# Punching Shear Behaviour of Slab-Column Edge Connections Reinforced with Fibre-Reinforced Polymer (FRP) Composite Bars

by

Mohammed Galal Osman Mohammed El-Gendy

A Thesis submitted to the Faculty of Graduate Studies of

The University of Manitoba

in partial fulfillment of the requirements of the degree of

**MASTER OF SCIENCE**

Department of Civil Engineering

University of Manitoba

Winnipeg, MB, Canada

# ABSTRACT

Recently, the use of fibre reinforced polymers (FRP) as an alternate to conventional steel has proved to be an effective solution to the corrosion problem. However, FRP reinforcing bars have a relatively low axial and transverse stiffness compared to steel bars which results in a lower shear capacity of FRP reinforced concrete (RC) elements compared to the steel-RC elements.

Flat plate systems are commonly used in structures like parking garages to take advantages of the absence of beams. They, however, are susceptible to punching shear failure where the column along with a surrounding part of the slab suddenly punches through the remainder of the slab.

An experimental program was conducted at the University of Manitoba to investigate the influence of different parameters on the punching shear behaviour of slab-column edge connections. Nine full-scale isolated slab-column edge connections were constructed and tested to failure. One connection was reinforced with steel flexural reinforcement, six with GFRP flexural reinforcement and two with GFRP flexural and shear reinforcement. The parameters investigated were the flexural reinforcement type and ratio, the moment-to-shear ratio and the spacing of the stud shear reinforcement.

The test results showed that GFRP-RC connections can undergo significant deformations leading to an ample warning before the brittle punching failure. Also, the well-anchored shear studs managed to control the propagation of diagonal shear cracks and transferred the mode of failure from a brittle punching shear mode to a deformable flexural mode.

*To Mom and Dad,*

*I hope this achievement gets me a step closer to making you proud of me.*

# ACKNOWLEDGMENTS

First of all, I would like to express my sincere gratitude and appreciation to my advisor Dr. Ehab El-Salakawy, PEng, Professor and Canada Research Chair in Durability and Modernization of Civil Structures, Department of Civil Engineering, University of Manitoba. He has been a tremendous mentor for me. I would like to thank him for trusting and encouraging me. His academic and personal advices have been priceless.

I would also like to thank my colleagues for their continuous support specially Mohamed Hasaballa and Karam Mahmoud whose comments and suggestions were remarkable.

The financial support provided by the Natural Science and Engineering Research Council of Canada (NSERC) through Discovery and Canada Research Chair programs is gratefully acknowledged.

My experimental program would have never been completed without the help and assistance of the W. R. McQuade structures laboratory technical staff, Chad Klowak, PEng, Brenden Pachal and Grant Whiteside during the construction and testing of the specimens.

A huge “thank you” to my dear friends Ahmed Hamdi Sakr, Mohammed Mady and Evan Coy for their priceless assistance, to my friends Ahmed Radwan and Ahmed Ghazy for their support and to my friend Khaled Ahmed, without him I wouldn’t have started my graduate studies.

At last, but definitely not least, I would like to thank my family. All the words in the world cannot describe how grateful I am for your sacrifices. Your wishes and prayers gave me the strength to persevere and warmed my heart.

*Mohammed Galal El-Gendy, September 2014*

# TABLE OF CONTENTS

# LIST OF TABLES

# LIST OF FIGURES

# LIST OF NOTATIONS

$a$ depth of equivalent rectangular stress block

$A$ effective tension area of concrete surrounding the flexural tension reinforcement and extending from the extreme tension fibre to the centroid of the flexural tension reinforcement and an equal distance past that centroid, divided by the number of bars

$A_b$ area of an individual reinforcing bar

$A_f$ area of longitudinal FRP reinforcement on the flexural tension side of a member

$A_g$ gross area of section

$A_s$ area of longitudinal steel reinforcement on the flexural tension side of a member

$A_{vf}$ area of FRP shear reinforcement within a distance $s$

$A_{vs}$ area of steel shear reinforcement within a distance $s$

$b$ width of cross section

$b_b$ band width of reinforced concrete slab extending a distance 1.5$h$ past the sides of the column

$b_o$ perimeter of critical section for shear in slabs

$b_1$ width of the critical section for shear in slabs measured in the direction of the span for which unbalanced moments are determined

$b_2$ width of the critical section for shear in slabs measured in the direction perpendicular to $b_1$

$c$ distance from extreme compression fibre to neutral axis

$c_1$ size of rectangular shear cross section in slabs measured in the direction of the span for which moments are being determined

$c_2$ size of rectangular shear cross section in slabs measured in the direction perpendicular to $c_1$

$C$ compression component of the bending moment acting on a section

$d$ distance from extreme compression fibre to centroid of tension reinforcement

$d_b$ diameter of reinforcing bar

$d_c$ distance from extreme tension fibre to centre of the longitudinal bar located closest to it

*D.L.* dead loads

$e$ distance from centroid of section for critical shear in slabs to the point where shear stress is being calculated

$E_c$ modulus of elasticity of concrete

$E_f$ modulus of elasticity of FRP reinforcement

$E_s$ modulus of elasticity of steel reinforcement

$f_c'$ specified compressive strength of concrete

$f_{fu}$ ultimate strength of FRP reinforcement

$f_{pcd}$ design compressive strength of concrete (according to JSCE 2007)

$f_r$ modulus of rupture of concrete

$f_s$ calculated stress in reinforcement at specified loads

$f_y$ specified yield strength of steel longitudinal reinforcement

$f_{yv}$ specified yield strength of steel shear reinforcement

$h_s$ overall thickness of a slab

$I$ moment of inertia of section about centroidal axis

$I_{cr}$ moment of inertia of cracked section

$I_e$ effective moment of inertia

$I_g$ moment of inertia of gross concrete section about centroidal axis, neglecting the reinforcement

$jd$ flexural lever arm (distance between tension and compression components of the bending moment applied at a section)

$J$ property of the critical shear section of slabs analogous to the polar moment of inertia deformability factor for slab-column connections

$k$ ratio of $c$ to $d$

$k_b$ coefficient dependent on the reinforcing bar bond characteristics

$k_i$ pre-cracking stiffness factor

$k_p$ post-cracking stiffness factor

$k_1$ bar location factor used for calculating development length

$k_2$ coating factor used for calculating development length

$k_3$ concrete density factor used for calculating development length

$k_4$ bar size factor used for calculating development length

$k_5$ welded deformed wire fabric factor used for calculating development length

$l_d$ development length of reinforcement

$l_n$ length of clear span in the direction that moments are being determined, measured face-to-face of supports

$L$ centre-to-centre spacing between columns

*L.L.* live load

$m_x$ bending moment per unit length on a section perpendicular to the $x$-axis

$m_y$ bending moment per unit length on a section perpendicular to the $y$-axis

$M_{cr}$ cracking moment

$M_f$ unbalanced moment about the centroid of the critical shear section in slabs

$M_n$ nominal flexural strength at section

$M_p$ equivalent plastic moment used in yield line theory calculations

$M_r$ factored moment resistance

$M_s$ moment due to specified loads

$M_u$ factored moment at section

$n$ number of items

$n_f$ ratio of modulus of elasticity of FRP bars to modulus of elasticity of concrete

$n_s$ ratio of modulus of elasticity of steel bars to modulus of elasticity of concrete

$Q$ first moment of inertia about the centroidal axis of the part of the cross section farther from the centroidal axis than the point where the shear stresses are being calculated, used for one-way shear calculations

$s$ maximum centre-to-centre spacing of transverse reinforcement

spacing of headed shear reinforcement measured perpendicular to $b_o$

$T$ Tension component of the bending moment acting on a section

$u$ peripheral length of the column (according to JSCE 2007)

$u_p$ peripheral length of the design cross-section at $d/2$ from the column face (according to JSCE 2007)

$v_c$ shear stress resistance provided by the concrete

$v_f$ factored shear stress

$v_n$ nominal shear stress

$v_r$ shear stress resistance

$v_s$ shear stress resistance provided by shear reinforcement

$V_c$ nominal shear strength provided by concrete

$V_f$ factored shear force

$V_{flex}$ predicted flexural failure load of a connection

$V_n$ nominal shear strength

$V_{pcd}$ design punching shear capacity (according to JSCE 2007)

$V_r$ shear force resistance

$V_s$ nominal shear strength provided by shear reinforcement

$V_{Test}$ actual failure load of a connection

$V_{Pred}$ predicted failure load of a connection

$V_u$ factored shear force at section

$w_f$ factored load per unit area

$x$ centroidal $x$-axis of a critical section

$y$ centroidal $y$-axis of a critical section

$y_t$ distance from centroidal axis of gross section, neglecting reinforcement, to extreme fibre in tension

$z$ quantity limiting distribution of flexural reinforcement

$\alpha$ factor takes into account the eccentricity of the shearing force (according to JSCE 2007)

$\alpha_s$ factor that adjusts $v_c$ for support dimensions

$\alpha_1$ ratio of average stress in rectangular compression block to the specified concrete strength

$\beta_c$ ratio of long side to short side of column

$\beta_1$ ratio of depth of rectangular compression block to depth to the neutral axis

$\gamma_b$ partial safety factor (according to JSCE 2007)

$\gamma_c$ density of concrete

$\gamma_f$ fraction of unbalanced moment transferred by flexure at slab-column connections

$\gamma_v$ fraction of unbalanced moment transferred by eccentricity of shear at slab-column connections

$\Delta_s$ deflection of a member at service

$\Delta_u$ curvature of a member at ultimate

$\varepsilon_{cu}$ maximum strain at the extreme concrete compression fibre at ultimate

$\varepsilon_{fu}$ ultimate strain of FRP reinforcement

$\varepsilon_s$ strain in steel reinforcement

$\varepsilon_y$ yield strain in steel reinforcement

$\lambda$ factor to account for low-density concrete

$\rho$ flexural reinforcement ratio

$\rho_b$ balanced flexural reinforcement ratio

$\sigma$ normal stress

$\varphi$ resistance factor applied to a specified material property or to the resistance of a member which for the limit state under consideration takes into account the variability of dimensions and material properties, quality of work, type of failure and uncertainty in the prediction of resistance (according to CAN/CSA A23.3-04)

$\Psi_s$ curvature of a section at service

$\Psi_u$ curvature of a section at ultimate

# CHAPTER 1: INTRODUCTION

## 1.1. BACKGROUND

Reinforced concrete structures are usually reinforced with conventional steel reinforcement. Steel, in the presence of moisture, is subjected to a significant durability problem which is corrosion. Initially, the alkaline nature of concrete protects the steel reinforcement against corrosion by providing a thin passive film that surrounds the steel reinforcement (Neville 1995). However, when RC structures are subjected to aggressive conditions, e.g., wet/dry cycles, freeze/thaw cycles and diffusion of de-icing salts through the concrete, this alkaline passive film is destroyed and the reinforcement is vulnerable to electrochemical corrosion.

Corrosion of steel reinforcement is one of the major durability issues resulting in the deterioration of structures which increases the number of repair cycles required for a structure to achieve its service life and, consequently, increases the repair and maintenance costs over the service life of the structure. In a study published by the U.S. Federal Highway Administration (Koch et al. 2002), the total annual direct cost of corrosion in the U.S. is estimated to be $276 billion which is approximately 3.1% of the nation's Gross Domestic Product "GDP". Of this cost, 16.4% is related to the corrosion of steel in infrastructures.

Many solutions have been proposed to overcome the corrosion problem such as increasing the concrete cover, improving the quality of the concrete and the use of different kinds of steel reinforcement (i.e., stainless steel, epoxy-coated steel and galvanised steel). However, besides being cost-ineffective, these solutions have managed only to delay the initiation of the corrosion process; none of them was able to completely prevent it. Recently, the use of fibre reinforced

polymers (FRP) composites as an alternate to the conventional steel has proved to be an effective solution to the corrosion problem.

Corrosion resistance is not the only advantage of FRP composites over conventional steel. They have many other advantages such as higher longitudinal tensile strength, higher fatigue endurance, no magnetic conductivity, light-weight, low electrical and thermal conductivity for certain types of fibres, and versatility of fabrication. On the other hand, unlike steel, FRP composites exhibit linear-elastic behaviour up to failure, i.e., they do not undergo any ductile phase in terms of a yielding plateau prior to the brittle rupture as shown in Figure 1.1. Moreover, FRP reinforcing bars, especially glass (G)FRP bars, have low transverse strength and stiffness which affects the shear strength of the bars. They also have a relatively low elastic stiffness and compressive strength compared to steel bars (ACI Committee 440 2006). Due to these differences, the published design codes and guidelines dealing with steel-RC structures cannot be directly applied to FRP-RC structures. Experimental investigations must be carried out to verify the behaviour of concrete elements reinforced with FRP composites.

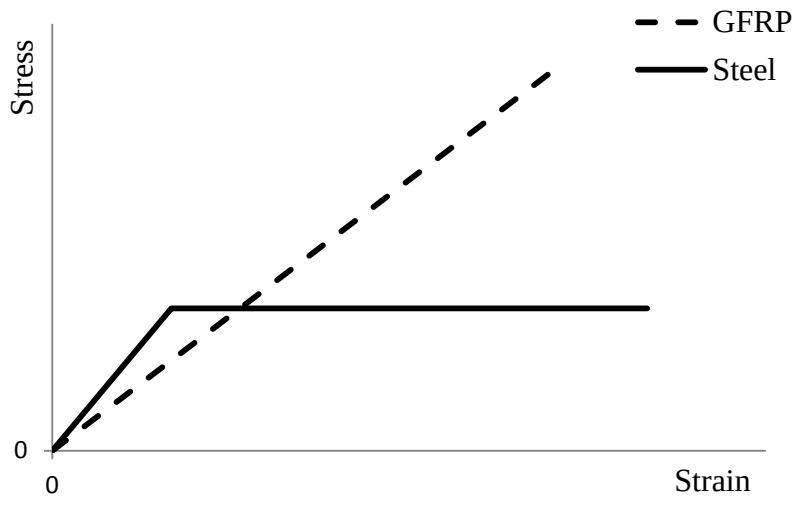


Figure 1.1: Typical stress-strain relationship

Much research have been conducted in the last two decades to investigate the behaviour of FRP-RC members and codes and guidelines for the design of such members have been published (Japan Society of Civil Engineering 1997; ACI Committee 440 2006; Canadian Standards Association 2012). However, little research has been conducted to investigate the shear behaviour of FRP-RC members in general and the punching shear behaviour of FRP-RC flat plates in particular.

## 1.2. PROBLEM DEFINITION

Concrete flat plate system is the simplest in terms of formwork construction since the slab is supported directly by columns (Figure 1.2) and its soffit is continuously flat (Lorenz and Trygestad 2005). In addition, the absence of beams provides flexibility for partition location and lower storey heights, which, in turn, results in an increased number of stories for the same height. This leads to cost saving in partition walls and many other construction details especially in case of medium and high rise buildings (Fanella 2000).

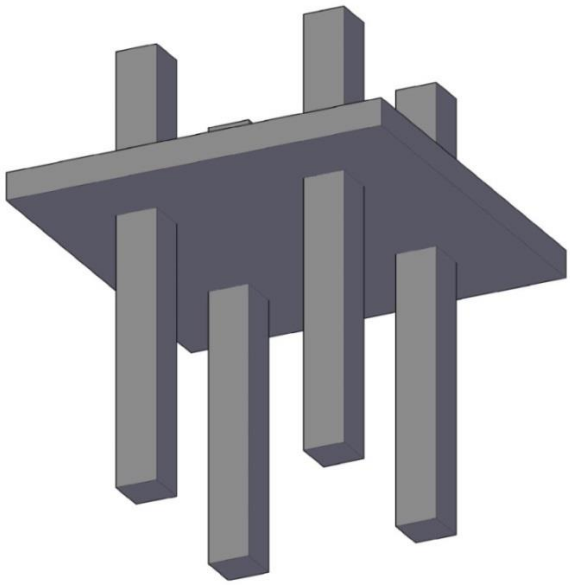

Figure 1.2: Typical flat plate system

Flat plate systems are commonly used in parking garage structures to take advantage of the absence of beams to allow for more clearance for the vehicles. In North America, parking garages are very vulnerable to corrosion of steel reinforcement because they are often subjected to harsh conditions such as freeze/thaw cycles, wet/dry cycles and de-icing salts. As mentioned earlier, the use of FRP reinforcement instead of the conventional steel reinforcement would overcome the corrosion problem.

Whether the flat plate system is reinforced with steel or FRP bars, it is susceptible to punching shear failure where the column along with a surrounding part of the slab suddenly punches through the remainder of the slab. This type of failure is extremely dangerous because of its brittle nature which does not give any warning to the occupants of the building before failure. Furthermore, the failure of one joint in the system may lead to loss of the structure integrity and, accordingly, a progressive collapse of the whole structure when the adjacent connections fail to support the additional loads imposed on it (Swamy and Ali 1982).

Punching shear failure occurs as a result of the high shear stresses caused by the inevitable combination of shear force and bending moment transferred between the slab and the column at a slab-column connection. The bending moment transfer occurs due to pattern loading conditions, different lengths of adjacent spans and/or the presence of lateral load. Precise calculations for the shear stresses at these connections in addition to reasonable predictions of the punching shear capacities of the connections are essential to prevent the undesirable punching shear failure.

The effects of different parameters on the punching shear behaviour of steel-RC slab-column connections have been extensively investigated (Richart 1948; Moe 1961; Vanderbilt 1972;

Zaghlool and Rawdon de Paiva 1973; Long 1975; Dilger and Ghali 1981; Swamy and Ali 1982; Mokhtar et al. 1985; Hawkins et al. 1989; Gardner 1990; Marzouk and Hussein 1991; Alexander and Simmonds 1992; Shaaban and Gesund 1994; Marzouk et al. 1996, 1998, 2000; Menetrey 1998; El-Salakawy et al. 1998, 2000; Ghannoum 1998; Osman et al. 2000; Dilger et al. 2005; Ozden et al. 2006; Stein et al. 2007; Widianto et al. 2009; Rizk et al. 2011) and provisions for the design of such connections have been included in different codes and guidelines (Canadian Standards Association 2004; Japan Society of Civil Engineering 2007; ACI Committee 318 2011). On the other hand, information on the behaviour of FRP-RC slab-column connections is relatively limited due to the lack of experimental and analytical studies. Little research has been conducted to study the punching shear behaviour of FRP-RC slab-column interior connection (Banthia et al. 1995; El-Ghandour et al. 1999, 2003; Matthys and Taerwe 2000; Ospina et al. 2003; Zaghloul and Razaqpur 2004; El-Gamal et al. 2005; Dulude et al. 2010; Hassan et al. 2013). Moreover, to the author's best knowledge, only one research study has been done to study the punching shear behaviour of FRP-RC slab-column edge connections using small scale specimens reinforced with carbon (C)FRP grid reinforcement (Zaghloul 2007).

## 1.3. SCOPE OF WORK

There are three different types for slab-column connections depending on their location: interior, edge and corner connections. The relatively higher moment transferred between the slab and the column at the edge and corner connections compared to the interior ones makes them more critical to punching shear failure.

Many solutions have been considered to prevent the punching shear failure for steel-RC slab-column connections. One of these solutions is using stud shear reinforcement (Dilger and Ghali 1981; Mokhtar et al. 1985; El-Salakawy et al. 2000; Stein et al. 2007). The scope of this

experimental study is to investigate the punching shear behaviour of isolated full-scale slab-column edge connections. The slabs are totally reinforced in flexure with GFRP longitudinal bars with or without GFRP stud shear reinforcement. The connections are subjected to three different moment-to-shear ratios (0.2 m, 0.4 m and 0.6 m).

## 1.4. OBJECTIVES

The objectives of this study are to:

- Investigate the punching shear behaviour of GFRP-RC slab-column edge connections with and without punching shear reinforcement subjected to gravity loads with different moment-to-shear ratios.
- Verify the punching shear provisions in the Canadian Standards Association code CAN/CSA S806-12 (Canadian Standards Association 2012), the American Concrete Institute guideline ACI 440.1R-06 (ACI Committee 440 2006) and the Japan Society of Civil Engineering code JSCE 1997 (Japan Society of Civil Engineering 1997).
- Provide recommendations for designers and researchers to predict the punching shear capacity of GFRP-RC slab-column edge connections with and without punching shear reinforcement.

In order to achieve these objectives, the effects of the following parameters on the punching shear behaviour of edge-slab column connections have been studied:

- The flexural reinforcement type and ratio.
- The presence and spacing of stud shear reinforcement.
- The moment-to-shear ratio.

## 1.5. WORK METHODOLOGY

In order to achieve the aforementioned objectives, an extensive experimental study is conducted in the W. R. McQuade Structures Laboratory at the University of Manitoba. In this study, a total of nine isolated full-scale GFRP-RC slab-column edge connections are constructed and tested under gravity loads up to failure. Each connection represents an edge column stub connected to an isolated portion of a 6500×6500×200 mm slab bounded by the slab edge and the lines of contraflexure.

## 1.6. THESIS ORGANIZATION

The thesis consists of five chapters as follows:

- Chapter one introduces the problem definition, the specific scope and objectives of the research, and the methodology followed to achieve these objectives.
- Chapter two provides information about FRP composites and their constituent materials, a comparison between the behaviour of beams and slabs in shear, an overview of the existing design provisions regarding punching shear in different codes and guidelines for both steel-RC and FRP-RC slab-column connections, and a critical review of previous research pertaining to punching shear behaviour of both steel-RC and FRP-RC slab-column connections.
- Chapter three provides a detailed description of the experimental program in terms of the details of the test connections (dimensions, properties of constituent materials and reinforcement detailing), the details of the instrumentations used to monitor the behaviour of the connections during the test (LVDTs, reinforcement and concrete strain gauges, and PI gauges) and the details of the test setup and test procedure (test frame and hydraulic machines applying the loads).

- Chapter four provides the analysis and discussion of the experimental test results in terms of cracking patterns and mode of failure, strains in the reinforcement and concrete, deflections, the ultimate punching capacity and comparisons to different code predictions.
- Chapter five presents a summary of the work, derived conclusions and recommendations for future research.

# CHAPTER 2: LITERATURE REVIEW

## 2.1. INTRODUCTION

Flat plates may fail in shear in two different mechanisms: (1) one-way shear and (2) two-way shear or punching shear as shown in Figure 2.1. However, the punching shear capacity of a slab is usually far less than its one-way shear capacity; thus, punching shear governs the design (Park and Gamble 2000). In a typical slab-column connection, not only concentric loads are transferred from the slab to the column, but also bending moments are transferred due to uneven loading schemes or unequal adjacent span lengths. The moment transfer is magnified in the case of slab-column edge connections and if the structure is to resist lateral loads. In any case, if the applied punching shear stresses are higher than the capacity of the connection, shear reinforcement is to be used to increase the punching shear capacity. Stud shear reinforcement, in particular, has been used to increase the capacity and ductility of steel-RC connections. It is easy to install inside thin slabs as it does not interrupt the flexural reinforcement; moreover, it has sufficient anchorages on both upper and lower ends to prevent bond slip prior to yielding (Mokhtar et al. 1985).

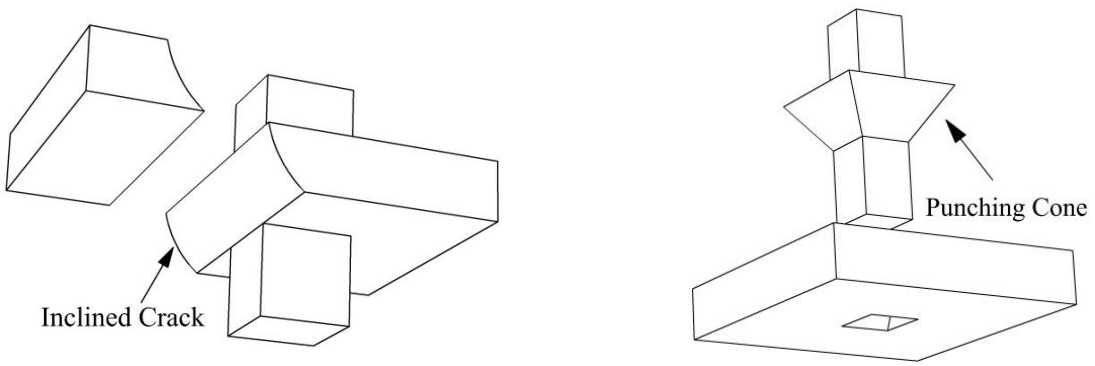


a) One-way shear b) Punching shear

Figure 2.1: One-way and two-way shear (reproduced from Wight and MacGregor 2011)

The behaviour of FRP-RC slab-column connections has been studied starting the late 1990's. It was demonstrated that the punching shear capacity of FRP-RC slab-column interior connections subjected to concentric loads is considerably less than that of steel-RC connections with a similar flexural strength (Matthys and Taerwe 2000). This conclusion is reasonable since the axial stiffness and the transverse strength of the FRP bars are relatively less than those of the steel bars, which reduce the shear capacity of FRP-RC concrete members (El-Sayed et al. 2005).

This chapter presents a detailed discussion of the previous research available on both steel-RC and FRP-RC slab-column connections with and without shear reinforcement. In addition, a summary of the punching shear provisions in the current codes and guidelines in North America and Japan is also presented.

## 2.2. PROPERTIES OF FRP COMPOSITE BARS

### 2.2.1. Physical Properties

The American Concrete Institute standard (ACI 440.1R-06) describes two important physical properties of FRP composites: (1) the density and (2) the coefficient of thermal expansion.

#### 2.2.1.1. Density

The density of the FRP composites is considerably lower than that of steel. Generally, the specific gravity of FRPs is about one-sixth to one-fourth that of steel reinforcements. Since the lower the density the lighter the bars are, the transportation and labor costs are considerably reduced. The densities of different types of reinforcing bars given by the ACI 440.1R-06 are listed in Table 2.1.

Table 2.1: Densities of reinforcing bars (ACI Committee 440 2006)

| Reinforcement type | Steel | GFRP | CFRP | AFRP |
|---|---|---|---|---|
| Density ($gm/cm^3$) | 7.9 | 1.25-2.1 | 1.5-1.6 | 1.25-1.4 |

#### 2.2.1.2. Coefficient of thermal expansion

Unlike steel reinforcement, FRP composites have different coefficients of thermal expansion in the longitudinal and transverse directions depending on the types of the constituents (fibres and resin) and the fibre-volume fraction. Furthermore, while the properties of the fibres control the longitudinal coefficient, the transverse coefficient is dependent on the properties of the resin (Bank 1993). The coefficients of thermal expansion of different types of reinforcing bars as given by the ACI 440.1R-06 are listed in Table 2.2. It is noted that the longitudinal coefficient of thermal expansion for CFRP bars is close to zero, which indicates that CFRP bars are not affected by changing the temperature. Furthermore, AFRP bars have a negative longitudinal coefficient of thermal expansion, which means that the length of AFRP bars decreases with increasing the temperature and increases with decreased temperature.

Table 2.2: Coefficient of thermal expansion (ACI Committee 440 2006)

| Reinforcement type | | Steel | GFRP | CFRP | AFRP |
|---|---|---|---|---|---|
| Coefficient ($x10^6/^oC$) | Longitudinal | 11.7 | 6 to 10 | -9 to 0 | -6 to -2 |
| | Transverse | 11.7 | 21 to 23 | 74 to 104 | 60 to 80 |

### 2.2.2. Mechanical Properties

#### 2.2.2.1. Tensile behaviour

FRP composites are brittle in nature. Unlike steel reinforcement, they do not undergo a yielding plateau prior to rupture when they are loaded in tension. Instead, they exhibit a linear elastic stress-strain relationship up to failure as shown in Figure 1.1.

Many parameters affect the tensile strength and modulus of an FRP bar; some of them are the type of fibres and resin, the fibre-volume fraction and the diameter of the bar. Moreover, the quality control of the manufacturing process also affects the mechanical characteristics (Wu 1990). Consequently, having two bars with the same diameter, made of the same constituent materials and with the same fibre-volume fraction does not mean that they have the exact same tensile properties. Accordingly, the tensile properties of FRP composite bars should be obtained directly from the manufacturer for each batch.

Since most FRP composite bars are made of thermosetting resin which cannot be reshaped after curing, they cannot be bent after being manufactured. Instead, FRP bent bars can be prefabricated with bends. In this case, a strength reduction of 40 to 50% in the bend portion compared with the strength of a straight bar is expected due to stress concentrations (Nanni et al. 1998). As shown in Table 2.3, the tensile strength of the FRP composite bars is much higher than the yield strength of the steel bars. On the other hand, the stiffness of the FRP bars is lower than that of the steel bars.

Table 2.3: Typical tensile properties of reinforcing bars (ACI Committee 440 2006)

| Reinforcement type | Steel | GFRP | CFRP | AFRP |
|---|---|---|---|---|
| Tensile strength (MPa) | 276-517* | 483-1600 | 600-3690 | 1720-2540 |
| Tensile modulus (GPa) | 200 | 35-51 | 120-580 | 41-125 |

*yield strength

#### 2.2.2.2. Compressive behaviour

The failure for FRP bars under axial compression may be triggered by transverse tensile failure, internal buckling of the fibres, and/or shear failure depending on the type of fibres and resin and the fibre-volume fraction.

The current design documents in North America (Canadian Standards Association 2012) and the American Concrete Institute guideline (ACI Committee 440 2006) consider the FRP reinforcement in compression zones to have zero compressive strength. In general, the compressive strength and compressive modulus of FRP bars is less than the tensile strength and modulus of the same product.

#### 2.2.2.3. Shear behaviour

In general, FRP bars are weak in interlaminar shear because the resin is usually unreinforced in the transverse direction of the bar and, consequently, interlaminar shear strength depends on the weak resin. Placing fibres in the transverse direction across the axial fibres will increase the shear resistance.

#### 2.2.2.4. Bond behaviour

Bond stresses between the FRP bars and the concrete is transferred by the adhesion between the concrete and the reinforcing bar (chemical bond), the frictional resistance due to roughness of the FRP bar's surface, the bearing of the bar deformations against the concrete (mechanical bond/interlock), the hydrostatic pressure exerted on the bars due to the shrinkage of the concrete and the expansion/swelling of the bars when subjected to high temperature (Benmokrane et al. 1996; Cosenza et al. 1997). When an FRP-RC element is tested, the chemical bond mechanism is the dominant mechanism transferring bond stresses between the concrete and the bars until initial pullout/slip of the bars; thereafter, frictional bond and mechanical interlock become the governing mechanisms depending on the surface texture.

The bond behaviour of FRP bars is fairly different from that of steel bars because of the different surface preparations and the considerable differences in the material properties in both

longitudinal and transverse directions (Cosenza et al. 1997). A reduction of 40% to 10% was found in the maximum bond strength of GFRP bars compared to steel bars with the same diameter. This was attributed to the fact that while the main contribution to the bond strength in case of steel reinforcement comes from the bearing of the bar rips against the concrete; the rips of the GFRP bars do not provide enough lateral confinement since they have different geometry and lower shear strength and stiffness than those of steel bars (Benmokrane et al. 1996).

## 2.3. ONE-WAY SHEAR (BEAM ACTION)

In general, flat plate systems may exhibit two different types of shear failure depending on the type of loading (distributed load or concentrated load) and the geometry of the slab-column connections (the size of the column, the thickness of the slab and the presence of column capitals). These two types are: 1) One-way shear or beam action and 2) Two-way shear or punching shear. In the one-way shear mechanism, the slab behaves as a wide rectangular beam where the failure occurs at an inclined crack extending across the entire width of the slab. The behaviour of beams subjected to shearing stresses can be divided into two stages: 1) pre-cracking behaviour and 2) post-cracking behaviour.

### 2.3.1. Pre-Cracking Behaviour

When a simply-supported beam is subjected to a concentrated load in mid-span as shown in Figure 2.2, the shear stress distribution on an uncracked section, *v*, is calculated from Equation 2.1.

$$v = \frac{VQ}{Ib} \qquad \text{Eq. [2.1]}$$

Where *V* is the shearing force at the cross section, *Q* is the first moment of inertia about the centroidal axis of the part of the cross section farther from the centroidal axis than the point

where the stresses are being calculated, *I* is the moment of inertia of the cross section and *b* is the width of the cross section.

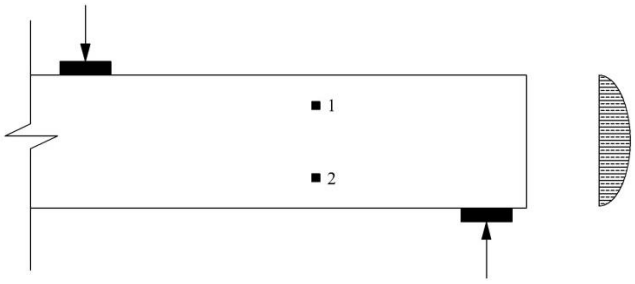


a) Shear stress distribution

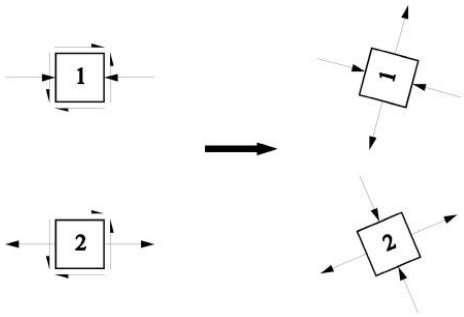


b) Flexural, shear and principal stresses on two elements in the shear span

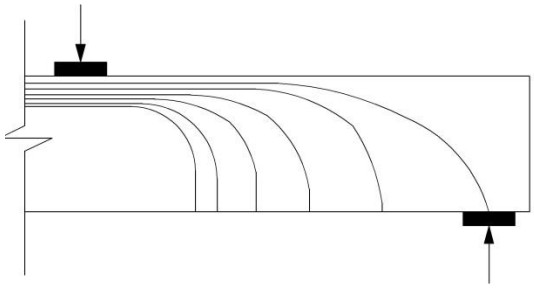

c) Principal compressive stresses paths in an uncracked beam

Figure 2.2: Stresses in an uncracked Beam (reproduced from Wight and MacGregor 2011)

The orientation of the principal stresses acting on two different elements in the beam is shown in Figure 2.2b. Following the surfaces on which principal tension stresses act in adjacent elements gives the cracking pattern shown in Figure 2.2c. The cracks are steeper at the bottom where there

are no shear stresses and the principal tension stress equals the tensile flexural stress acting parallel to the beam longitudinal axis. The diagonal shear stresses are maximum and the flexural stresses are zero at the longitudinal axis of the beam and, thus, $45^{o}$ inclined cracks appear in the mid-height of the beam. At the top, shear stresses are zero and the flexural stresses are compressive stresses which cause flatter cracks near the top of the beam (Wight and MacGregor 2011).

### 2.3.2. Post-Cracking Behaviour

After the beam is cracked, the shear stresses can be calculated from Equation 2.2 and the shear stress distribution of a cracked section is shown in Figure 2.3. This stress distribution assumes that about 30% of the shear stresses are transferred through the uncracked portion of the cross section while the remaining is transferred through the crack mainly by means of aggregate interlock and dowel action.

$$v = \frac{V}{b * jd} \qquad \text{Eq. [2.2]}$$

Where *jd* is the flexural lever arm (distance between tension and compression components of the bending moment applied at the section).

Shear failure occurs when inclined shear cracks take place. In most cases, vertical flexural cracks start first at the bottom of the beam and extend to form flexure-shear cracks. However, in certain cases when the shear span-to-depth ratio is small, shear stresses in the web are considerably higher than the flexural stresses at the bottom of the beam; thus, a diagonal shear crack occurs prior to the occurrence of flexural cracks.

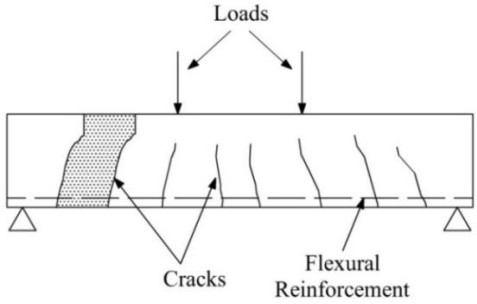


a) A cracked simply-supported beam

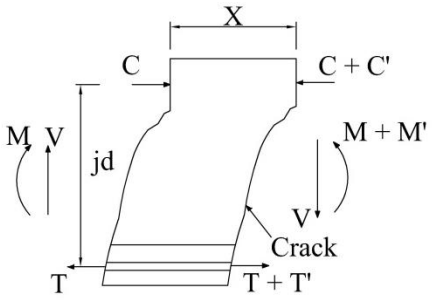


b) The portion between two cracks

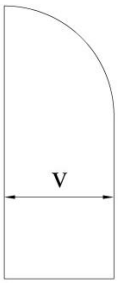


c) Shear stress distribution

Figure 2.3: Shear stresses in a cracked beam (reproduced from Wight and MacGregor 2011)

### 2.3.3. Shear Strength Provided by Concrete

The shear strength in beams without shear reinforcement is provided by five components as shown in Figure 2.4: (1) shear resistance of the compression zone (uncracked concrete), (2) aggregate interlock along the two surfaces of the crack, (3) dowel action of the flexural reinforcement crossing the shear crack, (4) arch action in deep members with shear span-to-depth ratio less than 2.5; and (5) residual tensile stress in the shear crack resulting from the small remaining connections between the two faces of the crack (ASCE-ACI Committee 426 1974). These five components of the shear strength of beams without shear reinforcement together are referred to as the shear provided by concrete. This description is somehow inaccurate since the flexural reinforcement has a great contribution to the shear strength; however, the description is still valid as it implies the absence of shear reinforcement.

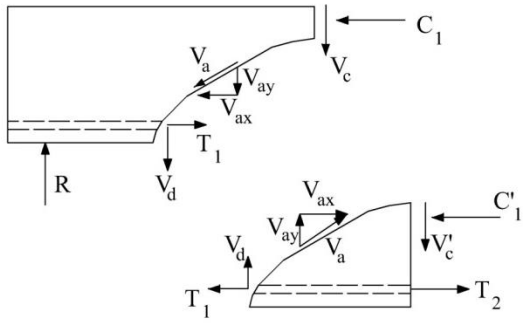


Figure 2.4: Forces in a cracked beam (reproduced from Wight and MacGregor 2011)

The shear strength provided by concrete is affected by the following parameters: (1) the tensile strength of concrete which determines the cracking load, (2) the flexural reinforcement ratio which affects the stiffness of the cross section and the shear resistance provided by the dowel action, (3) the shear span-to-depth ratio which controls the arch action, (4) the beam size which affects the cracks widths, (5) the presence of axial loads which delay the initiation of cracks and reduce crack widths in case of compressive forces or speed up the initiation of cracks and increase the crack widths in case of tensile forces and (6) the size of the coarse aggregate which controls the roughness of the crack interface.

### 2.3.4. Shear Strength Provided by Reinforcement (The Truss Analogy)

When the shear strength carried by the concrete is below the flexural strength of the member, shear reinforcement is to be used to ensure that the member will reach its flexural capacity before shear failure occurs.

When the beam is loaded, the strains in the stirrups are very low until inclined cracks start to develop. Therefore, stirrups do not prevent inclined cracks from developing; instead, they control the propagation and the width of the inclined cracks. As in the case of members without shear reinforcement, the entire shear is resisted by the whole uncracked section prior to cracking. After

flexural cracking and until inclined cracking, the shear is resisted by the shear strength provided by the concrete. Once inclined cracks start to propagate, the shear stress is transferred to the stirrup. Besides carrying shear stresses, stirrups will control the propagation of the inclined cracks leading to an increase in the aggregate interlock component.

The truss analogy proposed by (Ritter 1899) and (Mörsch 1902) for designing RC beams in shear provides a great conceptual model to explain the shear forces in a cracked RC beam. As shown in Figure 2.5, a simple beam with inclined cracks develops internal forces similar to the forces of a truss, i.e., compressive and tensile forces in the lower and upper flanges, respectively, tensile forces in the stirrups and diagonal compressive forces in the concrete web between the inclined cracks. In order to simplify the indeterminate system of forces shown in Figure 2.5a into the analogous truss shown in Figure 2.5b, some assumptions have to be made. All the stirrups passing through the inclined crack are lumped together into one vertical truss member. Similarly, a diagonal truss member represents the diagonal concrete under compression.

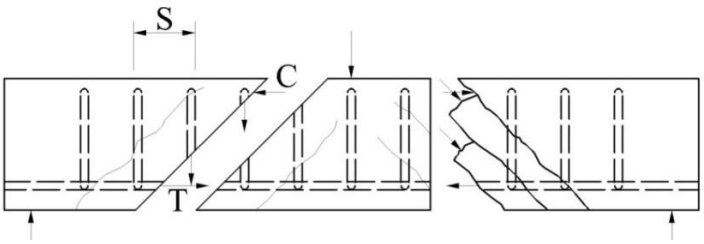


a) Internal forces in a cracked beam

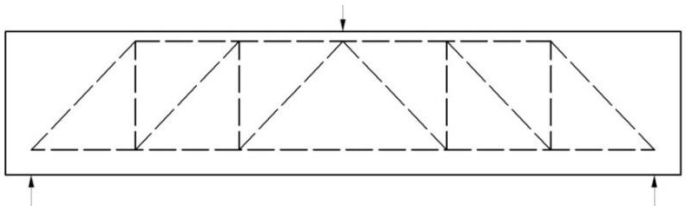

b) Pin-jointed truss

Figure 2.5: Truss analogy (reproduced from Wight and MacGregor 2011)

## 2.4. TWO-WAY SHEAR (PUNCHING SHEAR)

Punching shear failure is a local failure of the slab-column connection or at the locations of concentrated loads. In slab-column connections, the column along with a pyramid-shape part of the slab punches through the remainder of the slab as a result of the high shear stresses caused by the inevitable combination of shear forces and bending moments transferred between the slab and the column.

The behaviour of slab-column connections is very complex due to the multidimensional geometry of the connection which precludes the development of simple analysis procedures that realistically assess the actual stresses condition. Thus, away from the European attempts to develop models that implement a reasonable facsimile of the actual behaviour (Kinnunen and Nylander 1960; Kinnunen 1963), most of the available analyses in North America limit the maximum shear strength of a slab to a value determined empirically from experimental tests. This value is highly-dependent on the assumed location of the critical section since the critical section perimeter increases with the distance of the critical section from the column face.

### 2.4.1. Mechanism of Punching Shear Failure

Similar to the case of one-way shear, once the inclined cracks form in the absence of shear reinforcement, shear stresses are resisted by the five components of the shear strength provided by concrete (Section 2.3.3). However, when two-way bending occurs, the ultimate shear strength of a slab is generally higher than a beam. This increase is attributed to the following five factors: (1) the distribution of moments, (2) the lack of symmetry, (3) the inadequacy of a simple static analysis, (4) the in-plane forces generated by restraints provided by the supports and (5) the interaction of flexural and shear effects (ASCE-ACI Committee 426 1974).

#### 2.4.1.1. Distribution of moments

When a slab-column connection is subjected to a vertical shearing force, the first crack to form is a tangential flexural crack at the location of maximum radial bending moments, i.e., at the column face. Radial cracks then extend from the column face towards the supported edges due to bending moments in the tangential direction. Additional tangential cracks a distance away from the column face will not form until the applied load increases significantly since the radial moment decreases rapidly with increasing the distance from the column face. On another hand, inclined cracks must propagate in the tangential direction (perpendicular to radial cracks). Since flexural tangential cracks are not located where they can initiate inclined cracks, inclined cracks tend to originate at the middepth of the slabs and, accordingly, their characteristics are similar to web-shear cracks rather than flexural-shear cracks in the case of beams.

#### 2.4.1.2. Lack of symmetry

In most cases, orthogonal reinforcement mats are used in slabs. The use of orthogonal reinforcement mats, rather than circular/radial reinforcement mats, creates a complex pattern of in-plane forces in the slab (Lenschow and Sozen 1966, 1967). Figure 2.6 shows a part of a slab with a reinforcing mat at $45^{o}$ to the direction of the moment, $M_1$. The components of the reinforcement forces, $T$, in the y direction are balanced by compression forces in the concrete at the level of that reinforcement (since the moment in the y direction is zero). This means that in-plane forces develop in the slab wherever flexural cracks are not parallel to the reinforcing bars. Such in-plane forces increase the loads for any cracking that develops after the initial tangential and radial cracks.

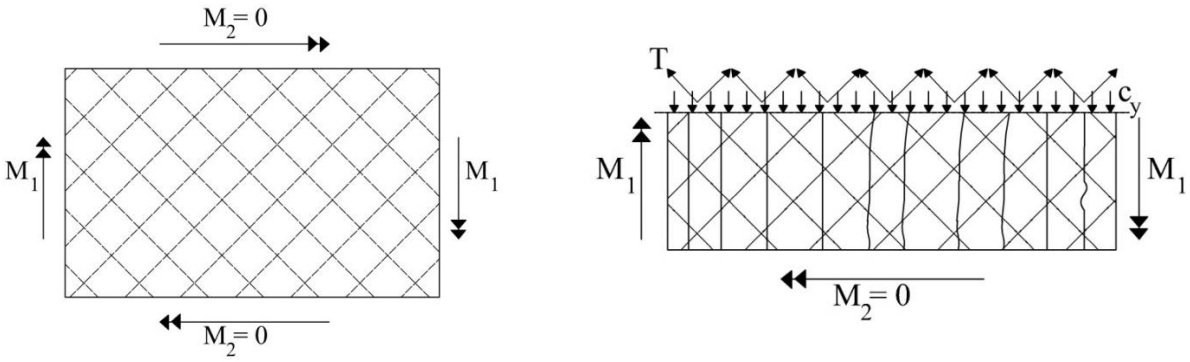


a) Moment and reinforcement orientation b) Internal forces at reinforcement level

Figure 2.6: In-plane forces in slabs (reproduced from ASCE-ACI Committee 426 1974)

#### 2.4.1.3. Inadequacy of static analyses

Figure 2.7 shows slab and beam cross sections at the location of the inclined cracks. For the beam, to satisfy equilibrium requirements, the tensile force, *T*, in the reinforcement crossing the inclined crack must equal the compressive force, *C*, acting above the inclined crack. On the other hand, for the slab, equilibrium requirements does not require the compressive force, $C_1$, acting below the inclined crack to equal the tensile force, $T_1$, developed in the reinforcement crossing the crack; instead, it requires that the summation of the compressive forces developed along the entire width of the slab, $C_1+C_2$, to equal the summation of the tensile forces developed in the reinforcement along the entire width of the slab, $T_1+T_2$. While maintaining equilibrium requirements, the force $C_1$ can be redistributed and the ratio between $C_1$ and $C_2$ may decrease with decreasing the depth of the uncracked concrete in the inclined crack location. However, there is no comparable mechanism for reducing the shear forces at that location. Concentrating the reinforcement through the failure perimeter may be thought to increase the compressive force, $C_1$ through increasing the depth of uncracked concrete; however, the force, $T_1$, in that reinforcement can be balanced by the compressive force developed outside the failure perimeter, $C_2$.

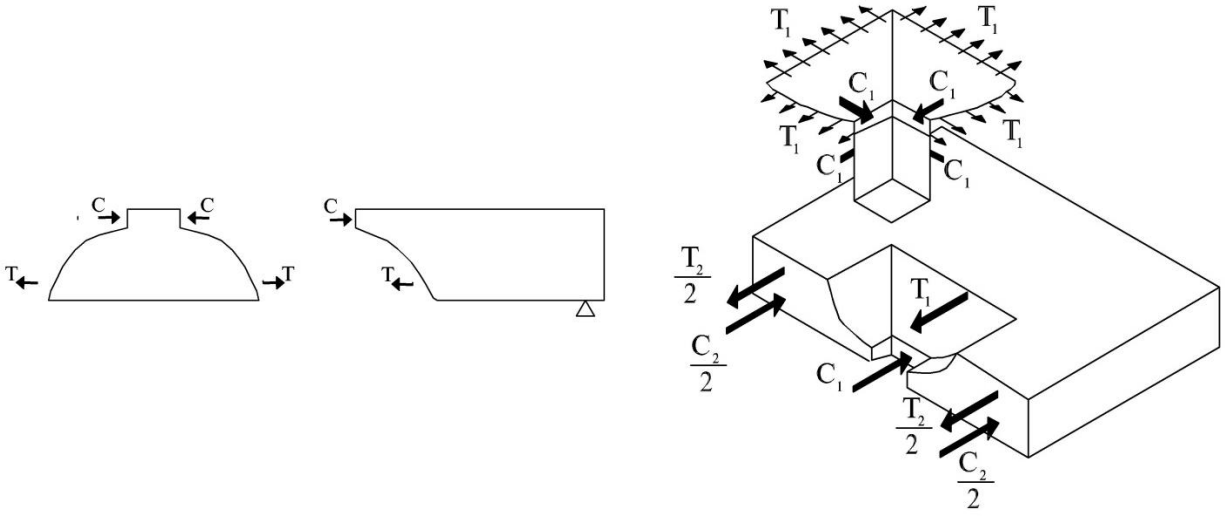


a) Beam b) Two-way slab

Figure 2.7: Forces at inclined cracks (reproduced from ASCE-ACI Committee 426 1974)

#### 2.4.1.4. In-plane forces generated by restraints

In-plane outward displacements tend to occur in the cracked region of the slab at the column vicinity. However, these displacements are restrained by the stiffness of the slab surrounding the failure region and, in turn, in-plane compression forces are developed in the slab. These forces increase the flexural and shear capacities of the slab-column connection. They, on the other hand, restrict the rotations of the cross sections and, subsequently, further reduce the ductility/deformability of the failure mode.

#### 2.4.1.5. Interaction of shear and flexural effects

The critical sections for maximum moment and shear in a slab-column connection coincide at the column face. Accordingly, moment-shear interaction is expected which makes it very difficult in most cases to classify the failure as either flexural failure or punching shear failure. Generally, the failure modes change from flexural failure to punching failure with increasing the slab reinforcement ratio.

### 2.4.2. Slab-Column Connections Transferring Shear and Unbalanced Moment

In most cases, slab-column connections are not subjected only to axial shearing forces but also to an unbalanced bending moment. Unbalanced moment is transferred at the exterior slab-column connections (edge and corner connections) due to the discontinuity of the slab and at the slab-column interior connections due to pattern loading. The value of the unbalanced moment transferred at a connection is dramatically increased if the connection is subjected to lateral loading. The transfer of the unbalanced moment causes the shear stress distribution around the column face to become nonuniform and reduces the shear capacity of the connection. Moreover, the punched region becomes confined to the area at the heavily loaded side of the column, i.e., where the direction of the shearing forces and unbalanced moment coincide, while the area at the opposite side may show little or no distress as shown in Figure 2.8.

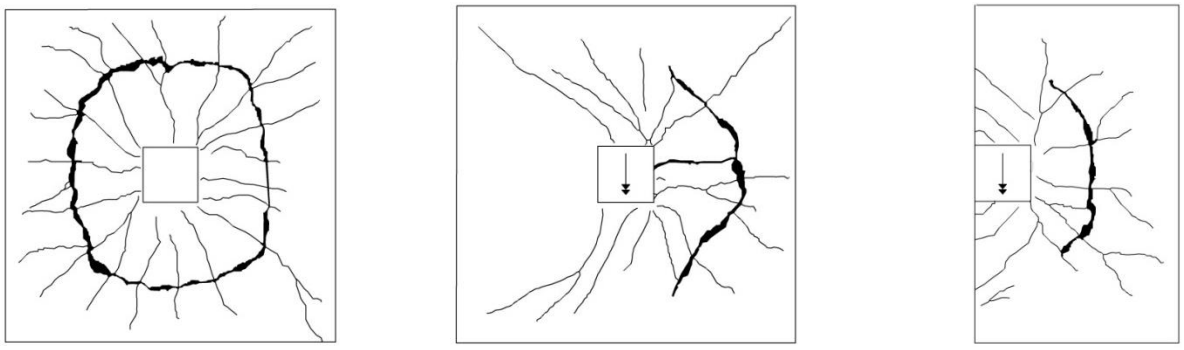

a) Interior – shear only b) Interior – shear & moment c) Edge

Figure 2.8: Different punching failures (reproduced from Alexander and Simmonds 1987)

### 2.4.3. Methods of Analysis

Four analytical approaches have been used to analyze the behaviour of slab-column connections transferring shear and unbalanced moment: (1) analysis based on a linear variation in shear

stress, (2) analysis based on thin plate theory, (3) analysis based on beam analogies and (4) analysis based on truss analogies.

#### 2.4.3.1. Analysis based on a linear variation of shear stress

This is the analysis implemented in the recent codes and guidelines in North America (Canadian Standards Association 2004; ACI Committee 318 2011). The shear stresses on a critical perimeter located a distance away from the column face is assumed to vary linearly with the distance from the centroidal axis of the perimeter as shown in Figure 2.9. Shear stresses are induced by the vertical shearing force and a portion of the unbalanced moment transferred through the connection. The remainder portion of the unbalanced moment is assumed to be resisted by flexure in the slab. The maximum shear stress, $v_f$, is calculated by Equation 2.3.

$$v_f = \frac{V_f}{b_o d} + \frac{\gamma_v M_f e}{J} \qquad \text{Eq. [2.3]}$$

Where $V_f$ is the factored shear force, $b_o$ is the perimeter of the critical section, $d$ is the slab average effective depth, $\gamma_v$ is the fraction of the unbalanced moment transferred between slab and column, $M_f$, and resisted by shear (Equation 2.4), $e$ is the distance from the centroid of the critical shear perimeter to the point where shear stress is being calculated and $J$ is a property of the critical shear section analogous to the polar moment of inertia calculated from Equations 2.5 and 2.6 for interior and edge connections, respectively.

$$\gamma_v = 1 - \frac{1}{1 + \frac{2}{3}\sqrt{\frac{b_1}{b_2}}} \qquad \text{Eq. [2.4]}$$

$$J = \frac{{b_1}^3 d + d^3 b_1}{6} + \frac{b_2 d {b_1}^2}{2} \qquad \text{Eq. [2.5]}$$

$$J = 2\left[\frac{{b_1}^3 d}{3} + \frac{d^3 b_1}{12}\right] - b_o d e^2 \qquad \text{Eq. [2.6]}$$

Where $b_1$ and $b_2$ are the widths of the critical perimeter measured in the direction of the span for which moments are determined and the perpendicular direction, respectively.

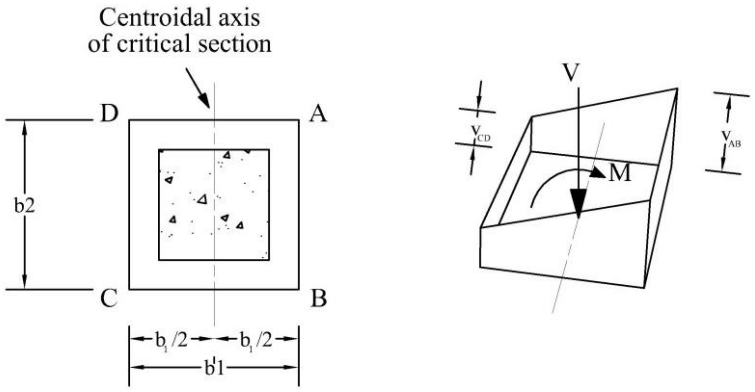


a) Interior connection

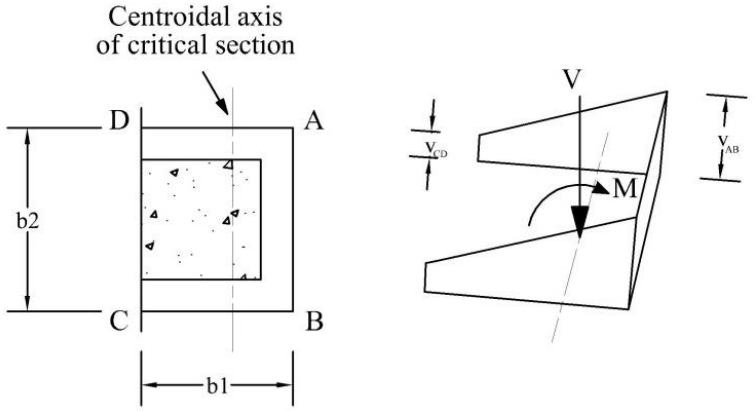


b) Edge connection

Figure 2.9: Linear shear stress distribution (reproduced from ACI Committee 318 2011)

#### 2.4.3.2. Analysis based on thin plate theory

This method was proposed in the early 1970s (Mast 1970a; b) to determine the stresses at slab-column connections based on the flexural theory of elastic plates. Unlike the straight-line shear stress theory, this method takes into account the shape of the column and the dimensions and boundary conditions of the slab. The shear stress distribution predicted by this method is nonlinear for rectangular columns. The predictions of this method are in good agreement with

those of the straight-line shear stress theory for the case of wide, rather than deep, columns, i.e., $C_2$ larger than $C_1$. On the contrary, for the case of deep columns, there is a considerable difference between the predictions of both methods.

#### 2.4.3.3. Analysis based on beam analogies

The slab strips framing orthogonally into each column face are considered to act as beams with constant widths of $C + d$ or $C + d/2$, as appropriate. These strips are subjected to shearing force and bending and torsional moments; thus, they are assumed to be capable of developing their shearing force and bending and torsional moments at the critical section. The strength of the connection is then calculated as the summation of the strengths of the four beams. Redistribution of stresses is permitted between the beams and the failure of the connection is assumed to occur when ultimate conditions are reached for at least three and two beams for interior and exterior connections, respectively.

#### 2.4.3.4. Analysis based on truss analogies

The first truss model was introduced to predict the ultimate capacity and load carrying mechanism of slab-column interior connections without shear reinforcement and subjected to a combination of shear and unbalanced moment (Alexander and Simmonds 1987; Simmonds and Alexander 1987). It provides a load path for shear forces in the presence of diagonal cracking and explains the role of flexural reinforcement in determining shear strength. As shown in Figure 2.10a, the truss model is a three dimensional space truss composed of concrete compression struts and tension ties. There are two types of compression struts: (1) struts parallel to the plane of the slab (anchoring struts) and (2) struts inclined at some angle to the plane of the slab (shear struts). When a slab-column interior connection is subjected to shearing force only, no anchoring struts develop. The gravity struts on the side faces of the column are gradually replaced by

anchoring struts as the ratio of moment-to-shear increases and, eventually, uplift shear struts develop at the back side of the column.

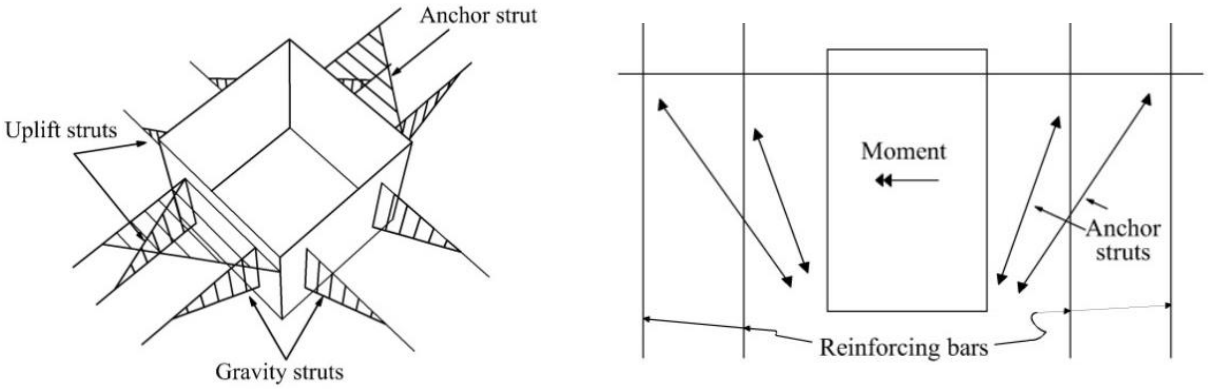


a) Struts in an interior connection b) Anchoring struts assembly

Figure 2.10: Truss model (reproduced from Alexander and Simmonds 1987)

Each connection comprises four anchoring struts as shown in Figure 2.10b; the force in each strut is balanced by two perpendicular reinforcing bars lying in the horizontal plane (one bar is passing through the column in the direction parallel to the axis about which the unbalanced moment is acting while the other bar is some distance away from the column). This assembly indicates that not only the bars passing through the column resist the unbalanced moment, but also the bars some distance from the column do.

The shear struts assembly is similar to the force diagram generated in a crane corbel as shown in Figure 2.11. The angle of the shear strut, the magnitude of the tensile force in the reinforcing bar and the magnitude of the compression force in the concrete strut are all essential to determine the geometry of the force system. In the case of the corbel, the angle of the shear strut is typically known since the loading point coincides with the conjunction of the tensile and compressive forces. On the other hand, the angle of the shear strut is a redundant since the slab is subjected to distributed loading rather than a concentrated load. Moreover, the vertical component of the

compressive force in the shear strut must be balanced by a tension field within the concrete. There are two types of shear struts according to their orientation: (1) gravity struts which oppose the relative downward movement of the slab and are tied by top reinforcing bars and (2) uplift struts which oppose the relative upward movement of the slab and are tied by bottom reinforcing bars, if any.

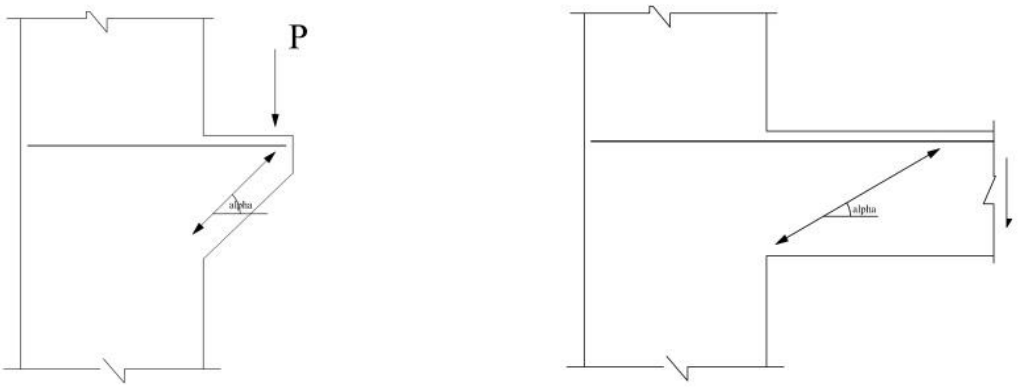


a) Corbel b) Shear strut

Figure 2.11: Shear strut vs. corbel forces (reproduced from Alexander and Simmonds 1987)

Tension struts tie the compression struts to the column. A portion of a tension tie can only be used by either an anchoring or a shear strut. Thus, a complete shear-moment interaction diagram can be generated by changing the portions of the tension ties assigned to anchoring and shear struts. The amount of reinforcing bars participating in the tension tie is not clearly defined. However, besides all the reinforcing bars passing through the column, it seems reasonable to assume that the bars at a distance *d* from the column face are included according to their distance from the column face, i.e., the contribution of a bar decreases linearly with increasing the distance from the column face (Alexander and Simmonds 1987). Three failure modes may be related to the truss analogy: (1) failure of the tension tie, (2) failure of the compression strut and (3) failure of the vertical (out-of-plan) component of the shear strut.

## 2.5. PUNCHING SHEAR REINFORCEMENT

If the shear capacity provided by concrete in a slab-column connection is not adequate to resist the applied shear stress, the punching shear capacity of the connection has to be increased to insure a ductile/deformable flexural failure rather than a brittle punching shear failure. This can be achieved by many methods such as: (1) increasing the area of concrete resisting shear stresses, i.e., increasing the thickness of the slab, providing a drop panel or a column head and/or increasing the column dimensions, (2) using concrete with higher compressive strength and (3) providing additional shear strength by placing shear reinforcement at the column vicinity. Although all these methods provide an increase in the punching shear capacity of the connections, only properly anchored shear reinforcement increased the ductility/deformability of the failure mode allowing for large slab-column deformations (Megally and Ghali 2000).

Although shear Reinforcement in the shape of shearheads were introduced in the 1930s (Wheeler 1936), it was not until the 1960s and the 1970s when design provisions for shear reinforcement were implemented in the ACI code for slabs thicker than 250 mm (ACI Committee 318 1963) and for thin slabs (ACI Committee 318 1971), respectively.

In a slab-column connection without shear reinforcement, the major inclined crack forms at an angle of approximately 30-35$^{o}$ with the plane of the slab. When shear reinforcement is present, it controls the inclined cracks propagation and provides additional confinement to the concrete. The crack inside the shear reinforced zone forms at a steeper angle of about 45$^{o}$ (Polak et al. 2005). Three main conditions have to be satisfied in order for the shear reinforcement to be effective: (1) the radial spacing of the reinforcement should be limited to insure that inclined cracks do not form between two adjacent reinforcing bars, (2) effective anchorage in both tension and compression zones must be provided for the shear reinforcement especially in thin

slabs and (3) the shear reinforcement should be placed without obstructing the placement of the flexural reinforcement.

There are three main types of shear reinforcement for steel-RC slab-column connections: (1) shear reinforcement consisting of bent bars and single- or multiple-leg stirrups (Figure 2.12a), (2) shear reinforcement consisting of structural steel sections (shearheads) and (3) headed shear stud reinforcement (Figure 2.12b). Strength and ductility considerations are the main criteria in choosing the type of shear reinforcement. However, other criteria such as proper anchorage in thin slabs, the ease of placing in the slab and economy have to be considered (Polak et al. 2005).

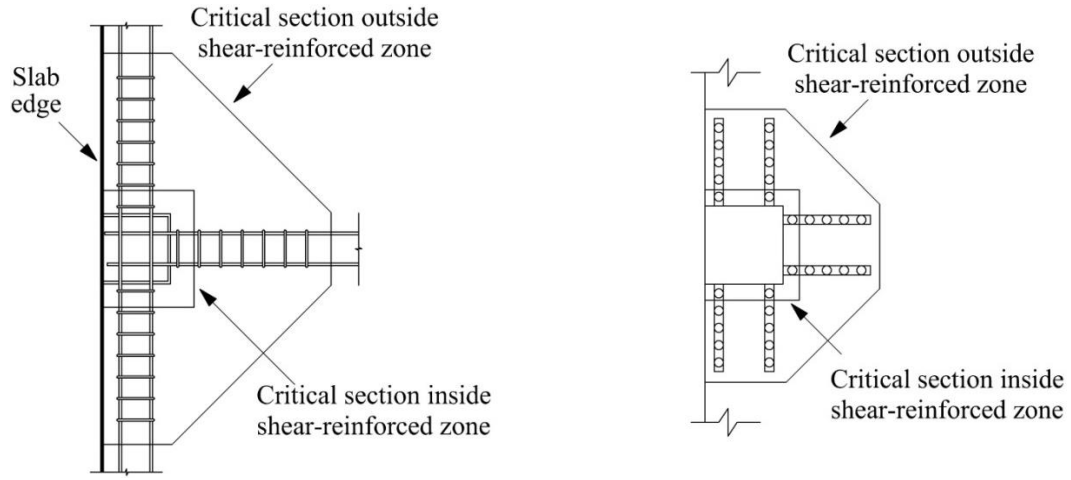


a) Stirrup shear reinforcement b) Headed shear stud reinforcement

Figure 2.12: Arrangement of shear reinforcement in edge slabs (reproduced from ACI Committee 318 2011)

## 2.6. BUILDING CODES PROVISIONS FOR PUNCHING SHEAR

This section summarizes the provisions for punching shear of both steel-RC and GFRP-RC slab-column connections in the codes and guidelines in North America and Japan. The discussion will be limited to the case of slab-column edge connections with stud shear reinforcement. Unlike

interior connections, the design of edge connections always has to consider the transfer of unbalanced moment due to the discontinuity of the slab.

### 2.6.1. Steel-RC Slab-Column Connections

While the Japanese code (Japan Society of Civil Engineering 2007) takes into account the effect of flexural reinforcement ratio on the punching shear capacity, both the North American codes (Canadian Standards Association 2004; ACI Committee 318 2011) do not include this effect in calculating the punching shear capacity.

The three codes consider the critical section for punching shear to be located at a distance *d/2* from the column face. Thus, the critical section may consist of four, three or two faces in the cases of slab-column interior, edge or corner connections, respectively. Moreover, the three codes adopt the linear variation of shear stresses theory discussed in Section 2.4.3.1 in calculating the applied shear stress.

#### 2.6.1.1. CAN/CSA A23.3-04 (Canadian Standards Association 2004)

The CAN/CSA A23.3-04 requires that the maximum factored shear stress, $v_f$, calculated from Equations 2.3 through 2.6 should not exceed the factored shear stress resistance, $v_r$.

##### *2.6.1.1.1. Shear stress resistance without shear reinforcement*

The factored shear stress resistance, $v_r$, shall be the smallest of Equations 2.7 to 2.9:

$$v_r = v_c = 0.19\left(1 + \frac{2}{\beta_c}\right)\lambda\,\varphi_c\,\sqrt{f_c'} \qquad \text{Eq. [2.7]}$$

$$v_r = v_c = \left(0.19 + \alpha_s\frac{d}{b_o}\right)\lambda\,\varphi_c\,\sqrt{f_c'} \qquad \text{Eq. [2.8]}$$

$$v_r = v_c = 0.38\,\lambda\,\varphi_c\,\sqrt{f_c'} \qquad \text{Eq. [2.9]}$$

Where $v_c$ is the factored shear resistance provided by the concrete, $\beta_c$ is the ratio of longer to shorter side of the column, $\lambda$ is a factor takes into account the concrete density (1.0 for normal density concrete), $\varphi_c$ is the resistance factor for concrete (0.65), $f_c^{'}$ is the concrete compressive strength (not to be taken greater than 64 MPa) and $\alpha_s$ is a factor takes into account the support condition (3 for edge connections).

The size factor is considered by multiplying the value obtained from the above three equations by *1300/ (1300 + d)* if the effective depth, *d*, exceeds 300 mm.

#### *2.6.1.1.2. Shear stress resistance with stud shear reinforcement*

In order to provide sufficient ductility, shear reinforcement shall be extended to a distance *2d* from the column face or to the section where the factored shear stress resistance outside the shear reinforced zone, $v_f$, is not greater than the value specified in Equation 2.10, whichever longer.

$$v_f = 0.19\,\lambda\,\varphi_c\,\sqrt{f_c'} \qquad \text{Eq. [2.10]}$$

Moreover, when properly anchored headed shear reinforcement is provided, $v_f$ shall not be greater than $0.75\,\lambda\,\varphi_c\,\sqrt{f_c'}$. The factored shear stress resistance within the shear reinforced zone, $v_r$, is the summation of the factored shear resistance provided by the concrete, $v_c$, (Equation 2.11) and the factored shear resistance provided by the stud shear reinforcement, $v_s$, (Equation 2.12).

$$v_c = 0.28\,\lambda\,\varphi_c\,\sqrt{f_c'} \qquad \text{Eq. [2.11]}$$

$$v_s = \frac{\varphi_s A_{vs} f_{yv}}{b_o s} \qquad \text{Eq. [2.12]}$$

Where $\varphi_s$ is the resistance factor for steel (0.85), $A_{vs}$ is the cross-sectional area of the headed shear reinforcement on a concentric line parallel to the perimeter of the column, $f_{yv}$ is the

specified yield strength of the headed shear reinforcement and *s* is the radial spacing between the parallel lines of studs.

The distance between the first line of studs and the column face shall be taken as *0.4d* while *s* shall be taking according to $v_f$ as follows:

When $v_f \leq 0.56\,\lambda\,\varphi_c\,\sqrt{f_c'}$ , $s \leq 0.75d$ When $v_f > 0.56\,\lambda\,\varphi_c\,\sqrt{f_c'}$ , $s \leq 0.5d$

**2.6.1.2. ACI 318-11 (ACI Committee 318 2011)**

The ACI 318-11 requires that the factored shear stress, $v_u$, resulting from the factored shear force, $V_u$, and the factored unbalanced moment, $M_u$, must not exceed the reduced nominal shear strength, $\varphi v_n$.

***2.6.1.2.1. Shear stress resistance without shear reinforcement***

The nominal shear stress resistance, $V_u$, shall be the smallest of Equations 2.13 through 2.15:

$$V_n = V_c = 0.083\left(2 + \frac{4}{\beta_c}\right)\lambda\sqrt{f_c'}\,b_o d \qquad \text{Eq. [2.13]}$$

$$V_n = V_c = 0.083\left(2 + \alpha_s\frac{d}{b_o}\right)\lambda\sqrt{f_c'}\,b_o d \qquad \text{Eq. [2.14]}$$

$$V_n = V_c = 0.33\lambda\sqrt{f_c'}\,b_o d \qquad \text{Eq. [2.15]}$$

Where $V_c$ is the nominal shear strength provided by the concrete and $\alpha_s$ is a factor takes into account the support condition (30 for edge connections).

It is to be noted that, although slightly different in format, the provisions of the ACI 318-11 yields the exact same results as those of the CAN/CSA A23.3-04. The nominal shear strength, $V_c$, calculated from Equations 2.12 to 2.14 is to be multiplied by a strength reduction factor, $\varphi$, equals 0.75.

#### *2.6.1.2.2. Shear stress resistance with stud shear reinforcement*

Shear reinforcement shall be extended to the section where $v_f$ is not greater than the value specified in Equation 2.16.

$$0.17\lambda\varphi\sqrt{f_c'} \quad \text{Eq. [2.16]}$$

Moreover, when properly anchored headed shear reinforcement is provided, $V_c$ and $V_n$ shall not be greater than the values specified in Equations 2.17 and 2.18, respectively.

$$0.25\,\lambda\sqrt{f_c'}b_o d \quad \text{Eq. [2.17]}$$

$$0.66\,\lambda\sqrt{f_c'}b_o d \quad \text{Eq. [2.18]}$$

The nominal shear stress resistance provided by the stud shear reinforcement, $v_s$, is given by Equation 2.19:

$$v_s = \frac{A_v f_{yv}}{b_o s} \geq 0.17\lambda\sqrt{f_c'} \quad \text{Eq. [2.19]}$$

Where $A_v$ is the cross-sectional area of the headed shear reinforcement on a concentric line parallel to the perimeter of the column and $f_{yv}$ is the specified yield strength of the headed shear reinforcement.

The distance between the first line of studs and the column face shall not exceed *0.5d* while *s* shall be taking according to $v_f$ as follows:

When $v_f \leq 0.50\lambda\varphi\sqrt{f_c'}$ , $s \leq 0.75d$ When $v_f > 0.5\,\lambda\,\varphi_c\sqrt{f_c'}$ , $s \leq 0.5d$

### 2.6.1.3. JSCE 2007 (Japan Society of Civil Engineering 2007)

#### *2.6.1.3.1. Shear stress resistance without shear reinforcement*

The design punching shear capacity, $V_{pcd}$, may be determined by Equations 2.20 through 2.25:

$$V_{pcd} = \beta_d \beta_p \beta_r \frac{f_{pcd} u_p d}{\gamma_b} * \frac{1}{\alpha} \quad \text{Eq. [2.20]}$$

$$\beta_d = \sqrt[4]{\frac{1000}{d}} \leq 1.5 \quad \text{Eq. [2.21]}$$

$$\beta_p = \sqrt[3]{100\rho} \leq 1.5 \quad \text{Eq. [2.22]}$$

$$\beta_r = 1 + \frac{1}{1 + 0.25\,{}^{u}/_{d}} \quad \text{Eq. [2.23]}$$

$$f_{pcd} = 0.2\sqrt{f'_{cd}} \leq 1.2 \quad \text{Eq. [2.24]}$$

$$\alpha = 1 + 1.5 * \frac{e_x + e_y}{\sqrt{b_x b_y}} \quad \text{Eq. [2.25]}$$

where, $f_{pcd}$ is the design compressive strength of concrete, $u_p$ is the peripheral length of the design cross-section at $d/2$ from the column face, $d$ is the average effective depth of both orthogonal directions, $\gamma_b$ is a partial safety factor, $\alpha$ is a factor takes into account the eccentricity of the shearing force, $\rho$ is the average flexural reinforcement ratio in both orthogonal direction, $u$ is the peripheral length of the column, $e_x$ and $e_y$ are the load eccentricity in the two orthogonal directions, and $b_x$ and $b_y$ are the dimensions of the critical section in the two orthogonal directions.

### 2.6.2. FRP-RC Slab-Column Connections

Similar to the CAN/CSA A23.3-04 and the ACI 318-11, the recently published CAN/CSA S806-12 (Canadian Standards Association 2012) and the ACI 440.1R-06 (ACI Committee 440 2006) adopt the theory of the linear variation of shear stresses discussed in Section 2.4.3.1 in calculating the applied factored shear stresses, $v_f$. They also consider the critical section for shear

to be located at a distance *d/2* from the column face. Both codes do not include any provision for designing slab-column connections with any kind of shear reinforcement.

#### 2.6.2.1. CAN/CSA S806-12 (Canadian Standards Association 2012)

Unlike the case of steel-RC slab-column connections, the shear strength of FRP-RC slab-column connections is more sensitive to the flexural reinforcement ratio/stiffness. This is attributed to the relatively low modulus of elasticity of FRP which causes the depth of the neutral axis of the cracked section to decrease significantly after cracking (El-Gamal et al. 2005). Accordingly, the recently published CAN/CSA S806-12 accounts for the flexural reinforcement stiffness in calculating the punching shear resistance of FRP-RC slab-column connections.

The factored shear stress resistance, $v_r$, shall not exceed the limits specified in CAN/CSA A23.3-04 (Section 2.6.1.1) and the smallest of the following calculated from Equations 2.26 through 2.28:

$$v_r = v_c = 0.028\left(1 + \frac{2}{\beta_c}\right)\lambda\,\varphi_c(E_F\rho_F f_c')^{\frac{1}{3}} \quad \text{Eq. [2.26]}$$

$$v_r = v_c = 0.147\left(0.19 + \alpha_s\frac{d}{b_o}\right)\lambda\,\varphi_c(E_F\rho_F f_c')^{\frac{1}{3}} \quad \text{Eq. [2.27]}$$

$$v_r = v_c = 0.056\lambda\,\varphi_c(E_F\rho_F f_c')^{\frac{1}{3}} \quad \text{Eq. [2.28]}$$

Where $E_f$ and $\rho_f$ are the elastic modulus and the flexural reinforcement ratio for the FRP flexural reinforcement, respectively, $f_c'$ is the concrete compressive strength (not to be taken greater than 60 MPa) and $\alpha_s$ is a factor takes into account the support condition (3 for edge connections).

If the effective depth of the slab exceeds 300 mm, then the size effect should be considered by multiplying the value of $v_c$ obtained from the above equations by $\left(300/d\right)^{0.25}$.

#### 2.6.2.2. ACI 440.1R-06 (ACI Committee 440 2006)

The nominal shear stress resistance, $V_n$, shall be calculated from Equation 2.29:

$$V_n = V_c = \frac{4}{5}\sqrt{f_c'}\,b_o c \qquad \text{Eq. [2.29]}$$

Where $V_c$ is the nominal shear strength provided by concrete and $c$ is the cracked transformed section neutral axis depth calculated from Equations 2.30 and 2.31:

$$c = kd \qquad \text{Eq. [2.30]}$$

$$k = \sqrt{2\rho_f n_f + \left(\rho_f n_f\right)^2} - \rho_f n_f \qquad \text{Eq. [2.31]}$$

Where $n_f$ is the modular ratio (ratio of modulus of elasticity of FRP bars to modulus of elasticity of concrete).

Equation 2.29 can be rewritten as shown in Equation 2.32 which is the equation adopted by the ACI 318-11 for steel-RC slab-column connections modified by the factor (5$k$/2) to account for the axial stiffness of the FRP reinforcement (El-Gamal et al. 2005).

$$V_n = V_c = \left(\frac{5}{2}k\right) 0.33\sqrt{f_c'}\,b_o d \qquad \text{Eq. [2.32]}$$

Equation 2.29 is a modification to the mathematical one-way shear model presented by Tureyen and Frosch (Tureyen and Frosch 2003) to account for the increased confinement provided by the two-way action at a slab-column connection (Ospina 2005). Tureyen and Forsch model (Equation 2.33) assumes that the shear stress is carried solely by the uncracked concrete, i.e., ignoring the contributions of the aggregate interlock and dowel action. Moreover, although the model was derived mathematically based on the stress state in the uncracked concrete region, they assumed a conservative value for the factor multiplied by the term $\sqrt{f_c'}\,b_o c$ to simplify the design calculations and to provide conservative estimates. Although the test results from the

literature suggested an average value of 0.54, they used a value of 0.4 in their model. All these conservative measures usually lead to very conservative estimates of Equation 2.29.

$$V_n = V_c = \frac{2}{5}\sqrt{f_c'}\, b_o c \qquad \text{Eq. [2.33]}$$

#### 2.6.2.3. JSCE 1997 (Japan Society of Civil Engineering 1997)

The design punching shear capacity $V_{pcd}$ is calculated in the same manner as in the case of steel-RC connections (Eqs. 2.20 through 2.25). The only difference is that Equation 2.22 is modified to take into account the difference in the elastic modulus between FRP and steel as shown in Equation 2.34:

$$\beta_p = \sqrt[3]{100\rho \frac{E_f}{E_s}} \leq 1.5 \qquad \text{Eq. [2.34]}$$

Where, $E_f$ and $E_s$ are the elastic modulus for the FRP and steel reinforcement, respectively.

## 2.7. RESEARCH ON STEEL-RC SLAB-COLUMN CONNECTIONS

### 2.7.1. Effect of Flexural Reinforcement Ratio

Increasing the flexural reinforcement ratio has a significant effect on increasing the punching shear capacity of slab-column connections. It also increases the post-cracking stiffness and decreases the ductility of the connections (Marzouk and Hussein 1991; Marzouk et al. 1998, 2000; Ozden et al. 2006; Widianto et al. 2009; Rizk et al. 2011). Furthermore, increasing the flexural reinforcement ratio changes the mode of failure from a ductile flexural mode to a brittle punching shear mode (Osman et al. 2000; Stein et al. 2007).

The significant increase of the punching shear capacity is attributed to the role of the increased flexural reinforcement in controlling flexural cracks. Significant yielding of the flexural reinforcement results in large (deep and wide) cracks. Wide cracks decrease the contribution of

the aggregate interlock contribution to the shear strength, while deep cracks decrease the area of the uncracked concrete. Therefore, the amount of flexural reinforcement has a significant influence on the punching capacity of slab-column connections (Richart 1948).

### 2.7.2. Effect of Shear Reinforcement (Stud Shear Reinforcement)

As mentioned in Section 2.5, there are many types of shear reinforcement for slab-column connections. This discussion, however, will be limited to the stud shear reinforcement type. The shear stud reinforcement was first introduced in the late 1970s at the University of Calgary (Dilger et al. 1978). Then, it was adopted in the Canadian Code CAN3-A23.3-M84 in 1984 (Canadian Standards Association 1984).

The main advantage of stud shear reinforcement over the traditional stirrups and bent bars is their feasibility to be installed in the congested region around columns in thin slabs while having proper anchorage at the top and bottom to develop yield in the studs before failure (Dilger et al. 1978; Seible et al. 1980; Dilger and Ghali 1981; Mokhtar et al. 1985; Elgabry and Ghali 1987).

Furthermore, implementing stud shear reinforcement in slab-column connections increases the ductility and ultimate capacity of the connections (El-Salakawy et al. 1998, 2000; Birkle and Dilger 2008; Heinzmann et al. 2012). However, the ultimate capacity of the connection will increase only if its flexural capacity is well above its punching capacity. Otherwise, the mode of failure will change from a brittle punching mode to a ductile flexural mode (Stein et al. 2007).

### 2.7.3. Effect of Moment-to-Shear Ratio

The unbalanced moments transferred to a slab-column connection can be increased significantly under the application of horizontal loads, e.g., wind or earthquake. Increasing the moment-to-shear ratio decreases the ultimate capacity of the connection (Zaghlool and Rawdon de Paiva 1973; Marzouk et al. 1996, 2000; El-Salakawy et al. 1998; Ozden et al. 2006). Furthermore, it

increases the zone of the slab affected by shear stresses (El-Salakawy et al. 1998; Marzouk et al. 2000). For slab-column edge connections, in the case of high moment-to-shear ratios, the shear stresses at the free edge reverse their direction. Consequently, the inclined cracks at the free edge propagate approximately perpendicular to the case of low moment-to-shear ratio (El-Salakawy et al. 1998).

## 2.8. YIELD LINE THEORY

The yield line theory has been initiated by Ingerslev (1923) and then extensively developed by Johansen (1943, 1946). It gives the values of the vertical shearing force, $V_{flex}$, and the unbalanced moment, $M_{flex}$, which produce flexural failure in slab-column connections in terms of the bending moment per unit width of the slab at yielding of the flexural reinforcement, $m_y$. These values represent the upper bound of the shearing force and the unbalanced moment that can be transferred between the column and the slab. The values are estimated by postulating a failure pattern compatible with the boundary conditions of the slab in the test set-up. A failure pattern consists of the lines of excessive cracking across which the tension steel has yielded, forming plastic hinges. These lines divide the slab into segments forming the failure pattern. However, the segments are not examined to ensure that their ultimate moment of resistance was not exceeded; thus, the resulting ultimate capacity may be overestimating if an incorrect pattern was used. Consequently, all the possible failure patterns should be examined (Park and Gamble 2000). The theory has been efficiently used to estimate the ultimate flexural capacities of steel-RC slab-column connections (Mortin 1989; Mortin and Ghali 1991; El-Salakawy et al. 2000; Ritchie et al. 2006; Stein et al. 2007) and different failure patterns were suggested as shown in Figure 2.13.

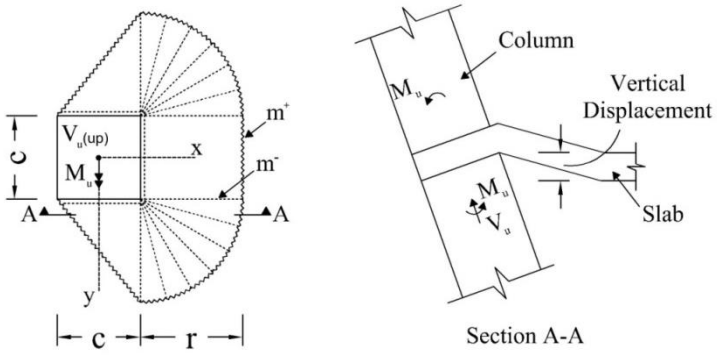


a) Pattern suggested by Park and Gamble (2000)

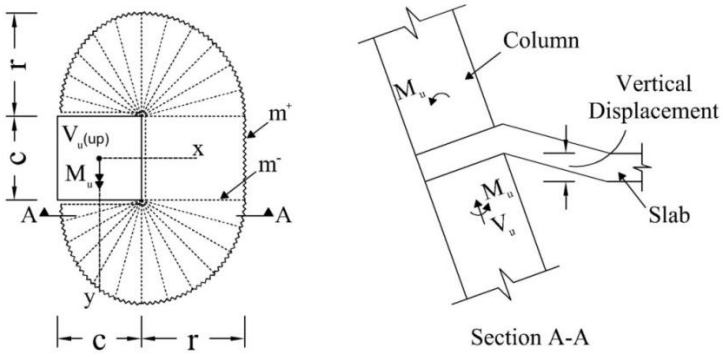


b) Pattern suggested by Ritchi et al. (2006) and Stein et al. (2007)

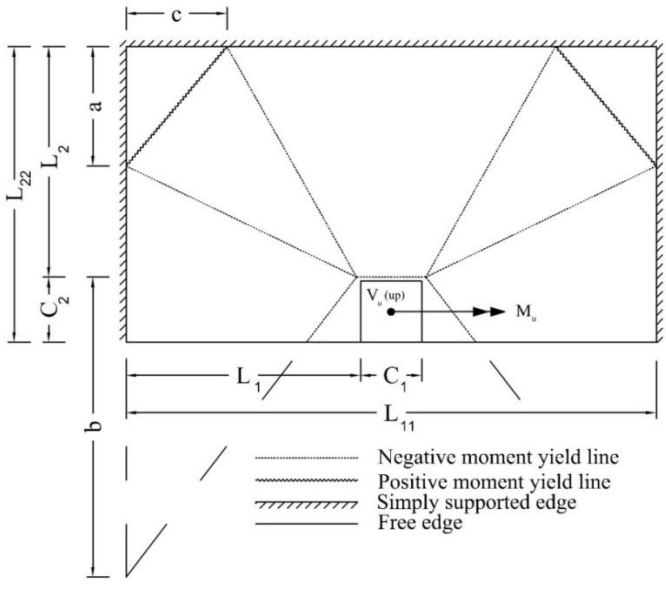


c) Pattern suggested by Mortin (1989)

Figure 2.13: Different yield line patterns for slab-column edge connections

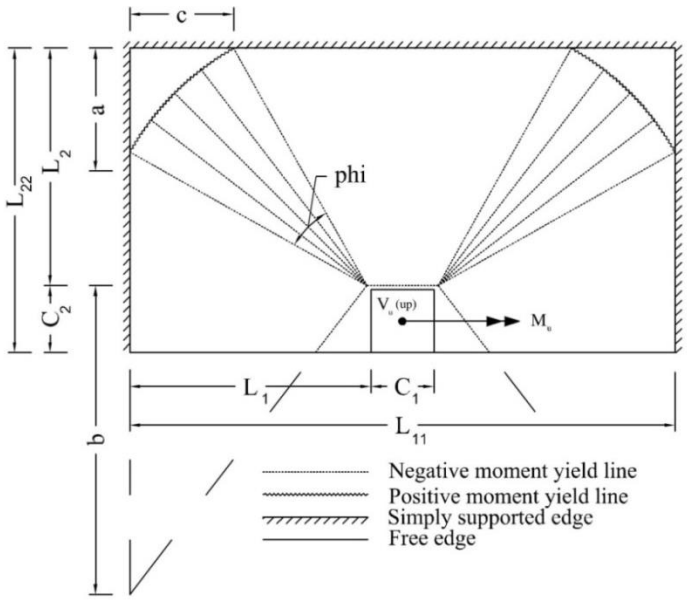


d) Pattern suggested by Mortin (1989)

Figure 2.13: Different yield line patterns for slab-column edge connections - continued

On the other hand, FRP reinforcement behaves linearly up to failure and there is no yielding point that identifies the formation of plastic hinges. However, due to the relatively low modulus of elasticity of the FRP reinforcement, FRP-RC slab-column connections experience large post-cracking deformations prior to flexural failure. Gar et al. (2014) suggested the use of an equivalent plastic moment capacity for FRP-RC slabs, $M_p$, as an analogous to the yielding moment capacity of steel-RC slabs. They theoretically idealized the flexural behaviour of FRP-RC sections into a trilinear behaviour as shown in Figure 2.14, where $EI_c$ and $EI_{cr}$ refer to the pre-cracking and post-cracking flexural stiffness of the section, respectively. The equivalent plastic moment was then obtained by simplifying the idealized tri-linear behaviour into an energy-equivalent bi-linear behaviour similar to that of the steel-RC elements where the area beneath the idealized trilinear and the simplified bi-linear responses are the same. The resulted formula for the plastic moment capacity, $M_p$, is shown in Equation 2.35:

$$M_p = 0.5M_n + 0.5\left(1 - \frac{I_{cr}}{2I_g}\right)\left(\frac{M_{cr}}{M_n}\right)M_{cr} \qquad \text{Eq. [2.35]}$$

Where $M_n$ and $M_{cr}$ are the nominal and cracking moment capacities of the section, respectively, and $I_g$ and $I_{cr}$ are the gross and cracked moment of inertia of the section, respectively.

## 2.9. RESEARCH ON FRP-RC SLAB-COLUMN CONNECTIONS

### 2.9.1. Previously Proposed Design Models

Banthia et al. (1995) tested four slabs, three reinforced with CFRP grids and one with steel grid. They came up with a conclusion that, despite the significant differences between the used CFRP and steel, no significant changes are needed to the code equations dealing with steel-RC connections when extending them to slabs reinforced with FRP reinforcement.

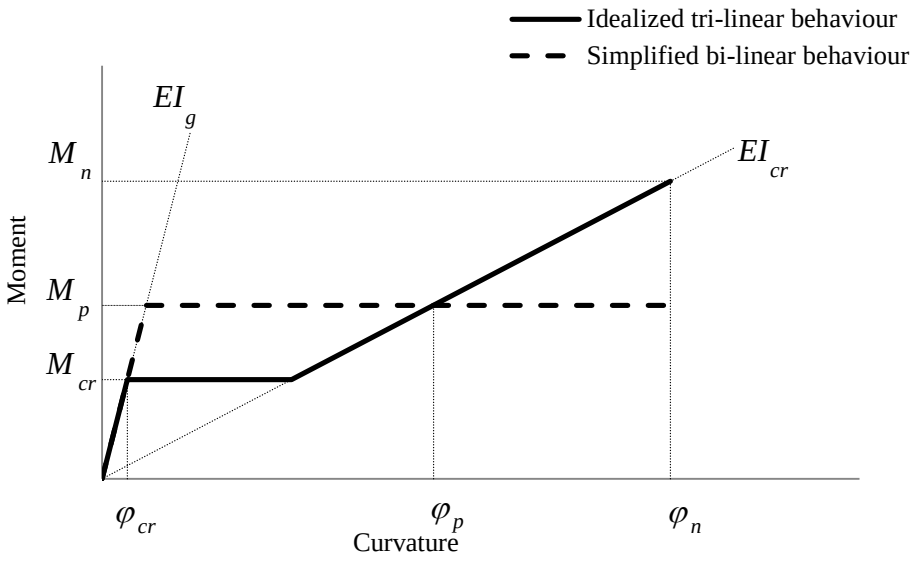


Figure 2.14: Moment-curvature response for FRP-RC sections (reproduced from Gar et al. 2014)

El-Ghandour et al. (1999) found that the ACI 318-95 code (ACI Committee 318 1995) overestimates the concrete shear resistance of FRP-RC slabs with low reinforcement ratios as it totally ignores the influence of flexural reinforcement. They proposed Equation 2.36 which is a

modification to the ACI-318-95 equation through multiplying the obtained shear strength value by the term $\left(\frac{E_f}{E_s}\right)^{1/3}$. Test results showed that this modification leads to accurate predictions of the punching capacity of tested FRP-RC slabs without shear reinforcement.

$$V_{c\,,El} = V_{c,ACI\ 318}\ x\ \left(\frac{E_f}{E_s}\right)^{1/3} = 0.33\sqrt{f_c'}\ \left(\frac{E_f}{E_s}\right)^{1/3}\ b_o d \qquad \text{Eq. [2.36]}$$

Similarly, Matthys and Taerwe (2000) suggested a modification to Equation 37 of the BS 8110-1: 1997 (British Standards Institution 1997) by introducing the equivalent reinforcement ratio $\rho\frac{E_f}{E_s}$ to account for the relatively low modulus of elasticity of FRP reinforcement as shown in Equation 2.38.

$$v_{c,BS} = 0.79\ (100\rho_s)^{1/3}\left(\frac{400}{d}\right)^{1/4}\left(\frac{f_{ck}}{25}\right)^{1/3} \qquad \text{Eq. [2.37]}$$

$$V_{c\,,MT}\ = 1.36\ \frac{\left(100\ \rho_f \frac{E_f}{E_s} f_c'\right)^{1/3}}{d^{1/4}}\ \ b_o d \qquad \text{Eq. [2.38]}$$

Where $\rho_f$ is the reinforcement ratio of the tensile FRP mat and $b_o$ is the rectangular or square control perimeter at a distance of 1.5*d* away from the loaded area.

Ospina et al. (2003) found that the modification of the ACI 318-95 equation introduced by El-Ghandour et al. (1999) gives worse agreement with their test results than what the original equation does. On the other hand, they supported the equation proposed by Matthys and Taerwe (2000); however, they added another modification to it as shown in Equation 2.39.

$$V_{c,Osp.} = 2.77\ \left(\ \rho_f\ f_c'\right)^{1/3}\ \sqrt{\frac{E_f}{E_s}}\ b_o d \qquad \text{Eq. [2.39]}$$

Zaghloul and Razaqpur (2004) proposed a new model to predict the punching shear capacity under combination of shear force and unbalanced moment. The new model is a modification to the expression for one-way shear given in the CAN/CSA S806-02 (Equation 2.40) as shown in Equation 2.41.

$$v_{c,\ CSA} = 0.035\lambda\ \varphi_c \left(f_c'\rho E_f \frac{V_f}{M_f} d\right)^{1/3} \quad \text{Eq. [2.40]}$$

$$V_{c\ ,\ zag.} = 0.07\ \varphi_c \left(f_c'\rho E_f\right)^{1/3} \quad \text{Eq. [2.41]}$$

El-Gamal et al. (2005) suggested a new model which is also a modification to the ACI 318-95 model with two new parameters: $\alpha$ to account for the flexural stiffness and $N$ to account for the continuity of the of the slab as shown in Equations 2.42 and 2.43.

$$V_c = 0.33\sqrt{f_c'} b_o d\ \ \alpha\ \ (1.2)^N \quad \text{Eq. [2.42]}$$

$$\alpha = 0.5(\rho E)^{1/3}\left(1 + {}^{8d}/_{b_o}\right) \quad \text{Eq. [2.43]}$$

Where $N$ is taken as 0, 1 and 2 for one panel slabs, slabs continuous along one axis and slabs continuous along their two axes, respectively.

### 2.9.2. Effect of Different Parameters

#### 2.9.2.1. Effect of flexural reinforcement type and ratio

Matthys and Taerwe (2000) investigated the punching shear behaviour of slab-column interior connections reinforced with CFRP grids. They tested seventeen 1000 mm square slabs with a depth of 120 mm or 150 mm. Four connections were reinforced with steel grids while the remaining thirteen were reinforced with CFRP grids. It was concluded that in order to obtain

similar punching capacity as the steel-RC slabs, FRP-RC slabs should have sufficiently high flexural stiffness by increasing the flexural reinforcement ratio and/or the slab depth.

Ospina et al. (2003) tested four full-scale slab-column interior connections; two reinforced with GFRP bars, one reinforced with GFRP grid and one reinforced with steel bars. It was found that the punching strength of a slab increases and the ultimate deflection decreases with increasing the elastic stiffness of the reinforcing mat.

Zaghloul and Razaqpur (2004) tested seven half-scale slab-column interior connections under eccentric loading. One connection was reinforced with steel bars and the other six were reinforced with CFRP grids. It was found that increasing the reinforcement axial stiffness has a more significant effect on increasing the capacity than increasing the reinforcement ratio; the capacity decreased by 22% when a 1.33% CFRP grid was used instead of 1.4% steel grid. The authors suggested that the punching shear capacity varies linearly with the cubic root of the axial stiffness of the reinforcement.

Zaghloul (2007) tested ten half-scale slab-column edge connections. Three connections were reinforced with steel bars and seven were reinforced with CFRP grids. Furthermore, two steel-RC connections and two CFRP-RC connections were reinforced with different types of shear reinforcement. The unbalanced moment was applied via changing the eccentricity of the vertical load applied on the upper column stub while no loads were applied at the lower column stub. The test variables were the flexural reinforcement ratio and type, moment-to-shear ratio, column width-to-slab depth ratio, column aspect ratio and the presence of shear reinforcement. Two connections were assigned to investigate the effect of the flexural reinforcement ratio. Increasing the reinforcement ratio by 46% increased the ultimate capacity by 21%; however, it had no effect

on the post-cracking stiffness. Another two connections were assigned to investigate the effect of flexural reinforcement type (steel bars and CFRP grids). The post cracking stiffness of the connection reinforced with steel bars was higher than that of the connections reinforced with CFRP grid; however, both connections had the same failure load.

Lee et al. (2009) tested six full scale slab-column interior connections under concentric loading. Two connections were reinforced with uniform and banded distributions of steel bars while the other four were reinforced with GFRP bars (one with uniform distribution and three with different ratios of banded distribution). The capacities of the connections reinforced with uniform and banded GFRP bars were 26% and 22% lower than their counterparts with steel bars, respectively. Moreover, it was found that banding the reinforcement in the column vicinity resulted in slightly higher punching shear strength, greater post-cracking stiffness and more uniform distribution of strains in the bars. In addition, it was observed that the failure plane for the slabs with banded reinforcement extended to a greater distance from the column faces. Increasing the GFRP reinforcement ratio from 1.18% to 2.15% increased the punching capacity by 10.8%. However, a further increase of the reinforcement ratio to 3% resulted in an increase in the capacity of 11.7% only which indicates that excessive concentrations of the slab reinforcement is ineffective in increasing the punching capacity.

Hassan et al. (2013) tested ten full-scale interior slab column connections under concentric loading to investigate the effects of the reinforcement type (steel and different grade of GFRP) and ratio (0.34% to 1.66%), slab thickness (200 mm and 350 mm) and concrete compressive strength (NSC and HSC) on the punching shear behaviour. The authors found that for the same slab and column dimensions, increasing the reinforcement ratio increases the punching capacity. For the 200 mm slabs with 300×300 mm columns, increasing the reinforcement ratio from

0.71% to 1.56% increased the ultimate capacity by 31%. Also, increasing the flexural reinforcement ratio decreased the deflections at the same load level, i.e., increased the post-cracking stiffness, due to the increased effective moment of inertia of the concrete section. On the other hand, changing the reinforcement type from steel bars to GFRP bars with maintaining the same flexural reinforcement ratio decreased the ultimate capacity by 32% and 37% and decreased the post-cracking stiffness by 60% and 57% for the 200 mm and 350 mm slabs, respectively.

Nguyen-Minh and Rovňák (2013) tested six full-scale slab-column interior connections under concentric loading. Three connections were reinforced with GFRP bars and three with steel bars. The only parameter was the flexural reinforcement ratio being 0.2%, 0.4% and 0.6% for both GFRP-RC and steel-RC connections. Again, increasing the GFRP flexural reinforcement ratio increased the ultimate capacity and the post-cracking stiffness. On the other hand, the GFRP-RC connections had lower capacity and post-cracking stiffness and wider cracks compared to their steel-RC counterparts.

#### 2.9.2.2. Effect of moment-to-shear ratio

Zaghloul and Razaqpur (2004) tested seven half-scale interior connections under eccentric loading. Three connections had different moment-to-shear ratios as the only parameter (0.0 m, 0.22 m and 0.3 m). The results showed that increasing the moment-to-shear ratio decreases the punching capacity. Increasing the moment-to-shear ratio from 0.0 m to 0.22 m and 0.3 m decreased the ultimate capacity by 27% and 43%, respectively.

Zaghloul (2007) investigated the influence of moment-to-shear ratio on the punching shear behaviour of half-scale CFRP-RC slab-column edge connections. The post cracking stiffness and the capacity of the connection subjected to the higher moment-to-shear ratio were higher than

those of the connection subjected to the lower moment-to-shear ratio. Increasing the moment-to-shear ratio from 0.265 m to 0.415 m increased the ultimate capacity by 12%. This unusual behaviour was attributed to the very huge difference in the concrete strength between both connections. The connection subjected to high ratio had a concrete strength of 56.8 MPa while the connection subjected to low ratio had a concrete strength of 26.7 MPa. Despite this huge difference in the concrete strength, the results were normalized regarding the concrete strength. The normalized results seem reasonable where the post-cracking stiffnesses for both connections are similar and the capacity of the connection subjected to high ratio is 15% less than that of the connection subjected to low ratio.

#### 2.9.2.3. Effect of shear reinforcement

El-Ghandour et al. (2003) investigated the effect of CFRP shear-bands on the punching shear behaviour of circular slab-column interior connections subjected to concentric loading. The shear-reinforced slabs showed larger deformability compared to those without shear reinforcement. Furthermore, implementing the shear-bands in a slab with a GFRP flexural reinforcement of 0.38% increased the ultimate capacity by 13.9% due to the role of the shear reinforcement in preventing the punching shear failure at lower load levels. The authors concluded that the concrete contribution to the punching shear resistance is substantially reduced after the initiation of the major shear crack; accordingly, they proposed that only 50% of the concrete shear resistance can be relied upon similar to the ACI 318-95 approach (ACI Committee 318 1995). They also recommended a strain limit of 0.0045 μs for designing shear reinforcement with a maximum spacing of 0.5*d* based on the results.

Zaghloul (2007) tested half-scale GFRP-RC edge and interior slab column connections to study the effect of a type of CFRP shear reinforcement on the punching shear behaviour of such

connections. Shear rails were cut from CFRP grids. A typical CFRP shear rail consisted of four legs 90 mm apart. The rails were placed orthogonally parallel to the column faces. The proposed shear reinforcement increased the ultimate capacity of the interior connections by 24.6% and 30.4% when the first leg of the rail was located 0.5*d* and 0.85*d* from the column face, respectively. However, the increase was only 9% for the edge connections with the first leg of the rail located 0.5*d* from the column face. In addition, the shear reinforcement increased the deformability of the connections. The authors recommended a relatively conservative value for the design limit strain and stress in the shear reinforcement for this specific type of reinforcement of 3000 με and 0.25$f_u$, respectively.

Hassan et al. (2014) tested ten full-scale slab-column interior connections under concentric loading. All the slabs had GFRP flexural reinforcement but only seven slabs had GFRP or CFRP closed, spiral or bundled spiral stirrups as shear reinforcement. The presence of the stirrups enhanced the performance of the connections in terms of reducing the brittleness of the failure and increasing the deformation capacity. The maximum strains in the stirrups were recorded at a distance of 0.5*d*–1.0*d* from the column faces and completely diminished at 2.5*d* from the column face for connections with 350-mm thick slabs. For the 200-mm thick slabs, the stirrups developed strains as high as 1500 microstrains at 2.5*d* from the column face. The authors concluded that the punching capacity was governed by the flexural reinforcement ratio rather than the strength of the FRP stirrups. Accordingly, specimens with very low flexural reinforcement ratios may not exhibit significant increases in punching shear capacity when FRP stirrups are used. They also recommended that the strain limits of 0.004 and 0.005 recommended by the ACI 440.1R-06 (ACI Committee 440 2006) and the CSA S806-12 (Canadian Standards Association 2012), respectively, can be used in the design.

# CHAPTER 3: EXPERIMENTAL PROGRAM

## 3.1. GENERAL

Based on the literature review, it is well demonstrated that several parameters have significant effects on the punching shear behaviour of slab-column connections. Some of the main parameters are the flexural reinforcement type and ratio, the moment-to-shear ratio and the shear reinforcement ratio. This chapter presents the details of the experimental study conducted in the W. R. McQuade Structures Laboratory at the University of Manitoba to study the effects of these parameters on the punching shear behaviour of slab-column edge connections.

## 3.2. MATERIALS

### 3.2.1. Concrete

All test connections were constructed using normal-weight, ready-mix concrete with a target compressive strength of 35 MPa at 28 days using a maximum aggregate size of 19 mm (except for the shear-reinforced connections where a maximum aggregate size of 13 mm was selected). All test prototypes were cast and wet-cured in the laboratory for 7 days. Standard 100×200 mm and 150×300 mm cylinders were cast from each batch and tested after 3, 7, 14 and 28 days and at the day of testing to determine the actual concrete compressive and tensile strengths, respectively.

### 3.2.2. Flexural Reinforcement

Three types of reinforcing bars were used as longitudinal reinforcement for the slabs: (1) No. 15M conventional deformed steel bars, (2) No. 19 sand-coated (SC) GFRP V-ROD$^{TM}$ bars (Pultrall Inc. 2013) and (3) No. 19 ribbed-deformed (RD) GFRP ComBAR$^{®}$ bars (Schoeck Canada Inc. 2013). On the other hand, No. 20M and No. 10M deformed steel bars and stirrups

were used to reinforce the columns in all connections, respectively. The mechanical properties of the deformed steel bars and the GFRP bars were obtained from standard tests carried out according to the ASTM A370-11 (ASTM A370 - 14 2014) and the ASTM D7205/D7205M-06 (ASTM D7205 / D7205M - 06 2011), respectively. Table 3.1 shows the mechanical properties of the used steel and GFRP bars.

Table 3.1: Mechanical properties of the used reinforcing bars

| Bar Material | Bar Size | Effective Diameter (mm) | Effective Area ($mm^2$) | Tensile Strength (MPa) | Elasticity Modulus (GPa) | Ultimate Strain (%) |
|---|---|---|---|---|---|---|
| Steel (Straight and Bent) | No.20M | 15.9 | 200 | 419* | 182 | 0.23* |
| SC-GFRP (Straight) | No.19 | 19.1 | 285 | 1484 | 65 | 2.3 |
| SC-GFRP (Bent - Straight Portion) | | | | 1232 | 52 | |
| RD-GFRP (Straight) | No. 19 | 20 | 314 | 1060 | 64 | 1.67 |
| RD-GFRP (Bent - Straight Portion) | | 19.1 | 287 | 900 | 54 | |
| RD-GFRP Studs | No. 13 | 12.0 | 113 | 1060 | 64 | |

*yield stress and strain for steel

### 3.2.3. Shear Reinforcement

Size No. 4 RD-GFRP bars with headed-ends were used as shear studs. The end head is made of a thermo-setting polymeric concrete with a compressive strength ranging between 100 and 120 MPa. The heads were cast on the end of the straight bar and hardened at higher temperatures. As shown in Figure 3.1, each head begins with a wide disk and then tapers in multiple steps towards the outer bar diameter. The outer diameter of wide disk is 30 mm, i.e., 2.5 times the bar diameter.

The length of the end head is 60 mm while the length of the stem of the stud is 50 mm. The mechanical properties of the RD-GFRP studs are listed in Table 3.1.

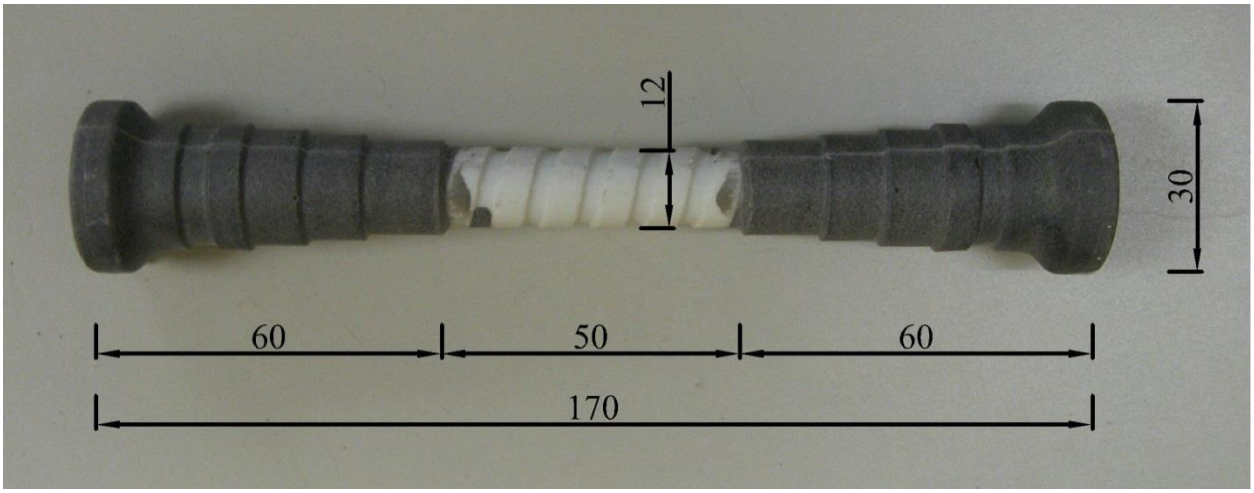


Figure 3.1: Ribbed-deformed GFRP stud with headed-ends (dimensions in mm)

### 3.3. TEST CONNECTIONS

Nine full-scale slab-column edge connections were constructed and tested to failure. The slabs were reinforced with deformed steel bars in one connection, SC-GFRP bars in five connections and RD-GFRP bars in three connections. Two connections of the three reinforced with RD-GFRP bars were reinforced with stud shear reinforcement at different spacing. The designation of the connections consists of four characters separated by dashes as follows: the first character indicates the reinforcement type (S for steel, GSC for SC-GFRP and GRD for RD-GFRP), the second character indicates the flexural reinforcement ratio in the direction perpendicular to the free edge (0.9 for $\rho$ = 0.9%, 1.35 for $\rho$ = 1.35% and 1.8 for $\rho$ = 1.8%), the third character indicates the spacing of the stud shear reinforcement (XX for no shear reinforcement, 50 for $S$ = 50 mm and 75 for S = 75 mm) and the fourth character indicates the moment-to-shear ratio applied to the connection (0.2 for moment-to-shear ratio = 0.2 m, 0.4 for moment-to-shear ratio = 0.4 m and 0.6 for moment-to-shear ratio = 0.6 m). For example, GRD-0.9-50-0.4 denotes a

connection reinforced with RD-GFRP bars in flexure with a reinforcement ratio of 0.9% in the direction perpendicular to the column, reinforced with shear studs spaced 50 mm centre-to-centre and subjected to a moment-to-shear ratio of 0.4 m.

The dimensions and reinforcement ratios of the connections were defined by performing two elastic analyses of a typical parking garage system consisting of three 6.5 m-long square bays in both directions (Appendix A). The slab of the system was reinforced with steel reinforcing bar in one analysis and with SC-GFRP bars in the other. Each slab-column connection simulates an isolated portion of a 6500×6500 mm slab bounded by the slab free edge and the lines of contra-flexure around the column which are assumed to be 0.2$L$ away from the centerlines of the column stub, where $L$ is the span between the centerlines of the columns as shown in Figure 3.2. The analyses were carried out according to the CAN/CSA A23.3-04 and the CAN/CSA S806-12 standards, when applicable (Appendix A). The system was designed to carry a specified gravity load $w_f$ = 8.2 kN/m$^2$, i.e., a specified dead load $D.L.$ = 5.8 kN/m$^2$ and a factored live load $L.L.$ = 2.4 kN/m$^2$ (NBCC 2010), resulting in a moment-to-shear ratio of 0.4 m. The details of test connections are listed in Table 3.2.

The resulting connections had dimensions of 2600×1450×200 mm; however, 2800×1550×200 mm slabs were cast to allow for a supporting clearance. The column stub extended 1000 mm above and below the slab with cross sectional area of 300×300 mm. On the other hand, although subjected to the same loads, the SC-GFRP flexural reinforcement ratio resulting from the analysis (1.8%) was twice the steel flexural reinforcement ratio (0.9%). The higher reinforcement ratio for the slabs reinforced with SC-GFRP is necessary to satisfy the serviceability requirements. The flexural reinforcement ratios resulting from the analyses of the steel and SC-GFRP reinforced systems have been employed in connections S-0.9-XX-0.4 and

GSC-1.8-XX-0.4, respectively. Also, the latter reinforcement ratio has been multiplied by 0.5 and 0.75 and used for connections GSC-0.9-XX-0.4 and GSC-1.35-XX-0.4, respectively, to study the effect of the flexural reinforcement ratio. Furthermore, the resulting moment-to-shear ratio (0.4 m) was applied to all test connections except connections GSC-0.9-XX-0.2 and GSC-0.9-XX-0.6 where it was multiplied by 0.5 (0.2 m) and 1.5 (0.6 m), respectively, to study the effect of moment-to-shear ratio. All connections were reinforced in tension side only with one orthogonal mesh. Straight bars were used in the direction parallel to the free edge while bent bars were used in the direction perpendicular to the free edge to provide the required anchorage. The columns for all the connections were heavily reinforced with 4-20M bars and No.10M stirrups to prevent premature failure. The dimensions and details of the reinforcement for the tested connections are shown in Figures 3.4 to 3.6.

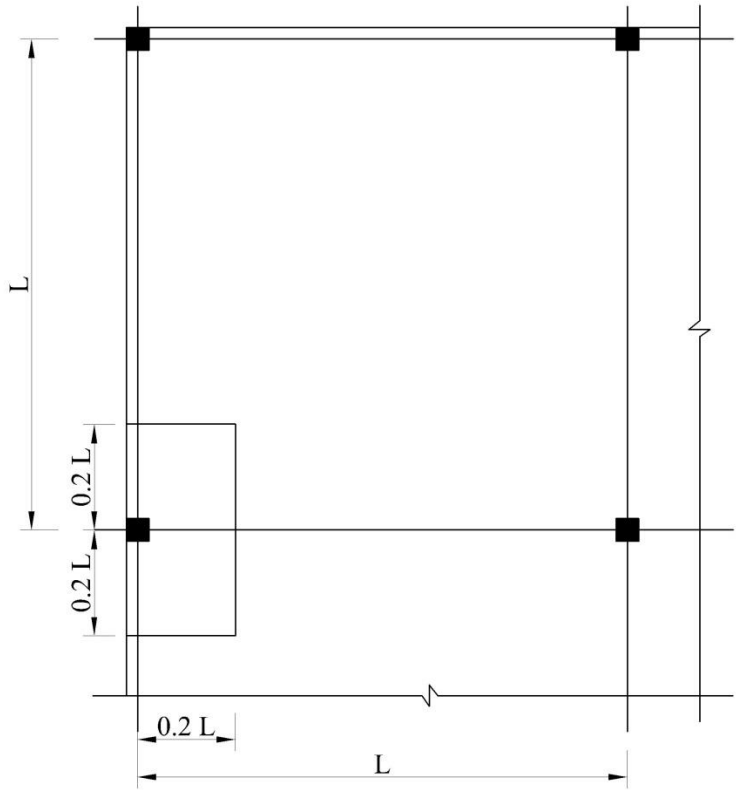


Figure 3.2: The portion of slab under consideration

Table 3.2: Details of test connections

| Connection | Reinf. type | Reinforcement ratio, $\rho$ (%) and spacing, $S$ (mm) | | | | Stud spacing (mm) | Moment-to-shear ratio (m) |
|---|---|---|---|---|---|---|---|
| | | Perpendicular to edge | | Parallel to edge | | | |
| | | $\rho$ | $s$ | $\rho$ | $s$ | | |
| S-0.9-XX-0.4 | Steel | 0.93 | 128 | 0.79 | 166 | NA | 0.4 |
| GSC-0.9-XX-0.4 | SC-GFRP | 0.9 | 186 | 0.82 | 232 | | |
| GSC-1.35-XX-0.4 | | 1.35 | 124 | 1.23 | 155 | | |
| GSC-1.8-XX-0.4 | | 1.8 | 93 | 1.64 | 116 | | |
| GSC-0.9-XX-0.2 | | 0.9 | 128 | 0.79 | 166 | | 0.2 |
| GSC-0.9-XX-0.6 | | | | | | | 0.6 |
| GRD-0.9-XX-0.4 | RD-GFRP | 0.87 | 193 | 0.84 | 249 | | 0.4 |
| GRD-0.9-75-0.4 | | | | | | 120 | |
| GRD-0.9-50-0.4 | | | | | | 80 | |

For the two shear-reinforced connections, the shear studs were arranged in parallel peripheral rows around the column; each row contains six studs. The spacing between the first row and the column face was 0.4*d* while the spacing between the stud rows was 0.75*d* and 0.5*d* for connections GRD-0.9-75-0.4 and GRD-0.9-50-0.4, respectively. The studs extended to a distance of 3.4*d* from the column face, i.e., the critical section outside the shear-reinforced zone is located at 3.9*d* from the column face as shown in Figure 3.5.

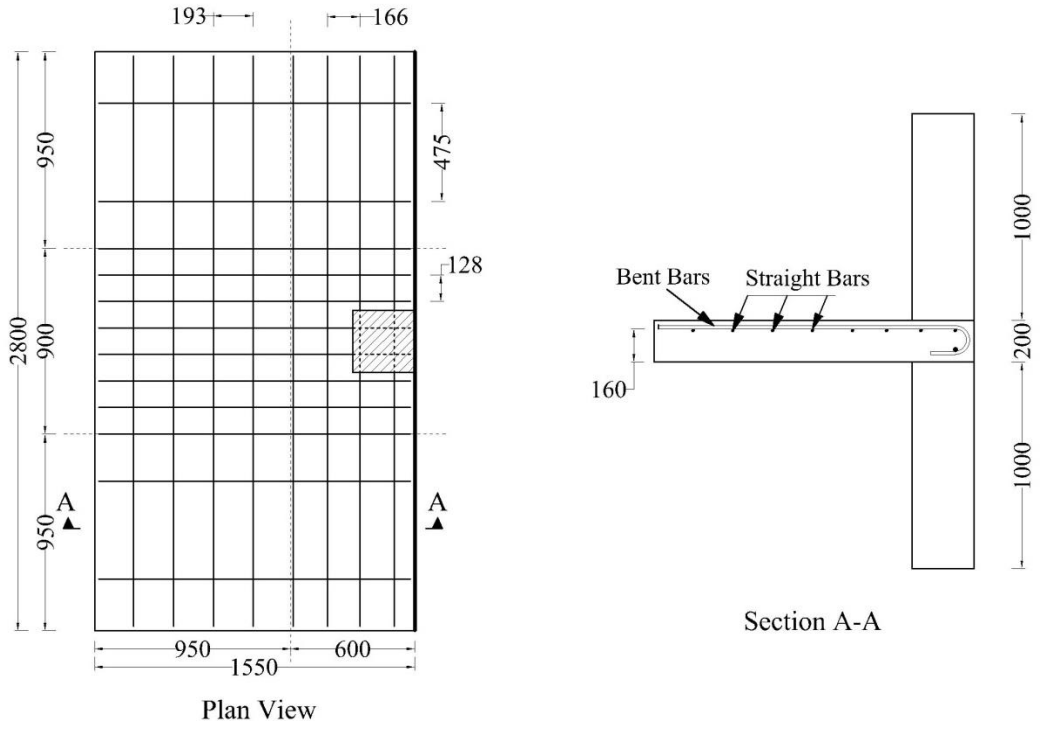


a) Connection S-0.9-XX-0.4

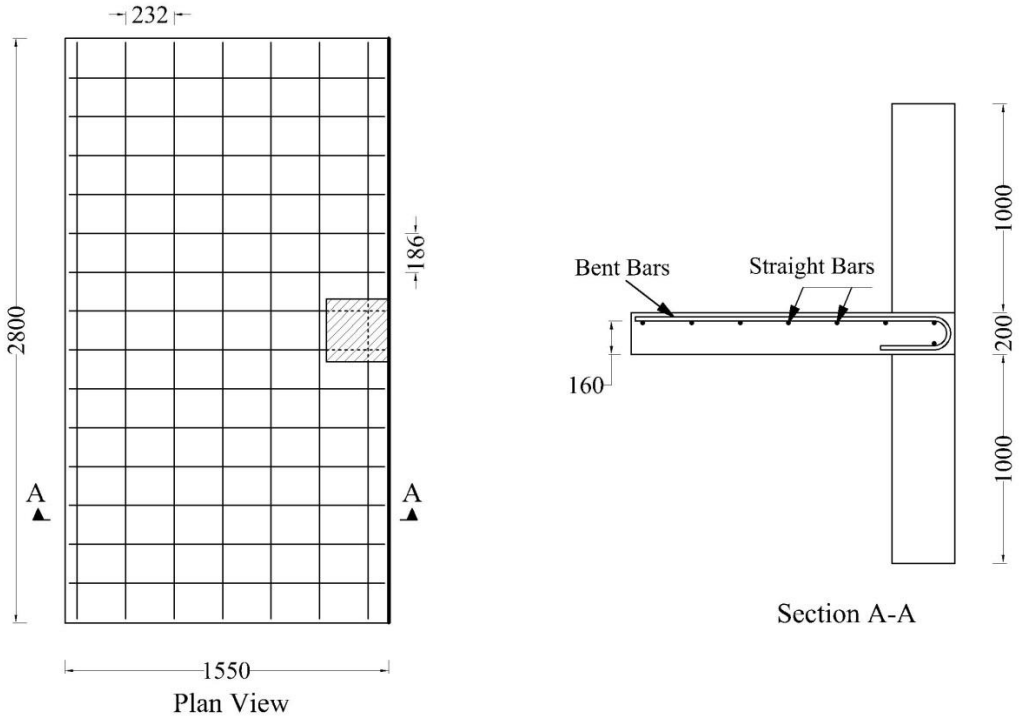


b) Connections GSC-0.9-XX-0.2, GSC-0.9-XX-0.4 and GSC-0.9-XX-0.6

Figure 3.3: Dimensions and flexural reinforcement layout (Dimensions in mm)

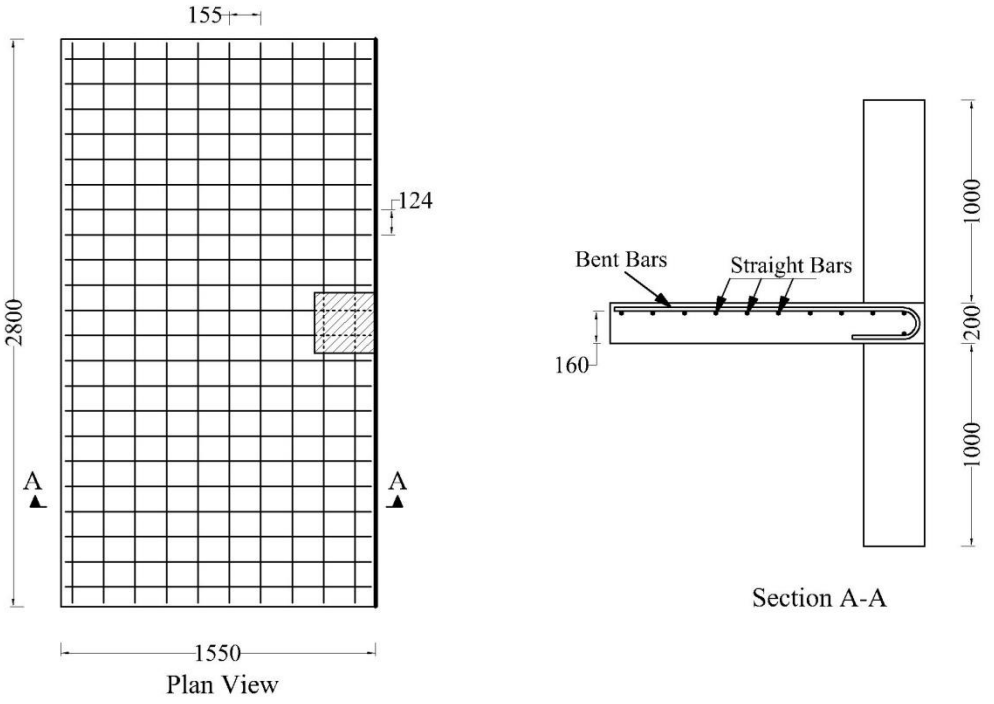


c) Connection GSC-1.35-XX-0.4

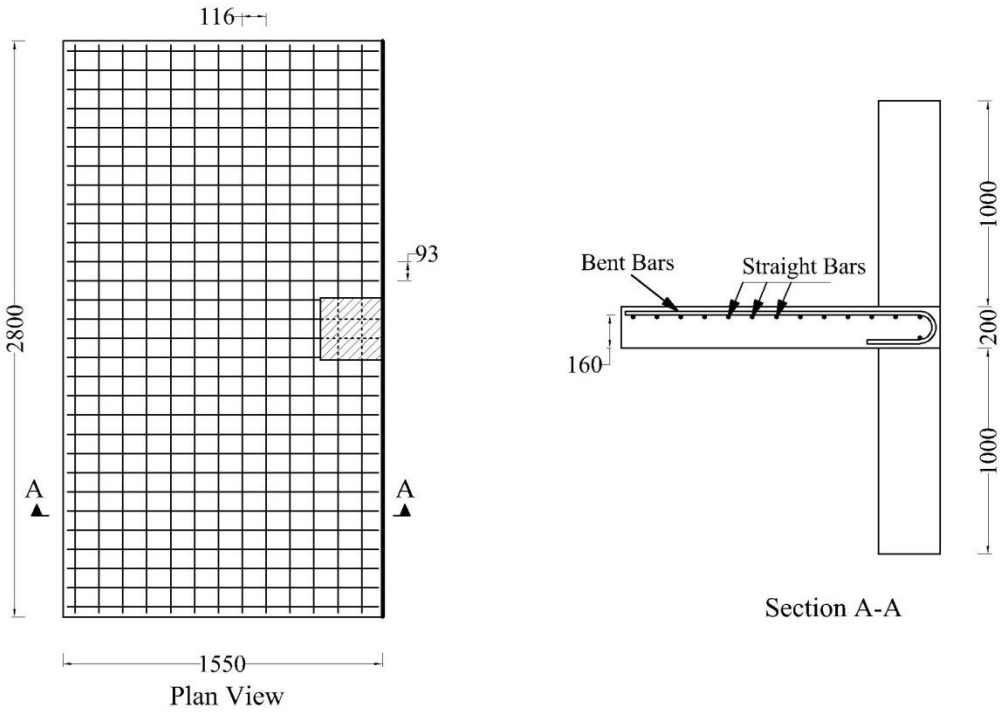


d) Connection GSC-1.8-XX-0.4

Figure 3.3: Dimensions and flexural reinforcement layout – continued (Dimensions in mm)

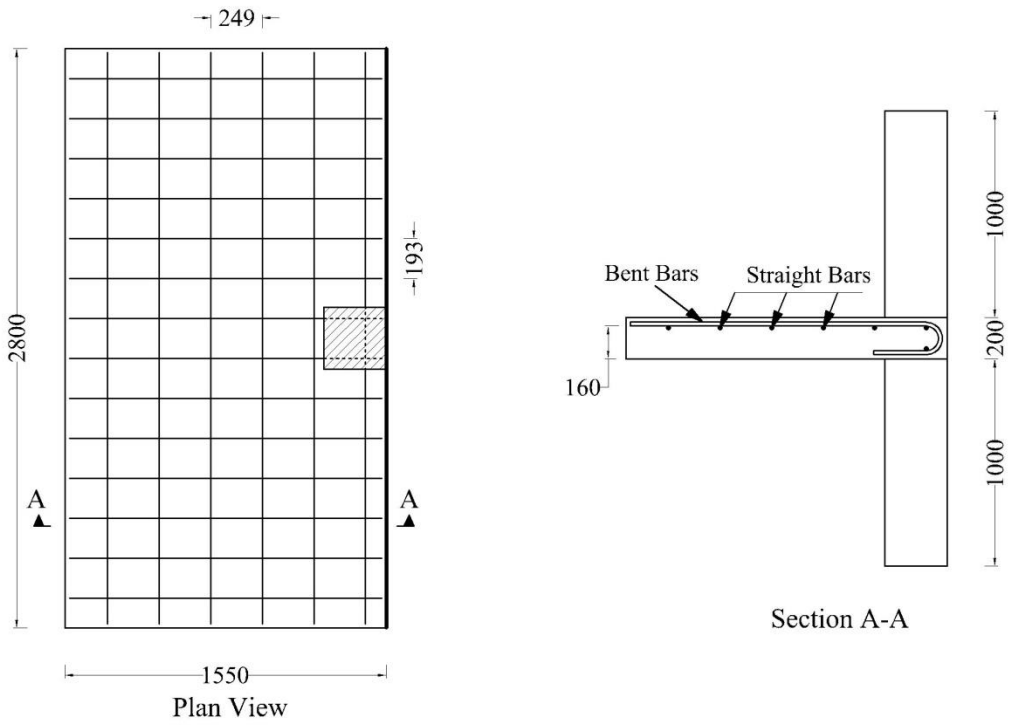


e) Connections GRD-0.9-XX-0.4, GRD-0.9-75-0.4 and GRD-0.9-50-0.4

Figure 3.3: Dimensions and flexural reinforcement layout – continued (Dimensions in mm)

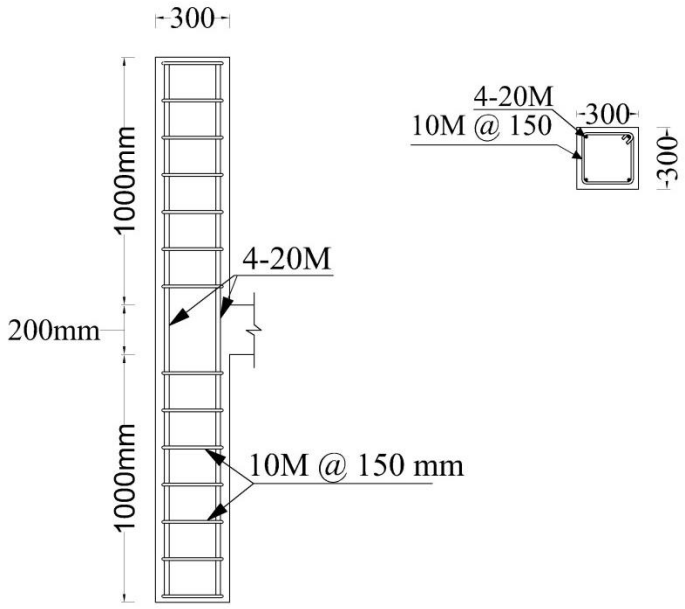


Figure 3.4: Column details (Dimensions in mm)

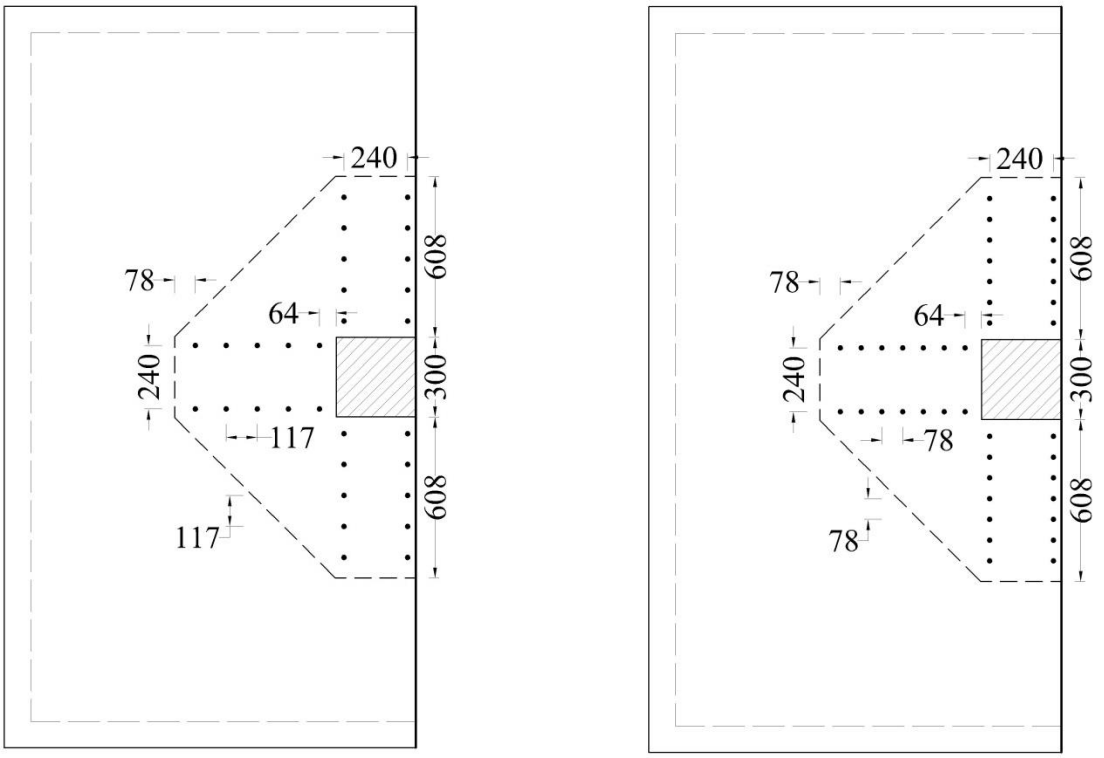


a) GRD-0.9-75-0.4 b) GRD-0.9-50-0.4

Figure 3.5: Stud shear reinforcement layout (Dimensions in mm)

a) Connection GSC-0.9-XX-0.4

Figure 3.6: Reinforcement configuration

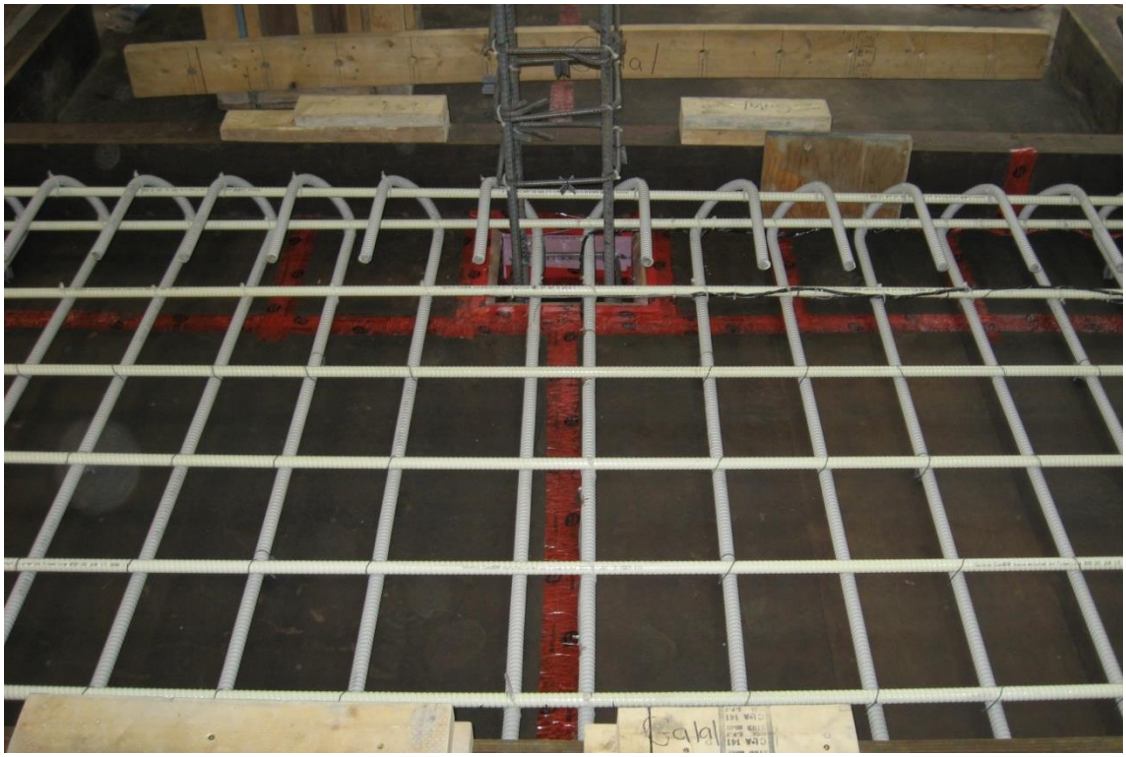

b) Connection GRD-0.9-XX-0.4

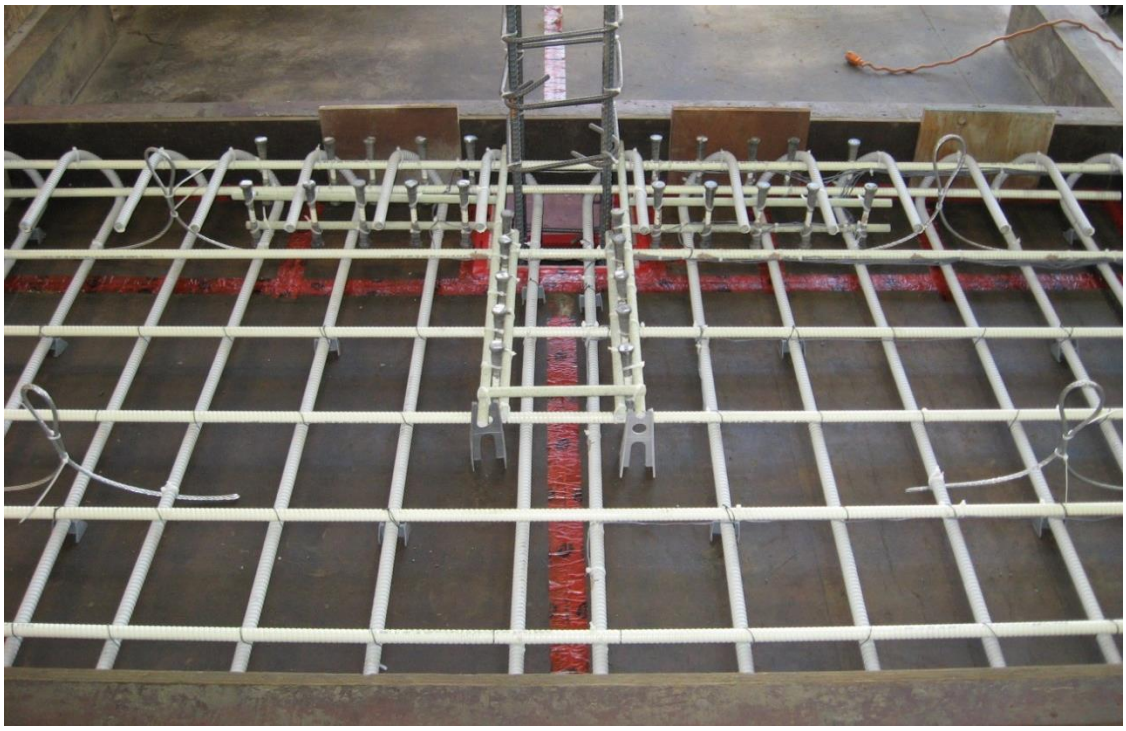

c) Connection GRD-0.9-75-0.4

Figure 3.6: Reinforcement configuration - continued

## 3.4. TEST INSTRUMENTATION

Both internal (reinforcement strain gauges) and external (load cells, PI-gauges, concrete strain gauges and LVDTs) instrumentation were used to provide a real-time monitoring of the behaviour of the connections during the test. All instrumentation was connected to a computerized data acquisition system (DAQ) to record the readings during the test. The propagation of cracks was carefully marked during the test.

### 3.4.1. Reinforcement Strain Gauges

For the flexural reinforcement, twelve electrical resistance strain gauges were attached to three reinforcing bars passing through the column as shown in Figure 3.7. For the shear studs, electrical resistance strain gauges were attached to the mid height of the stems at different locations as shown in Figure 3.8.

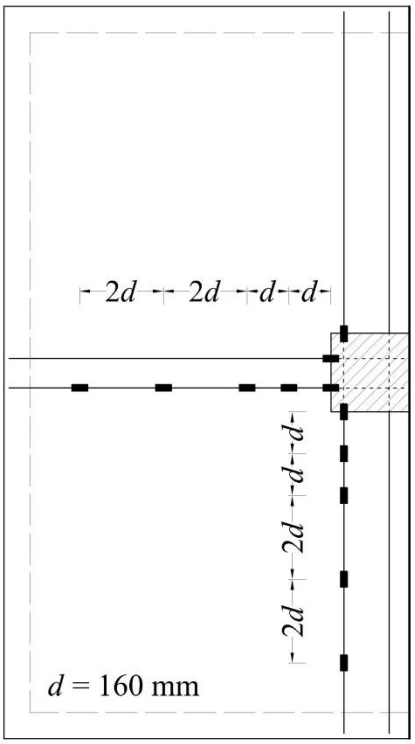


Figure 3.7: Strain gauges layout on the flexural reinforcement

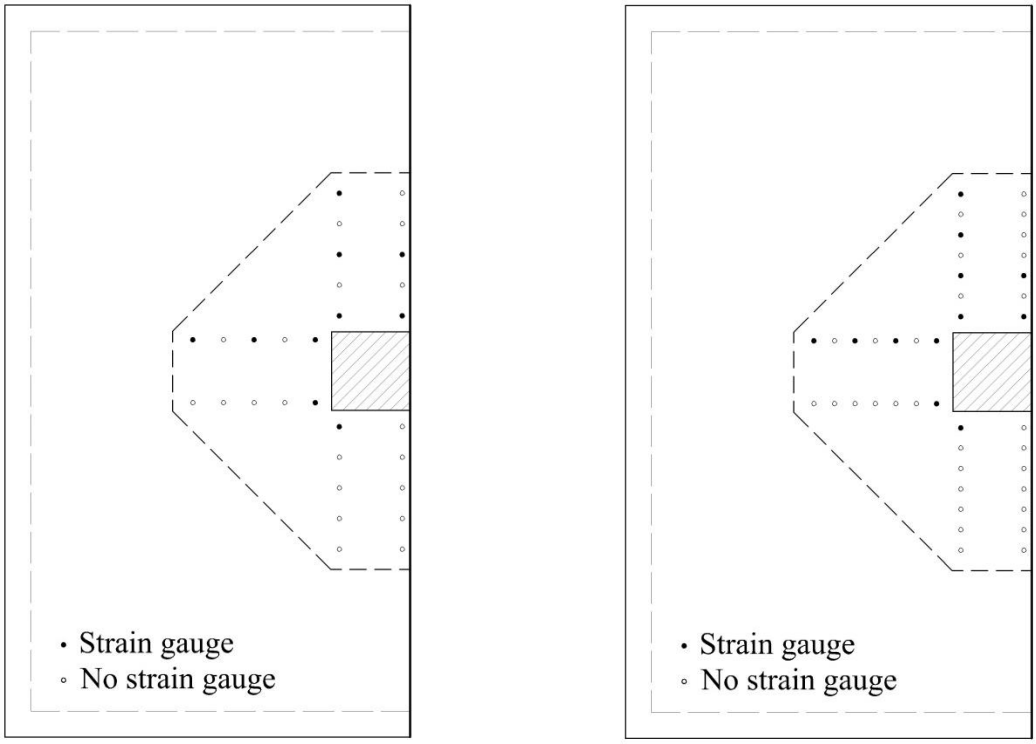


a) GRD-0.9-75-0.4 b) GRD-0.9-50-0.4

Figure 3.8: Strain gauges layout on the shear reinforcement

### 3.4.2. PI-Gauges and Concrete Strain Gauges

For all slabs, two PI-gauges were attached to the compression side of the slab near the column face in order to capture the maximum concrete strains in both orthogonal directions as shown in Figure 3.9. For connections GSC-0.9-XX-0.2, GSC-0.9-XX-0.6, GRD-0.9-75-0.4 and GRD-0.9-50-0.4, concrete strain gauges were glued to the concrete surface at the same location to verify the readings of the PI-gauges.

### 3.4.3. Load Cells

One load cell was attached to each of the hydraulic machines (two jacks and one actuator) (Section 3.5) to measure the applied loads.

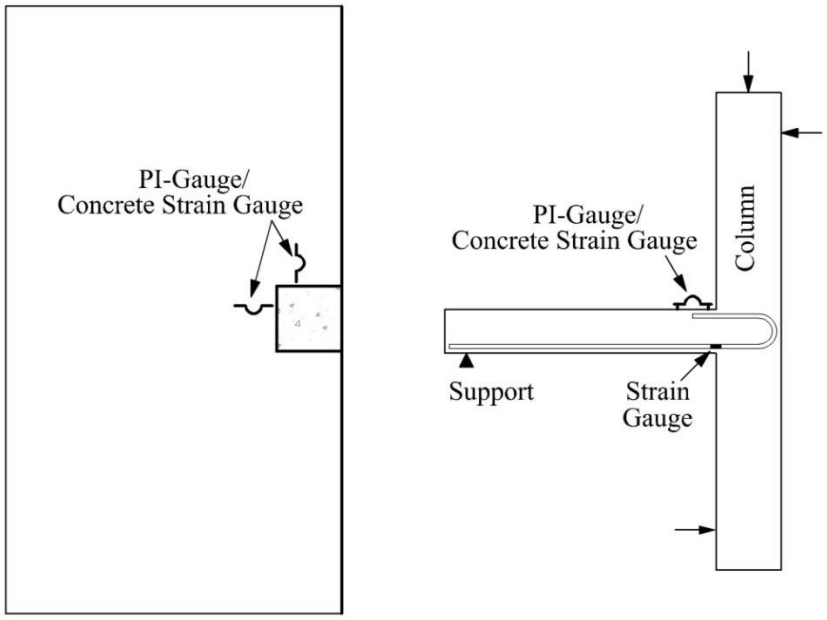


Figure 3.9: PI-gauges/concrete strain gauges locations

### 3.4.4. Linear Variable Differential Transducers (LVDTs)

The deflection profiles of the slabs were obtained by measuring the deflections at several locations on the slab using twelve LVDTs as shown in Figure 3.10.

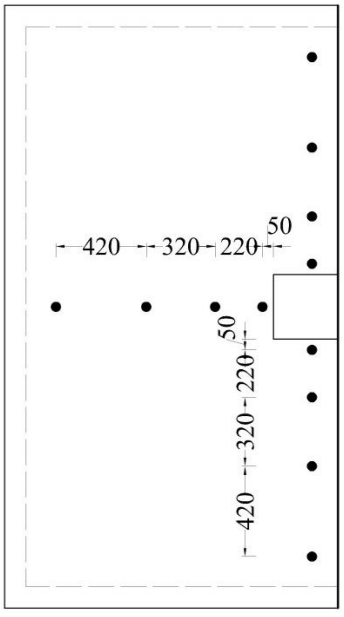


Figure 3.10: Typical arrangement of LVDTs (Dimensions in mm)

## 3.5. TEST SET-UP AND PROCEDURE

The connections were tested in an upside-down position with respect to the position of a real structure. This was done due to the test setup available in the laboratory which allows the vertical shearing force to be applied from top to bottom. Therefore, tension cracks appeared at the bottom side of the slabs.

The slabs were simply supported on heavy steel I-beam arrangement along three of the four edges while the fourth edge was left free. Thin 20-mm wide steel plates were used as bearing plates between the slabs and the steel supports. In addition, neoprene strips were inserted on top of the bearing plates to ensure a uniform distribution of the loads along the edges.

A 1000-kN hydraulic actuator was used to apply the vertical shearing force on the top of the upper column stub. While, two hydraulic jacks were used to apply the lateral forces causing the unbalanced moment at the tips of the upper and lower column stubs. The three hydraulic machines were fixed to a rigid steel frame that was fixed to the laboratory strong ground. Figure 3.11 shows the details of the test setup.

Vertical and horizontal loads were applied simultaneously. Loads were monotonically applied until failure. The hydraulic actuator applied the vertical shearing force under a displacement control rate of 0.75 mm/min until the first crack is detected and then the rate was increased to 1.5 mm/min. On the other hand, the horizontal loads were applied under load control mode with a rate of 4 kN/min to maintain a constant moment-to-shear ratio during the whole test.

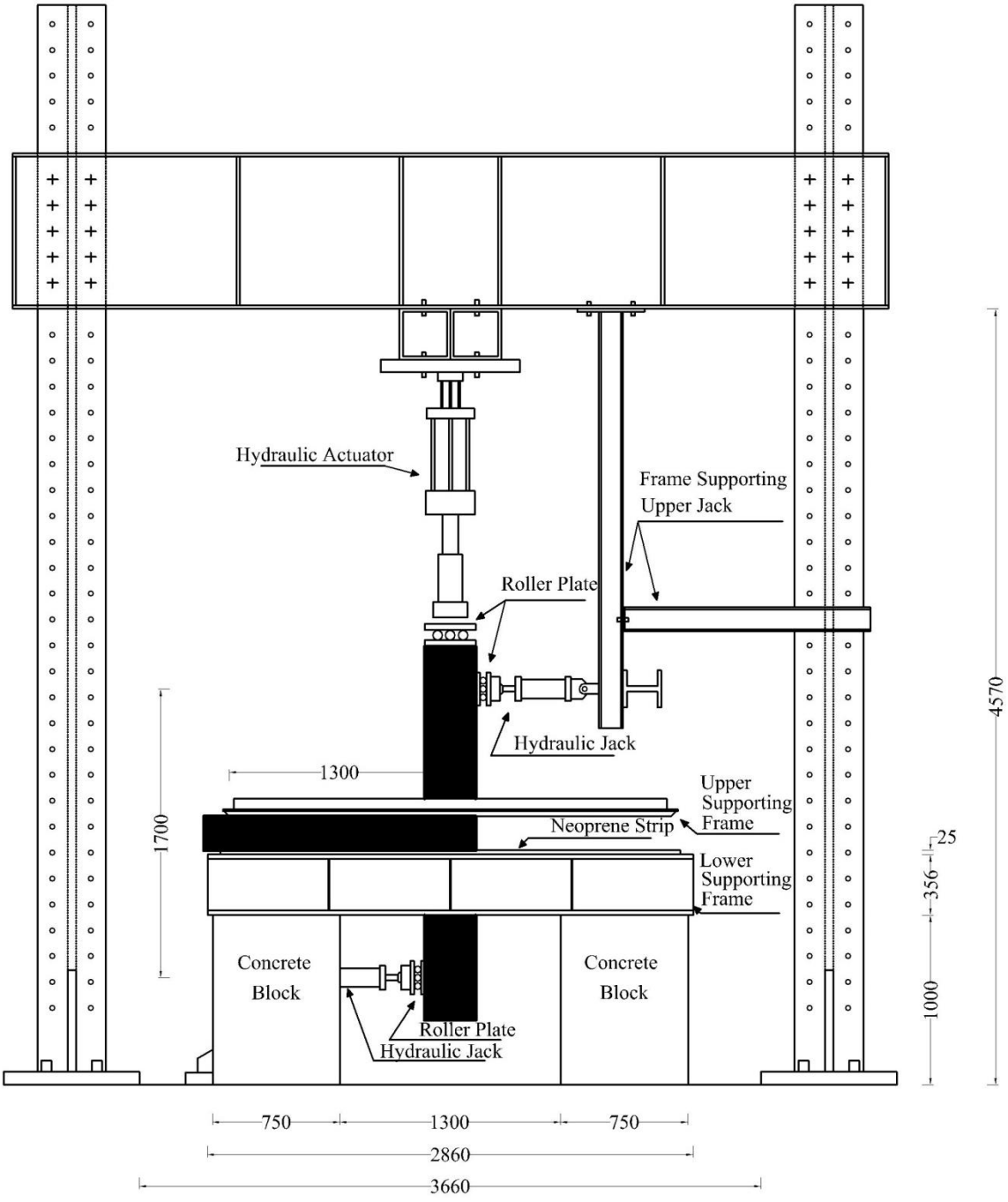


a) Elevation View

Figure 3.11: Test setup (Dimensions in mm)

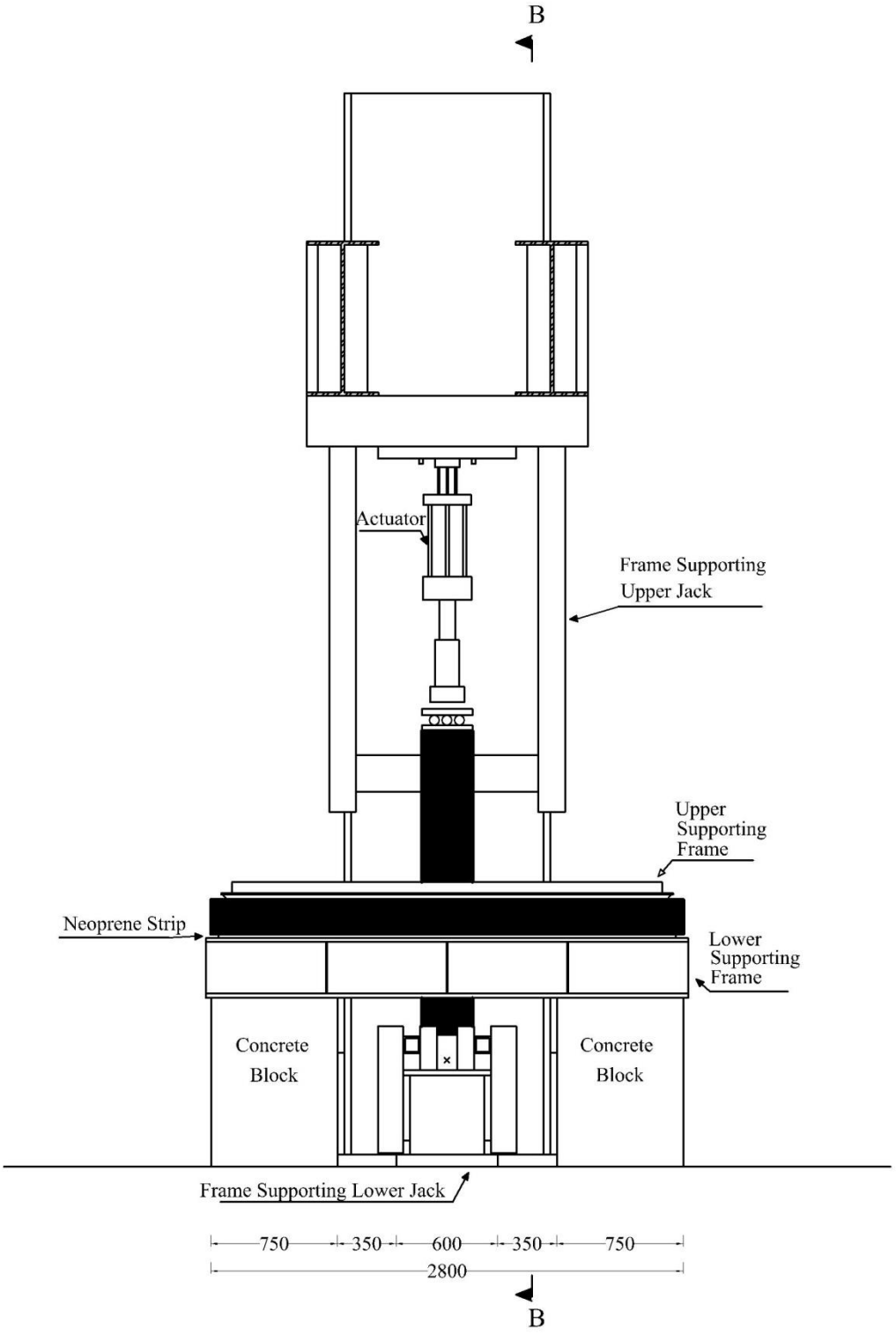


b) Section A-A

Figure 3.11: Test setup – continued (Dimensions in mm)

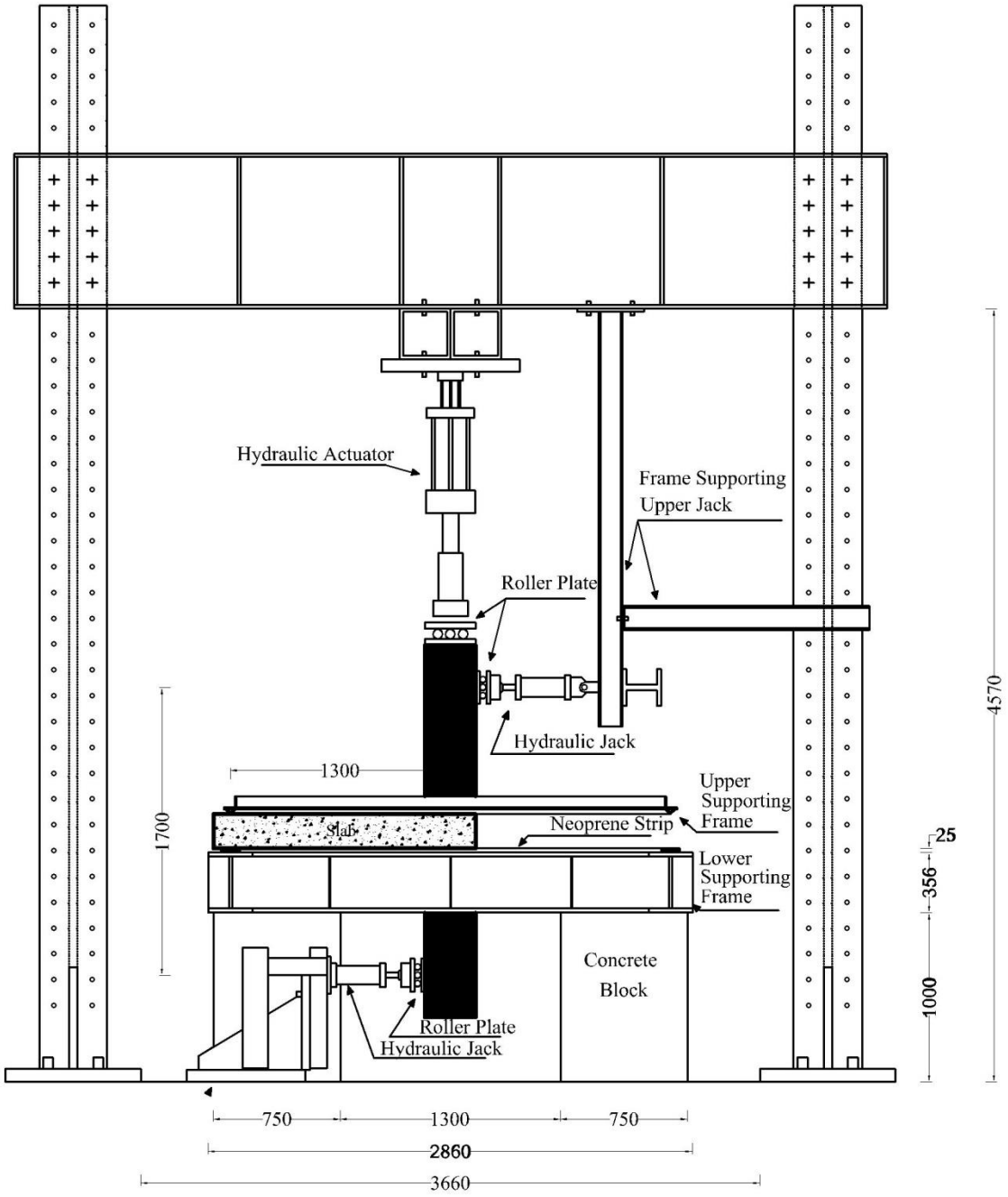


c) Section B-B

Figure 3.11: Test setup – continued (Dimensions in mm)

d) Photo of the set-up

Figure 3.11: Test setup – continued (Dimensions in mm)

# CHAPTER 4: EXPERIMENTAL RESULTS AND DISCUSSION

## 4.1. GENERAL

This chapter summarizes the experimental results for all tested connections. The behaviour of the connections is discussed in terms of the cracking pattern and mode of failure, deflection measurements, strain measurements, the ultimate capacity and the predictions of different codes.

It is to be noted that, for all connections, the deflections at the column face are the deflection readings taken from the LVDT located 50 mm from the column face in the direction perpendicular to the free edge. Also, the reinforcement strain at the column face refers to the reinforcement strain readings taken from the strain gauge located 20 mm from the column face on one of the bars passing through the column perpendicular to the free edge. While the concrete strain at the column face are the concrete strain readings taken from the PI-gauge located at the same position on the compression face of the slab. Furthermore, all the flexural reinforcement strain profiles perpendicular and parallel to the free edge are established at increments of 20% of the failure load for one of the bars passing through the column in each direction.

## 4.2. SERIES I - EFFECT OF FLEXURAL REINFORCEMENT RATIO

Three connections were assigned to investigate the effect of the GFRP flexural reinforcement ratio on the punching shear behaviour, i.e., GSC-0.9-XX-0.4, GSC-1.35-XX-0.4 and GSC-1.8-XX-0.4. However, connection S-0.9-XX-0.4 is included in this discussion to compare its behaviour to that of connection GSC-1.8-XX-0.4 as they both were designed to carry the same specified loads according to the CAN/CSA A23.3-04 (Canadian Standards Association 2004) and the CAN/CSA S806-12 (Canadian Standards Association 2012), respectively (Appendix A).

### 4.2.1. Cracking Pattern and Mode of Failure

The four connections failed in a brittle punching shear mode with no signs of flexural failure, i.e. concrete crushing at the compression face of the slab. The failure was characterized by a drastic drop in the vertical load when the column along with a conical portion of the slab punched through the remainder of the slab.

The four connections showed similar cracking behaviour. On the tension face of the slab, flexural cracks were first observed at the inner corners of the column, i.e. the location of maximum bending moment, at a vertical load of 40, 32, 46 and 36 kN for connections S-0.9-XX-0.4, GSC-0.9-XX-0.4, GSC-1.35-XX-0.4 and GSC-1.8-XX-0.4, respectively, as listed in Table 4.1. The relatively higher cracking load for connection GSC-1.35-XX-0.4 has affected the connection's behaviour as will be discussed later. These initial flexural cracks propagated around the column periphery until they reached the free edge forming a fairly tangential crack. At the same time, two cracks were developed from the interior face of the column towards the supported edge of the slab in the direction perpendicular to the free edge. With increasing the load, radial cracks started to form at the column vicinity propagating through the entire slab. Circumferential cracks then appeared at about 50% of the failure load for the four connections. The cracking patterns on the tension face at failure are shown in Figure 4.1. This behaviour is similar to that reported by Matthys and Taerwe (2000) and El-Salakawy et al. (1998) for FRP-RC interior connections and steel-RC edge connections, respectively.

Table 4.1: Test results for Series I connections

| Connection | Load (kN) | | | Deflection (mm) | | | Reinforcement Strain (μs) | | | Stiffness Factor (kN/mm) | | Deformability Factor, $J$ | Concrete Strength, $f_c'$ (MPa) |
|---|---|---|---|---|---|---|---|---|---|---|---|---|---|
| | Cr | Ser | Fail | Cr | Ser | Fail | Cr | Ser | Fail | $k_i$ | $k_p$ | | |
| S-0.9-XX-0.4 | 40 | 180 | 306 | 0.4 | 6.7 | 19.2 | 113 | 1367 | 10804[#] | 128.7 | 11.1 | 1.8[^] | 41 |
| GSC-0.9-XX-0.4 | 32 | | 227 | 0.4 | 25.5 | 39.3 | 175 | 6930 | 9776 | 91.8 | 3.7 | 24.1 | 41 |
| GSC-1.35-XX-0.4 | 46 | | 268 | 0.3 | 11.8 | 28.4 | 116 | 5120 | 8168 | 128.1 | 6.0 | 21.4 | 41 |
| GSC-1.8-XX-0.4 | 36 | | 277 | 0.5 | 10.6 | 24.1 | 199 | 2900 | 5087 | 85.9 | 8.1 | 7.6 | 45 |

[*]Cr, at first cracking; Ser, at service level; Fail, at failure; $K_i$, pre-cracking stiffness factor; and $k_p$, post-cracking stiffness factor
[#]parallel to the free edge
[^]Ductility = deflection at failure/deflection at first yielding

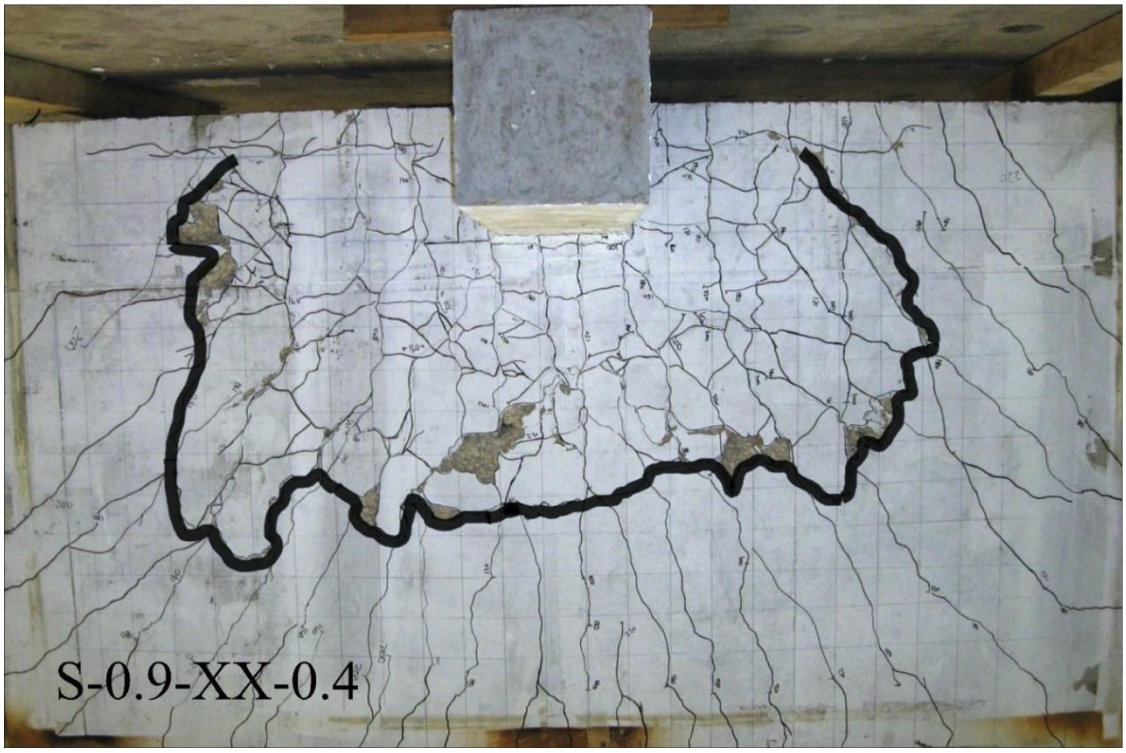


a) Connection S-0.9-XX-0.4


b) Connection GSC-0.9-XX-0.4

Figure 4.1: Cracking on the tension face at failure for Series I connections

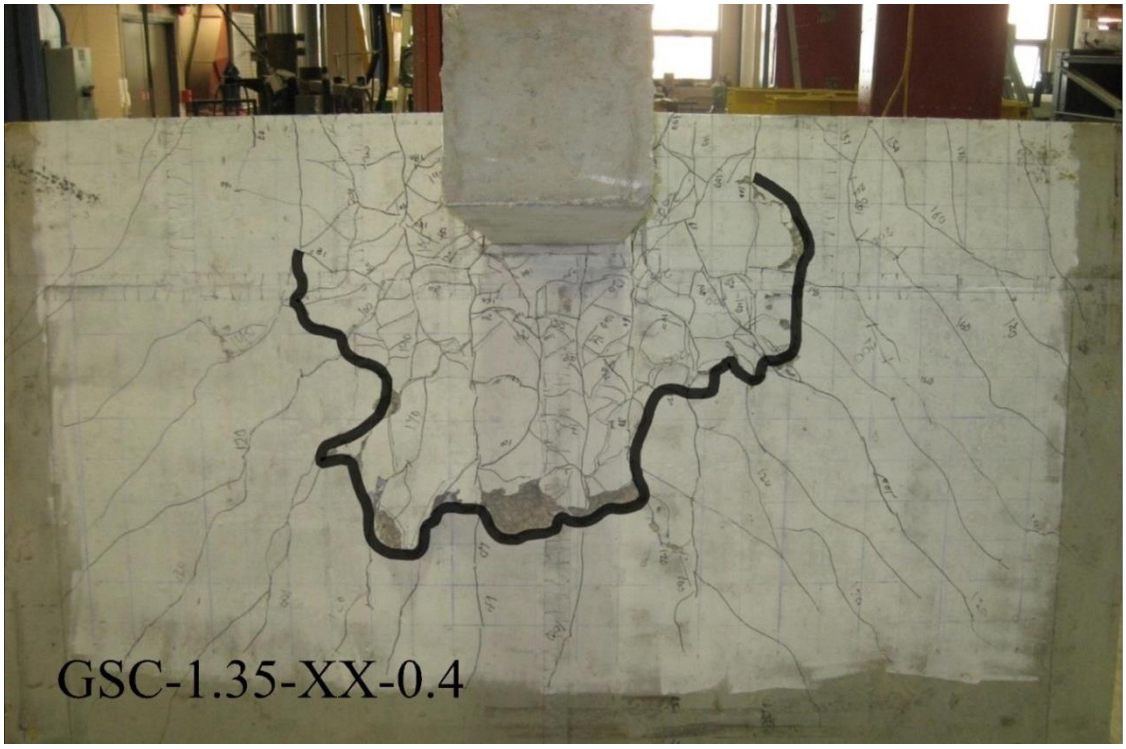


c) Connection GSC-1.35-XX-0.4

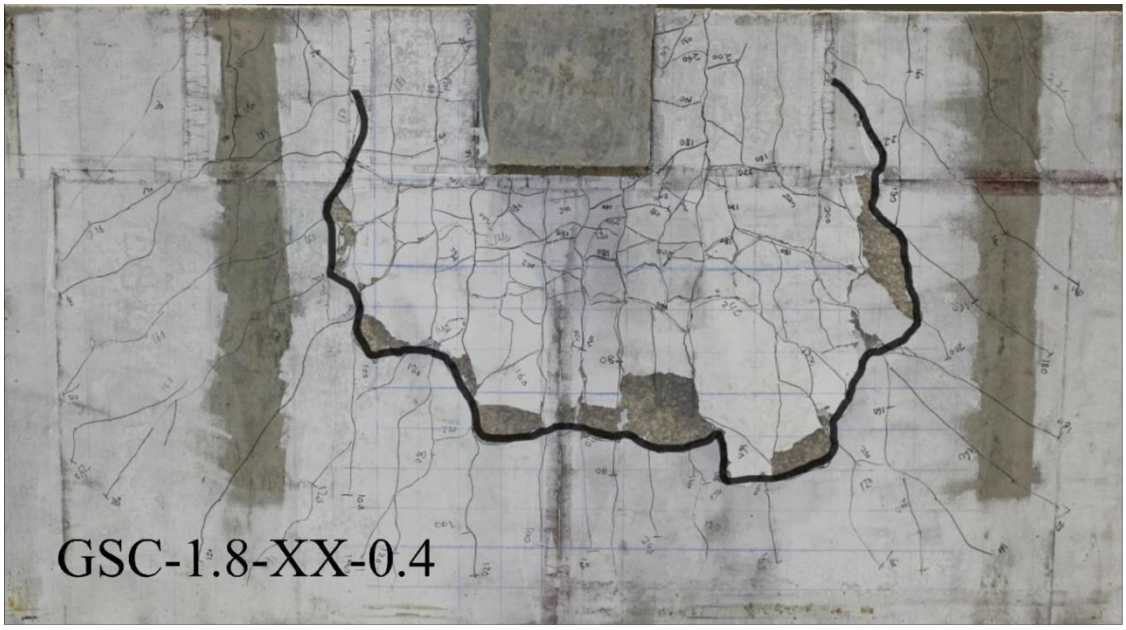


d) Connection GSC-1.8-XX-0.4

Figure 4.1: Cracking on the tension face at failure for Series I connections - continued

On the free edge, for connection S-0.9-XX-0.4, the first crack started from the bottom column corner and extended 60 mm in the transverse direction at a vertical load of 40 kN. This crack, then, propagated making an approximate angle of $66^{o}$ with the horizontal plane at a vertical load of 100 kN. Punching failure eventually occurred at this diagonal crack. Similarly, for connection GSC-0.9-XX-0.4, the first crack formed at the bottom column corner at a vertical load of 40 kN but extended instantaneously in the transverse direction to a height of 165 mm from the slab soffit. Other cracks then started to form at the free edge at farther distances from the column corner. The failure diagonal crack, located at 130 mm from the column corner, was making an approximate angle of $56^{o}$ with the horizontal plane at a vertical load of 80 kN.

Also, for connection GSC-1.35-XX-0.4, the first crack started from the bottom column corner and extended instantaneously in the transverse direction to a height of 160 mm from the slab soffit at a vertical load of 55 kN. The failure diagonal crack propagated from the flexural crack 100 mm away from the column corner making an approximate angle of $71^{o}$ with the horizontal plane at a vertical load of 100 kN. Furthermore, for connection GSC-1.8-XX-0.4, three cracks formed simultaneously in the column vicinity at a vertical load of 60 kN. The crack closest to the bottom column corner extended instantaneously in the transverse direction to a distance of 170 mm from the slab soffit. This crack, then, propagated making an approximate angle of $78^{o}$ with the horizontal plane at a vertical load of 100 kN eventually causing punching failure. Accordingly, increasing the GFRP flexural reinforcement ratio by 50% and 100% increased the angle of the failure cone on the free edge by 22% and 34%, respectively. The cracking patterns on the free edge at failure for the four connections are shown in Figure 4.2.

a) Connection S-0.9-XX-0.4

b) Connection GSC-0.9-XX-0.4

c) Connection GSC-1.35-XX-0.4

d) Connection GSC-1.8-XX-0.4

Figure 4.2: Cracking on the free edge at failure for Series I connections

### 4.2.2. Deflections

In general, the load-deflection relationship for steel-RC slab-column connections can be approximated by three straight lines defining three different stages of behaviour according to the significant changes in the stiffness (Alexander and Simmonds 1992). Stage I represents the

uncracked behaviour of the slab from the start of loading until the point of first cracking. At this stage, since the slab is uncracked, the slab stiffness depends mainly on the dimensions of the concrete cross section. Stage II represents the cracked behaviour of the connection; it begins after cracks have stabilized and extends up to the point where reinforcement yielding takes place. At this stage, the slab stiffness depends mainly on the axial stiffness of the flexural reinforcement, i.e., the product of the flexural reinforcement ratio and the reinforcement modulus of elasticity, $\rho E$, rather than the cross-sectional dimensions. Stage III represents the extensive plastic deformations of the slab after yielding of reinforcement (Alexander and Simmonds 1992). On the other hand, a typical load-deflection relationship for FRP-RC slab-column connections failing in punching shear has only the first two stages since FRP reinforcement does not yield. Stages I and II are quantified herein using the pre-cracking and post-cracking stiffness factors, $k_i$ and $k_p$, respectively (Table 4.1). These factors represent the slope of the load-deflection curve before and after cracking, respectively.

Figure 4.3 shows the relationship between the vertical load and the deflection at the column face. The self-weight of the connections was neither included in deflection nor vertical load values. It is obvious that connection S-0.9-XX-0.4 exhibited only the first two stages because the punching failure occurred before extensive yielding of the reinforcement has taken place. For the GFRP-RC connections, increasing the flexural reinforcement ratio had a considerable effect on the post-cracking stiffness. Increasing the flexural reinforcement ratio by 50% and 100% increased the post-cracking stiffness factor by 62% and 119%, respectively. Consequently, increasing the flexural reinforcement ratio decreased the deflections at the same load level. However, it can be seen that, up to a vertical load of 110 kN, connection GSC-1.8-XX-0.4 had higher deflections than connection GSC-1.35-XX-0.4 which have a 25% less reinforcement ratio. This is attributed

to the higher cracking load for connection GSC-1.35-XX-0.4 which delayed the initiation of flexural cracks and, in turn, delayed the transition of the behaviour of the section from a gross moment of inertia-dependent behaviour to an effective moment of inertia-dependent one. Furthermore, increasing the flexural reinforcement ratio by 50% and 100% decreased the maximum deflections 50 mm from the column face by 28% (from 39 mm to 28 mm) and 39% (from 39 mm to 24 mm), respectively. It can be seen in Figure 4.4 that the post-cracking stiffness factor increases approximately linearly with increasing the flexural reinforcement ratio.

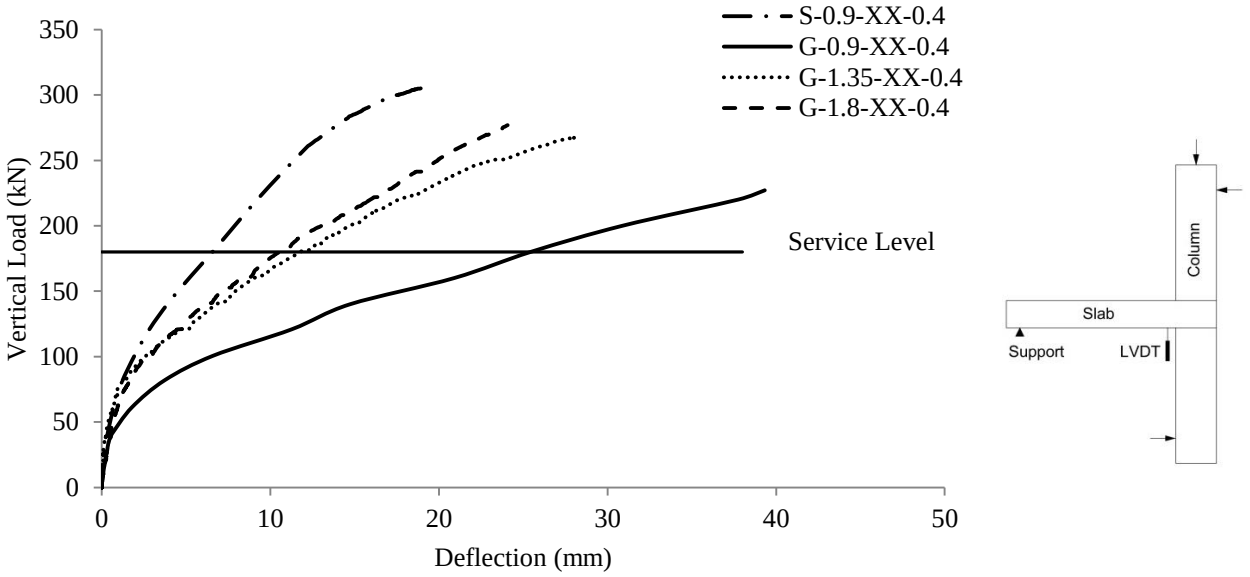


Figure 4.3: Load-deflection relationship for Series I connections

The post-cracking stiffness factor for connection S-0.9-XX-0.4 was 11.1 kN/mm. This is 37% higher than that of connection GSC 1.8-XX-0.4 (8.1 kN/mm). Moreover, the deflection at the service level for connection S-0.9-XX-0.4 was 6.7 mm which is 37% less than that of connection GSC-1.8-XX-0.4 (10.6 mm) although they both were designed to satisfy the serviceability requirements relevant to each type of reinforcement. This is attributed to the more relaxed serviceability requirement for the FRP-RC elements. The serviceability requirements of both

connections were governed by the crack control parameter provision (Appendix A). This parameter implicitly limits the maximum crack width for steel-RC flexural members to 0.4 and 0.33 mm for interior and exterior exposure, respectively (Cement Association of Canada 2006). While for FRP reinforcement, which does not corrode, these limitations are relaxed in the case of FRP- RC elements to 0.7 and 0.5 mm, respectively (Canadian Standards Association 2006, 2012).

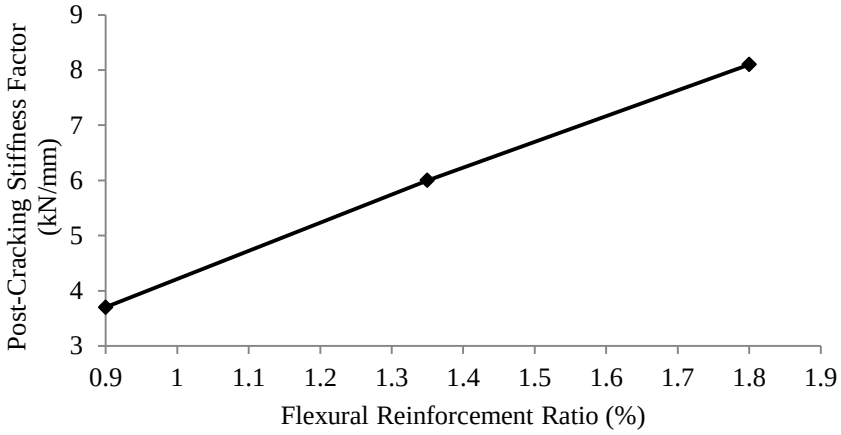


Figure 4.4: Reinforcement ratio vs. the post-cracking stiffness factor relationship

Ductility is the ability of a structural element to undergo substantial plastic deformations before fracture. In steel-RC slab-column connections, ductility is quantified by a rotation or a displacement ductility factor which is calculated as the ratio of the rotation or displacement at ultimate to those at steel reinforcement yielding (Marzouk et al. 1996). These factors provide means of comparison between levels of safety at ultimate and service states. Although FRP reinforcement does not yield, FRP-RC structures exhibit substantial deflections before fracture due to the low modulus of elasticity of FRP reinforcement. CHBDC S6-06 (Canadian Standards Association 2006) assesses this deformable behaviour of FRP-RC structures by the deformability factor, *J*, which is an analogues factor to the ductility factor and was first introduced in 1995

(Jaeger et al. 1995). The deformability factor is calculated using Equation 4.1 where $M$ and $\Psi$ are the moment and curvature of a section, respectively, and the subscripts $u$ and $s$ stand for the ultimate and service levels, respectively. The CHBDC S6-06 defines the service state as the state corresponding to a compressive strain in the outermost concrete fibres of 1000 με, i.e., when the extreme compression fibres of concrete reach its proportional limit.

Some of the connections tested herein did not reach a compressive strain of 1000 με in the extreme compression fibres. This, according to the aforementioned definition of deformability, implies that these connections did not show any ample warning before the brittle punching failure. However, another definition for the service condition was introduced by Newhook et al. (2002) and later adopted by ISIS Canada (2001), consider it as the state corresponding to a tensile strain in the flexural reinforcement of 2000 με. In this study, the latter definition will be used for comparison purposes. Moreover, in this discussion, the deformability factor will be calculated using Equation 4.2 which incorporates vertical loads, $P$, and displacements, $\Delta$, instead of moments and curvatures at failure and service states.

$$J = \frac{M_u \psi_u}{M_s \psi_s} \qquad \text{Eq. [4.1]}$$

$$J = \frac{P_u \Delta_u}{P_s \Delta_s} \qquad \text{Eq. [4.2]}$$

The deformability factors for the three GFRP-RC connections are listed in Table 4.1. The deformability factors were 24.1, 21.4 and 7.6 for connections GSC-0.9-XX-0.4, GSC-1.35-XX-0.4 and GSC-1.8-XX-0.4, respectively. Increasing the reinforcement ratio by 50% and 100% decreased the deformability factor by 11% and 68%, respectively. Yet, the three values are considerably above the minimum limit of 4 adopted by ISIS Canada (ISIS Canada 2001).

Therefore, using reinforcement ratios as high as 1.8%, which is 5.3 times the balanced reinforcement ratio, still allows the connection to give ample warning before failure.

### 4.2.3. Flexural Reinforcement and Concrete Strains

Figure 4.5 shows the relationship between the vertical load and the reinforcement and concrete strains at the column face. It is to be noted that the gauge in connection S-0.9-XX-0.4 malfunctioned at 88% of the failure load (269 kN). This happened before showing any signs of yielding at this location at a reading of 2420 μs. However, yielding of steel reinforcement at the column face was recorded on the bars parallel to the free edge at a load of 78% of the failure load (240 kN).

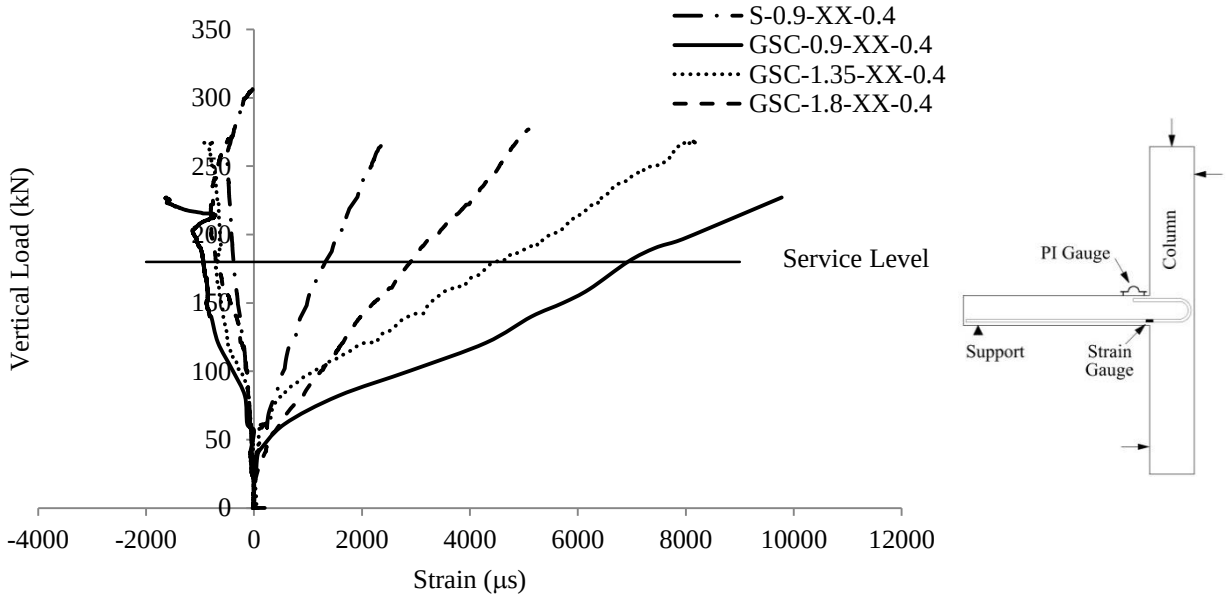


Figure 4.5: Load-strain relationship for Series I connections

The reinforcement strains after cracking varied approximately linearly with increasing the load for the four connections. For the GFRP-RC connections, increasing the flexural reinforcement ratio decreased the reinforcement strains at the same load level. This is a direct result of providing additional reinforcement to carry the same load/moment. However, the measured

reinforcement strains in connection GSC-1.8-XX-0.4 were higher than those in connection GSC-1.35-XX-0.4, which has 25% less reinforcement ratio, up to a load of about 110 kN. Again, this is attributed to the higher cracking load of connection GSC-1.35-XX-0.4 compared to that of connection GSC-1.8-XX-0.4 which delayed the onset of cracking in connection GSC-1.35-XX-0.4 and, consequently, the development of tensile strains in the reinforcing bar in this connection.

Furthermore, increasing the flexural reinforcement ratio decreased the reinforcement strain at failure; increasing the reinforcement ratio by 50% and 100% decreased the maximum reinforcement strain by 16% and 48%, respectively. The maximum reinforcement strains were recorded on the bar passing through the column perpendicular to the free edge for the three GFRP-RC connections as listed in Table 4.1. The maximum strain in the reinforcing bars occurred in connection GSC-0.9-XX-0.4, i.e. the one with the lowest GFRP flexural reinforcement ratio, and was 9780 με; this is 42.5% of the ultimate tensile strain of the used GFRP bars. Moreover, the maximum recorded concrete strains for the three connections were well below 3500 με, i.e. the concrete crushing strain specified by the CAN/CSA S806-12. This confirms that the failure mode was pure punching rather than a flexural failure.

The reinforcement strain at the service level for connection GSC-1.8-XX-0.4 was 2900 με. This is 50% less than the service strain limit specified by the CAN/CSA S806-12 which is 25% of the rupture strain of the used bars (5750 με). However, it is 112% higher than that of connection S-0.9-XX-0.4 (1370 με). Again, this is attributed to the more relaxed crack control limitations in the case of FRP-RC elements compared to the case of steel-RC elements.

Figures 4.6 and 4.7 show the reinforcement strain profiles in the directions perpendicular and parallel to the free edge, respectively. The strain profiles in both orthogonal directions for the

three connections clearly demonstrate that the strains were inversely proportional to the distance of the strain gauge from the column face. This implies a good bond between the sand-coated GFRP bars and the surrounding concrete. Similar behaviour of slab-column interior connections reinforced with sand-coated GFRP bars subjected to concentric loading was reported in the literature (Hussein et al. 2004; Dulude et al. 2013).

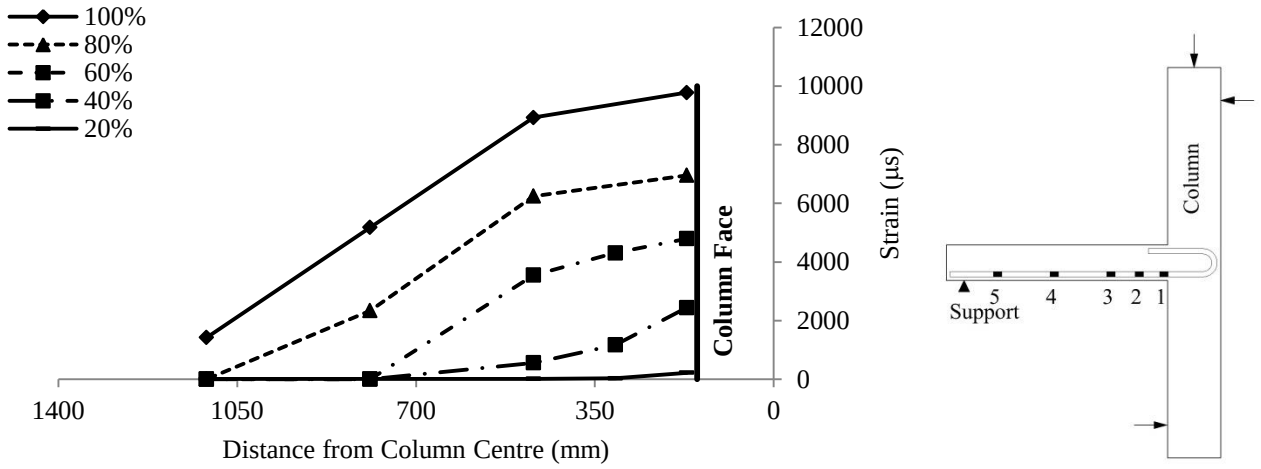


a) Connection GSC-0.9-XX-0.4

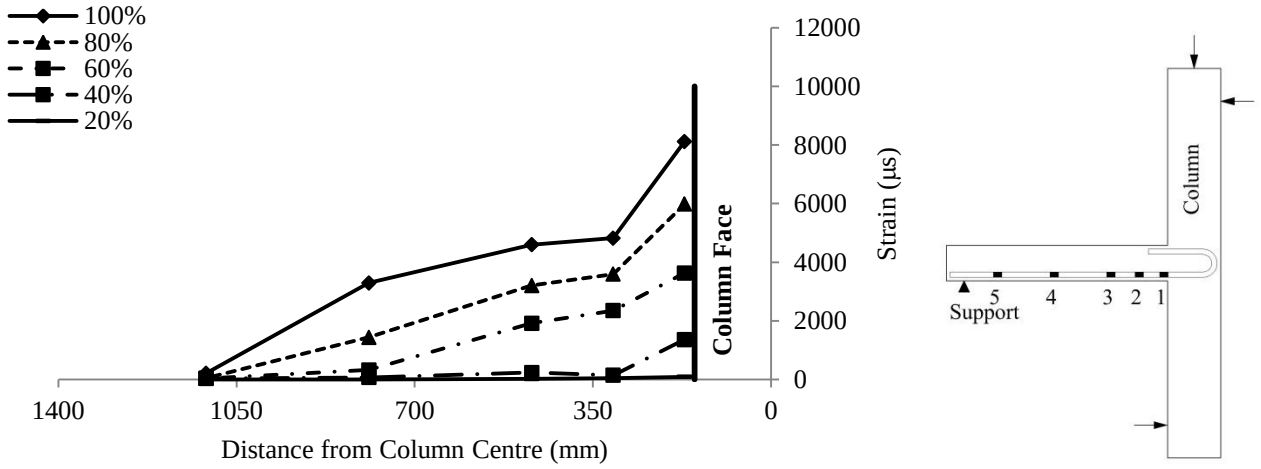


b) Connection GSC-1.35-XX-0.4

Figure 4.6: Reinforcement strain profile perpendicular to the free edge

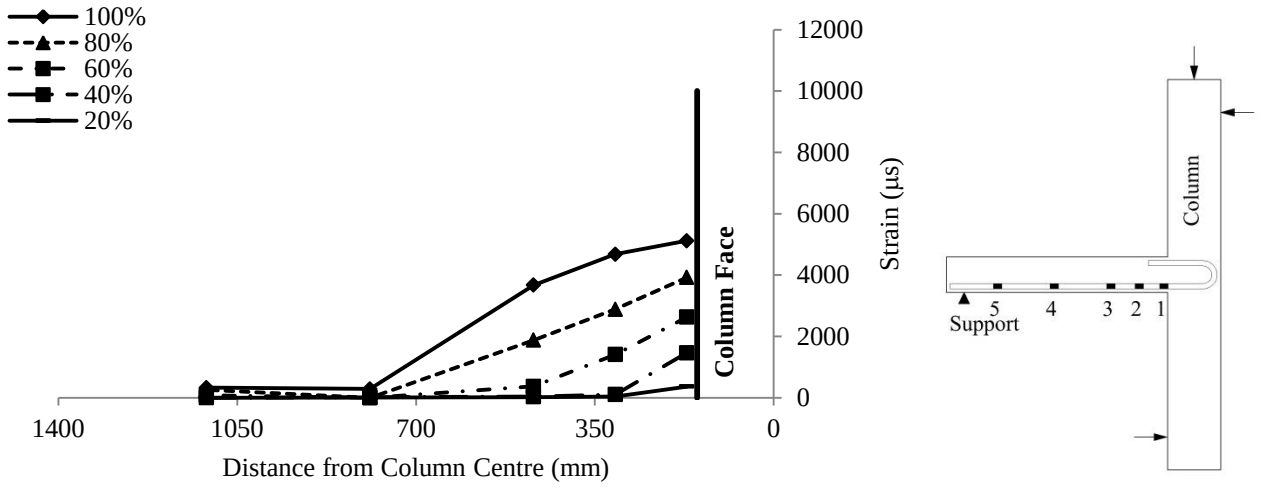


c) Connection GSC-1.8-XX-0.4

Figure 4.6: Reinforcement strain profile perpendicular to the free edge – continued

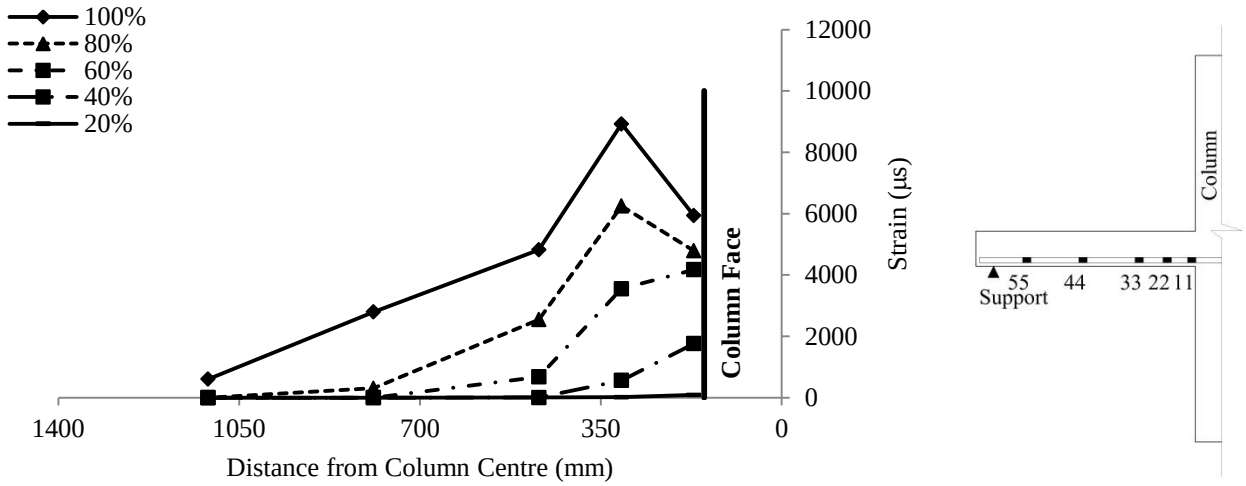


a) Connection GSC-0.9-XX-0.4

Figure 4.7: Reinforcement strain profile parallel to the free edge

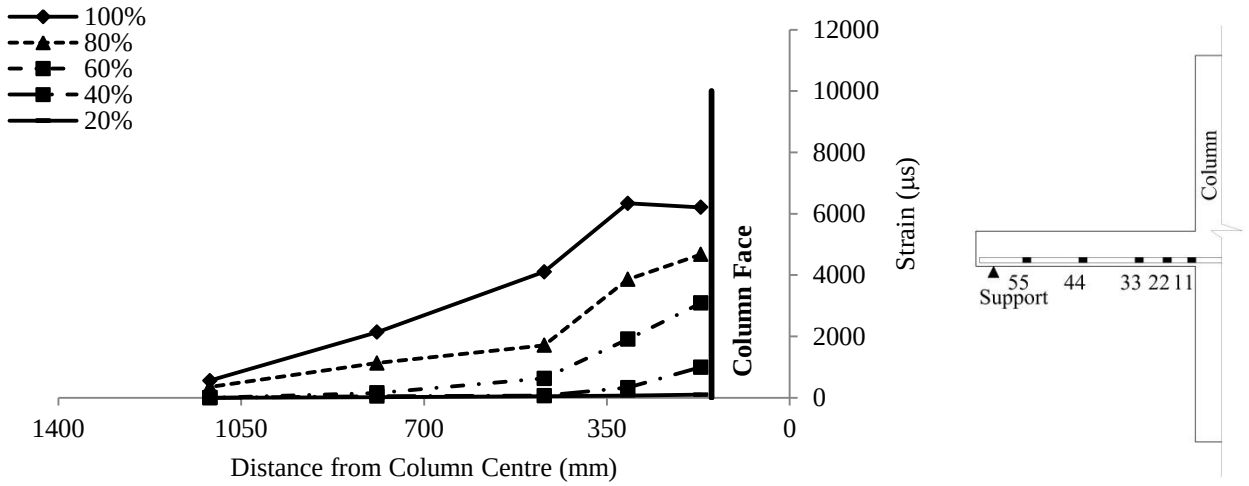


b) Connection GSC-1.35-XX-0.4

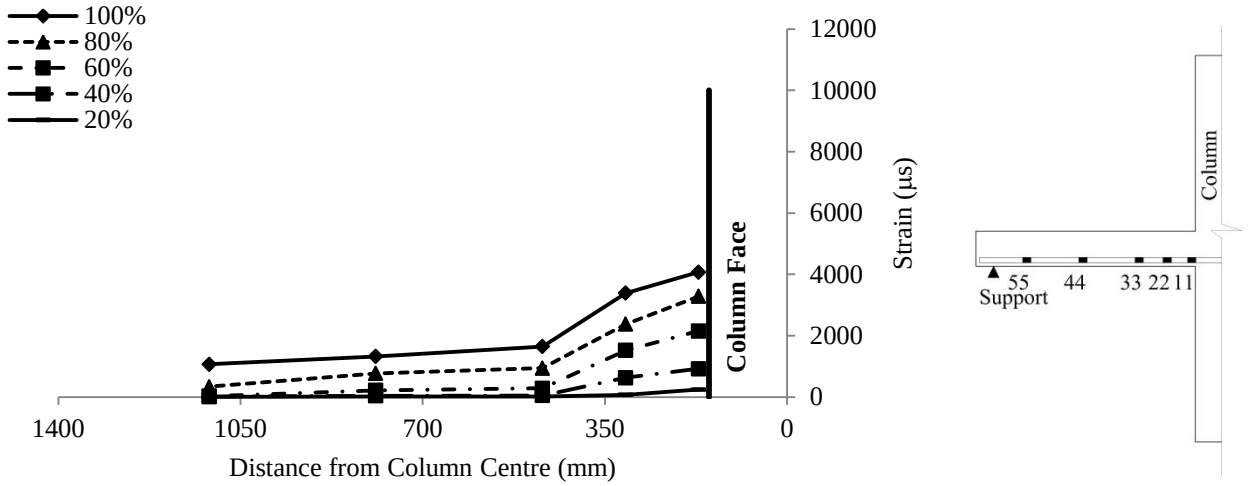


c) Connection GSC-1.8-XX-0.4

Figure 4.7: Reinforcement strain profile parallel to the free edge - continued

### 4.2.4. Punching Shear Capacity

The failure loads of the connections were normalized by being multiplied by $\sqrt[3]{40/f_c'}$, where $f_c'$ is the actual concrete compressive strength, in MPa, of the connection at the day of testing and 40 MPa is a reference strength based on the average concrete strengths of the tested connections, to eliminate the effect of the relative differences in the concrete strengths. The cubic root was

used rather than the square root to align with the CAN/CSA S806-12 equation for punching shear which considers the effect of the concrete compressive strength to the power of 1/3. The actual and normalized failure loads are listed in Table 4.2.

Increasing the reinforcement ratio from 0.9% to 1.35% increased the normalized capacity by 18.2%. This is attributed to the increased reinforcement axial stiffness, $\rho E$. Increasing the reinforcement axial stiffness controls the propagation of cracks leading to narrower and shorter cracks. This increases the contribution of the aggregate interlock component to the shear strength of the section and increases the depth of the uncracked concrete. In addition, increasing the flexural reinforcement ratio increases the contribution of the dowel action. This effect, however, is not as significant as the earlier two because the transverse strength and stiffness of the FRP bars is considerably small. However, further increasing the reinforcement ratio to 1.8% did not result in a further increase in the normalized capacity. This unexpected behaviour is hard to explain; however, having in mind the superior initial behaviour of connection GSC-1.35-XX-0.4 due to its higher cracking load, it seems that the high capacity of connection GSC-1.35-XX-0.4 is the unusual behaviour rather than the low capacity of connection GSC-1.8-XX-0.4. Figure 4.8 shows the relationship between the flexural reinforcement ratio and the normalized failure load.

Table 4.2: Actual and normalized failure loads for Series I connections

| Connection | Flexural Reinforcement Ratio, $\rho$ (%) | Concrete Compressive Strength, $f_c'$ (MPa) | Actual Failure Loads (kN) | Normalized Failure Loads (kN) |
|---|---|---|---|---|
| S-0.9-XX-0.4 | 0.9 | 41.3 | 306.4 | 303.2 |
| GSC-0.9-XX-0.4 | 0.9 | 41.1 | 227.1 | 225.1 |
| GSC-1.35-XX-0.4 | 1.35 | 41.0 | 268.2 | 266 |
| GSC-1.8-XX-0.4 | 1.8 | 45.6 | 276.9 | 265 |

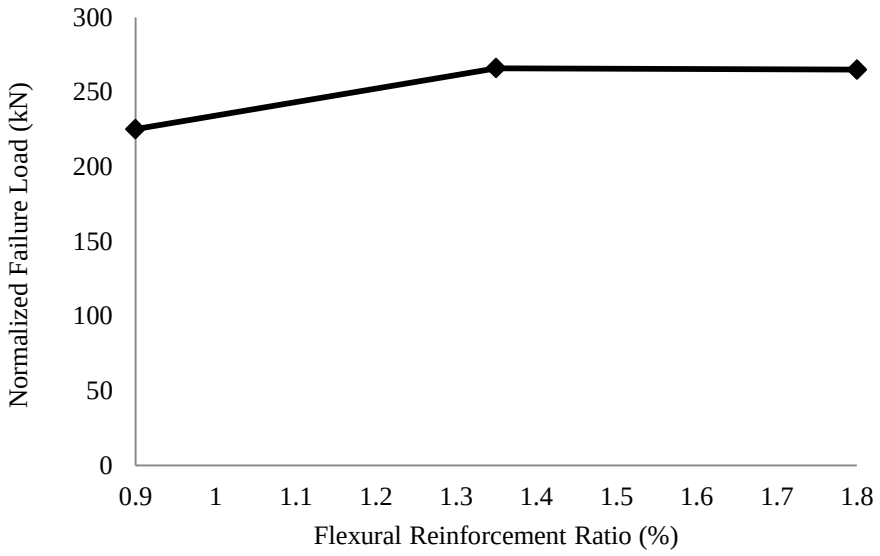


Figure 4.8: Reinforcement ratio-normalized failure load relationship

### 4.2.5. Code Comparisons

The punching shear capacities of the tested connections were calculated using the provisions of the CAN/CSA S806-12, the ACI 440.1R-06 and the JSCE 1997. All the safety factors in the code equations were set to 1.0 to predict the nominal punching shear capacity. Moreover, the flexural capacities of the connections were estimated using the yield line theory. The failure pattern proposed by Mortin (1989) was adopted (see Section 2.8).

Table 4.3 shows comparisons between the actual failure loads and the predicted punching and flexural capacities of the three GFRP-RC connections. The ultimate capacities of the three connections were lower than the upper bound predictions of the yield line theory with an average $V_{Test}/V_{flex}$ of 0.8 ± 0.05. This confirms that the connections failed in a brittle punching mode rather than a deformable flexural mode. On the other hand, the punching capacity predictions of the CAN/CSA S806-12 and the JSCE 1997 are very close, yet slightly conservative, to the actual capacities with an average $V_{Test}/V_{pred}$ of 1.29 ± 0.07 and 1.25 ± 0.04, respectively. However, the

ACI 440.1R-06 highly underestimates the capacities with an average $V_{Test}/V_{pred}$ of 2.19 ± 0.17. The reason behind this underestimation is that the punching shear equation in the ACI 440.1R-06 is originally derived from the one-way shear model proposed by Tureyen and Frosch (2003). This model accounts for the uncracked concrete contribution only to resist the applied shear stresses and ignores the aggregate interlock and the dowel action contributions as discussed in Section 2.6.2.2.

## 4.3. SERIES II - EFFECT OF FLEXURAL REINFORCEMENT TYPE

Three connections were assigned to investigate the effect of flexural reinforcement type on the punching shear behaviour, i.e., S-0.9-XX-0.4, GSC-0.9-XX-0.4 and GRD-0.9-XX-0.4.

### 4.3.1. Cracking Pattern and Mode of Failure

The three connections failed in a brittle punching shear mode with no signs of flexural failure. However, connection GRD-0.9-XX-0.4 exhibited a less brittle punching failure than the other two connections characterized by significant deflections/deformations at a steady load level just before the drastic load drop due to the punching failure. This deformable behaviour could be attributed to loss of bond between the reinforcing bars and the surrounding concrete a short time before failure as will be discussed in Section 4.3.3. The test results are listed in Table 4.4. Figure 4.9 shows the cracking pattern at failure on the tension face and the free edge for connection GRD-0.9-XX-0.4. The final cracking patterns for the three connections (Figures 4.1, 4.2 and 4.9) and the propagation of cracks were similar despite the different reinforcement types.

Table 4.3: Code comparisons for Series I connections

| Connection | Actual Failure Loads, $V_{Test}$ (kN) | Punching Shear Capacity Predictions, $V_{Pred}$ | | | | | | | |
|---|---|---|---|---|---|---|---|---|---|
| | | CAN/CSA S806-12 | | ACI 440.1R-06 | | JSCE 1997 | | Yield Line Theory | |
| | | $V_{Pred}$ | $V_{Test}/V_{Pred}$ | $V_{Pred}$ | $V_{Test}/V_{Pred}$ | $V_{Pred}$ | $V_{Test}/V_{Pred}$ | $V_{Pred}$ | $V_{Test}/V_{Pred}$ |
| GSC-0.9-XX-0.4 | 227.1 | 173.5 | 1.31 | 98.5 | 2.31 | 181.4 | 1.25 | 275.9 | 0.82 |
| GSC-1.35-XX-0.4 | 268.2 | 198.2 | 1.35 | 118.7 | 2.26 | 207.9 | 1.29 | 321.6 | 0.83 |
| GSC-1.8-XX-0.4 | 276.9 | 226.2 | 1.22 | 137.7 | 2.01 | 228.6 | 1.21 | 373 | 0.74 |
| Mean | | | 1.29 | | 2.19 | | 1.25 | | 0.8 |
| Standard Deviation | | | 0.07 | | 0.17 | | 0.04 | | 0.05 |

Table 4.4: Test results for Series II connections

| Connection | Load (kN) | | Deflection (mm) | | Reinforcement Strain (μs) | | Stiffness Factor (kN/mm) | | Deformability Factor, $J$ | Concrete Strength, $f_c'$ (MPa) |
|---|---|---|---|---|---|---|---|---|---|---|
| | Cr | Fail | Cr | Fail | Cr | Fail | $k_i$ | $k_p$ | | |
| S-0.9-XX-0.4 | 40 | 306.4 | 0.4 | 19.2 | 113 | 10804[#] | 128.7 | 11.1 | 1.8[^] | 41.3 |
| GSC-0.9-XX-0.4 | 32 | 227.1 | 0.4 | 39.3 | 175 | 9776 | 91.8 | 3.7 | 24.1 | 41.1 |
| GRD-0.9-XX-0.4 | 36 | 191.2 | 0.5 | 38 | 138[#] | 7979 | 85 | 3.9 | 19.4 | 41 |

[*]Cr, at first cracking; Fail, at failure; $k_i$, pre-cracking stiffness factor; $k_p$, post-cracking stiffness factor; and $f_c'$, concrete compressive strength.
[#]parallel to the free edge
[^]Ductility = deflection at failure/deflection at first yielding


a) Tension face

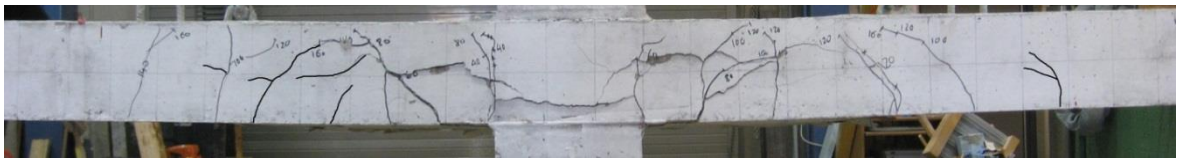

b) Free edge

Figure 4.9: Cracking at failure for connection GRD-0.9-XX-0.4

### 4.3.2. Deflections

Figure 4.10 shows the relationship between the vertical load and the deflection at the column face. Although FRP reinforcement does not yield, connection GRD-0.9-XX-0.4 exhibited a plateau similar to that defining the yielding of steel reinforcement in steel-RC elements before failure. That is, while the load increased only by 2% (from 187.4 to 191.2 kN), the deflections

increased by 15.8% (from 32.8 to 38 mm). This plateau is attributed to the loss of bond between the bar and the surrounding concrete (see Section 4.3.3).

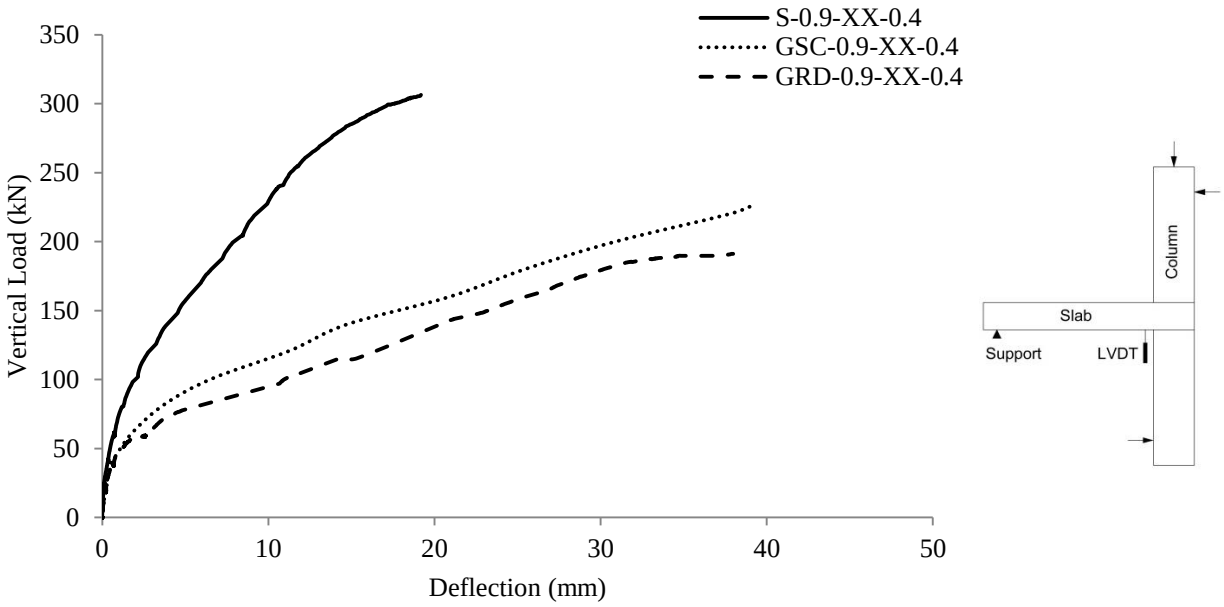


Figure 4.10: Load-deflection relationship for Series II connections

Although the three connections had the same flexural reinforcement ratio, connection S-0.9-XX-0.4 had 200% and 185% higher post-cracking stiffness factor, $k_p$, than connections GSC-0.9-XX-0.4 and GRD-0.9-XX-0.4, respectively. This is attributed to the higher axial stiffness of the steel bars compared to the GFRP bars. As shown in Figure 4.11, connection S-0.9-XX-0.4 had 275% and 260% higher effective reinforcement ratio, $\rho E_{used}/E_{steel}$, than connections GSC-0.9-XX-0.4 and GRD-0.9-XX-0.4, respectively.

On the other hand, connections GSC-0.9-XX-0.4 and GRD-0.9-XX-0.4 had very similar effective reinforcement ratios and, consequently, had very close post-cracking stiffness factors. Yet, as shown in Figure 4.10, connection GRD-0.9-XX-0.4 exhibited higher post-cracking deflections at the same load level than connection GSC-0.9-XX-0.4. This is attributed to a more

abrupt loss of the uncracked stiffness for connection GRD-0.9-XX-0.4 than that for connection GSC-0.4XX-0.4. Figure 4.12 shows the relationship between the vertical load and the deflection at the column face at early load stages. Also, Figure 4.13 shows the relationship between the vertical load and the flexural reinforcement strain at the column face at early load stages.

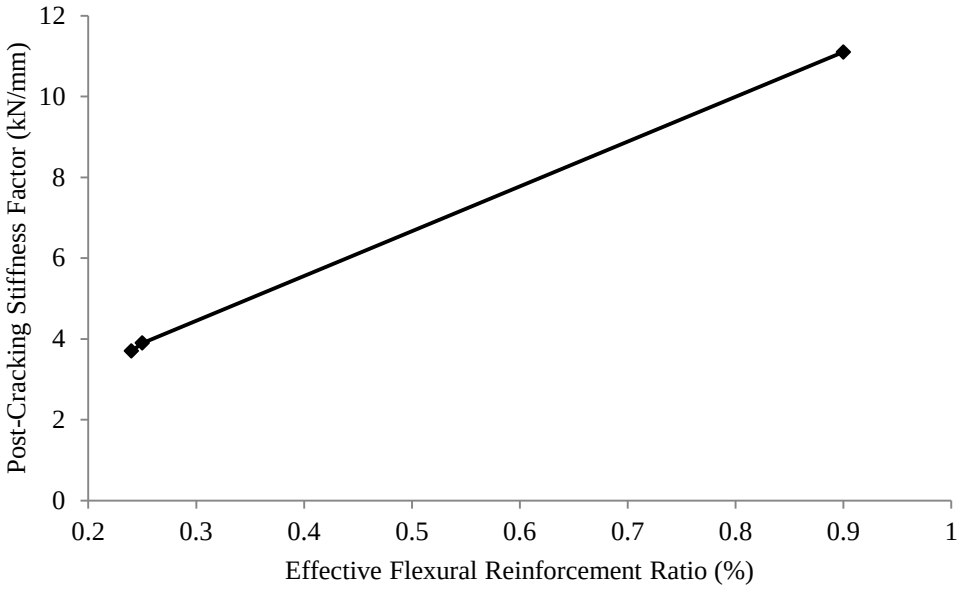


Figure 4.11: Effective reinforcement ratio vs. post-cracking stiffness

As shown in Figure 4.12, while connection GSC-0.9-XX-0.4 exhibited a smooth gradual loss of its uncracked stiffness, an abrupt loss of stiffness took place in connection GRD-0.9-XX-0.4 between vertical loads of 47 kN and 59 kN followed by a relatively high constant rate of losing the stiffness until a vertical load of 100 kN when the crack formation stabilized and the cracked stiffness of the section was maintained. Correspondingly, as shown in Figure 4.14, while the reinforcement strains in connection GSC-0.9-XX-0.4 started to increase gradually after first cracking, the bars in connection GRD-0.9-XX-0.4 did not develop any strains up to a vertical load of 57 kN. The concrete surface at the inner column face remained uncracked until a crack suddenly formed at a vertical load of 57 kN releasing a high amount of energy. This, in turn, led

to a sudden increase in the reinforcement strains and a sudden reduction in the stiffness of the slab. The slope of the load-strain curve increased once the formation of the cracks stabilized at a vertical load of 100 kN. The formation of a relatively wide crack at the inner column face in connection GRD-0.9-XX-0.4 was visually marked during the test as shown in Figure 4.14.

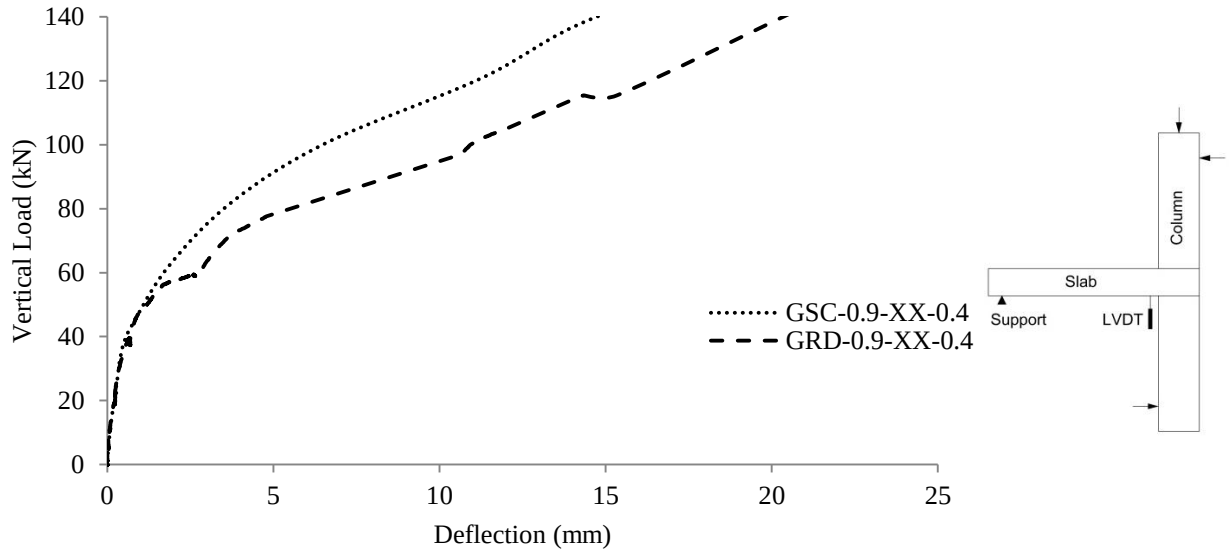


Figure 4.12: Load-deflection relationship at early load stages

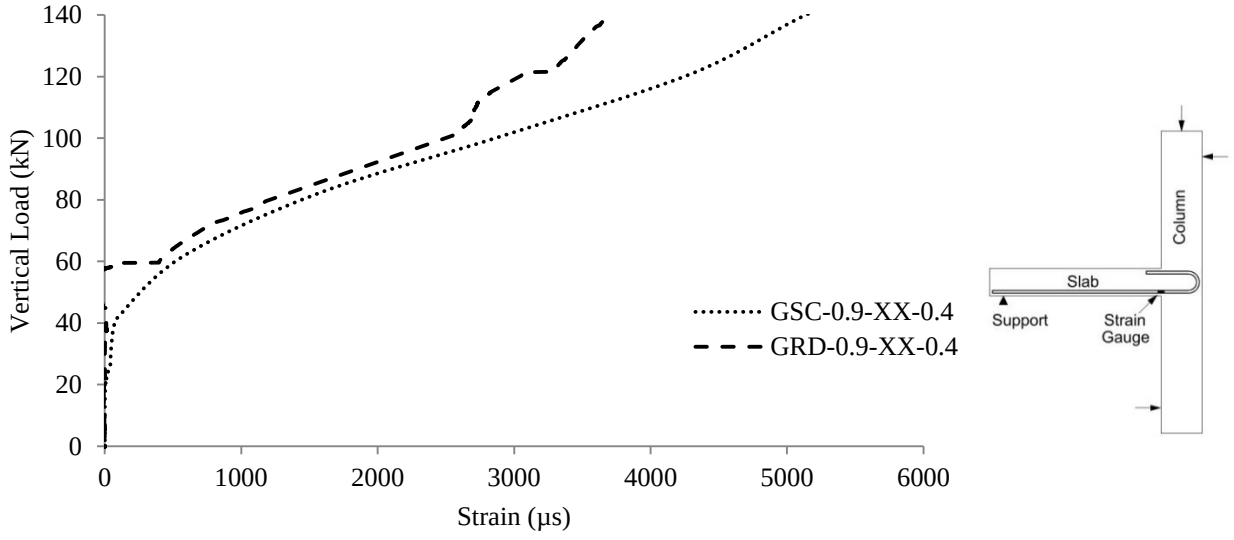


Figure 4.13: Load-reinforcement strain at early load stages

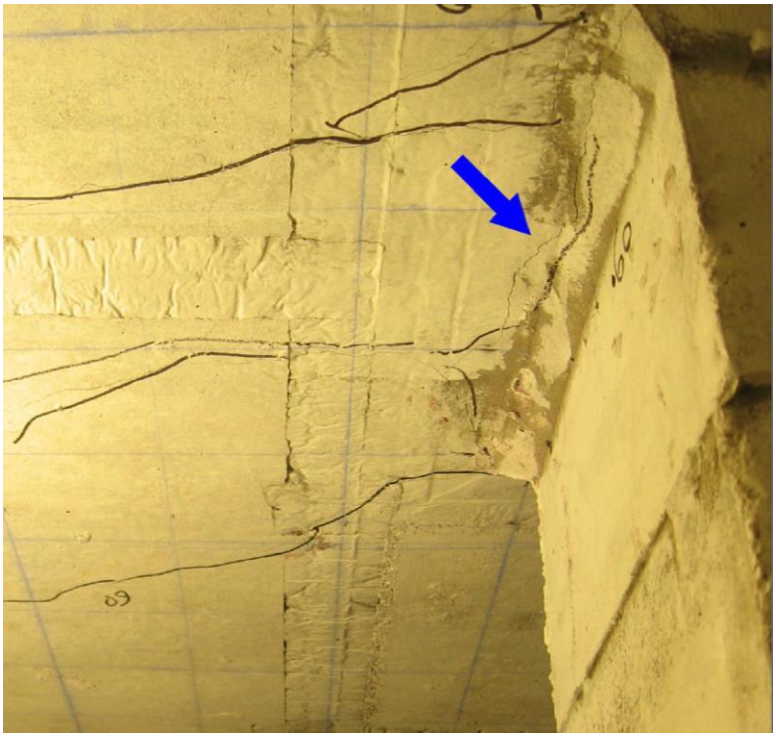

Figure 4.14: The formation of a crack at the inner column face in connection GRD-0.9-XX-0.4

The deformability factors, *J*, for the GFRP-RC connections are listed in Table 4.4. The connections showed considerable deformability with a deformability factor of 24.1 and 19.4 for connections GSC-0.9-XX-0.4 and GRD-0.9-XX-0.4, respectively. This demonstrates the capability of the GFRP-RC connections to provide an ample warning before failure.

### 4.3.3. Flexural Reinforcement and Concrete Strains

Figure 4.15 shows the relationship between the vertical load and the reinforcement and concrete strains at the column face. The maximum reinforcement and concrete strain for connection GRD-0.9-XX-0.4 were 7980 μs and 1460 μs which are 47.8% and 41.6% of the ultimate tensile strain of the used ribbed-deformed GFRP bars and the concrete crushing strain specified by the CAN/CSA S806-12, respectively. This indicates that the failure of the connection was pure punching shear rather than flexural failure.

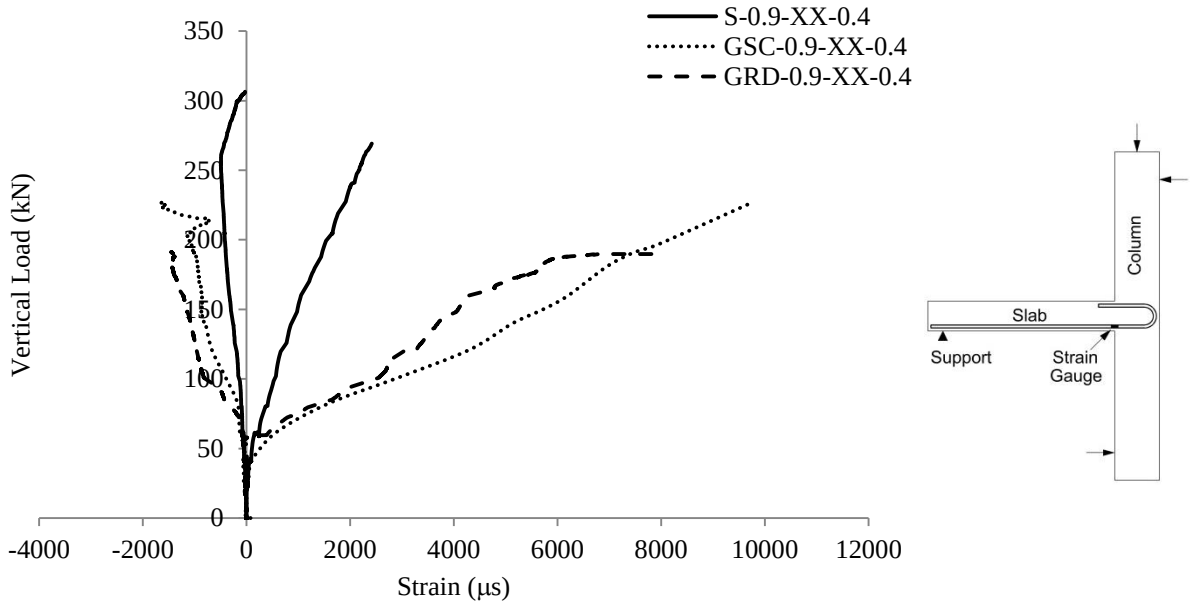


Figure 4.15: Load-strain relationship for Series II connections

For the three connections, the strains after cracking varied linearly with increasing the vertical load; however, there were two distinctive characters describing the behaviour of connection GRD-0.9-XX-0.4. The first is a kink in the load-reinforcement strain curve at a load of approximately 100 kN which depicts the stabilization of crack formation at the column face (Section 4.3.2). The second is a plateau before failure similar to the yielding plateau that defines the behaviour of steel-RC connections after reinforcement yielding. This plateau is characterized by an increase in the strains from 6000 μs at a load of 187 kN to 7980 μs at a load of 191.2 kN (at failure); this is a 33% increase in the strain with only 2% increase in the load. This sudden increase in the strain readings before failure was evident not only at the column face but approximately along the whole length of the reinforcing bars passing through the column in the directions perpendicular and parallel to the free edge as shown in Figure 4.16.

Figure 4.16 shows the strain profiles for these two bars. In the direction perpendicular to the free edge, the strains are inversely proportional to the distance from the column face up to 90% of the

failure load when the strains suddenly increased. The increase was 66%, 56%, 215% and 146% for gauges number 1, 3, 4 and 5, respectively, while gauge number 2 malfunctioned at 70% of the failure load. Furthermore, in the direction parallel to the free edge, the strain profile became approximately uniform along the whole length of the bar as the strains increased at 90% of the failure load by 30%, 97%, 57% and 82% for gauges number 22, 33, 44 and 55, respectively, while gauge number 11 malfunctioned at 90% of the failure load. This indicates a loss of bond between the reinforcing bar and the surrounding concrete.

Ospina et al. (2003) reported a similar behaviour of ribbed-deformed GFRP bars. They tested four full-scale slab-column interior connections; one reinforced with conventional steel bars, one reinforced with a two-dimensional GFRP grid and two were reinforced with ribbed-deformed GFRP bars with flexural reinforcement ratios of 0.73% and 1.46%. They reported a uniform strain distribution at failure in the connection reinforced with a 0.73% reinforcement ratio of ribbed-deformed GFRP bars.

Connection GSC-0.9-XX-0.4 which had the same flexural reinforcement ratio and the same bar diameter as connection GRD-0.9-XX-0.4 did not experience such behaviour (Figures 4.6 and 4.7). This implies that the used sand-coated bars have better bond characteristics than the used ribbed-deformed bars. Similar conclusions were found by other researchers (Cosenza et al. 1997; Kassem et al. 2011).

### 4.3.4. Punching Shear Capacity

The actual and the normalized failure loads for the three connections are listed in Table 4.5. Connections GSC-0.9-XX-0.4 and GRD-0.9-XX-0.4 had 26% and 37% less capacity than connection S-0.9-XX-0.4, respectively. This is attributed to the lower modulus of elasticity of the

GFRP bars (sand-coated and ribbed-deformed) compared to that of the steel bars. However, the decrease in the capacity was more pronounced for connection GRD-0.9-XX-0.4 than connection GSC-0.9-XX-0.4 due to the loss of bond experienced in connection GRD-0.9-XX-0.4. Consequently, connection GRD-0.9-XX-0.4 had 15.8% less capacity than connection GSC-0.9-XX-0.4 although they have very similar effective flexural reinforcement ratio.

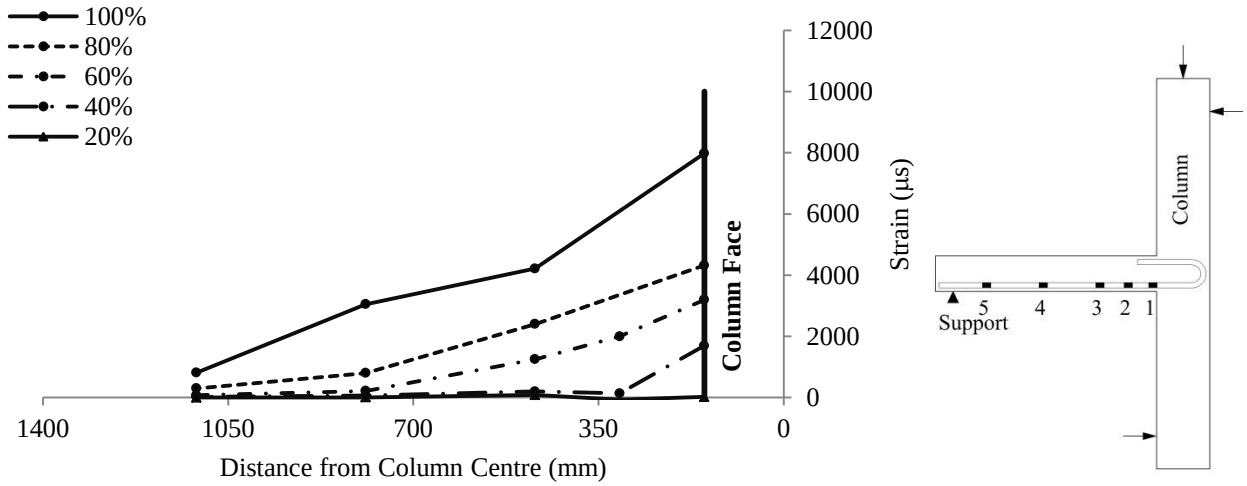


a) Perpendicular to the free edge

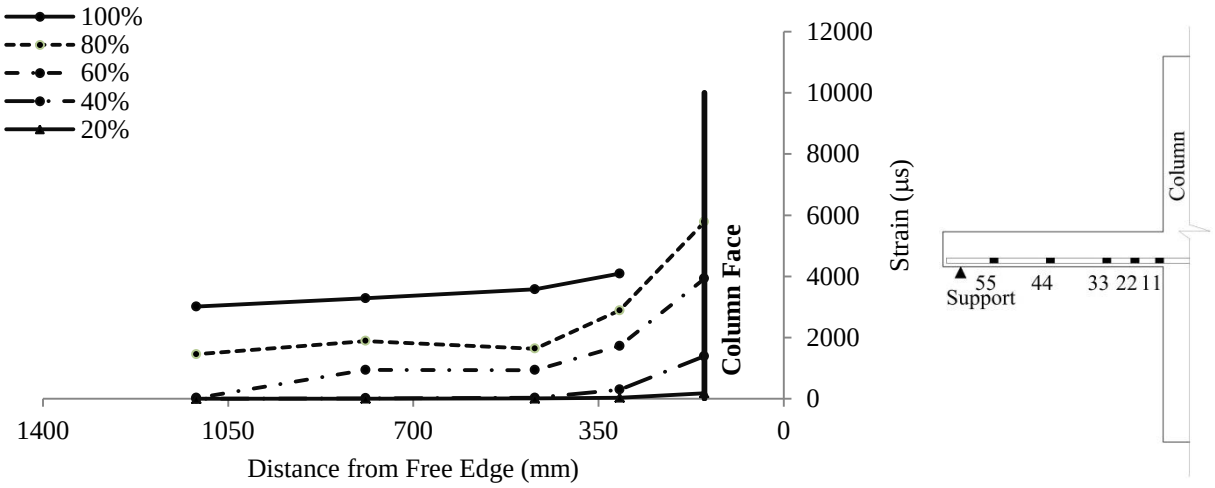


b) Parallel to the free edge

Figure 4.16: Reinforcement strain profile for connection GRD-0.9-XX-0.4

Table 4.5: Actual and normalized failure loads for Series II connections

| Connection | Effective Flexural Reinforcement Ratio, $\rho E/E_s$ (%) | Concrete Compressive Strength, $f_c'$ (MPa) | Actual Failure Loads (kN) | Normalized Failure Loads (kN) |
|---|---|---|---|---|
| S-0.9-XX-0.4 | 0.9 | 41.3 | 306.4 | 303.2 |
| GSC-0.9-XX-0.4 | 0.24 | 41.1 | 227.1 | 225.1 |
| GRD-0.9-XX-0.4 | 0.25 | 41.0 | 191.2 | 189.6 |

### 4.3.5. Code Comparisons

Table 4.6 shows a comparison between the actual failure loads and the predicted punching and flexural capacities of the three GFRP-RC connections. For the GFRP-RC connections, the ultimate capacities were considerably lower than the predictions of the yield line theory with an average $V_{Test}/V_{flex}$ of 0.75 ± 0.1 which confirms that the connections failed in a brittle punching mode. On the other hand, the CAN/CSA S806-12 and the JSCE 1997 give very close predictions; their predictions are slightly conservative with an average $V_{Test}/V_{Pred}$ of 1.21 ± 0.14 and 1.16 ± 0.13, respectively. This conservatism allowed both codes to provide an adequate safety margin for the loss of bond in connection GRD-0.9-XX-0.4. On the contrary, the ACI 440.1R-06 highly underestimates the capacities with an average $V_{Test}/V_{Pred}$ of 2.13 ± 0.26. For connection S-0.9-XX-0.4 reinforced with steel bars, the failure load was close to the flexural capacity with a $V_{Test}/V_{flex}$ of 0.92. However, yielding of the steel reinforcement was localized at the column vicinity only which indicates that a yield line pattern did not form and that the failure mode was brittle punching shear. Furthermore, the JSCE 2007 gives very good estimates with a $V_{Test}/V_{Pred}$ of 1.14. Also, although they do not consider the effect of the flexural reinforcement ratio, the CAN/CSA A23.3-04 and the ACI 440.1R-06 give good predictions with a $V_{Test}/V_{Pred}$ of 1.13 and 1.34, respectively.

For steel-RC connections, since the steel bars have a high modulus of elasticity, the depth of the neutral axis does not vary significantly with varying the flexural reinforcement ratio; therefore, the punching shear capacity is governed mainly by the concrete compressive strength. Accordingly, unlike the case of the FRP-RC connections, the design formulas that do not consider the effect of flexural reinforcement ratio or modulus will yield good results for the steel-RC connections (El-Ghandour et al. 1999).

## 4.4. SERIES III - EFFECT OF MOMENT-TO-SHEAR RATIO

Three connections were assigned to investigate the effect of moment-to-shear ratio on the punching shear behaviour, namely GSC-0.9-XX-0.2, GSC-0.9-XX-0.4 and GSC-0.9-XX-0.6.

### 4.4.1. Cracking Pattern and Mode of Failure

The three connections failed in a brittle punching shear mode with no signs of flexural failure, i.e. concrete crushing at the compression face of the slab. Also, the cracking behaviour of the three connections was similar. For connection GSC-0.9-XX-0.2, flexural cracks on the tension face of the slab were first observed at the column face at a vertical load of 35 kN (Table 4.7). Then, radial cracks started to propagate from all column faces towards the supported edges. The first circumferential crack formed 290 mm from the inner column face at a vertical load of 100 kN. Similarly, for connection GSC-0.9-XX-0.6, the first crack was observed at the side face of the column at a vertical load of 34 kN. Radial cracks then started to propagate from the column vicinity towards the supported edges at a load of 80 kN. The first circumferential crack formed 350 mm from the inner column face at a vertical load of 100 kN. Figure 4.17 shows the cracking pattern at failure for both connections on the tension face.

Table 4.6: Code comparisons for Series II connections

| Connection | Actual Failure Loads, $V_{Test}$ (kN) | Punching Shear Capacity Predictions, $V_{Pred}$ | | | | | | | |
|---|---|---|---|---|---|---|---|---|---|
| | | CAN/CSA S806-12 | | ACI 440.1R-06 | | JSCE 1997 | | Yield Line Theory | |
| | | $V_{Pred}$ | $V_{Test}/V_{Pred}$ | $V_{Pred}$ | $V_{Test}/V_{Pred}$ | $V_{Pred}$ | $V_{Test}/V_{Pred}$ | $V_{Pred}$ | $V_{Test}/V_{Pred}$ |
| S-0.9-XX-0.4 | 306.4 | 272.1[*] | 1.13 | 229.5[$] | 1.34 | 269.2[#] | 1.14 | 332.6 | 0.92 |
| GSC-0.9-XX-0.4 | 227.1 | 173.5 | 1.31 | 98.5 | 2.31 | 181.4 | 1.25 | 275.9 | 0.82 |
| GRD-0.9-XX-0.4 | 191.2 | 172.4 | 1.11 | 98.5 | 1.94 | 180.8 | 1.06 | 279.2 | 0.68 |
| Mean[^] | | | 1.21 | | 2.13 | | 1.16 | | 0.75 |
| Standard Deviation[^] | | | 0.14 | | 0.26 | | 0.13 | | 0.1 |

[*]CAN/CSA A23.3-04
[$]ACI 318-11
[#]JSCE 2007
[^]for connections GSC-0.9-XX-0.4 and GRD-0.9-XX-0.4

Table 4.7: Test results for Series III connections

| Connection | Load (kN) | | Deflection (mm) | | Reinforcement Strain (μs) | | Stiffness Factor (kN/mm) | | Deformability Factor, $J$ | Concrete Strength, $f_c'$ (MPa) |
|---|---|---|---|---|---|---|---|---|---|---|
| | Cr | Fail | Cr | Fail | Cr | Fail | $k_i$ | $k_p$ | | |
| GSC-0.9-XX-0.2 | 35 | 239.4 | 0.3 | 52.1 | 97 | 9264[#] | 87.6 | 3.2 | 24.5 | 37.3 |
| GSC-0.9-XX-0.4 | 32 | 227.1 | 0.4 | 39.3 | 175 | 9776 | 91.8 | 3.7 | 24.1 | 41.1 |
| GSC-0.9-XX-0.6 | 34 | 159.1 | 0.3 | 18.9 | 100 | 7013[$] | 90.7 | 4.6 | 16.1 | 36.5 |

[*]Cr, at first cracking; Fail, at failure; $K_i$, pre-cracking stiffness factor; $k_p$, post-cracking stiffness factor; and $f_c'$, concrete compressive strength.
[#]parallel to the free edge
[$]at 89% of the failure load


a) Connection GSC-0.9-XX-0.2


b) Connection GSC-0.9-XX-0.6

Figure 4.17: Cracking on the tension face at failure for Series III connections

On the free edge, for connection GSC-0.9-XX-0.2, the first crack formed at the bottom corner of the column and extended instantaneously in the transverse direction to a distance of 120 mm from the slab soffit at a vertical load of 40 kN. Other cracks then started to form at farther distances from the column face. At a vertical load of approximately 100 kN, diagonal cracks started to propagate from all flexural cracks. The failure diagonal crack propagated from the flexural crack at the bottom column corner making an approximate steep angle of $67^{o}$ with the horizontal away from the column. However, all other diagonal cracks propagated towards the column. Similarly, for connection GSC-0.9-XX-0.6, the first crack formed at the bottom corner of the column and extended instantaneously in the transverse direction until it approximately reached the top surface of the slab at a height of 190 mm from the slab soffit at a vertical load of 60 kN. At a vertical load of 80 kN, the failure diagonal crack propagated from the flexural crack located 100 mm away from the column corner and extended rapidly through the thickness of the slab making an approximate angle of $44^{o}$ with the horizontal plane. Figure 4.18 shows the cracking pattern at failure for both connections on the free edge. In general, increasing the moment-to-shear ratio decreased the number of cracks at failure on both the tension face and the free edge of the slab. Increasing the moment-to-shear ratio increased the shear stresses applied to the critical section which caused diagonal shear cracks to propagate faster and shear failure to occur before significant flexural cracks form.

Connections GSC-0.9-XX-0.2 and GSC-0.9-XX-0.6 were saw-cut in the direction perpendicular to the free edge after the test to investigate the propagation of diagonal cracks inside the slabs as shown in Figures 4.19 and 4.20. The diagonal shear crack extended from the column face at the compression face of the slab to the tension face of the slab with different inclination angles. Increasing the moment-to-shear ratio pushed the failure surface on the tension face of the slab

away from the column and led to a flatter angle of the diagonal crack. Increasing the ratio from 0.2 to 0.6 m decreased the diagonal crack angle with the horizontal at the tension face by 10% (from 28.3$^{o}$ to 25.5$^{o}$) and at the free edge by 34%. This agrees with the findings of El-Salakawy et al. (1998) and Marzouk et al. (2000).

a) Connection GSC-0.9-XX-0.2

b) Connection GSC-0.9-XX-0.6

Figure 4.18: Cracking on the free edge at failure for Series III connections


a) Connection GSC-0.9-XX-0.2

Figure 4.19: Internal diagonal cracks in the direction perpendicular to the free edge at failure

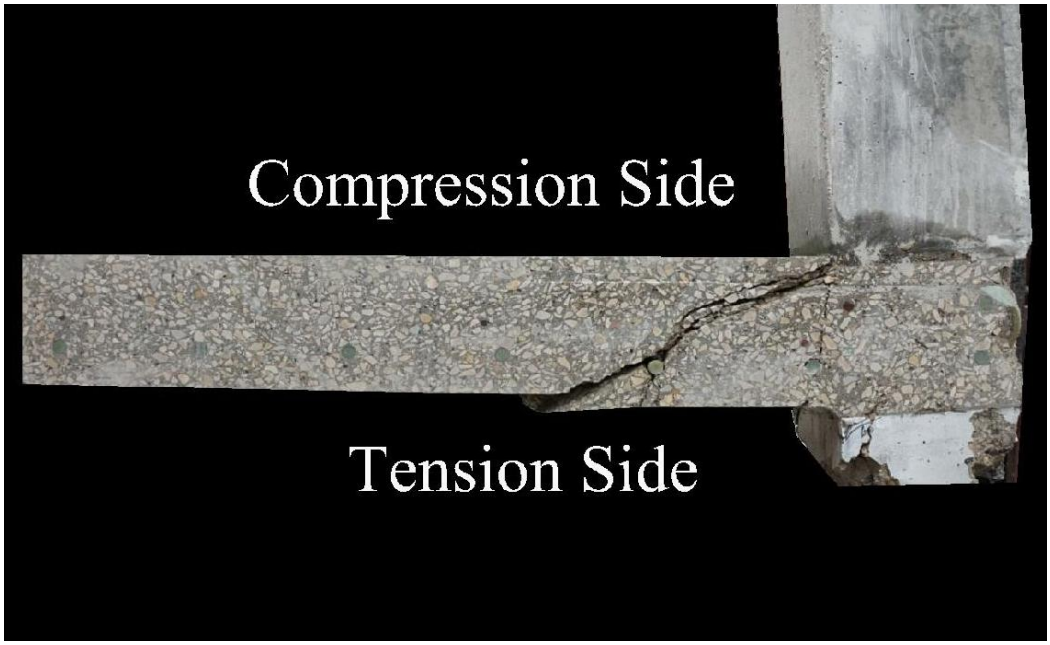


b) Connection GSC-0.9-XX-0.6

Figure 4.19: Internal diagonal cracks in the direction perpendicular to the free edge at failure - continued

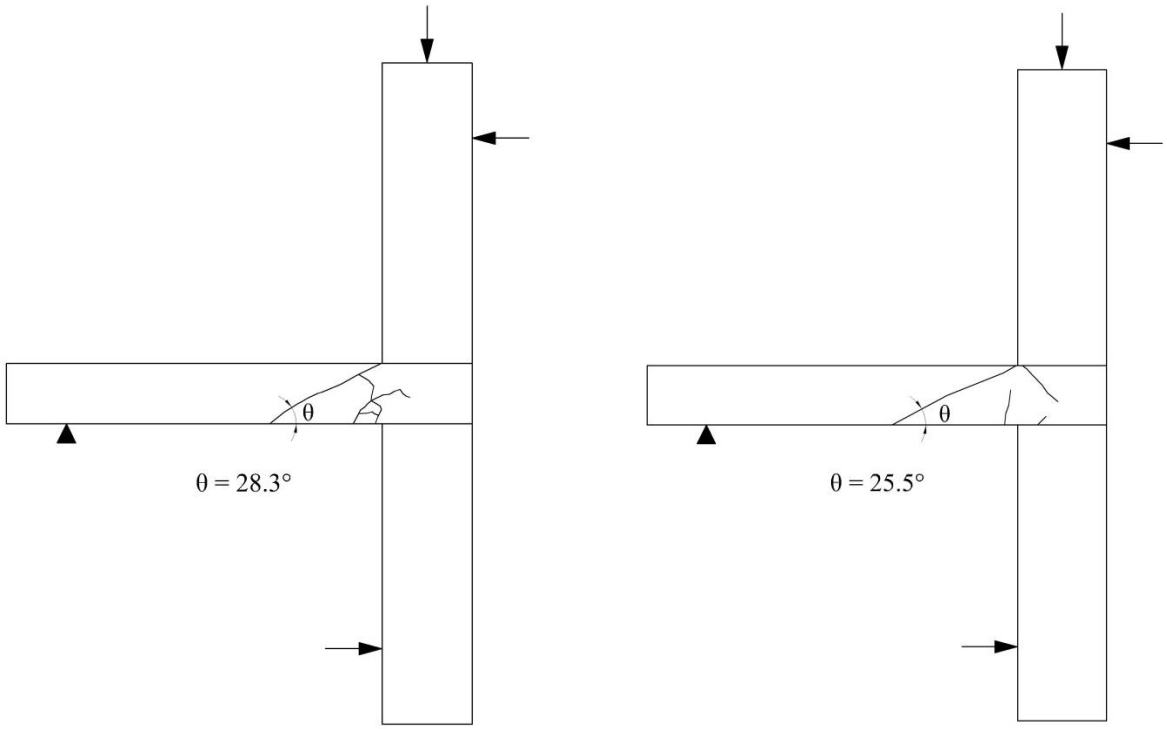


a) GSC-0.9-XX-0.2 b) GSC-0.9-XX-0.6

Figure 4.20: Schematic drawing of the internal cracks

Figure 4.21 shows the shear stress distribution on the critical shear perimeter located 0.5*d* from the column face at a slab-column edge connection for different loading cases. Depending on the value of the unbalanced moment transferred between the column and the slab, the shear stresses on the two perimeter sides, perpendicular to the free edge, will act on either one direction or two different directions as shown in Figure 4.21d and 4.21e, respectively. For the three connections discussed herein, the latter case took place. Accordingly, the failure cone will form as shown in Figure 4.22; while the diagonal cracks at the inner face of the column propagated from the tension face towards the column, the cracks at the free edge propagated from the tension face away from the column. The inclination angle in both cases depends on the value of the shear stresses. Furthermore, increasing the moment-to-shear ratio will change the shear stress distribution at the same vertical load level in the manner shown in Figure 4.23. The shear stress on the free edge at the same load level increases with increasing the moment-to-shear ratio. As a result, the angle of the shear cracks with the horizontal at the free edge is decreased.

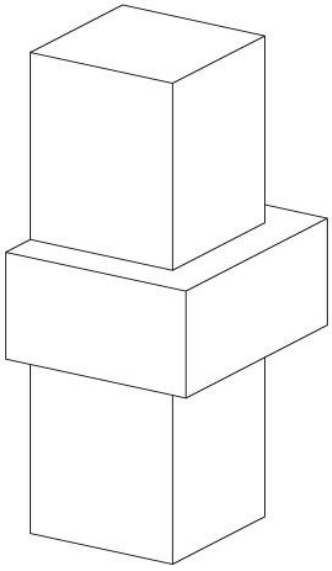

a) Critical section at an edge connection

Figure 4.21: Shear stress distribution on the shear perimeter

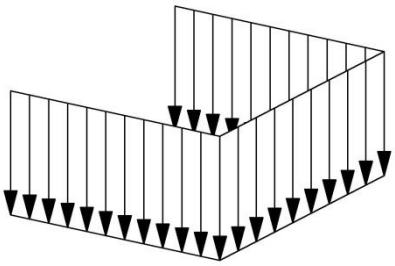

b) Shear stress due to shear force only

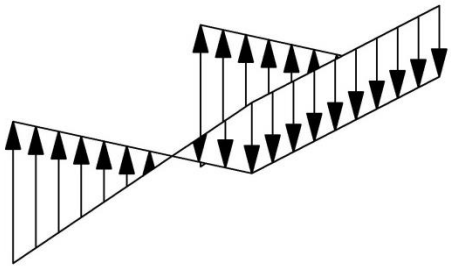

c) Shear stress due to moment only

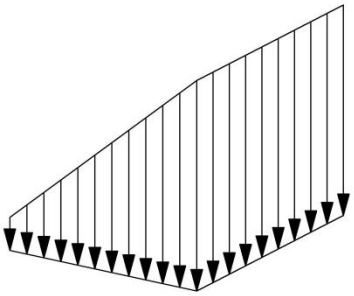

d) Total shear stress (high shear force)

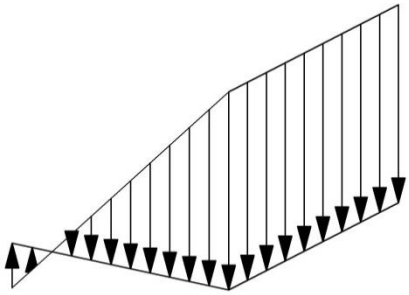

e) Total shear stress (high moment)

Figure 4.21: Shear stress distribution on the shear perimeter - continued

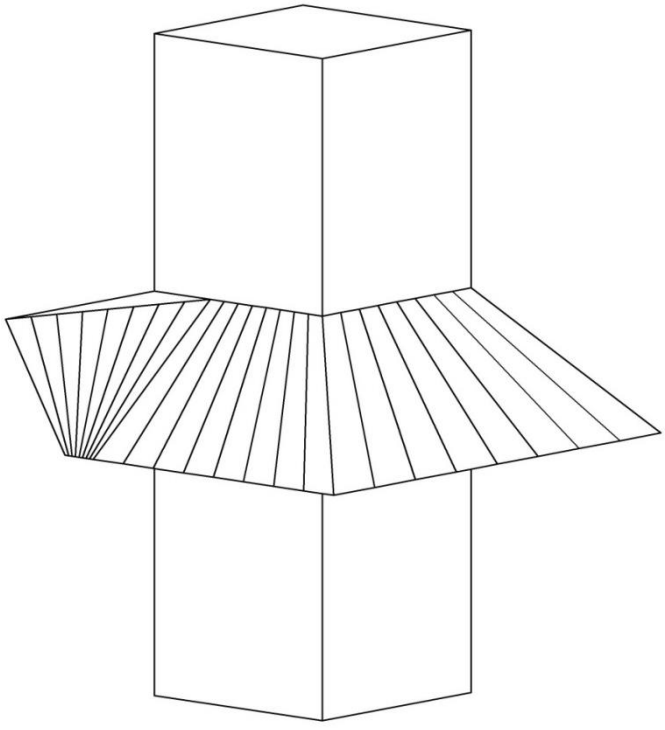

Figure 4.22: Expected failure cone (reproduced from Mortin 1989)

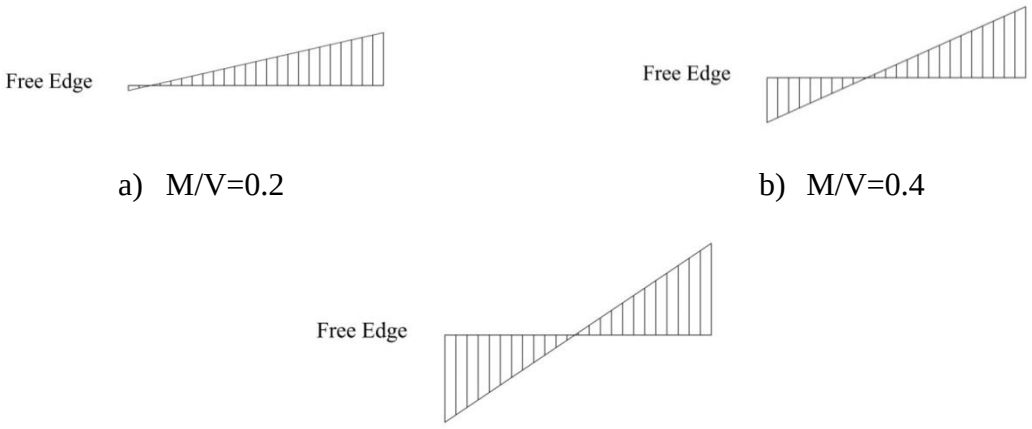


a) M/V=0.2

b) M/V=0.4

c) M/V=0.6

Figure 4.23: Shear stress distribution on the side face of the critical section, perpendicular to the free edge, at the same shear load level

### 4.4.2. Deflections

Figure 4.24 shows the relationship between the vertical load and the deflection at the column face. The moment-to-shear ratio has an insignificant effect on both the pre- and post-cracking stiffness of the connections. However, increasing the moment-to-shear ratio from 0.2 m to 0.4 m and 0.6 m decreased the maximum deflections by 21.4% and 62.2%, respectively.

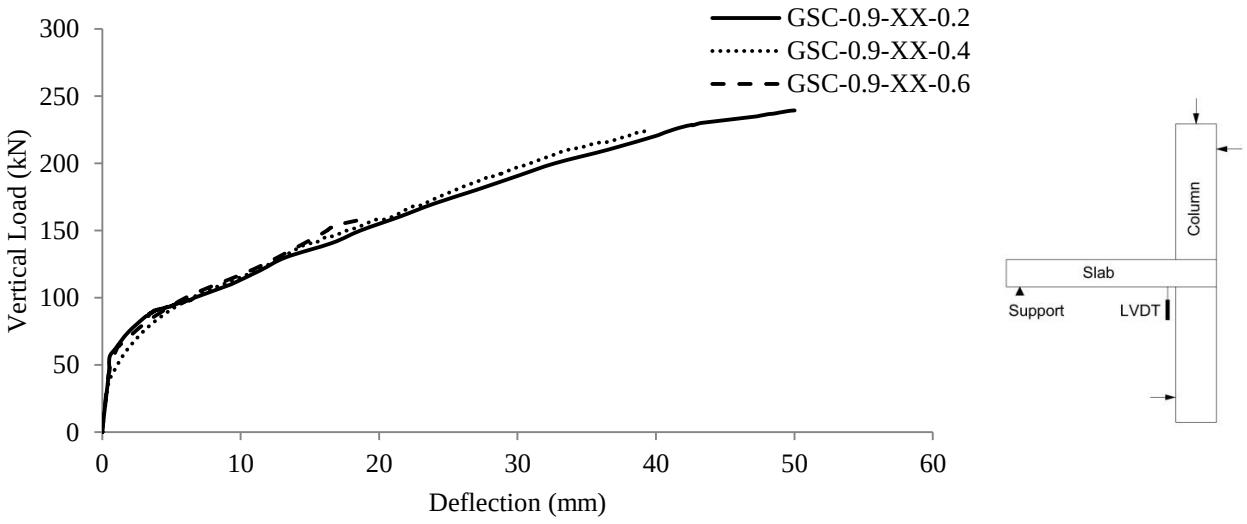


Figure 4.24: Load-deflection relationship for Series III connections

### 4.4.3. Flexural Reinforcement and Concrete Strains

Figure 4.25 shows the relationship between the vertical load and the reinforcement and concrete strains at the column face. It is to be noted that the reinforcement strain gauge in connection GSC-0.9-XX-0.6 malfunctioned at 85.5% of the failure load at a reading of 6754 μs. The reinforcement strains after cracking varied approximately linearly with the increasing the load; however, the rate of developing strains in connection GSC-0.9-XX-0.2 decreased abruptly at a vertical load of 95 kN due to the formation of a second circumferential crack farther from the column face. This is confirmed from Figure 4.26 which shows the strain distribution on the bar passing through the column in the direction perpendicular to the free edge for connection GRD-0.9-XX-0.4. It is obvious that gauge number 3 started to pick up strains at the same load level when the graph of gauges number 1 and 2 started to propagate steeper.

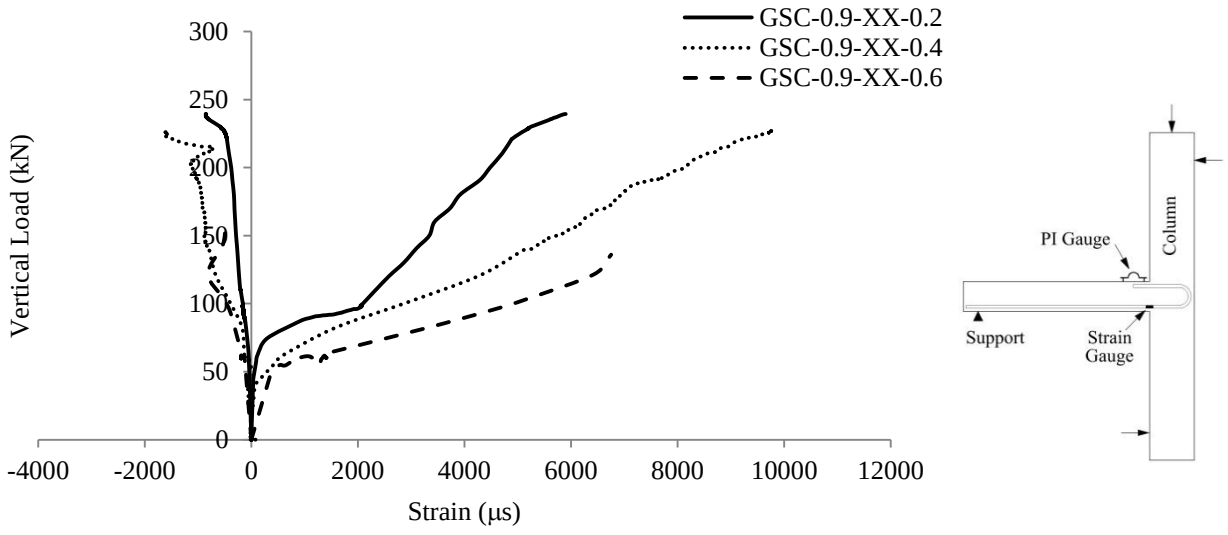


Figure 4.25: Load-strain relationship for Series III connections

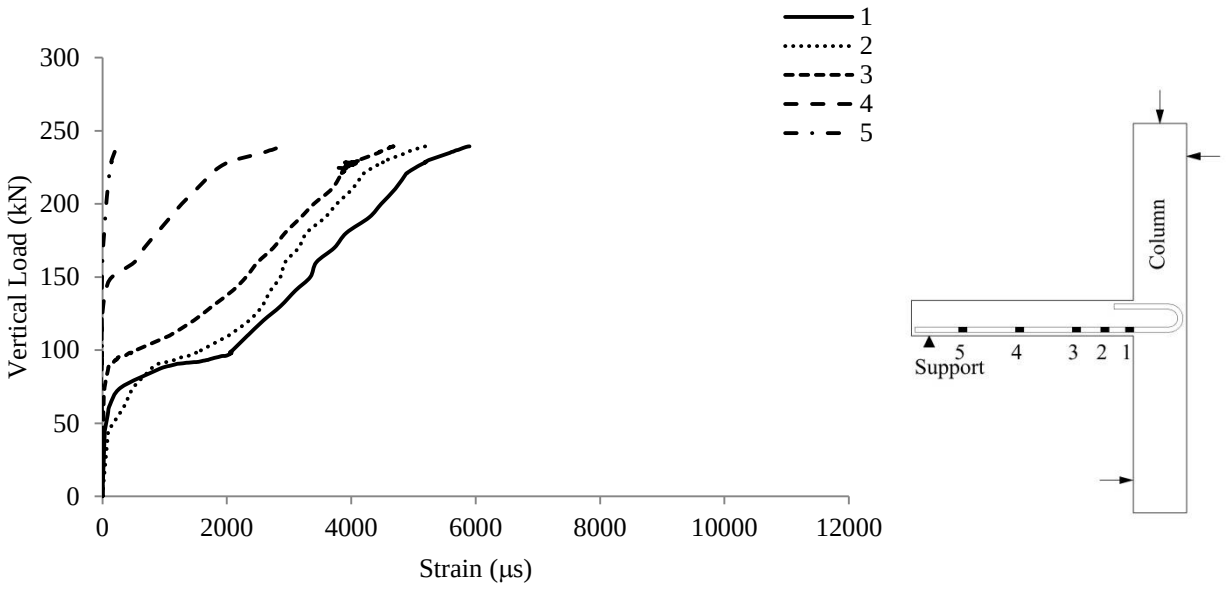


Figure 4.26: Load-reinforcement strain for connection GSC-0.9-XX-0.2

Increasing the moment-to-shear ratio increased the reinforcement and concrete strains at the same load level since increasing the applied unbalanced moment increases the longitudinal stresses applied at the slab section. The maximum recorded reinforcement strains at the column face are 9261 μs, 9776 μs and 6754 μs while the maximum recorded concrete strains are 736 μs, 1619 μs and 815 μs for connections GSC-0.9-XX-0.2, GSC-0.9-XX-0.4 and GSC-0.9-XX-0.6, respectively. These values were recorded in the direction perpendicular to the free edge for connections GSC-0.9-XX-0.4 and GSC-0.9-XX-0.6 and in the direction parallel to the free edge for connection GSC-0.9-XX-0.2. This indicates that applying a moment-to-shear ratio as low as 0.2 m reduced the radial moments in the strip perpendicular to the free edge compared to the strip parallel to the free edge.

This can be noticed in Figure 4.27 which shows the relationship between the vertical load and the reinforcement and concrete strains at the column face perpendicular and parallel to the free edge for the three connections. It can be seen that the perpendicular strains are less than the

parallel ones at all load levels in connection GSC-0.9-XX-0.2. With increasing the moment-to-shear ratio to 0.4 m, the perpendicular strains approaches the parallel ones and exceed them at higher load levels. With a further increase in the moment-to-shear ratio to 0.6 m, the perpendicular strains exceed the parallel ones at all load levels.

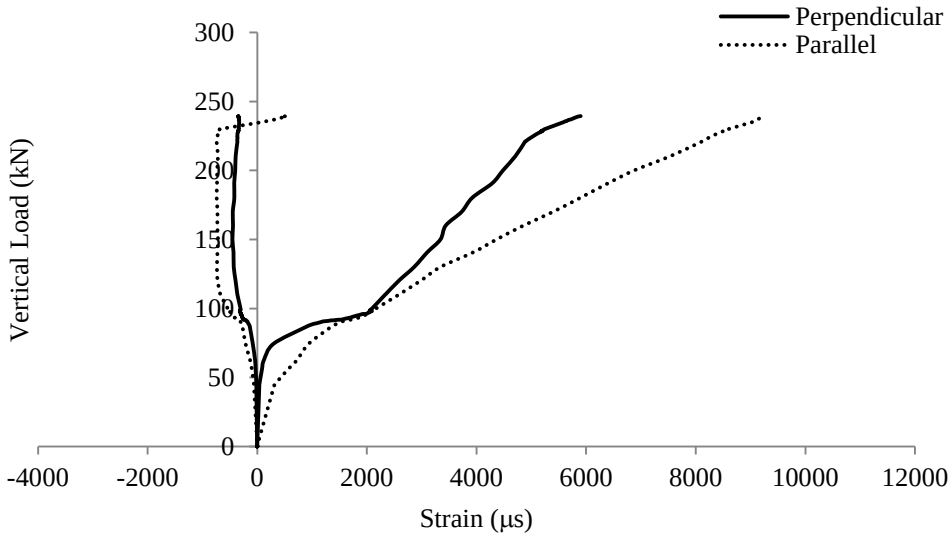


a) Connection GSC-0.9-XX-0.2

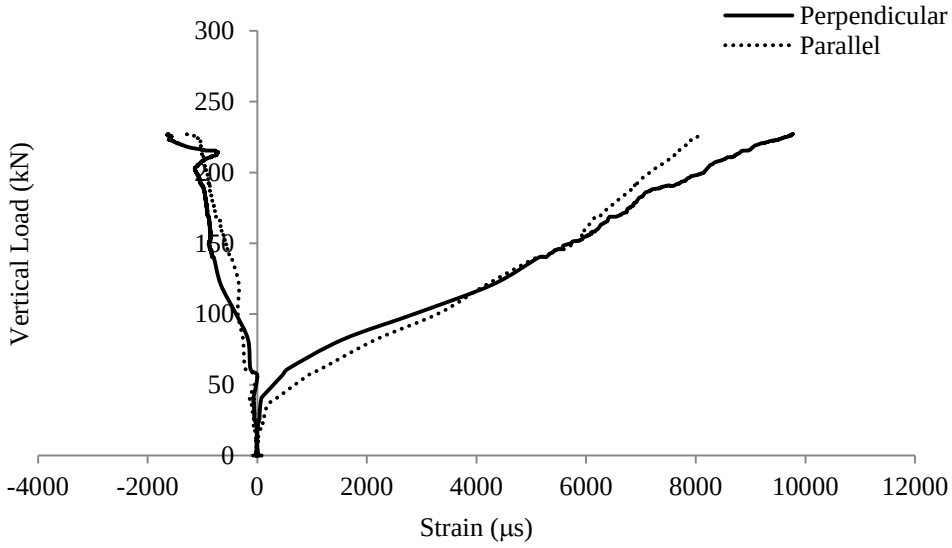


b) Connection GSC-0.9-XX-0.4

Figure 4.27: Load-reinforcement strain at the column face relationship

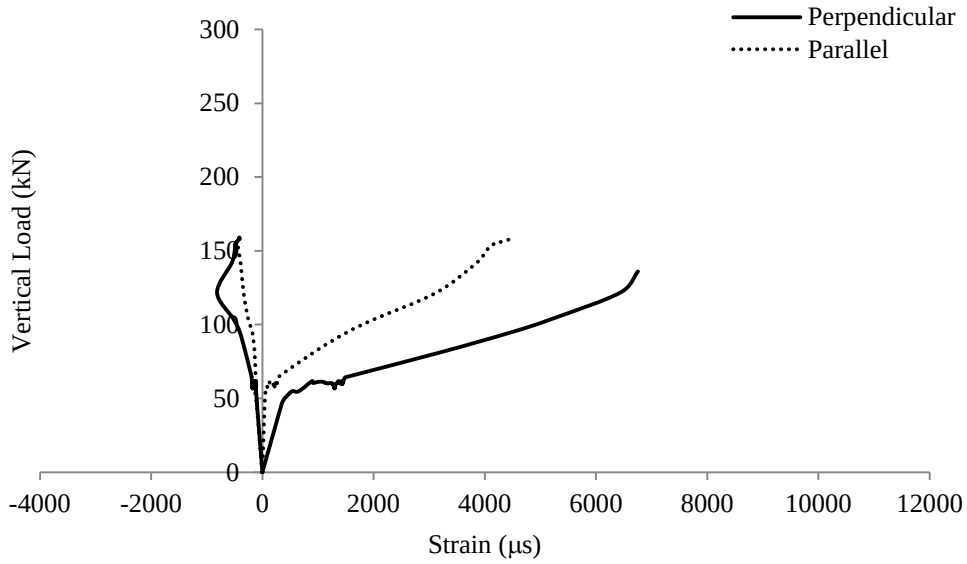


c) Connection GSC-0.9-XX-0.6

Figure 4.27: Load-reinforcement strain at the column face relationship - continued

Figure 4.28 and 4.29 show the reinforcement strain profiles connections GSC-0.9-XX-0.2 and GSC-0.9-XX-0.6 in the directions perpendicular and parallel to the free edge, respectively. For both connections, the strains are inversely proportional to the distance of the gauge from the free edge which indicates a good bond behaviour between the bars and the surrounding concrete. It is noted that the strains in the perpendicular direction along the whole length of the bar are lower than those in the parallel direction for connection GSC-0.9-XX-0.2 and higher for connection GSC-0.9-XX-0.6 due to the increased moment-to-shear ratio.

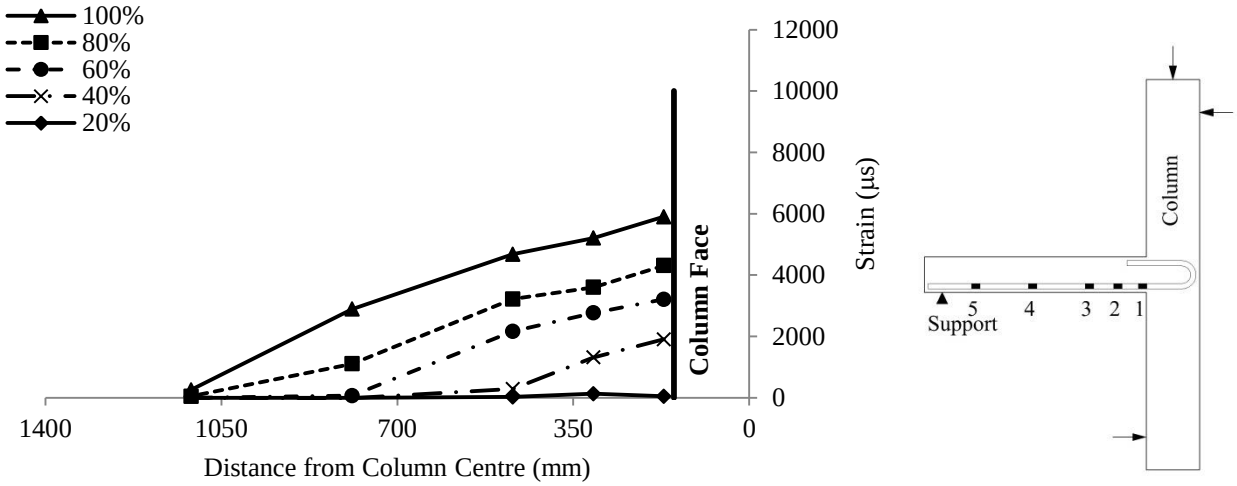


a) Connection GSC-0.9-XX-0.2

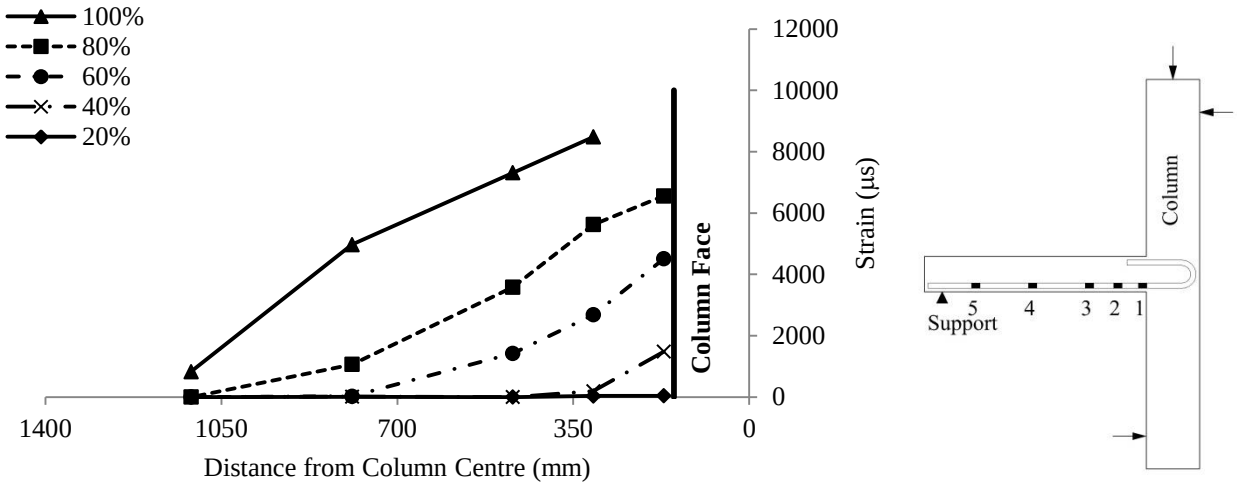


b) Connection GSC-0.9-XX-0.6

Figure 4.28: Reinforcement strain profile perpendicular to the free edge for Series III connections

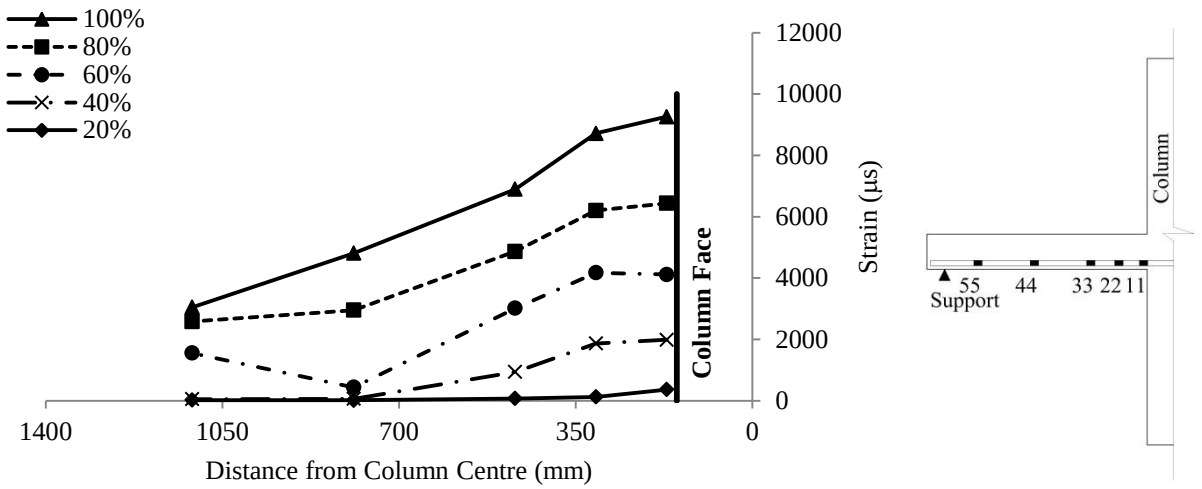


a) Connection GSC-0.9-XX-0.2

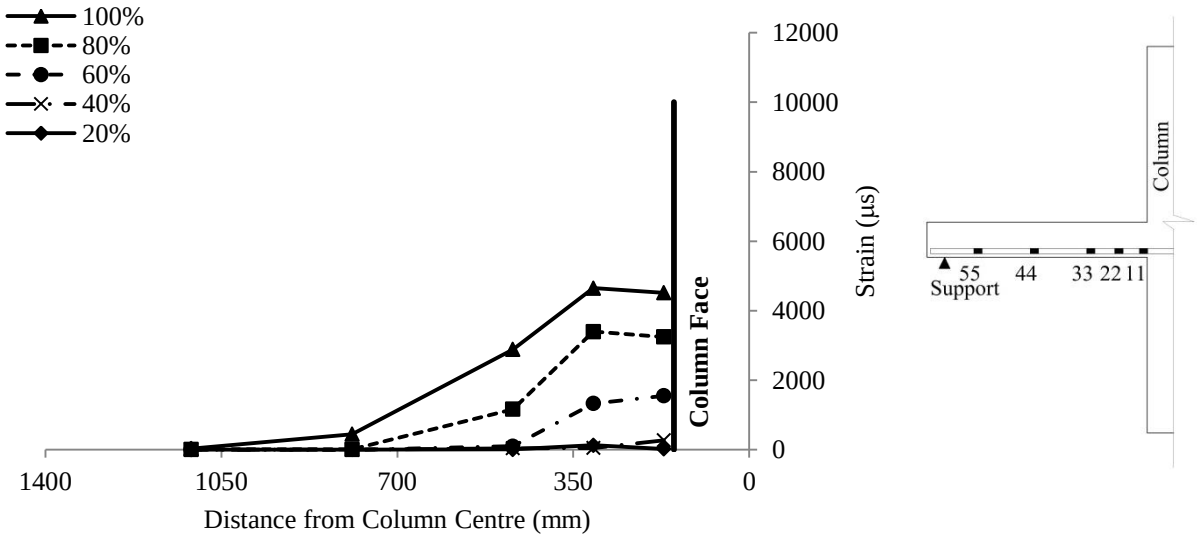


b) Connection GSC-0.9-XX-0.6

Figure 4.29: Reinforcement strain profile parallel to the free edge for Series III connections

### 4.4.4. Punching Shear Capacity

The actual and normalized failure loads are listed in Table 4.8 and the relationship between the moment-to-shear ratio and the normalized failure vertical load is shown in Figure 4.30. Increasing the moment-to-shear ratio from 0.2 m to 0.4 m and 0.6 m decreased the normalized

capacity by 8.1% and 33.1%, respectively. This is a result of the increased shear stresses at the critical shear perimeter due to the increased unbalanced moment as shown in Equation 2.3 (Section 2.4.3.1).

Table 4.8: Actual and normalized failure loads for Series III connections

| Connection | Moment-to-Shear Ratio, *M/V* (m) | Concrete Compressive Strength, $f_c'$ (MPa) | Actual Failure Loads (kN) | Normalized Failure Loads (kN) |
|---|---|---|---|---|
| GSC-0.9-XX-0.2 | 0.2 | 37.3 | 239.4 | 245.0 |
| GSC-0.9-XX-0.4 | 0.4 | 41.1 | 227.1 | 225.1 |
| GSC-0.9-XX-0.6 | 0.6 | 36.5 | 159.1 | 164.0 |

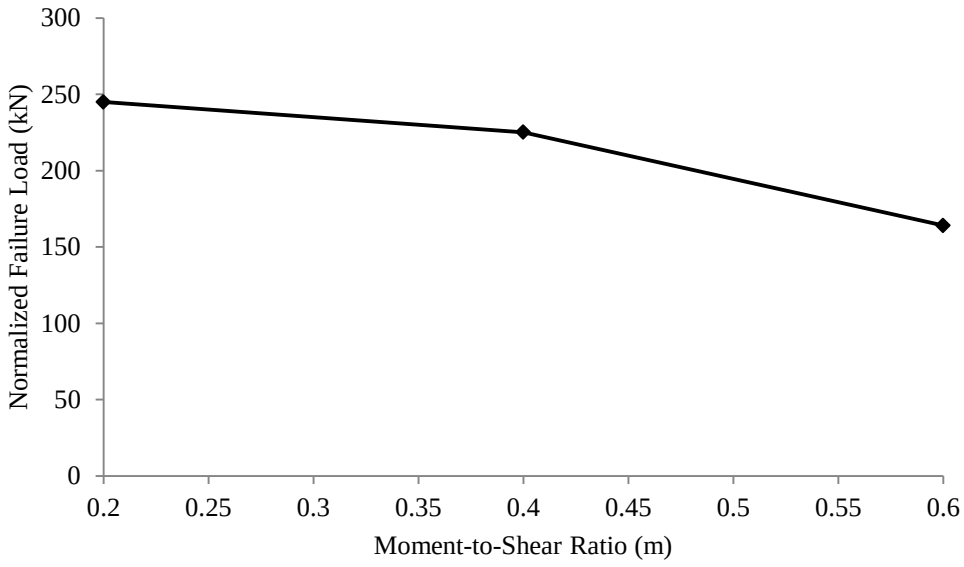


Figure 4.30: Effect of moment-to-shear ratio on the normalized failure load

### 4.4.5. Code Comparisons

Table 4.9 shows comparisons between the actual failure loads and the predicted punching and flexural capacities of the three connections. The ultimate capacities of the three connections were considerably lower than the predictions of the yield line theory with an average $V_{Test}/V_{flex}$ of 0.74

± 0.07 which confirms that the connections failed in a brittle punching mode rather than a deformable flexural mode. On the other hand, the CAN/CSA S806-12 and the JSCE 1997 give reasonable predictions with an average $V_{Test}/ V_{Pred}$ of 1.18 ± 0.16 and 1.11 ± 0.16, respectively. However, the JSCE 1997 overestimates the capacity of connection GSC-0.9-XX-0.2 with a $V_{Test}/ V_{Pred}$ of 0.93. Furthermore, ACI 440.1R-06 highly underestimates the capacities of the connections with an average $V_{Test}/ V_{Pred}$ of 2.07 ± 0.29. However, the degree of conservatism is considerably less for connection GSC-0.9-XX-0.2.

## 4.5. SERIES IV - EFFECT OF SHEAR REINFORCEMENT

Three connections were assigned to investigate the effect of shear reinforcement on the punching shear behaviour, i.e., GRD-0.9-XX-0.4, GRD-0.9-75-0.4 and GRD-0.9-50-0.4.

### 4.5.1. Cracking Pattern and Mode of Failure

Connection GRD-0.9-XX-0.4 (without shear reinforcement) failed in a brittle punching shear mode with some deformability due to the loss of bond between flexural reinforcing bar and the surrounding concrete as discussed in Section 4.3.1. On the contrary, connections GRD-0.9-75-0.4 and GRD-0.9-50-0.4 (with shear reinforcement) failed in a deformable flexure mode with considerable ample warning of impending failure. The flexural failure was characterized by substantial deflections before failure along with crushing of the concrete on the compression face of the slab at the column face as shown in Figure 4.31. The final cracking patterns on the tension face for the three connections (Figures 4.9 and 4.32) were very similar. Also, the cracking behaviour was similar to that described in Section 4.2.1. The only difference was that connection GRD-0.9-XX-0.4 showed a punching cone at failure while the other two connections did not. The test results are listed in Table 4.10.

Table 4.9: Code comparisons for Series III connections

| Connection | Actual Failure Loads, $V_{Test}$ (kN) | Punching Shear Capacity Predictions, $V_{Pred}$ | | | | | | | |
|---|---|---|---|---|---|---|---|---|---|
| | | CAN/CSA S806-12 | | ACI 440.1R-06 | | JSCE 1997 | | Yield Line Theory | |
| | | $V_{Pred}$ | $V_{Test}/V_{Pred}$ | $V_{Pred}$ | $V_{Test}/V_{Pred}$ | $V_{Pred}$ | $V_{Test}/V_{Pred}$ | $V_{Pred}$ | $V_{Test}/V_{Pred}$ |
| GSC-0.9-XX-0.2 | 239.4 | 238.5 | 1.00 | 136.7 | 1.75 | 257.6 | 0.93 | 331.6 | 0.72 |
| GSC-0.9-XX-0.4 | 227.1 | 173.5 | 1.31 | 98.5 | 2.31 | 181.4 | 1.25 | 275.9 | 0.82 |
| GSC-0.9-XX-0.6 | 159.1 | 128.7 | 1.24 | 74.3 | 2.14 | 140 | 1.14 | 232.5 | 0.68 |
| Mean | | | 1.18 | | 2.07 | | 1.11 | | 0.74 |
| Standard Deviation | | | 0.16 | | 0.29 | | 0.16 | | 0.07 |

Table 4.10: Test results for Series IV connections

| Connection | Load (kN) | | Deflection (mm) | | Reinforcement Strain (μs) | | Stiffness Factor (kN/mm) | | Deformability Factor, $J$ | Concrete Strength, $f_c'$ (MPa) |
|---|---|---|---|---|---|---|---|---|---|---|
| | Cr | Fail | Cr | Fail | Cr | Fail | $k_i$ | $k_p$ | | |
| GRD-0.9-XX-0.4 | 36 | 191.2 | 0.5 | 38.0 | 138[#] | 7979 | 85 | 3.9 | 19.4 | 41.0 |
| GRD-0.9-75-0.4 | 42 | 255.9 | 0.5 | 48.1 | 150[#] | 7683 | 95 | 3.7 | 22.9 | 40.7 |
| GRD-0.9-50-0.4 | 36 | 272.9 | 0.3 | 75.1 | 149[#] | 7878 | 117 | 3.6 | 36.1 | 37.7 |

[*]Cr, at first cracking; Fail, at failure; $k_i$, pre-cracking stiffness factor; $k_p$, post-cracking stiffness factor; and $f_c'$, concrete compressive strength.
[#]parallel to the free edge

a) Connection GRD-0.9-75-0.4

b) Connection GRD-0.9-50-0.4

Figure 4.31: Concrete crushing at the compression face of the slab for Series IV connections

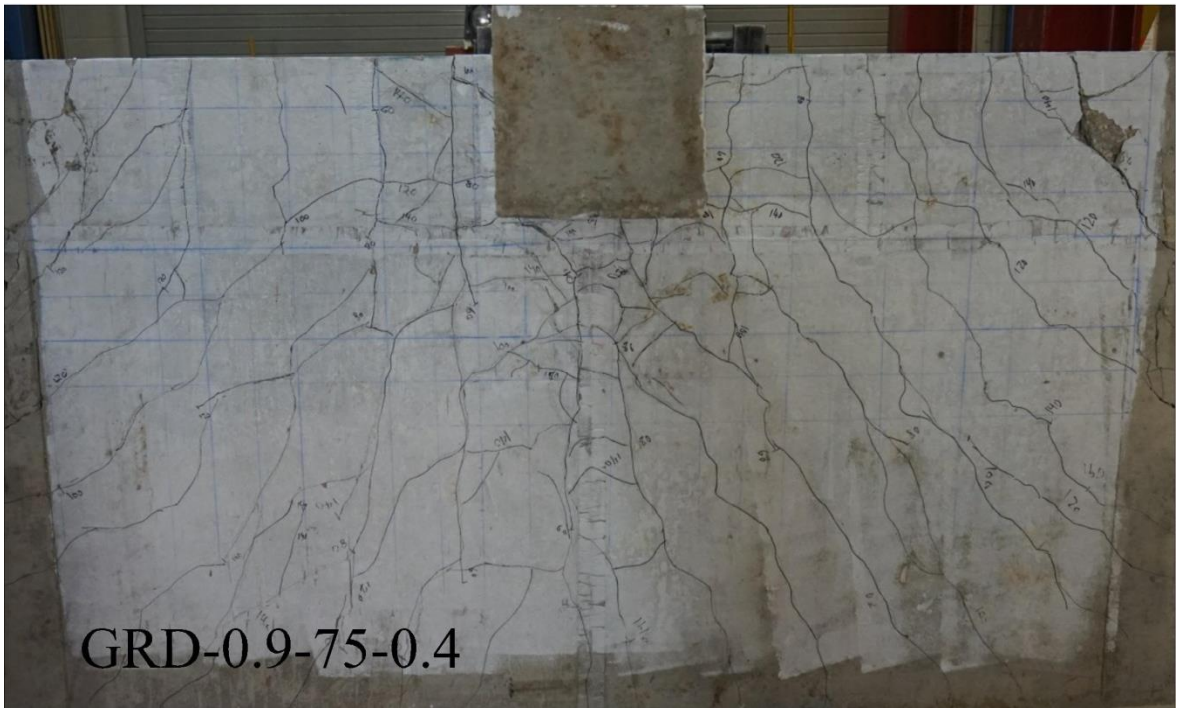


a) Connection GRD-0.9-75-0.4

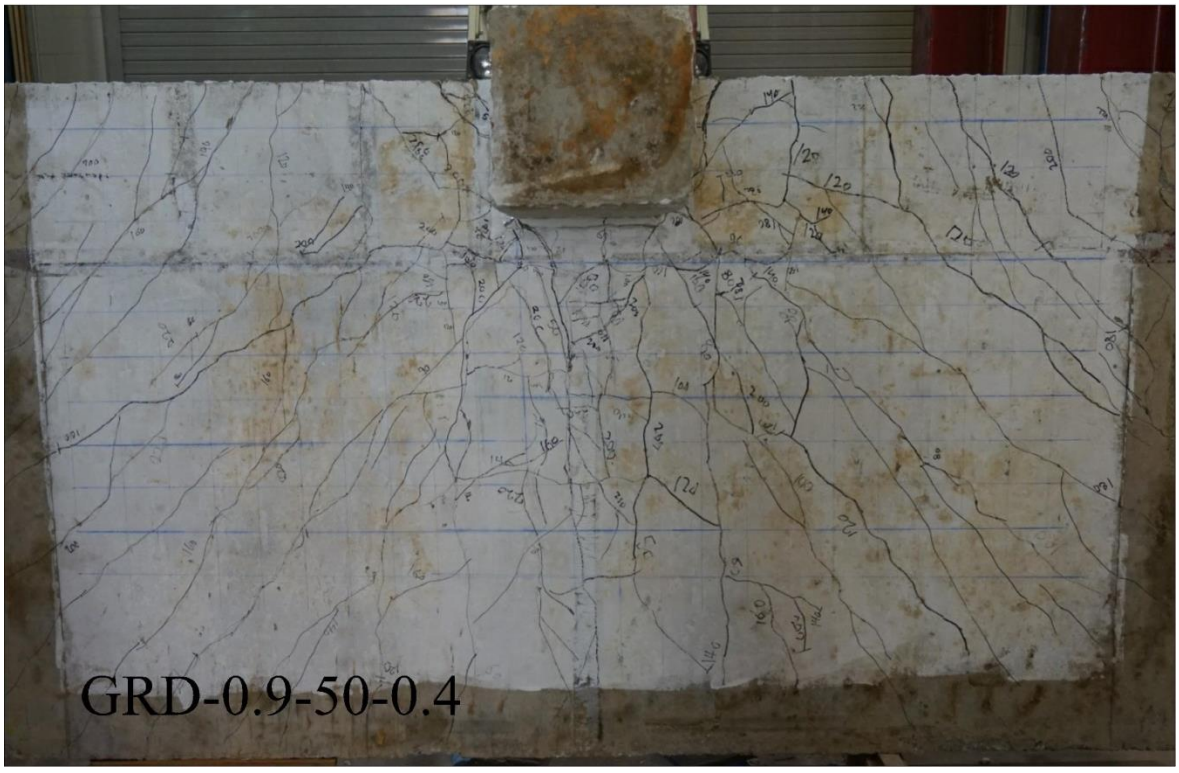


b) Connection GRD-0.9-50-0.4

Figure 4.32: Cracking on the tension face at failure for Series IV connections

Connections GRD-0.9-75-0.4 and GRD-0.9-50-0.4 were saw-cut in the direction perpendicular to the free edge after the test to investigate the propagation of diagonal cracks inside the slabs as shown in Figures 4.33 and 4.34. Although the columns did not punch in these two connections, fine diagonal cracks can be seen in the vicinity of the column (inside the shear-reinforced zone). The presence of the shear studs, however, controlled the propagation and prevented the widening of these diagonal cracks which allowed the connections to reach their flexural capacity. For both connections, the diagonal crack started from the compression face of the slab at the column face and crossed the first line of studs (located at a distance 0.4*d* from the column face) at the upper head. This crack, then, propagated making a relatively mild angle of $24^{o}$ with the horizontal in connection GRD-0.9-75-0.4 and crossed the following two lines of studs. However, in connection GRD-0.9-50-0.4, the diagonal crack propagated making a steeper angle of $63^{o}$ with the horizontal and did not cross the second line of studs. Similar behaviour was reported in the literature on steel-RC slab-column connections (Lips et al. 2012).


a) Connection GRD-0.9-75-0.4

Figure 4.33: Internal cracks in the direction perpendicular to the free edge at failure


b) Connection GRD-0.9-50-0.4

Figure 4.33: Internal cracks in the direction perpendicular to the free edge at failure - continued

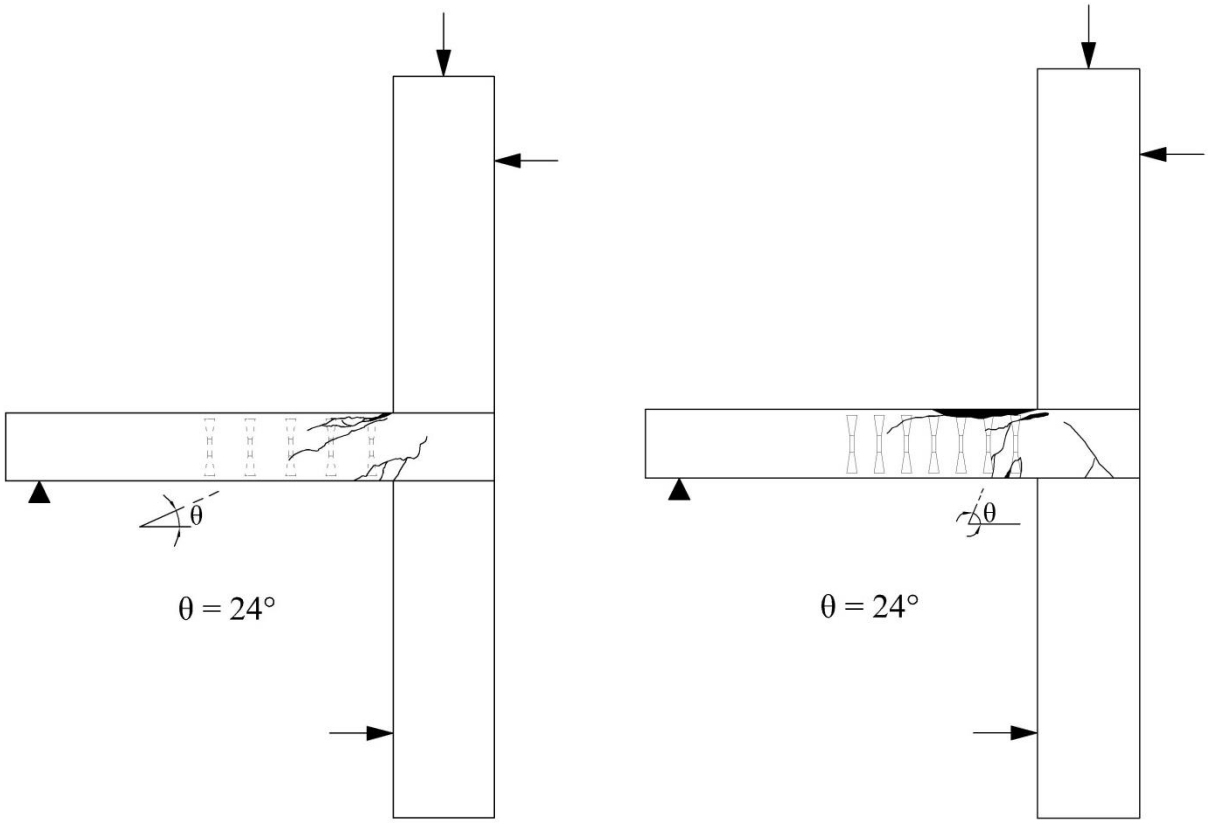


a) Connection GRD-0.9-75-0.4 b) Connections GRD-0.9-50-0.4

Figure 4.34: Schematic drawing of the internal cracks

On the free edge, for connection GRD-0.9-75-0.4, the first crack started from the bottom column corner and extended to a height of 140 mm in the transverse direction at a vertical load of 40 kN. With increasing the load, other cracks started to form at farther distances from the column corners. The main diagonal crack propagated from the flexural crack located 110 mm away from the bottom column corner making an approximate angle of $42^{o}$ with the horizontal at a vertical load of 140 kN. However, the shear studs managed to control the widening of this crack preventing the brittle punching shear failure. Connection GRD-0.9-50-0.4 behaved similarly; however, the main diagonal crack propagated with a steeper angle of $71^{o}$ with the horizontal. Figure 4.35 shows the cracking patterns on the free edge at failure for both shear-reinforced connections.

a) Connection GRD-0.9-75-0.4

b) Connection GRD-0.9-50-0.4

Figure 4.35: Cracking on the free edge at failure for Series IV connections

### 4.5.2. Deflections

Figure 4.36 shows the relationship between the vertical load and the deflection at the column face. The shear reinforcement had very insignificant effect on the post-cracking stiffness. It, however, significantly increased the deformability of the connections. Connection GRD-0.9-75-0.4 (with shear studs spaced at 0.*75d*) had 18% higher deformability factor than connection

GRD-0.9-XX-0.4 (without shear studs). Furthermore, decreasing the spacing of the shear studs from 0.75*d* in connection GRD-0.9-75-0.4 to 0.5*d* in connection GRD-0.9-50-0.4 increased the deformability factor by 58% (from 22.9 to 36.1). Also, the well-anchored double-headed shear studs substantially increased the deformation capacity of the connections. Connections GRD-0.9-75-0.4 and GRD-0.9-50-0.4 had 27% and 98% higher deflections at failure than connection GRD-0.9-XX-0.4.

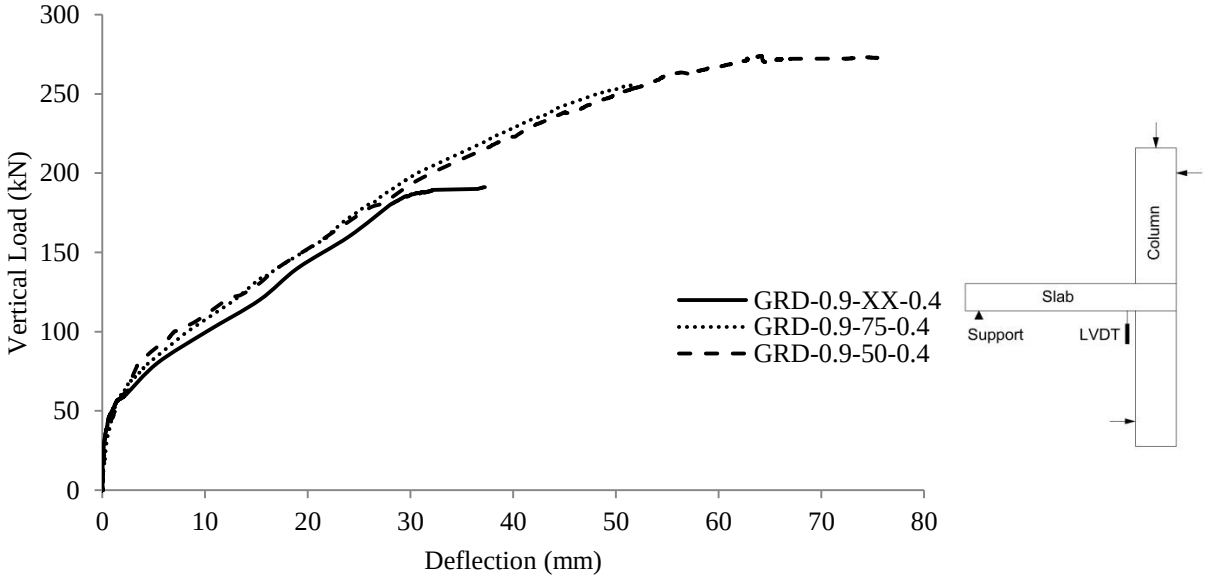


Figure 4.36: Load-deflection relationship for Series IV connections

### 4.5.3. Flexural Reinforcement and Concrete Strains

Figure 4.37 shows the relationship between the vertical load and the reinforcement and concrete strains at the column face. Again, for the three connections, the reinforcement strains after cracking varied approximately linearly with increasing the vertical load except for connection GRD-0.9-XX-0.4 where a plateau was experienced before failure due to the loss of bond between the bar and the surrounding concrete at this location (Section 4.3.3). Accordingly, although it failed at a lower load, connection GRD-0.9-XX-0.4 had higher reinforcement strain at

failure (7979 με) than connections GRD-0.9-75-0.4 (7683 με) and GRD-0.9-50-0.4 (7878 με). The maximum concrete strains were 1455 με, 2312 με and 5382 με for connections GRD-0.9-XX-0.4, GRD-0.9-75-0.4 and GRD-0.9-50-0.4, respectively, which might indicate that only connection GRD-0.9-50-0.4 exhibited a flexural failure mode. However, concrete crushing at the column face on the compression face of the slab was observed for both connections with shear reinforcement, i.e., connections GRD-0.9-75-0.4 and GRD-0.9-50-0.4), as shown in Figure 4.31.

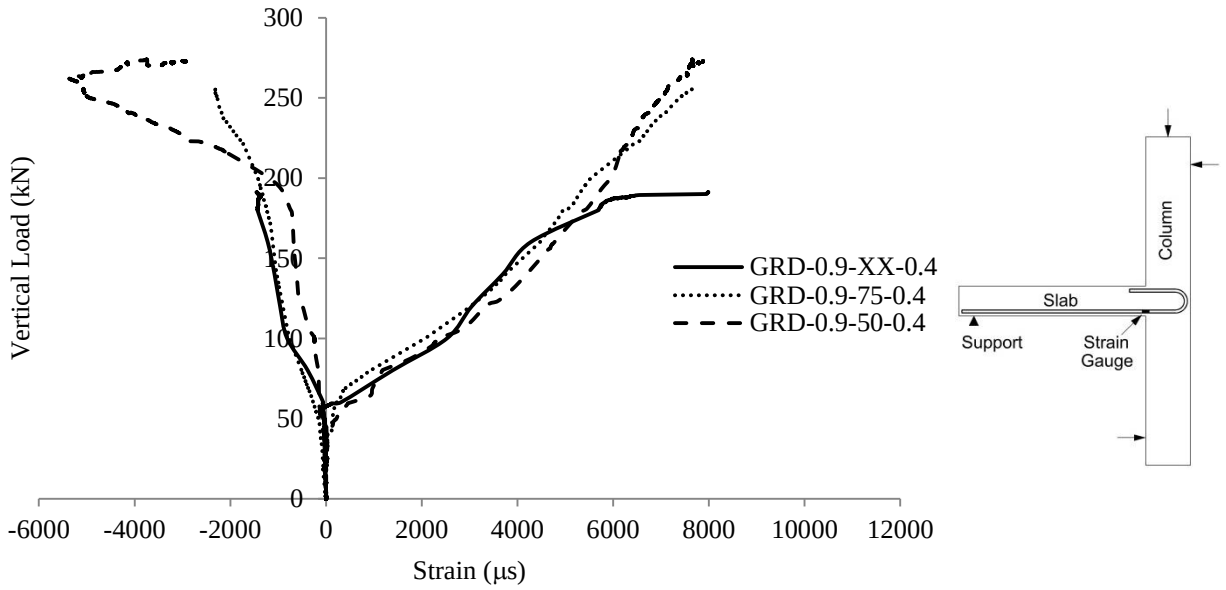


Figure 4.37: Load-strain relationship for Series IV connections

Figures 4.38 and 4.39 show the strain profiles for the three connections in the directions perpendicular and parallel to the free edge, respectively. Similar to connection GRD-0.9-XX-0.4 (see Section 4.3.3), connection GRD-0.9-50-0.4 exhibited a loss of bond between the bar and the surrounding concrete before failure. This can be seen from the approximately uniform strain distribution in both directions at failure.

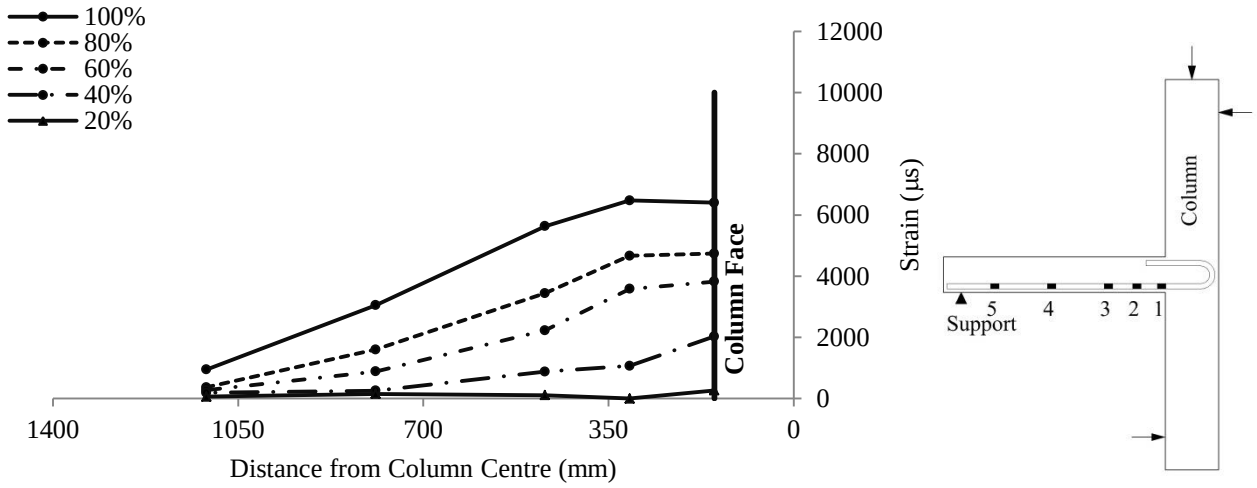


a) Connection GRD-0.9-75-0.4

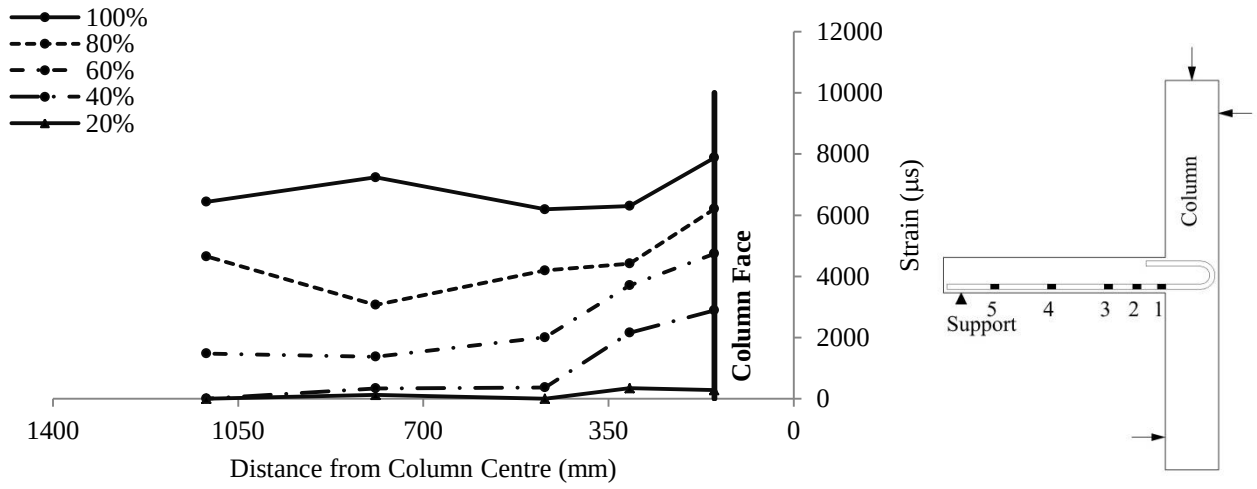


b) Connection GRD-0.9-50-0.4

Figure 4.38: Reinforcement strain profile perpendicular to the free edge for Series IV connections

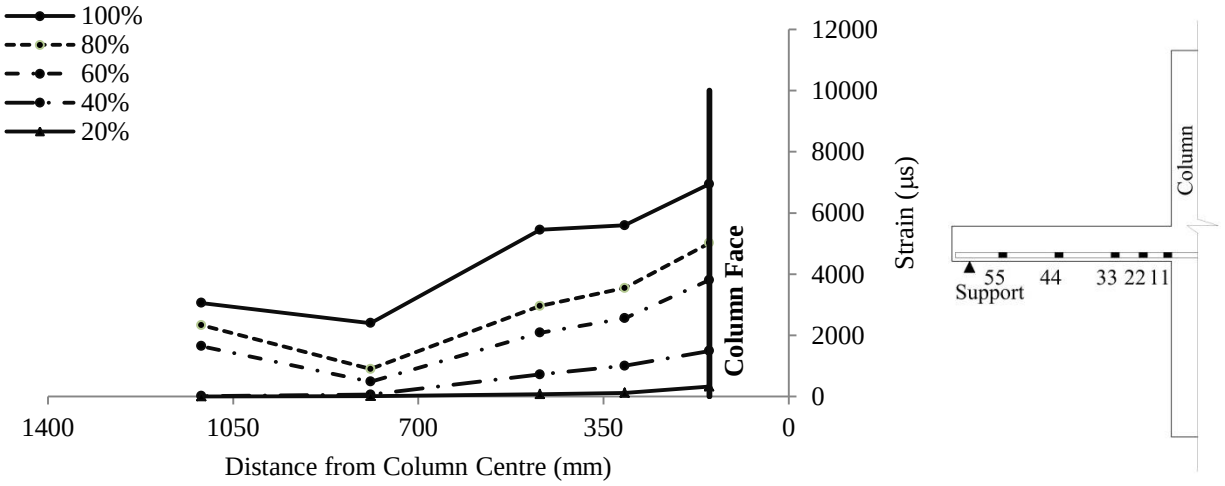


a) Connection GRD-0.9-75-0.4

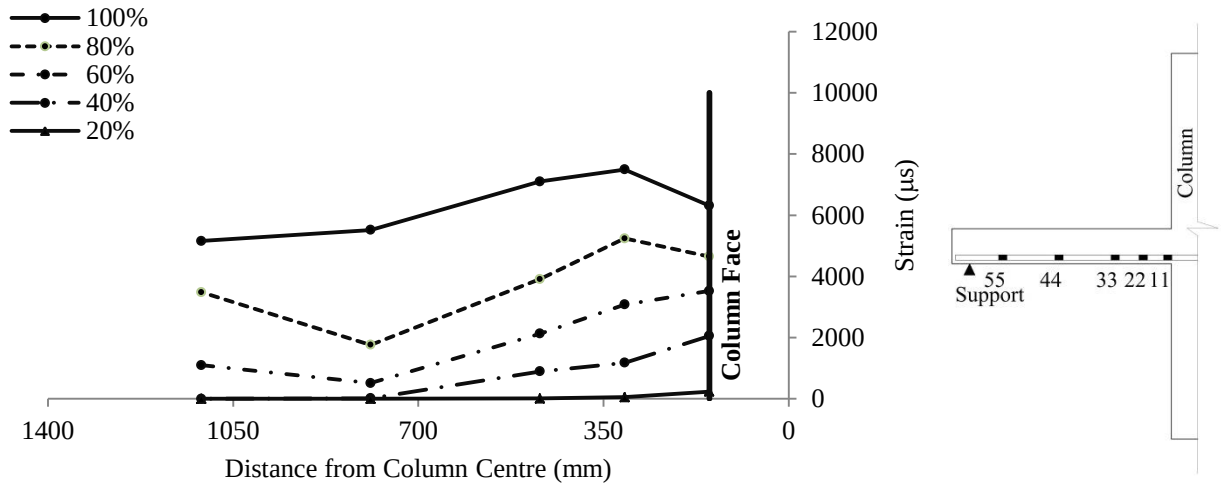


b) Connection GRD-0.9-50-0.4

Figure 4.39: Reinforcement strain profile parallel to the free edge for Series IV connections

### 4.5.4. Shear Reinforcement Strains

Figures 4.40 and 4.41 show the strains in the vertical stems of shear studs at increments of 20% of the failure load versus the distance from the column face divided by the average effective depth of the slab ($d$ = 160 mm) in the directions perpendicular and parallel to the free edge, respectively. In the direction perpendicular to the free edge, the highest strain reading was

recorded from the stud at a distance 1.9*d* (1706 με) and 0.4*d* (1982 με) from the column faces for connections GRD-0.9-75-0.4 and GRD-0.9-50-0.4, respectively. These measurements are in good agreement with the internal cracking pattern (Section 4.5.1) where the diagonal crack intersected with the three stud rows closest to the column face (up to a distance of 1.9*d* from the column face) in connection GRD-0.9-75-0.4. While in connection GRD-0.9-50-0.4, the steeper diagonal crack crossed only the first row of studs. Parallel to the free edge, the highest strain reading was recorded from the stud at a distance 0.4*d* (2314 με) from the column face for connections GRD-0.9-75-0.4 while other studs in this connection and all the studs in connection GRD-0.9-50-0.4 developed relatively low strains. The CAN/CSA S806-12 and the ACI 440.1R-06 limits the maximum strain in the vertical stem of the transverse FRP reinforcement to 5000 με and 4000 με, respectively. The maximum strain in the studs was 2314 με and was recorded in connection GRD-0.9-75-0.4. This value is only 46% and 58% of these two limits, respectively.

### 4.5.5. Punching Shear Capacity

The actual and the normalized failure loads for the three connections are listed in Table 4.11. The ultimate capacity of the connections increased considerably with providing the stud shear reinforcement. Connections GRD-0.9-75-0.4 and GRD-0.9-50-0.4 had 34% and 47% higher capacity than connection GRD-0.9-XX-0.4 (without shear reinforcement), respectively. It should be noted, however, that the full shear capacity of the latter two connections was not reached since they failed in a deformable flexural failure mode.

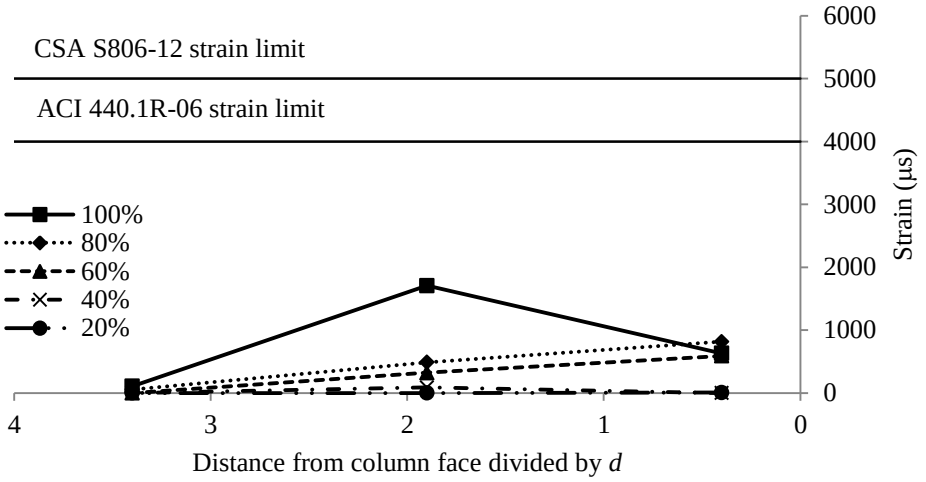


a) Connection GRD-0.9-75-0.4

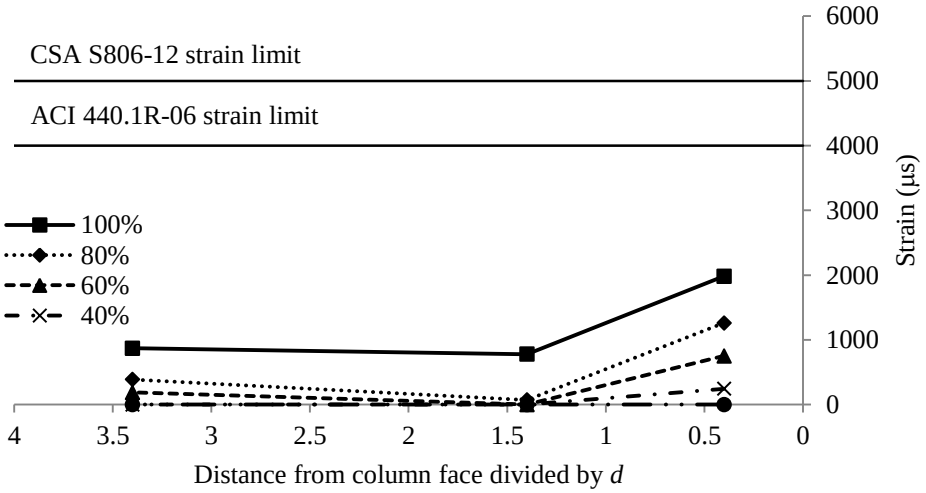


b) Connection GRD-0.9-50-0.4

Figure 4.40: Strains in studs vs. distance from column face perpendicular to the free edge

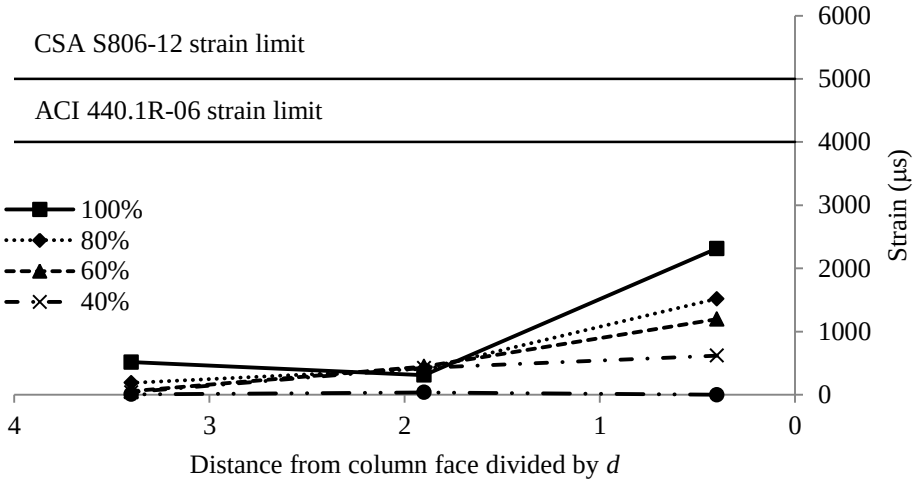


a) Connection GRD-0.9-75-0.4

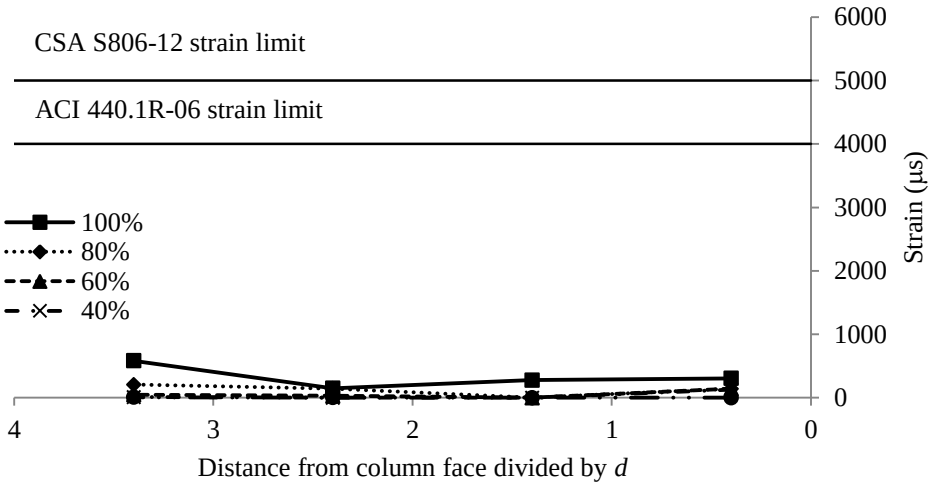


b) Connection GRD-0.9-50-0.4

Figure 4.41: Strains in studs vs. distance from column face parallel to the free edge

Table 4.11: Actual and normalized failure loads for Series IV connections

| Connection | Concrete Compressive Strength, $f_c'$ (MPa) | Actual Failure Loads (kN) | Normalized Failure Loads (kN) |
|---|---|---|---|
| GRD-0.9-XX-0.4 | 41.0 | 191.2 | 189.6 |
| GRD-0.9-75-0.4 | 40.7 | 255.9 | 253.7 |
| GRD-0.9-50-0.4 | 37.7 | 272.9 | 278.3 |

### 4.5.6. Proposed Design Equations for Shear-Reinforced Slab-Column Connections

Neither the CAN/CSA S806-12 nor the ACI 440.1R-06 includes design provisions regarding the design of FRP-RC slab-column connections with shear reinforcement. In this section, the provisions regarding the design of FRP-RC slab-column connections without shear reinforcement are modified to consider the shear reinforcement. The modifications are based on the relationship between the provisions regarding the connections with and without shear reinforcement in both the CAN/CSA A23.3-04 and the ACI 318-11 as follows.

#### 4.5.6.1. Modifications of the CAN/CSA S806-12 provisions

In the CAN/CSA A23.3-04, for connections with shear reinforcement, the punching strength provided by the concrete inside (Equation 2.11) and outside (Equation 2.10) the shear reinforced zone is 75% and 50% of the strength of a connection without shear reinforcement (Equation 2.9), respectively. Consequently, for FRP-RC connections, the punching equation of a connection without shear reinforcement in the CAN/CSA S806-12 (Equation 2.28) is multiplied by the same factors to obtain Equations 4.1 and 4.2 for the punching strength inside and outside the shear reinforced zone, respectively.

$$v_{c,inside} = 0.041\lambda\,\varphi_c(E_F\rho_F f_c')^{\frac{1}{3}} \qquad \text{Eq. [4.1]}$$

$$v_{c,outside} = 0.028\lambda\,\varphi_c(E_F\rho_F f_c')^{\frac{1}{3}} \qquad \text{Eq. [4.2]}$$

Moreover, the equation of the punching strength provided by the shear studs in the CAN/CSA A23.3-04 (Equation 2.12) is used in the case of FRP-RC connections with replacing the yield strength of the studs, $f_y$, by the ultimate strength of the studs with a limiting strain of 5000 μs, $f_{fu}$ = 0.005 $E_f$, as shown in Equation 4.3.

$$v_s = \frac{\varphi_s A_{vs} f_{fu}}{b_o s}$$ Eq. [4.3]

#### 4.5.6.2. Modifications of the ACI 440.1R-06 provisions

Similarly, in the ACI 318-11, the punching strength provided by the concrete inside (Equation 2.17) and outside (Equation 2.16) the shear reinforced zone is 75% and 50% of the strength of a connection without shear reinforcement (Equation 2.15), respectively. Consequently, the punching equation of a connection without shear reinforcement in the ACI 440.1R-06 (Equation 2.29) is multiplied by the same factors to obtain Equations 4.4 and 4.5 for the punching strength inside and outside the shear reinforced zone, respectively.

$$V_{n,inside} = V_{c,inside} = \frac{3}{5}\sqrt{f_c'} b_o c$$ Eq. [4.4]

$$V_{n,inside} = V_{c,inside} = \frac{2}{5}\sqrt{f_c'} b_o c$$ Eq. [4.5]

In addition, the equation of the punching strength provided by the shear studs in the ACI 318-11 (Equation 2.19) is used in the case of FRP-RC connections with replacing the yield strength of the studs, $f_y$, by the ultimate strength of the studs with a limiting strain of 4000 μs, $f_{fu} = 0.004\ E_f$, as shown in Equation 4.6.

$$v_s = \frac{A_v f_{fu}}{b_o s}$$ Eq. [4.6]

### 4.5.7. Comparisons with the Proposed Equations

Table 4.12 shows the predictions of the two modified approaches to predict the punching capacity of FRP-RC connections with shear reinforcement, the predictions of the yield line theory and a comparison between the actual failure loads and these predictions. For connections GRD-0.9-75-0.4 and GRD-0.9-50-0.4 with shear reinforcement, the actual failure loads were 0.91 and 0.86 of the failure loads predicted by the proposed models. These results are in good

agreement with the observed flexural failure mode of the two connections. However, since the full punching capacities of the two connections were not reached, the proposed equations are not completely verified. On the other hand, the predictions of the yield line theory closely match the failure loads of the two shear-reinforced connections with an average $V_{Test}/V_{flex}$ of 0.97 ± 0.07.

Table 4.12: Code comparisons for Series IV connections

| Connection | Actual Failure Loads, $V_{Test}$ (kN) | Punching Shear Capacity Predictions, $V_{Pred}$ | | | | | |
|---|---|---|---|---|---|---|---|
| | | Proposed Equations | | | | Yield Line Theory | |
| | | Based on CAN/CSA S806-12 | | Based on ACI 440.1R-06 | | | |
| | | $V_{Pred}$ | $V_{Test}/V_{Pred}$ | $V_{Pred}$ | $V_{Test}/V_{Pred}$ | $V_{Pred}$ | $V_{Test}/V_{Pred}$ |
| GRD-0.9-XX-0.4 | 191.2 | 172.4* | 1.11 | 98.5# | 1.94 | 279.2 | 0.68 |
| GRD-0.9-75-0.4 | 255.9 | 281.1 | 0.91 | 181.8 | 1.41 | 279.2 | 0.92 |
| GRD-0.9-50-0.4 | 272.9 | 316.9 | 0.86 | 181.8 | 1.5 | 267 | 1.02 |

* calculated by the CAN/CSA S806-12 provisions
# calculated by the ACI 440.1R-06 provisions

# CHAPTER 5: CONCLUSIONS AND FUTURE WORK

## 5.1. SUMMARY AND CONCLUSIONS

Nine full-scale slab-column edge connections were constructed and tested to failure under a combination of a vertical shearing force and an unbalanced moment. The slab of one connection was reinforced with steel bars while the slabs of the other eight connections were reinforced with GFRP bars. Moreover, two of the GFRP-RC slabs were reinforced with double-headed GFRP studs as shear reinforcement. The main objective of this investigation was to investigate the punching shear behaviour of slab-column edge connections reinforced with different configurations of GFRP longitudinal and transverse reinforcement and subjected to different combinations of vertical loads and unbalanced moments.

Based on the results of the tested connections, the following conclusions can be drawn:

1. All tested connections without shear reinforcement failed in a brittle punching shear mode with no signs of flexural failure. The punching failure was characterized by a drastic drop in the vertical load when the column along with a conical portion of the slab punched through the remainder of the slab.

2. The double-headed GFRP shear studs managed to control the propagation of the diagonal shear cracks allowing the connections to reach their flexural capacity before punching shear failure occurs. The flexural failure was characterized by substantial deflections before failure along with crushing of the concrete on the compression side of the slab at the column vicinity.

3. The headed-ends of the shear studs provided adequate anchorage which allowed the studs to develop tensile strains as high as 2314 με (13.9% of their ultimate tensile strain) without any signs of slippage. This strain value represents 46% and 58% of the strain limits in the transverse FRP reinforcement specified in the CAN/CSA S806-12 and the ACI 440.1R-06, respectively.

4. The used sand-coated GFRP bars had better bond performance than the used ribbed-deformed GFRP bars. Two of the three tested connections reinforced with ribbed-deformed GFRP bars experienced loss of bond between the reinforcing bars and the surrounding concrete before failure.

5. For the steel-RC connection, localized reinforcement yielding was observed at the column face. However, punching failure occurred before extensive yielding takes place.

6. The flexural reinforcement type and ratio had a significant effect on the post-cracking stiffness of the connections. The post-cracking stiffness factor increased in approximately linear manner with increasing the flexural reinforcement ratio; increasing the flexural reinforcement ratio by 50% and 100% increased the post-cracking stiffness factor by 62% and 119%, respectively. Similarly, the steel-RC connection had three times the post-cracking stiffness factor of its counterpart reinforced with sand-coated GFRP reinforcement due to the higher axial reinforcement stiffness of the steel bars. On the other hand, the moment-to-shear ratio and the presence of stud shear reinforcement had no effect on the post-cracking stiffness.

7. The shear-reinforced connections GRD-0.9-75-0.4 and GRD-0.9-50-0.4, which had failed in a deformable flexural mode, showed a considerable ample warning before failure with

ultimate deflections of 48.1 mm and 75.1 mm and deformability factors of 22.9 and 36.1, respectively. For the connections without shear reinforcement, increasing the flexural reinforcement ratio by 50% and 100% decreased the deformability factor by 11% and 68%, respectively. Furthermore, increasing the moment-to-shear ratio from 0.2 m to 0.6 m decreased the deformability factor by 34%. However, all connections without shear reinforcement had deformability factors ranging from 7.6 to 24.5, which allow for an ample warning before failure.

8. The flexural reinforcement type and ratio had a significant effect on the punching capacity of the connections. Doubling the GFRP flexural reinforcement ratio from 0.9% to 1.8% increased the punching capacity of the edge connection by 18%. Similarly, connections S-0.9-XX-0.4 reinforced with steel bars had 35% higher punching capacity than its counterpart connection GSC-0.9-XX-0.4 reinforced with sand-coated GFRP bars due to the increased reinforcement axial stiffness of the steel bars. Moreover, increasing the moment-to-shear ratio from 0.2 m to 0.4 m and 0.6 m decreased the punching capacity by 8.1% and 33.1%, respectively, due to the increased shear stresses at the critical shear perimeter.

9. For the connections without shear reinforcement, the CAN/CSA S806-12 and the JSCE 1997 provided reasonable, but slightly conservative, predictions with an average $V_{Test}/V_{pred}$ of 1.21 ± 0.13 and 1.15 ± 0.13, respectively. On the other hand, the ACI 440.1R-06 highly underestimated the capacities with an average $V_{Test}/V_{pred}$ of 2.07 ± 0.21. The reason behind this underestimation is that the punching shear equation in the ACI 440.1R-06 accounts for the uncracked concrete contribution only to resist the applied shear stresses and ignores the aggregate interlock and the dowel action contributions.

10. The application of the yield line theory on the GFRP-RC edge connections using the equivalent plastic moment approach (Gar et al. 2014) yielded reasonable predictions with an average $V_{test}/V_{pred}$ of 0.97 ± 0.07 for the connections failed in flexure.

11. Increasing the moment-to-shear ratio decreased the number of cracks at failure on both the tension side and the free edge of the slabs. This was due to the increased shear stresses applied to the critical section which caused shear failure to occur before significant flexural cracks form.

12. Increasing the moment-to-shear ratio pushed the failure surface on the tension side of the slab away from the column face and led to a flatter angle of the diagonal crack with the horizontal plane. Increasing the moment-to-shear ratio from 0.2 m in connection GSC-0.9-XX-0.2 to 0.6 m in connection GSC-0.9-XX-0.6 decreased the diagonal crack angle with the horizontal on the tension face of the slab by 10% (from $28.3^o$ to $25.5^o$).

13. The proposed design equations for the shear-reinforced GFRP-RC slab-column connections seems to yield good predictions; however, further investigation on connections with high flexural reinforcement ratios is required.

## 5.2. FUTURE WORK

The following are suggestions for further studies on the punching shear behaviour of GFRP-RC slab-column edge connections:

1. Studying the seismic response of FRP-RC slab-column edge connections.
2. Studying the influence of different anchorage types in the direction perpendicular to the free edge, i.e., bent bars and headed-end bars.

3. Studying the performance of the headed-end shear studs in slab-column edge connections with higher flexural reinforcement ratios (between four and six times the balanced reinforcement ratio).
4. Investigating the influence of different parameters on the punching shear behaviour of slab-column edge connections such as, but not limited to:
    a. The effect of high strength concrete.
    b. The size effect (e.g., slab thickness, column size, column aspect ratio and column width-to-slab depth ratio).
    c. The configuration of the transverse reinforcement.
5. Studying the punching shear behaviour of slab-column corner connections.

# REFERENCES

ACI Committee 318. (1963). *Building Code Requirements for Reinforced Concrete (ACI 318-63)*. American Concrete Institute, Detroit, Michigan, 144.

ACI Committee 318. (1971). *Building Code Requirements for Reinforced Concrete (ACI 318-71)*. American Concrete Institute, Detroit, Michigan, 78.

ACI Committee 318. (1995). *Building Code Requirements for Structural Concrete (ACI 318-95)*. American Concrete Institute, Detroit, Michigan.

ACI Committee 318. (2011). *Building Code Requirements for Structural Concrete (ACI 318-11) and Commentary*. American Concrete Institute, Detroit, Michigan, 509.

ACI Committee 440. (2006). *Guide for the Design and Construction of Structural Concrete Reinforced with FRP Bars*. American Concrete Institute, Farmington Hills, Michigan, 44.

Alexander, S. B., and Simmonds, S. H. (1987). "Ultimate Strength of Slab-Column Connections." *ACI Structural Journal*, 84(3), 255–261.

Alexander, S. B., and Simmonds, S. H. (1992). "Punching Shear Tests of Concrete Slab-Column Joints Containing Fiber Reinforcement." *ACI Structural Journal*, 89(4), 425–432.

ASCE-ACI Committee 426. (1974). "The Shear Strength of Reinforced Concrete Members - Slabs." *Journal of the Structural Division*, 100(8), 1543–1590.

ASTM A370 - 14. (2014). "Standard Test Methods and Definitions for Mechanical Testing of Steel Products." *American Society for Testing and Materials*, ASTM International, West Conshohocken, PA, 1(1), 50.

ASTM D7205 / D7205M - 06. (2011). "Standard Test Method for Tensile Properties of Fiber Reinforced Polymer Matrix Composite Bars." *American Society for Testing and Materials*, ASTM International, West Conshohocken, PA, 15(3), 12.

Bank, L. C. (1993). "Properties of FRP Reinforcements for Concrete." *Fiber-Reinforced-Plastic (FRP) Reinforcement for Concrete StructuresProperties and Applications*, Elsevier, 59–86.

Banthia, N., Al-Asaly, M., and Ma, S. (1995). "Behavior of Concrete Slabs Reinforced with Fiber-Reinforced Plastic Grid." *Journal of materials in civil engineering*, 7(4), 252–257.

Benmokrane, B., Tighiouart, B., and Chaallal, O. (1996). "Bond Strength and Load Distribution of Composite GFRP Reinforcing Bars in Concrete." *ACI Materials Journal*, 93(3), 254–259.

Birkle, G., and Dilger, W. H. W. (2008). "Influence of slab thickness on punching shear strength." *ACI Structural Journal*, 105(2), 180–188.

British Standards Institution. (1997). *Structural Use of Concrete - Code of Practice for Design and Construction*. BSI, 168.

Canadian Standards Association. (1984). *Design of Concrete Structures for Buildings, CAN3-A23.3-M84*. Canadian Standards Association, Toronto, Ontario, 281.

Canadian Standards Association. (2004). *Design of Concrete Structures, CAN/CSA-A23.3-04*. Canadian Standards Association, Toronto, Ontario, 240.

Canadian Standards Association. (2006). *Canadian Highway Bridge Design Code*.

Canadian Standards Association. (2012). *Design and Construction of Building structurSs with Fibre-Reinforced Polymer, CAN/CSA S806-12*. Canadian Standards Association, Toronto, Ontario, 198.

Cement Association of Canada. (2006). *Concrete design handbook*. Ottawa, ON.

Cosenza, E., Manfredi, G., and Realfonzo, R. (1997). "Behavior and Modeling of Bond of FRP Rebars to Concrete." *Journal of Composites for Construction*, 1(2), 40–51.

Dilger, W., Birkle, G., and Mitchell, D. (2005). "Effect of Flexural Reinforcement on Punching Shear Resistance." *ACI Special Publication*, 232, 57–74.

Dilger, W., Elmasri, M., and Ghali, A. (1978). "Flat Plates with Special Shear Reinforcement Subjected to Static Dynamic Moment Transfer." *ACI Journal Proceedings*, 75(10), 543–549.

Dilger, W., and Ghali, A. (1981). "Shear Reinforcement for Concrete Slabs." *Journal of the Structural Division*, 107(12), 2403–2420.

Dulude, C., Ahmed, E., and Benmokrane, B. (2010). "Punching Shear Strength of Concrete Flat Slabs Reinforced with GFRP Bars." *2nd International Structures Specialty Conference*, Winnipeg, Manitoba, 1–9.

Dulude, C., Hassan, M., Ehab, A., and Benmokrane, B. (2013). "Punching Shear Behavior of Flat Slabs Reinforced with Glass Fiber-Reinforced Polymer Bars." *ACI Structural Journal*, 110(5), 723–734.

Elgabry, A., and Ghali, A. (1987). "Tests on Concrete Slab-Column Connections with Stud-Shear Reinforcement Subjected to Shear-Moment Transfer." *ACI Structural Journal*, 84(5), 433–442.

El-Gamal, S., El-Salakawy, E. F., and Benmokrane, B. (2005). "A New Punching Shear Equation for Two-Way Concrete Slabs Reinforced with FRP Bars." *ACI Special Publication*, 230, 877–894.

El-Ghandour, A. W., Pilakoutas, K., and Waldron, P. (1999). "New Approach for Punching Shear Capacity Prediction of Fiber Reinforced Polymer Reinforced Concrete Flat Slabs." *ACI Special Publication*, 188, 135–144.

El-Ghandour, A. W., Pilakoutas, K., and Waldron, P. (2003). "Punching Shear Behavior of Fiber Reinforced Polymers Reinforced Concrete Flat Slabs: Experimental Study." *Journal of Composites for Construction*, 7(3), 258–265.

El-Salakawy, E. F., Polak, M. A., and Soliman, M. H. (1998). "Slab-Column Edge Connections Subjected to High Moments." *Canadian Journal of Civil Engineering*, 25(3), 526–538.

El-Salakawy, E., Polak, M., and Soliman, M. (2000). "Reinforced Concrete Slab-Column Edge Connections with Shear Studs." *Canadian Journal of Civil Engineering*, 27(2), 338–348.

El-Sayed, A., El-Salakawy, E. F., and Benmokrane, B. (2005). "Shear Strength of One-Way Concrete Slabs Reinforced With Fiber-Reinforced Polymer Composite Bars." *Journal of Composites for Construction*, 9(2), 147–157.

Fanella, D. A. (2000). *Concrete Floor Systems: Guide to Estimating and Economizing*. Portland Cement Association, Illinois, USA, 41.

Gar, S. P., Mander, J., Head, M., and Hurlebaus, S. (2014). "FRP Slab Capacity Using Yield Line Theory." *Journal of Composites for Construction*.

Gardner, N. (1990). "Relationship of the Punching Shear Capacity of Reinforced Concrete Slabs with Concrete Strength." *ACI Structural Journal*, 87(1), 66–71.

Ghannoum, C. M. (1998). "Effect of High-Strength Concrete on the Performance of Slab-column Specimens." McGill University.

Hassan, M., Ahmed, E., and Benmokrane, B. (2013). "Punching-Shear Strength of Normal and High-Strength Two-Way Concrete Slabs Reinforced with GFRP Bars." *Journal of Composites for Construction*, 17(6).

Hassan, M., Ahmed, E., and Benmokrane, B. (2014). "Punching Shear Behavior of Two-Way Slabs Reinforced with FRP Shear Reinforcement." *Journal of Composites for Construction*, 04014030(13).

Hawkins, N. M., Bao, A., and Yamazaki, J. (1989). "Moment Transfer From Concrete Slabs to Columns." *ACI Structural Journal*, 86(6), 705–716.

Heinzmann, D., Etter, S., Villiger, S., and Jaeger, T. (2012). "Punching Tests on Reinforced Concrete Slabs with and without Shear Reinforcement." *ACI Structural Journal*, 109(6), 787–794.

Hussein, A., Rashid, I., and Benmokrane, B. (2004). "Two-way concrete slabs reinforced with GFRP bars." *Advanced Composite Materials in Bridges and …*, Calgary, Alberta, 1–8.

Ingerslev, A. (1923). "The Strength of Rectangular Slabs." *Journal of the Institution of Civil Engineers*, 1(1), 3–14.

ISIS Canada. (2001). *Reinforcing Concrete Structures with Fibre Reinforced Polymers*. Winnipeg, Manitoba, 158.

Jaeger, L. G., Mufti, A. A., and Tadros, G. (1995). *Balanced Section, Ductility and Deformability in Concrete with FRP Reinforcement*. Halifax, NS, 50.

Japan Society of Civil Engineering. (1997). *Recommendation for Design and Construction of Concrete Structures using Continuous Fibre Reinforcing Materials*. Concrete Engineering Series 23, Tokyo, Japan, 325.

Japan Society of Civil Engineering. (2007). *Standard Specifications for Concrete Structures*. Tokyo, Japan, 469.

Johansen, K. W. (1943). *Yield Line Theory*. London, UK, 189.

Johansen, K. W. (1946). *Yield Line Formula for Slabs*. London, UK, 186.

Kassem, C., Farghaly, A. S., and Benmokrane, B. (2011). "Evaluation of Flexural Behavior and Serviceability Performance of Concrete Beams Reinforced with FRP Bars." *Journal of Composites for Construction*, 15(5), 682–695.

Kinnunen, S. (1963). *Punching of Concrete Slabs with Two-Way Reinforcement: With Special Reference to Dowel Effect and Deviation of Reinforcement from Polar Symmetry*. Henrik Lindståhls bokhandel, distr, 108.

Kinnunen, S., and Nylander, H. S. E. (1960). *Punching of Concrete Slabs without Shear Reinforcement*. Stockholm : KTH, Stockholm, Sweden, 112.

Koch, G. H., Brongers, M., Thompson, N. G., Virmani, Y. P., and Payer, J. H. (2002). *Corrosion Cost and Preventive Strategies in the United States*. 773.

Lee, J. H., Yoon, Y. S., Cook, W. D., and Mitchell, D. (2009). "Improving Punching Shear Behavior of Glass Fiber-Reinforced Polymer Reinforced Slabs." *ACI Structural journal*, 106(4), 427–434.

Lenschow, R. J., and Sozen, M. A. (1966). *A Yield Criterion for Reinforced Concrete Under Biaxial Moments and Forces*. Urbana, Illinois, 590.

Lenschow, R. J., and Sozen, M. A. (1967). "A Yield Criterion for Reinforced Concrete Slabs." *ACI Journal Proceedings*, 64(5), 266–273.

Lips, S., Ruiz, M., and Muttoni, A. (2012). "Experimental Investigation on Punching Strength and Deformation Capacity of Shear-Reinforced Slabs." *ACI Structural Journal*, (109), 889–900.

Long, A. E. (1975). "A two-phase approach to the prediction of the punching strength of slabs." *ACI Journal Proceedings*, 72(2), 37–45.

Lorenz, E. B., and Trygestad, A. R. (2005). "Formwork Considerations for Economical Concrete Projects." *Concrete International*, 61–64.

Marzouk, H., Emam, M., and Hilal, M. (1996). "Effect of High-Strength Concrete Columns on the Behavior of Slab-Column Connections." *ACI structural journal*, 93(5), 545–552.

Marzouk, H., Emam, M., and Hilal, M. S. (1998). "Effect of High-Strength Concrete Slab on the Behavior of Slab-Column Connections." *ACI Structural Journal*, 95(3), 227–236.

Marzouk, H., and Hussein, A. (1991). "Experimental Investigation on the Behavior of High-Strength Concrete Slabs." *ACI Structural Journal*, 88(6), 701–713.

Marzouk, H., Osman, M., and Helmy, S. (2000). "Behavior of High-Strength Lightweight Aggregate Concrete Slabs under Column Load and Unbalanced Moment." *ACI Structural Journal*, 97(6), 860–866.

Mast, P. E. (1970a). "Stresses in Flat Plates near Columns." *ACI Journal Proceedings*, 67(10), 761–768.

Mast, P. E. (1970b). "Plate Stresses at Columns near the Free Edge." *ACI Journal Proceedings*, 67(11), 898–902.

Matthys, S., and Taerwe, L. (2000). "Concrete Slabs Reinforced with FRP Grids. II: Punching Resistance." *Journal of Composites for Construction*, 4(3), 154–161.

Megally, S., and Ghali, A. (2000). "Seismic Behavior of Edge Column-Slab Connections with Stud Shear Reinforcement." *ACI Structural Journal*, 97(1), 53–60.

Menetrey, P. (1998). "Relationships between Flexural and Punching Failure." *ACI Structural journal*, 93(4), 412–419.

Moe, J. (1961). *Shearing Strength of Reinforced Concrete Slabs and Footings under Concentrated Loads*. Illinois, USA, 139.

Mokhtar, A. S., Ghali, A., and Dilger, W. H. (1985). "Stud Shear Reinforcement for Flat Concrete Plates." *ACI Journal Proceedings*, 82(5), 676–683.

Mörsch, E. (1902). *Reinforced Concrete, Theory and Application*. Beton-und Stahlbetonbau, Stuttgart, Germany.

Mortin, J. D. (1989). "Connections of Concrete Slabs with Edge Columns." University of Calgary.

Mortin, J., and Ghali, A. (1991). "Connection of flat plates to edge columns." *ACI Structural Journal*, (88), 191–198.

Nanni, A., Rizkalla, S., Bakis, C. E., Conrad, J. O., and Abdelrahman, A. A. (1998). "Characterization of GFRP Ribbed Rod Used for Reinforced Concrete Construction." *Proceedings of the International Composites Exhibition (ICE-98)*, Nashville, Tennessee, 1–6.

NBCC. (2010). *National Building Code of Canada*. National Research Council of Canada, Ottawa, Ontario, 1222.

Neville, A. (1995). "Chloride Attack of Reinforced Concrete: An Overview." *Materials and Structures*, 28(176), 63–70.

Newhook, J., Ghali, A., and Tadros, G. (2002). "Concrete Flexural Members Reinforced with Fiber Reinforced Polymer: Design for Cracking and Deformability." *Canadian Journal of Civil Engineering*, 29(1), 125–134.

Nguyen-Minh, L., and Rovňák, M. (2013). "Punching Shear Resistance of Interior GFRP Reinforced Slab-Column Connections." *Journal of Composites for Construction*, 17(1), 2–13.

Osman, M., Marzouk, H., and Helmy, S. (2000). "Behavior of High-Strength Lightweight Concrete Slabs under Punching Loads." *ACI Structural Journal*, 97(3), 492–498.

Ospina, C. (2005). "Alternative for Concentric Punching Capacity Evaluation of Reinforced Concrete Two-Way Slabs." *Concrete International*, 53–57.

Ospina, C. E., Alexander, S. D. B., and Cheng, J. J. R. (2003). "Punching of Two-Way Concrete Slabs with Fiber-Reinforced Polymer Reinforcing Bars or Grids." *ACI structural Journal*, 100(5), 589–598.

Ozden, S., Ersoy, U., and Ozturan, T. (2006). "Punching Shear Tests of Normal- and High-Strength Concrete Flat Plates." *Canadian Journal of Civil Engineering*, 33(11), 1389–1400.

Park, R., and Gamble, W. L. (2000). *Reinforced Concrete Slabs*. John Wiley & Sons, Inc., New York, USA, 736.

Polak, M. A., El-Salakawy, E. F., and Hammill, N. (2005). "Shear Reinforcement for Concrete Flat Slabs." *ACI Special Publication*, 232, 75–96.

Pultrall Inc. (2013). "V-ROD Technical Data Sheet." <http://www.vrod.ca/en/downloads.asp>.

Richart, F. E. (1948). "Reinforced Concrete Wall and Column Footings." *ACI Journal Proceedings*, 45(10), 97–127.

Ritchie, M., Ghali, A., Dilger, W., and Gayed, R. (2006). "Unbalanced moment resistance by shear in slab-column connections: experimental assessment." *ACI structural journal*, (103).

Ritter, W. (1899). "Construction Techniques of Hennebique." *Swiss Bauzeitung*, 33(5), 41–43.

Rizk, E., Marzouk, H., Hussein, A., and Hossin, M. (2011). "Effect of Reinforcement Ratio on Punching Capacity of RC Plates." *Canadian Journal of Civil Engineering*, 38(7), 729–740.

Schoeck Canada Inc. (2013). "Schock ComBAR - Technical Information." <http://www.schoeck.ca/en_ca/downloads?product=4&type=7&filter=1>.

Seible, F., Ghali, A., and Dilger, W. (1980). "Preassembled Shear Reinforcing Units for Flat Plates." *ACI Journal Proceedings*, 77(1), 28–35.

Shaaban, A. M., and Gesund, H. (1994). "Punching Shear Strength of Steel Fiber Reinforced Concrete Flat Plates." *ACI Structural Journal*, 91(4), 406–414.

Simmonds, S. H., and Alexander, S. B. (1987). "Truss Model for Edge Column-Slab Connections." *ACI Structural Journal*, 84(4), 296–303.

Stein, T., Ghali, A., and Dilger, W. (2007). "Distinction between Punching and Flexural Failure Modes of Flat Plates." *ACI structural journal*, 104(3), 357–365.

Swamy, R. N., and Ali, S. A. R. (1982). "Punching Shear Behavior of Reinforced Slab-Column Connections Made with Steel Fiber Concrete." *ACI Journal Proceedings*, 79(5), 392–406.

Tureyen, A., and Frosch, R. (2003). "Concrete Shear Strength: Another Perspective." *ACI Structural Journal*, 100(5), 609–615.

Vanderbilt, M. (1972). "Shear Strength of Continuous Plates." *Journal of the Structural Division*, 98(5), 961–973.

Wheeler, W. H. (1936). "Thin Flat-Slab Floors Prove Rigid Under Test." *Engineering News-Record*, 116(2), 49–50.

Widianto, Bayrak, O., and Jirsa, J. O. (2009). "Two-Way Shear Strength of Slab-Column Connections: Reexamination of ACI 318 Provisions." *ACI Structural Journal*, 106(2), 160–170.

Wight, J. K., and MacGregor, J. G. (2011). *Reinforced Concrete: Mechanics and Design*. Prentice Hall, 1177.

Wu, W. P. (1990). "Design of Slabs, Beams and Foundations." West Virginia University.

Zaghlool, E. R. F., and Rawdon de Paiva, A. (1973). "Tests of Flat-Plate Corner Column-Slab Connections." *Journal of the Structural Division*, 99(3), 551–572.

Zaghloul, A. (2007). "Punching Shear Strength of Interior and Edge Column-Slab Connections in CFRP Reinforced Flat Plate Structures Transferring Shear and Moment." Carlton University.

Zaghloul, A., and Razaqpur, A. (2004). "Punching Shear Strength of Concrete Flat Plates Reinforced with CFRP Grids." *Proceedings of the 4th Conference on Advanced Composite Materials in Bridges and Structures*, Calgary, Alberta, 1–8.

# APPENDIX A

# Analyses of a Parking Garage Flat Plate

## A.1. Layout of the Flat Plate System

Figures A.1a and A.1b show the load and bending moment distribution on a typical parking garage system consisting of three 6.5 m-long square bays in both directions. The edge slab-column connections are bounded by the slab free edge and the lines of contra-flexure around the column as shown in Figure A.1c. Two orthogonal strips are designed: perpendicular and parallel to the free edge as shown in Figure A.2.

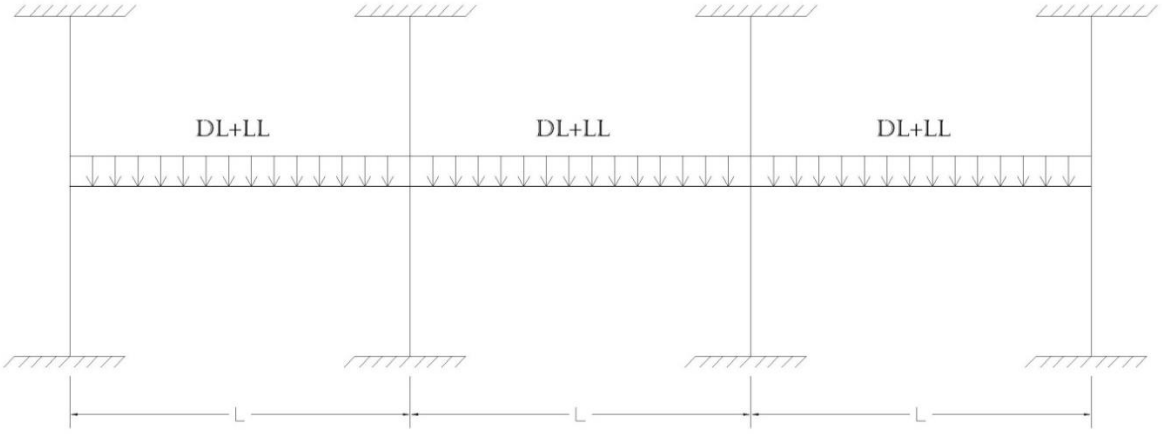


a) Applied loads

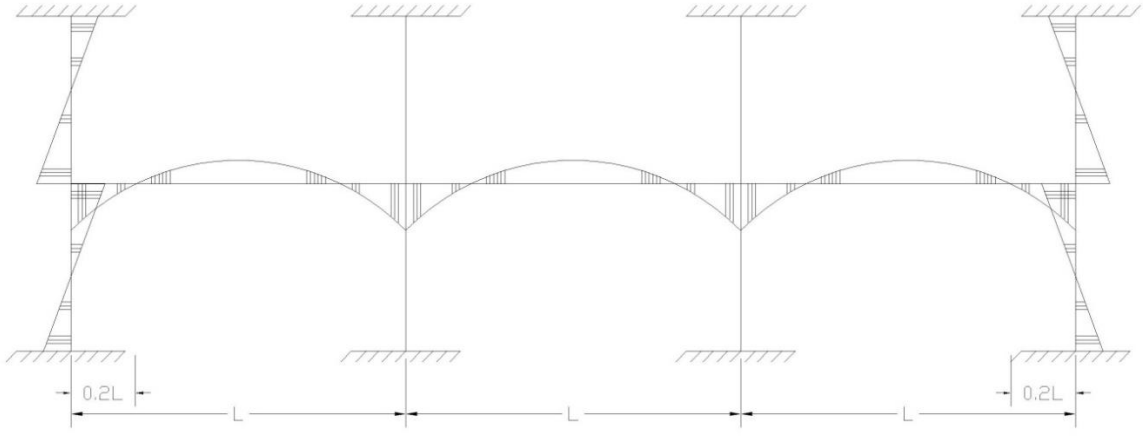


b) Bending moment diagram

Figure A.1: Parking garage frame

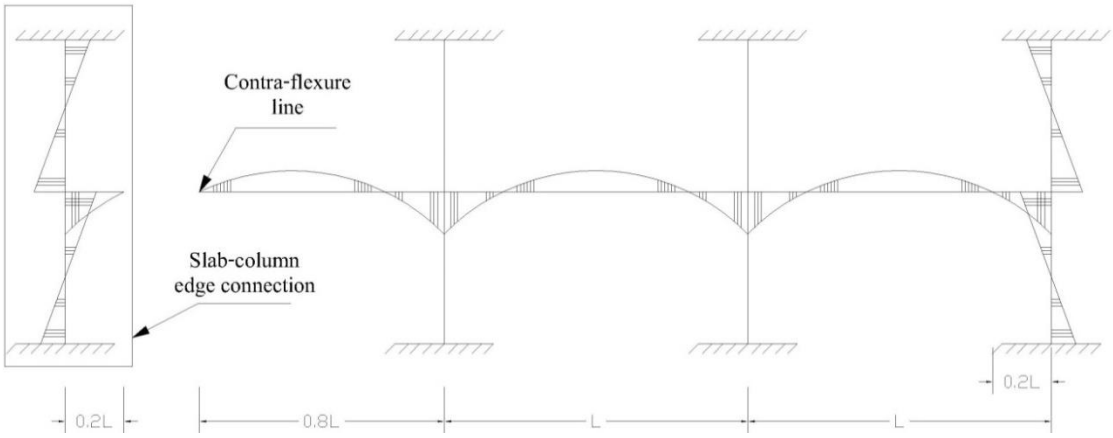


c) Lines of contra-flexure

Figure A.1: Parking garage frame - continued

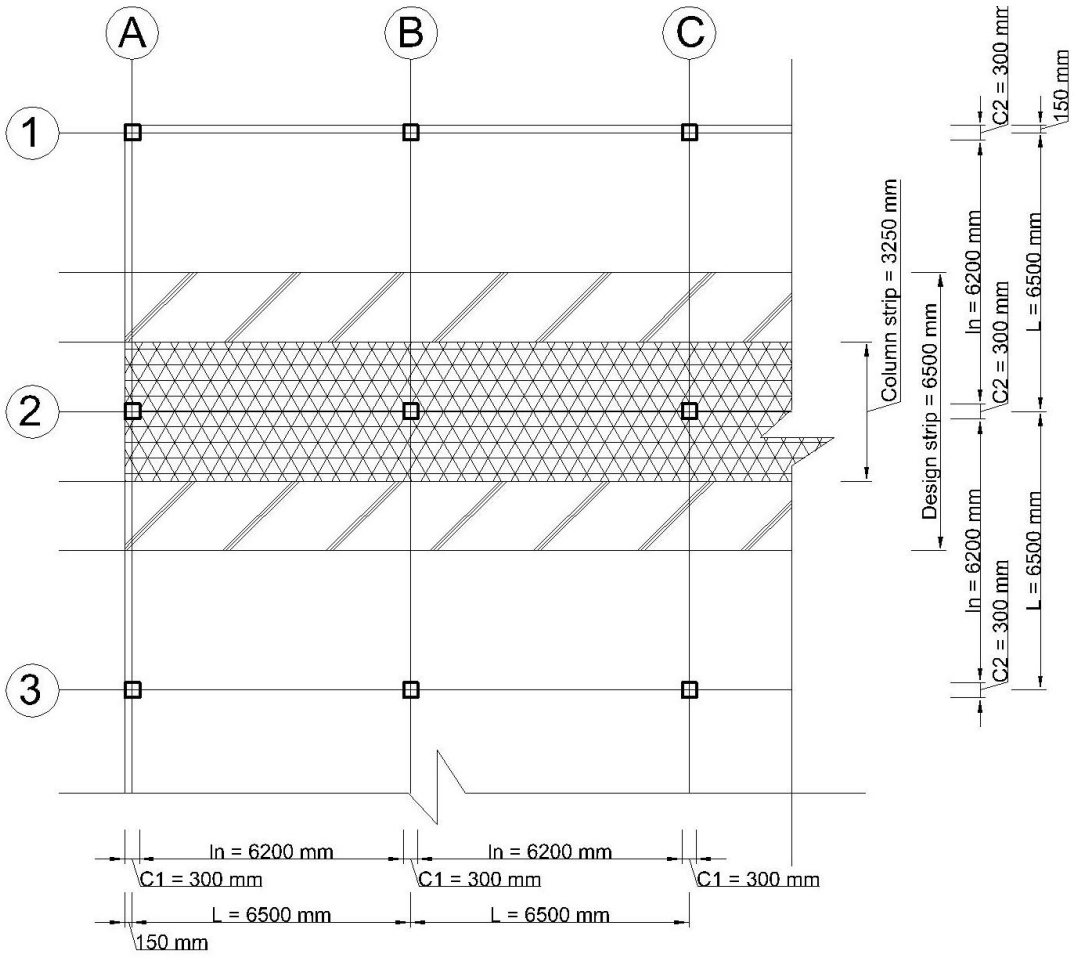


a) The strip perpendicular to the free edge

Figure A.2: Design strips

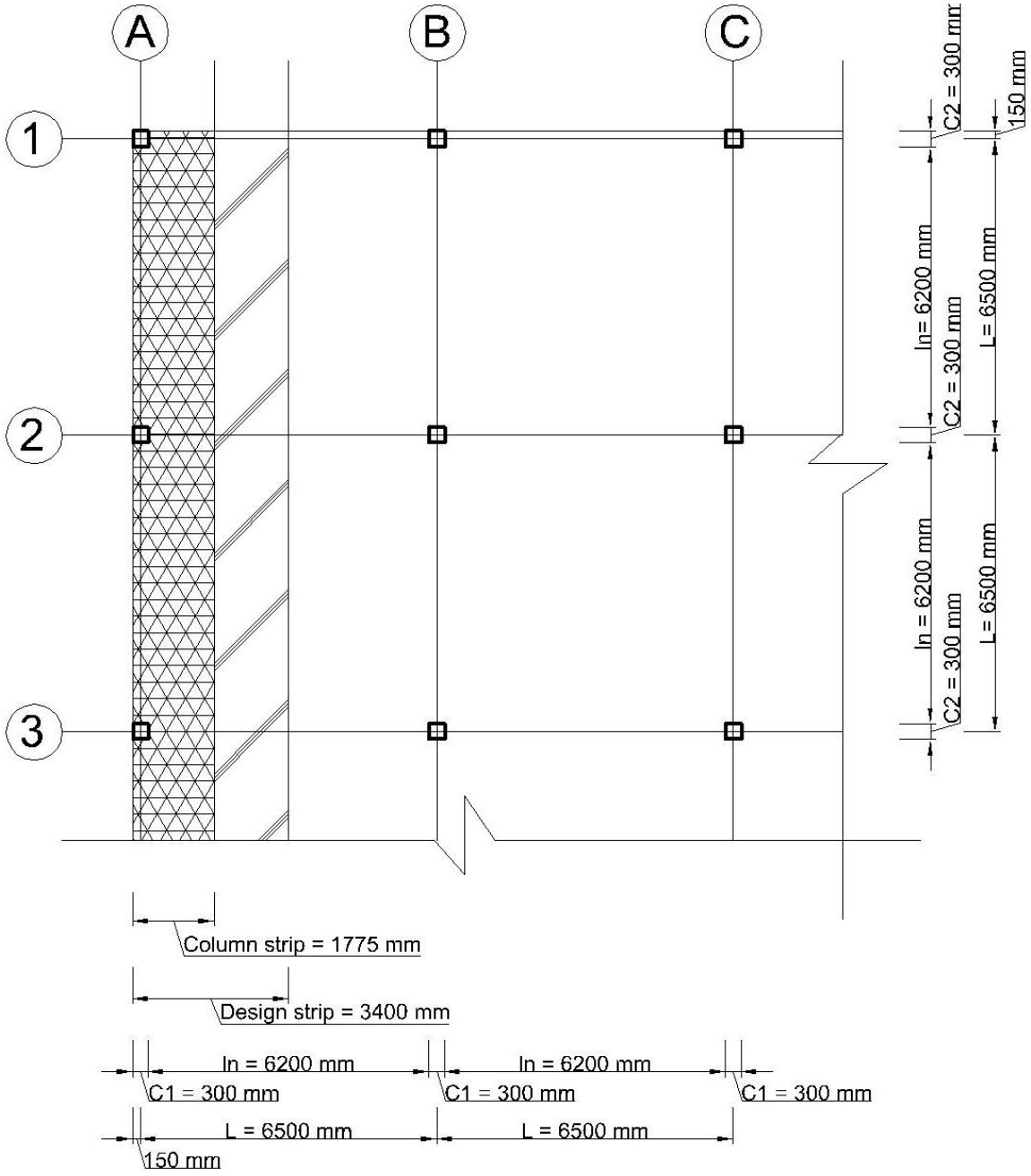


b) The strip parallel to the free edge

Figure A.2: Design strips - continued

## A.2. Properties of Concrete

Compressive strength of concrete $f_c' = 35\ MPa$

Material resistance factor $\phi_c = 1.0$

Ultimate compressive strain for concrete $\varepsilon_{c_u} = 0.0035$ **Clause 10.1.3 (A23.3-04)**

$\alpha_1 = 0.85 - 0.0015 f_c' = 0.85 - 0.0015(35) = 0.7975$ **Clause 10.1.7 (A23.3-04)**

$\beta_1 = 0.97 - 0.0025 f_c' = 0.97 - 0.0025(35) = 0.8825$ **Clause 10.1.7 (A23.3-04)**

**A.3. Loads**

$L.L. = 2.4\ kN/m^2$ (NBCC 2010)

$D.L. = self\ weight + partition\ allowance = 24 * 0.2 + 1.0 = 5.8\ kN/m2$ (NBCC 2010)

Factored load $w_f = 1.4\ D.L. = 1.4 * 5.8 = 8.12\ kN/m^2$ (NBCC 2010)

or $= 1.25\ D.L. + 1.5\ L.L. = 1.25 * 5.8 + 1.5 * 2.4$

$= 7.25 + 3.6 = 10.85\ kN/m^2$ (Governs)

**A.4. Slab Thickness "$h_s$"**

Minimum slab thickness $h_s = 1.1 * \frac{l_n\left(0.6+\frac{f_y}{1000}\right)}{30}$ **Clause 13.2.3 (A23.3-04)**

$= 1.1 * \frac{6200\left(0.6+\frac{415}{1000}\right)}{30} = 230.7\ mm$

Take $h_s = 200\ mm$

**A.5. Analysis of a steel-RC Parking Garage Flat Plate (According to CSA A23.3-04)**

**A.5.1. Properties of Reinforcement**

Use No. 15M bars $d_b = 16\ mm$ $A_b = 200\ \text{mm}^2$

Yield strength of steel $f_y = 415\ MPa$

Material resistance factor $\phi_s = 1.0$

Yield strain for steel $\varepsilon_y = 0.0021$

**A.5.2. The Strip Perpendicular to the Free Edge**

**A.5.2.1. Effective Depth "$d$"**

Take concrete clear cover $= 24.1mm$

→ Effective depth $d = h_s - clear\ cover - \frac{d_b}{2} = 200 - 24 - \frac{16}{2} = 168\ mm$

### A.5.2.2. Design Moments

$M_o = \frac{w_f * l_{2a} * l_n^2}{8} = \frac{10.85 * 6.5 * 6.2^2}{8} = 338.87\ kN.m$ **Clause 13.9.2**

Table A.1: Moment distribution in a design strip perpendicular to the free edge

| Axis | A | | B | | | C | Units | Clause |
|---|---|---|---|---|---|---|---|---|
| $l_n$ | 6200 | | | 6200 | | | | |
| $M_{Design}$ | 26 | 52 | 70 | 65 | 35 | 65 | % | 13.9.3 |
| | 88.1 | 176.2 | 237.2 | 220.3 | 118.6 | 20.3 | kN.m | |
| $M_{Col\ Str}$ | 100 | 60 | 70-90 | 70-90 | 55-65 | 70-90 | % | 13.11.2 |
| | **88.1** | 105.7 | 166.1-213.5 | 154.2-198.2 | 65.2-77.1 | 154.2-198.2 | kN.m | |
| $M_{Fld.Str}$ | 0 | 40 | 30-10 | 30-10 | 45-35 | 30-10 | % | 13.11.2 |
| | 0 | 70.5 | 71.2-23.7 | 66.1-22 | 53.4-41.5 | 66.1-22 | kN.m | |

### A.5.2.3. Reinforcement

$M_{Design} = 88.11 kN.m$

- Reinforcement for the total factored negative moment transferred to the exterior columns shall be placed within a band width $b_b = c + 3h_s$ **Clause 13.10.3**

❖ **For the Band Width $b_b = c + 3h_s$:**

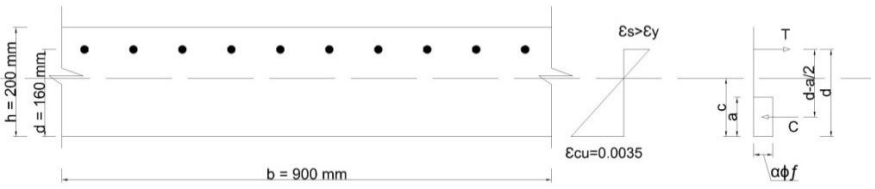


Figure A.3: Strain distribution and equivelant stress block

$b_b = c + 3h_s = 300 + 3 * 200 = 900\ mm$

$a = \frac{\phi_s A_s f_y}{\alpha_1 \phi_c f_c' b} = \frac{1.0 * A_s * 415}{0.7975 * 1.0 * 35 * 900} = 16.52 * 10^{-3} A_s$

$M_r = \phi_s A_s f_y * \left(d - \frac{a}{2}\right)$

→ $88.11 * 10^6 = 1.0 * A_s * 415 * (168 - \frac{16.52 * 10^{-3} A_s}{2})$

$\rightarrow 3.428A_s{}^2 - 69720A_s + 88.11 * 10^6 = 0$

$\rightarrow A_s = 1397.9\ mm^2$

$A_s = \frac{b}{S} * A_b \rightarrow 1397.9 = \frac{900}{S} * 200 \rightarrow S = 128.8\ mm$ Use 15M @ 128 mm c/c

$\rightarrow\ A_{s_{act.}} = \frac{b}{S_{act.}} * A_b = \frac{900}{128} * 200 = 1406.25\ mm^2$

➢ **Check for the Balanced Reinforcement Ratio "$\rho_b$":**

$\rho = \frac{1406.25}{168*900} = 0.93\ \%$

$\rho_b = \alpha_1\beta_1 \frac{\phi_c f_c'}{\phi_s f_y} * \frac{\varepsilon_{c_u}}{\varepsilon_{c_u} + \varepsilon_y}$

$\rho_b = 0.7975 * 0.8825 * \frac{1.0*35}{1.0*415} * \frac{0.0035}{0.0035+0.0021} = 3.71\ \%$

$\rightarrow \rho < \rho_b$ Under-reinforced Ok

❖ **For the Rest of the Column Strip:**

- Use minimum reinforcement "$A_{s_{min}}$" **Clause 13.10.9**

$A_{s_{min}} = 0.002A_g = 0.002 * (200 * 1000) = 400mm^2/m$ **Clause 7.8.1**

$A_{s_{min}} = \frac{b}{S} * A_b \rightarrow 400 = \frac{1000}{S} * 200 \rightarrow S = 500mm$

Maximum spacing $s_{max} = 3h_s = 3 * 200 = 600mm$ **Clause 13.10.4**

Or $= 500\ mm$ (Governs) Use 15M @ 475 mm c/c

**A.5.2.4. Development Length "$l_d$"** **Clause 12.2**

$l_d = 0.45k_1k_2k_3k_4 \frac{f_y}{\sqrt{f_c'}} d_b$ **Clause 12.2.3**

$k_1 = 1.0\ for\ horizontal\ reinforcement\ placed\ in\ such\ a\ way\ that\ less\ than\ 300\ mm\ of\ fresh\ concrete\ is\ cast\ in\ the\ member\ below\ the\ development\ length$

$k_2 = 1.0\ for\ uncoated\ reinforcement$

$k_3 = 1.0\ for\ normal\ density\ concrete$

$k_4 = 0.8\ for\ 20M\ and\ smaller\ bars\ and\ deformed\ wires$

$\rightarrow l_d = 0.45 * 1.0 * 1.0 * 1.0 * 0.8 * \frac{415}{\sqrt{35}} * 16 = 404.1\ mm > \frac{300}{2} - 30 = 120mm$

Use bent bars

$l_{dh} = 100\frac{d_b}{\sqrt{f'_c}} = 100 * \frac{16}{\sqrt{35}} = 270.4\ mm$ **Clause 12.5**

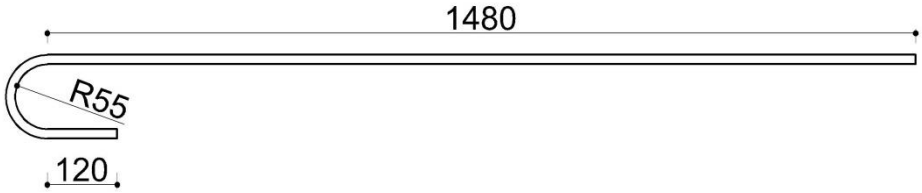


Figure A.4: Typical deformed steel bent bar dimensions

**A.5.2.5. Serviceability Check**

**A.5.2.5.1. Service Stress Calculations**

Specified load $w_s = D.L. + L.L. = 5.8 + 2.4 = 8.2\ kN/m^2$ (NBCC 2010)

Service moment $M_s = \frac{w_s * l_{2a} * l_n^2}{8} = \frac{8.2 * 6.5 * 6.2^2}{8} = 256.11\ kN.m$ **Clause 13.9.2**

Service moment at the edge connection $= M_s * 0.26 = 256.11 * 0.26 = 66.6\ kN.m$

**Clause 13.10.3**

$n = \frac{E_S}{E_c} = \frac{197000}{29878} = 6.59$

$k = \sqrt{2\rho n + (\rho n)^2} - \rho n = \sqrt{2 * 0.0093 * 6.59 + (0.0093 * 6.59)^2} - 0.0093 * 6.59 = 0.294$

$j = 1 - \frac{k}{3} = 1 - \frac{0.294}{3} = 0.902$

Service stress $f_s = \frac{M_s}{A_s jd} = \frac{66.6 * 10^6}{1406 * 0.902 * 168} = 312.5\ MPa$

**A.5.2.5.2. Crack Control Parameter**

$d_c = h - d = 200 - 168 = 32\ mm$

$A = 2 * S * d_c = 2 * 128 * 32 = 8192\ mm$

$z = f_s \sqrt[3]{d_c A} = 312.5 * \sqrt[3]{32 * 8192} = 20000\ N/mm < 30000\ N/mm$ OK

**Clause 10.6.1 (A23.3-04)**

**Summary:**

- **Place 15M @ 128 mm c/c in a band 900 mm wide centered on the column.**
- **Place 15M @ 475 mm c/c for the rest of the strip.**

### A.5.3. The Strip Parallel to the Free Edge

#### A.5.3.1. Effective Depth "$d$"

$d = h_s - clear\ cover - d_b - \frac{d_b}{2} = 200 - 24 - 16 - \frac{16}{2} = 152\ mm$

#### A.5.3.2. Design Moments

$M_o = \frac{w_f * l_a * l_n^2}{8} = \frac{10.85 * 3.4 * 6.2^2}{8} = 177.26\ kN.m$ **Clause 13.9.2**

Table A.2: Moment distribution in a design strip parallel to the free edge

| Axis | 1 | | | 2 | | 3 | Units | Clause |
|---|---|---|---|---|---|---|---|---|
| $l_n$ | 6200 | | | 6200 | | | | |
| $M_{Design}$ | 26 | 52 | 70 | 65 | 35 | 65 | % | 13.9.3 |
| | 46.1 | 92.2 | 124.1 | 115.2 | 62.04 | 115.2 | kN.m | |
| $M_{Col\ Str}$ | 100 | 60 | 70-90 | 70-90 | 55-65 | 70-90 | % | 13.11.2 |
| | 46.1 | 55.3 | **86.9-111.7** | 80.7-103.7 | 34.1-40.3 | 80.7-103.7 | kN.m | |
| $M_{Fld.Str}$ | 0 | 40 | 30-10 | 30-10 | 45-35 | 30-10 | % | 13.11.2 |
| | 0 | 36.9 | 37.2-12.4 | 34.6-11.5 | 27.9-21.7 | 34.6-11.5 | kN.m | |

#### A.5.3.3. Reinforcement

$M_{Design} = 86.86\ kN.m - 111.67\ kN.m$

- At interior columns, the band width $b_b$ shall be designed to resist at least one-third of the total factored negative moment in the entire design strip. **Clause 13.11.2.7**

❖ **For the Band Width $b_b = c + 1.5h_s$:**

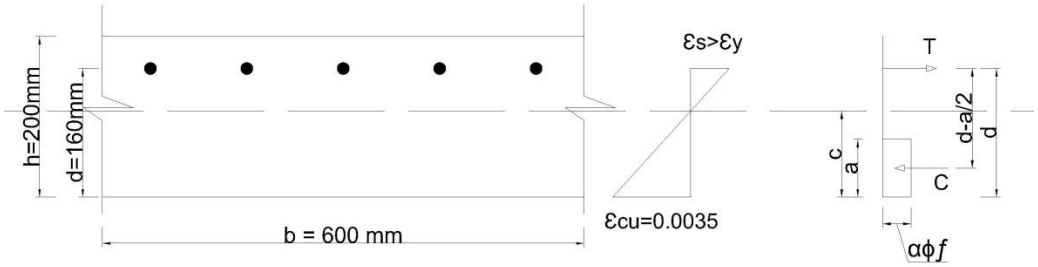


Figure A.5: Strain distribution and equivelant stress block

$b_b = c + 1.5h_s = 300 + 1.5 * 200 = 600\ mm$

$a = \frac{\phi_s A_s f_y}{\alpha_1 \phi_c f'_c b} = \frac{1.0 * A_s * 415}{0.7975 * 1.0 * 35 * 600} = 24.78 * 10^{-3}\ A_s$

$M = {}^{1}/_{3} * 124.08 = 41.36\ kN.m$

$M_r = \phi_s A_s f_y * \left(d - \frac{a}{2}\right)$

$\rightarrow 41.36 * 10^6 = 1.0 * A_s * 415 * (152 - \frac{24.78 * 10^{-3}\ A_s}{2})$

$\rightarrow 5.142 {A_s}^2 - 63080 A_s + 41.36 * 10^6 = 0$

$\rightarrow A_s = 719.1\ mm^2$

$A_s = \frac{b}{S} * A_b \rightarrow 719.1 = \frac{600}{S} * 200 \rightarrow S = 166.9\ mm$ Use 15M @ 166 mm c/c

$\rightarrow A_{s_{act}} = \frac{600}{166} * 200 = 722.89\ mm^2$

➢ **Check for the Unbalanced Moment:** **Clause 13.9.4**

$M_{Unb.} = 0.07 * \left[\left(w_{df} + 0.5\ w_{lf}\right) l_{2a} l_n^2 - w'_{df} l'_{2a} (l'_n)^2\right]$

$= 0.07\ [(7.25 + 0.5 * 3.6) * 3.4 * 6.2^2 - 7.25 * 3.4 * 6.2^2] = 16.47\ kN.m$

- The fraction to be carried by flexure within width $b_b$ is $\gamma_f$ **Clause 13.10.2**

$\gamma_f = \frac{1}{1 + \frac{2}{3}\sqrt{\frac{b_1}{b_2}}} = \frac{1}{1 + \frac{2}{3}\sqrt{\frac{380}{459}}} = 0.62$ **Clause 13.3.5.3**

$\gamma_f * M_{Unb} = 0.62 * 16.47 = 10.25\ kN.m < (M_r = 41.36\ kN.m)$ OK

➢ **Check for the Balanced Reinforcement Ratio "$\rho_b$":**

$\rho = \frac{722.89}{152*600} = 0.8 * 10^{-2}$

$\rho_b = 3.71 * 10^{-2}$

$\rightarrow\ \rho < \rho_b$ Under-reinforced OK

❖ **For the Rest of the Strip:**

$b = 1775 - 600 = 1175\ mm$

$M = 111.67 - 41.36 = 70.31\ kN.m$

$a = \frac{\phi_s A_s f_y}{\alpha_1 \phi_c f'_c b} = \frac{1.0*A_s*415}{0.7975*1.0*35*1175} = 12.65 * 10^{-3}\ A_s$

$M_r = \phi_s A_s f_y * \left(d - \frac{a}{2}\right)$

$\rightarrow\ 70.31 * 10^6 = 1.0 * A_s * 415\ (152 - \frac{12.65*10^{-3}\ A_s}{2})$

$\rightarrow 2.626\ {A_s}^2 - 63080 A_s + 70.31 * 10^6$

$\rightarrow A_s = 1211.8\ mm^2$

$A_s = \frac{b}{S} * A_b \rightarrow 1211.8 = \frac{1175}{S} * 200 \rightarrow S = 193.9\ mm$ Use 15M @ 193 mm c/c

**A.5.3.4. Development Length "$l_d$"** **Clause 12.2**

$l_d = 0.45 k_1 k_2 k_3 k_4 \frac{f_y}{\sqrt{f'_c}}\ d_b$ **Clause 12.2.3**

$k_1 = 1.0\ for\ horizontal\ reinforcement\ placed\ in\ such\ a\ way\ that\ less\ than\ 300\ mm$

$of\ fresh\ concrete\ is\ cast\ in\ the\ member\ below\ the\ development\ length$

$k_2 = 1.0\ for\ uncoated\ reinforcement$

$k_3 = 1.0\ for\ normal\ density\ concrete$

$k_4 = 0.8\ for\ 20M\ and\ smaller\ bars\ and\ deformed\ wires$

$\rightarrow l_d = 0.45 * 1.0 * 1.0 * 1.0 * 0.8 * \frac{415}{\sqrt{35}} * 16 = 404.1\ mm$ OK

**A.5.3.5. Serviceability Check**

**A.5.3.5.1. Service Stress Calculations**

Specified load $w_s = D.L. + L.L. = 5.8 + 2.4 = 8.2\ kN/m^2$ (NBCC 2010)

Service moment $M_s = \frac{w_s * l_{2a} * l_n^2}{8} = \frac{8.2 * 3.4 * 6.2^2}{8} = 133.96\ kN.m$ **Clause 13.9.2**

Service moment at the edge connection $= M_s * 0.7 * 0.33 = 133.96 * 0.7 * 0.33 =$

$31.26\ kN.m$

$n = \frac{E_s}{E_c} = \frac{197000}{29878} = 6.59$

$k = \sqrt{2\rho n + (\rho n)^2} - \rho n = \sqrt{2 * 0.0079 * 6.59 + (0.0079 * 6.59)^2} - 0.0079 * 6.59 = 0.275$

$j = 1 - \frac{k}{3} = 1 - \frac{0.275}{3} = 0.908$

Service stress $f_s = \frac{M_s}{A_s jd} = \frac{31.3 * 10^6}{723 * 0.908 * 152} = 313.25\ MPa$

**A.5.3.5.2. Crack Control Parameter**

$d_c = h - d = 200 - 152 = 48\ mm$

$A = 2 * S * d_c = 2 * 166 * 48 = 15936\ mm$

$z = f_s \sqrt[3]{d_c A} = 313.3 * \sqrt[3]{48 * 15936} = 28652.8\ N/mm < 30000\ N/mm$ OK

**Clause 10.6.1 (A23.3-04)**

**Summary:**

- **Place 15M @ 166 mm c/c in a band 600 mm wide beneath the column.**
- **Place 15M @ 193 mm c/c for the rest of the strip.**

## A.6. Analysis of a sand-coated GFRP-RC Parking Garage Flat Plate (According to CSA A23.3-04 and CSA S806-12)

### A.6.1. Properties of Reinforcement:

Material resistance factor $\phi_f = 1.0$

#### A.6.1.1. Bent Bars

Use No. 19 bars $d_{b_{ext.}} = 20.5\ mm$ $A_b = 285\ mm^2$

Ultimate tensile strength of GFRP $f_{frp_u} = 1232.3\ MPa$

Ultimate tensile strain for GFRP $\varepsilon_{frp_u} = 0.023$

Modulus of elasticity for GFRP $E_{frp} = 52.46\ GPa$

#### A.6.1.2. Straight Bars

Use No. 19 bars $d_{b_{ext.}} = 22\ mm$ $A_b = 285\ mm^2$

Ultimate tensile strength of GFRP $f_{frp_u} = 1484\ MPa$

Ultimate tensile strain for GFRP $\varepsilon_{frp_u} = 0.023$

Modulus of elasticity for GFRP $E_{frp} = 65.374\ GPa$

### A.6.2. The Strip Perpendicular to the Free Edge

#### A.6.2.1. Effective Depth "$d$"

Take concrete clear cover $= 19.5\ mm$

→ Effective depth "$d$" $= h_s - clear\ cover - \frac{d_b}{2} = 200 - 19.5 - \frac{20.5}{2} = 170.25\ mm$

#### A.6.2.2. Design Moments

$M_o = \frac{w_{f^*}\, l_{2a^*}\, l_n^2}{8} = \frac{10.85 * 6.5 * 6.2^2}{8} = 338.87\ kN.m$ **Clause 13.9.2 (A23.3-04)**

Table A.3: Moment distribution in a design strip perpendicular to the free edge

| Axis | A | | | B | | C | Units | Clause |
|---|---|---|---|---|---|---|---|---|
| $l_n$ | 6200 | | | 6200 | | | | |
| $M_{Design}$ | 26 | 52 | 70 | 65 | 35 | 65 | % | 13.9.3 |
| | 88.1 | 176.2 | 237.2 | 220.3 | 118.6 | 20.3 | kN.m | |
| $M_{Col\ Str}$ | 100 | 60 | 70-90 | 70-90 | 55-65 | 70-90 | % | 13.11.2 |
| | **88.1** | 105.7 | 166.1-213.5 | 154.2-198.2 | 65.2-77.1 | 154.2-198.2 | kN.m | |
| $M_{Fld.Str}$ | 0 | 40 | 30-10 | 30-10 | 45-35 | 30-10 | % | 13.11.2 |
| | 0 | 70.5 | 71.2-23.7 | 66.1-22 | 53.4-41.5 | 66.1-22 | kN.m | |

### A.6.2.3. Reinforcement

$M_{Design} = 88.11\ kN.m$

- Reinforcement for the total factored negative moment transferred to the exterior columns shall be placed within a band width $b_b = c + 3h_s$ **Clause 13.10.3 (A23.3-04)**

❖ **For the Band Width $b_b = c + 3h_s$:**

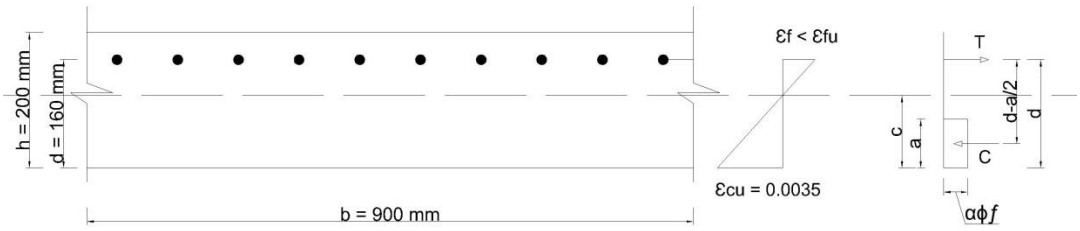


Figure A.6: Strain distribution and equivelant stress block

$b_b = c + 3h_s = 300 + 3 * 200 = 900\ mm$

$M_r = \alpha_1 \phi_c f_c' b \beta c * \left(d - \frac{\beta c}{2}\right)$

$\rightarrow 88.11 * 10^6 = 0.7975 * 1.0 * 35 * 900 * 0.8825 * c * \left(170.25 - \frac{0.8825 * c}{2}\right)$

$\rightarrow 9782.29c^2 - 3774357.91c + 88.11 * 10^6 = 0$

$\rightarrow c = 24.96\ mm$

From strain compatibility:

$\varepsilon_f = \varepsilon_{c_u} * \left(\frac{d}{c} - 1\right) = 0.0035 * \left(\frac{170.25}{24.96} - 1\right) = 20.37 * 10^{-3}$

$\rightarrow f_f = E_f * \varepsilon_f = 52460 * 20.37 * 10^{-3} = 1068.8\ MPa$

$C = T$

$\rightarrow \alpha_1 \phi_c f_c' b \beta c = \phi_f A_f f_f$

$\rightarrow 0.7975 * 1.0 * 35 * 900 * 0.8825 * 24.96 = 1.0 * A_f * 1068.8$

$\rightarrow A_f = 517.74\ mm^2$

$A_{f_{min}} = \frac{400}{E_f} * A_g = \frac{400}{52460} * (200 * 900) = 1372.47\ mm^2$ (Governs) **Clause 8.4.2.3 (S806-12)**

$A_f = \frac{b}{s} * A_b \rightarrow 1372.47 = \frac{900}{s} * 285 \rightarrow s = 186.89\ mm$ Use No. 19 @ 186 mm c/c

➢ **Check for the Balanced Reinforcement Ratio "$\rho_b$":**

$A_{f_{act}} = \frac{b}{s} * A_b = \frac{900}{186} * 285 = 1379.03\ mm^2$

$\rho = \frac{1379.03}{900 * 170.25} = 0.9\%$

$\rho_b = \alpha_1 \beta_1 \frac{\phi_c f_c'}{\phi_f f_{fu}} * \frac{\varepsilon_{c_u}}{\varepsilon_{c_u} + \varepsilon_{fu}}$

$\rho_b = 0.7975 * 0.8825\ \frac{1.0 * 35}{1.0 * 1232.3} * \frac{0.0035}{0.0035 + 0.023} = 0.26\%$

$\rightarrow\ \rho > \rho_b$ Over-Reinforced OK

❖ **For the Rest of the Strip:**

- Use minimum reinforcement "$A_{s_{min}}$"

$A_{f_{min}} = \frac{400}{E_f} * A_g = \frac{400}{52460} * (200 * 1000) = 1524.97\ mm^2/m$ (Governs)

**Clause 8.4.2.3 (S806-12)**

Or $= 0.0025 A_g = 0.0025 * (200 * 1000) = 500\ mm^2/m$

Maximum spacing $s_{max} = 3h_s = 3 * 200 = 600\ mm$ **Clause 8.4.2.3 (S806-12)**

Or $= 300\ mm$ (Governs)

$A_f = \frac{b}{s} * A_b \rightarrow 1524.97 = \frac{1000}{s} * 285 \rightarrow s = 186\ mm$

### A.6.2.4. Development Length "$l_d$" **Clause 9.5 (S806-12)**

$$f_f = 0.5E_f\varepsilon_{c_u}\left[\left(1 + \frac{4\alpha_1\beta_1\phi_c f_c'}{\rho_f\phi_f E_f\varepsilon_{c_u}}\right)^{1/2} - 1\right]$$

$$= 0.5 * 52460 * 0.0035 * \left[\left(1 + \frac{4*0.7975*0.8825*1.0*35}{0.009*1.0*52460*0.0035}\right)^{1/2} - 1\right]$$

$\rightarrow f_f = 623\ MPa$

$l_d = \frac{f_f}{3.1} k_2 \frac{d_b}{\sqrt{f_c'}}$ When $520\ MPa < f_{frp} \leq 1040\ MPa$

$k_2 = 1.0\ for\ normal\ density\ concrete$

$l_d = \frac{623}{3.1} * 1.0 * \frac{20.5}{\sqrt{35}} = 696.4\ mm$

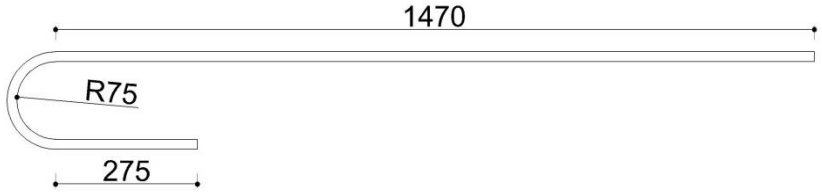


Figure A.7: Typical sand-coated GFRP bent bar dimensions

### A.6.2.5. Serviceability Check

#### A.6.2.5.1. Service Stress Calculations

Specified load $w_s = D.L. + L.L. = 5.8 + 2.4 = 8.2\ kN/m^2$ (NBCC 2010)

Service moment $M_s = \frac{w_s * l_{2a} * l_n^2}{8} = \frac{8.2 * 6.5 * 6.2^2}{8} = 256.11\ kN.m$ **Clause 13.9.2**

Service moment at the edge connection $= M_s * 0.26 = 256.11 * 0.26 = 66.6\ kN.m$

**Clause 13.10.3**

$n = \frac{E_f}{E_c} = \frac{52460}{29906} = 1.75$

$k = \sqrt{2\rho n + (\rho n)^2} - \rho n = \sqrt{2 * 0.009 * 1.75 + (0.009 * 1.75)^2} - 0.009 * 1.75 = 0.162$

$j = 1 - \frac{k}{3} = 1 - \frac{0.162}{3} = 0.946$

Service stress $f_s = \frac{M_s}{A_s jd} = \frac{66.6*10^6}{1379*0.946*170.25} = 299.87\ MPa$

**A.6.2.5.2. Crack Control Parameter**

$d_c = h - d = 200 - 170.25 = 29.75\ mm$

$A = 2 * S * d_c = 2 * 186 * 29.75 = 11067\ mm$

$z = f_s k_p \frac{E_s}{E_f} \sqrt[3]{d_c A} = 299.9 * 1.2 * \frac{197000}{52460} \sqrt[3]{29.75 * 11067} = 93318.5\ N/mm \gg 45000\ N/mm$

**Clause 8.3.1.1. (S806-12)**

Try No. 19 @ 93 mm c/c for the whole specimen

$k = \sqrt{2\rho n + (\rho n)^2} - \rho n = \sqrt{2 * 0.018 * 1.75 + (0.018 * 1.75)^2} - 0.018 * 1.75 = 0.221$

$j = 1 - \frac{k}{3} = 1 - \frac{0.221}{3} = 0.926$

Service stress $f_s = \frac{M_s}{A_s jd} = \frac{66.6*10^6}{2758*0.926*170.25} = 153.17\ MPa$

$A = 2 * S * d_c = 2 * 93 * 29.75 = 5533.5\ mm$

$z = f_s k_p \frac{E_s}{E_f} \sqrt[3]{d_c A} = 153.17 * 1.2 * \frac{197000}{52460} \sqrt[3]{29.75 * 5533.5} = 37828.7\ N/mm <$

$45000\ N/mm$ ok

**A.6.2.5.3. Reinforcement Strain Limit** **Clause 7.1.2.2. (S806-12)**

$0.25 f_u = 0.25 * 1232.3 = 308.08\ MPa > f_s = 153.17\ MPa$ OK

**Summary:**

- **Place No. 19 @ 93 mm c/c for the whole specimen.**

### A.6.3. The Strip Parallel to the Free Edge

#### A.6.3.1. Effective Depth "$d$"

$$d = h_s - clear\ cover - d_b - \frac{d_b}{2} = 200 - 19.5 - 20.5 - \frac{22}{2} = 149\ mm$$

#### A.6.3.2. Design Moments

$$M_o = \frac{w_f * l_a * l_n^2}{8} = \frac{10.85 * 3.4 * 6.2^2}{8} = 177.26\ kN.m$$ **Clause 13.9.2 (A23.3-04)**

Table A.4: Moment distribution in a design strip parallel to the free edge

| Axis | 1 | | 2 | | | 3 | Units | Clause |
|---|---|---|---|---|---|---|---|---|
| $l_n$ | 6200 | | | 6200 | | | | |
| $M_{Design}$ | 26 | 52 | 70 | 65 | 35 | 65 | % | 13.9.3 |
| | 46.1 | 92.2 | 124.1 | 115.2 | 62.04 | 115.2 | kN.m | |
| $M_{Col\ Str}$ | 100 | 60 | 70-90 | 70-90 | 55-65 | 70-90 | % | 13.11.2 |
| | 46.1 | 55.3 | **86.9-111.7** | 80.7-103.7 | 34.1-40.3 | 80.7-103.7 | kN.m | |
| $M_{Fld.Str}$ | 0 | 40 | 30-10 | 30-10 | 45-35 | 30-10 | % | 13.11.2 |
| | 0 | 36.9 | 37.2-12.4 | 34.6-11.5 | 27.9-21.7 | 34.6-11.5 | kN.m | |

#### A.6.3.3. Reinforcement

$$M_{Design} = 86.86\ kN.m - 111.67\ kN.m$$

- At interior columns, the band width $b_b$ shall be designed to resist at least one-third of the total factored negative moment in the entire design strip. **Clause 13.11.2.7 (A23.3-04)**

- **For the Band Width $b_b = c + 1.5h_s$:**

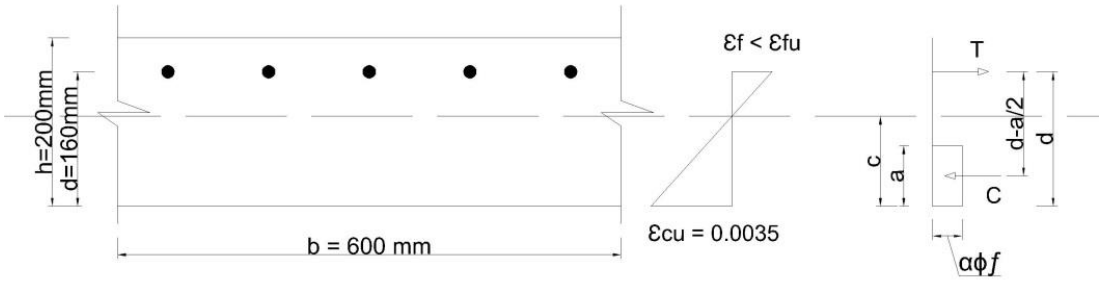


Figure A.8: Strain distribution and equivelant stress block

$b_b = c + 1.5h_s = 300 + 1.5 * 200 = 600\ mm$

$M = {}^{1}/_{3} * 124.08 = 41.36\ kN.m$

$M_r = \alpha_1 \phi_c f_c' b \beta c * \left(d - \frac{\beta c}{2}\right)$

$\rightarrow 41.36 * 10^6 = 0.7975 * 1.0 * 35 * 600 * 0.8825 * c * \left(149 - \frac{0.8825 * c}{2}\right)$

$\rightarrow 6521.53c^2 - 2202170.64c + 41.36 * 10^6 = 0$

$\rightarrow c = 19.96\ mm$

From strain compatibility:

$\varepsilon_f = \varepsilon_{c_u} * \left(\frac{d}{c} - 1\right) = 0.0035 * \left(\frac{149}{19.96} - 1\right) = 22.63 * 10^{-3}$

$\rightarrow f_f = E_f * \varepsilon_f = 65374 * 22.63 * 10^{-3} = 1479.23\ MPa \cong f_{f_u}$

Try $A_{f_{min}} = \frac{400}{E_f} * A_g = \frac{400}{65374} * (200 * 600) = 734.24\ mm^2$

$\alpha_1 \phi_c f_c' b \beta c = \phi_f A_f f_f$

$0.7975 * 1.0 * 35 * 600 * 0.8825 * c = 1.0 * 734.24 * 65374 * \varepsilon_f$

$\varepsilon_f = 3.08 * 10^{-4} * c = \varepsilon_{c_u} * \left(\frac{d}{c} - 1\right) = 0.0035 * \left(\frac{149}{c} - 1\right)$

$3.08 * 10^{-4} c^2 + 0.0035c - 0.5215 = 0$

$c = 35.86\ mm$

$\rightarrow \varepsilon_f = 3.08 * 10^{-4} * 35.86 = 11.04 * 10^{-3}$

$\rightarrow f_{frp} = 65374 * 11.04 * 10^{-3} = 721.83\ MPa < f_{f_u}$

$\rightarrow M_r = \phi_f A_f f_f * \left(d - \frac{\beta c}{2}\right) = 1.0 * 734.24 * 721.83 * \left(149 - \frac{0.8825*35.86}{2}\right) = 70.58\ kN.m >$

$M_f = 41.36\ kN.m$

$A_f = \frac{b}{s} * A_b \rightarrow 734.24 = \frac{600}{s} * 285 \rightarrow s = 232.89\ mm$ Use No. 19 @ 232 mm c/c

❖ **For the Rest of the Strip:**

Use $A_{f_{min}}$ Use No. 19 @ 232 mm c/c

$\rho_{frp} = \frac{737.07}{600*149} = 0.82\%$

**A.6.3.4. Development Length "$l_d$"** **Clause 9.3.2 (S806-12)**

$l_d = 1.15\ \frac{k_1 k_2 k_3 k_4 k_5}{d_{cs}} \frac{f_f}{\sqrt{f_c'}}\ A_b$

$k_1 = 1.0\ for\ horizontal\ reinforcement\ placed\ in\ such\ a\ way\ that\ less\ than\ 300\ mm\ of\ fresh\ concrete\ is\ cast\ in\ the\ member\ below\ the\ development\ length$

$k_2 = 1.0\ for\ normal\ density\ concrete$

$k_3 = 0.8\ for\ A_b < 300mm^2$

$k_4 = 1.0\ for\ GFRP$

$k_5 = 1.0\ sand\ coated\ bars$

$l_d = 1.15 * \frac{1*1*0.8*1*1}{66.5} * \frac{726.08}{\sqrt{35}} * 285 = 483.91\ mm$ OK

**A.6.3.5. Serviceability Check**

**A.6.3.5.1. Service Stress Calculations**

Specified load $w_s = D.L. + L.L. = 5.8 + 2.4 = 8.2\ kN/m^2$ (NBCC 2010)

Service moment $M_s = \frac{w_s * l_{2a} * l_n^2}{8} = \frac{8.2 * 3.4 * 6.2^2}{8} = 133.96\ kN.m$ **Clause 13.9.2**

Service moment at the edge connection $= M_s * 0.7 * 0.33 = 133.96 * 0.7 * 0.33 = 31.3\ kN.m$

**Clause 13.10.3**

$n = \frac{E_f}{E_c} = \frac{65374}{29906} = 2.19$

$k = \sqrt{2\rho n + (\rho n)^2} - \rho n = \sqrt{2 * 0.0082 * 2.19 + (0.0082 * 2.19)^2} - 0.0082 * 2.19 = 0.172$

$j = 1 - \frac{k}{3} = 1 - \frac{0.172}{3} = 0.943$

Service stress $f_s = \frac{M_s}{A_s jd} = \frac{31.3*10^6}{737*0.943*149} = 302.26\ MPa$

**A.6.3.5.2. Crack Control Parameter**

$d_c = h - d = 200 - 149 = 51\ mm$

$A = 2 * S * d_c = 2 * 232 * 51 = 23664\ mm$

$z = f_s k_p \frac{E_s}{E_f} \sqrt[3]{d_c A} = 302.3 * 1.2 * \frac{197000}{65374} \sqrt[3]{51 * 23664} = 116385.8\ N/mm \gg 38000\ N/mm$

**Clause 8.3.1.1. (S806-12)**

Try No. 19 @ 116 mm c/c for the whole specimen

$k = \sqrt{2\rho n + (\rho n)^2} - \rho n = \sqrt{2 * 0.0164 * 2.19 + (0.0164 * 2.19)^2} - 0.0164 * 2.19 = 0.234$

$j = 1 - \frac{k}{3} = 1 - \frac{0.234}{3} = 0.922$

Service stress $f_s = \frac{M_s}{A_s jd} = \frac{31.3*10^6}{1474*0.922*149} = 154.57\ MPa$

$A = 2 * S * d_c = 2 * 116 * 51 = 11832\ mm$

$z = f_s k_p \frac{E_s}{E_f} \sqrt[3]{d_c A} = 154.57 * 1.2 * \frac{197000}{65374} \sqrt[3]{51 * 11832} = 47232.8\ N/mm \cong 45000\ N/mm$

ok

**Summary:**

- **Place No. 19 @ 232 mm c/c for the whole strip.**

# APPENDIX B

## Shear Capacity of Connections without Shear Reinforcement

## B.1. Properties of the Critical Section

$d_v = 160\ mm$

$b_1 = c + \frac{d_v}{2} = 300 + \frac{160}{2} = 380\ mm$

$b_2 = c + 2 * \frac{d_v}{2} = 300 + 2 * \frac{160}{2} = 460\ mm$

$b_o = 2 * b_1 + b_2 = 2 * 380 + 460 = 1220\ mm$

$e = \frac{{b_1}^2}{2b_1 + b_2} = \frac{380^2}{2*380+460} = 118.4\ mm$

$J = 2\left(\frac{{b_1}^3 * d_v}{3} + \frac{{d_v}^3 * b_1}{12}\right) - b_o * d_v * e^2$

$= 2\left(\frac{380^3 * 160}{3} + \frac{160^3 * 380}{12}\right) - 1220 * 160 *$

$118.4^2 = 3377852377\ mm^4$

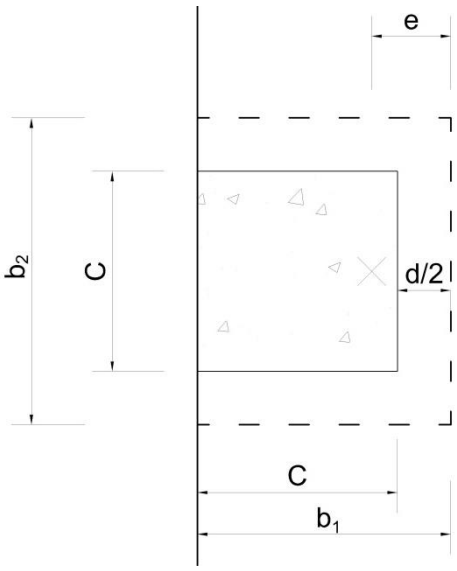


Figure B.1: Critical section at d/2 from column face

Where *e* is the distance between the centroid and the inner side of the critical section and J is a property of the critical shear section analogous to the polar moment of inertia

$\beta_c = \frac{c}{c} = 1$

$\gamma_v = 1 - \frac{1}{1+\frac{2}{3}\sqrt{\frac{b_1}{b_2}}} = 1 - \frac{1}{1+\frac{2}{3}\sqrt{\frac{380}{460}}} = 0.38$

$\frac{M_o}{V} = \frac{M}{V} - \left(b_1 - e - \frac{c}{2}\right) = 0.2 - \left(0.38 - 0.1184 - \frac{0.3}{2}\right) = 0.0884\ m \ \ when\ \frac{M}{V} = 0.2\ m$

$\frac{M_o}{V} = \frac{M}{V} - \left(b_1 - e - \frac{c}{2}\right) = 0.4 - \left(0.38 - 0.1184 - \frac{0.3}{2}\right) = 0.2884\ m \ \ when\ \frac{M}{V} = 0.4\ m$

$\frac{M_o}{V} = \frac{M}{V} - \left(b_1 - e - \frac{c}{2}\right) = 0.6 - \left(0.38 - 0.1184 - \frac{0.3}{2}\right) = 0.4884\ m \ \ when\ \frac{M}{V} = 0.6\ m$

## B.2. Connection S-0.9-XX-0.4

### B.2.1. Material Properties

#### B.2.1.1. Concrete

Actual compressive strength of concrete $f_c' = 41\ MPa$

Material resistance factor $\phi_c = 1.0$

Concrete density factor $\lambda = 1.0$

#### B.2.1.2. Flexural Reinforcement

Reinforcement ratio perpendicular to the free edge, $\rho_p = 0.0093$

Reinforcement ratio parallel to the free edge, $\rho_l = 0.0079$

Average reinforcement ratio, $\rho = \frac{\rho_p * b_2 + 2 * \rho_l * b_1}{b_o} = \frac{0.0093 * 460 + 2 * 0.0079 * 380}{1220} = 0.0084$

### B.2.2. Shear Capacity according to CAN/CSA A23.3-04 **Clause 13.3**

$v_r = v_c = 0.19 * \left(1 + \frac{2}{\beta_c}\right) \lambda \varphi_c \sqrt{f_c'} = 0.19 * \left(1 + \frac{2}{1}\right) * 1.0 * 1.0 * \sqrt{41} = 3.65\ MPa$

$v_r = v_c = \left(0.19 + \alpha_s \frac{d_v}{b_o}\right) \lambda \varphi_c \sqrt{f_c'} = \left(0.19 + 3 * \frac{160}{1220}\right) * 1.0 * 1.0 * \sqrt{41} = 3.74\ MPa$

$v_r = v_c = 0.38 \lambda \varphi_c \sqrt{f_c'} = 0.38 * 1.0 * 1.0 * \sqrt{41} = 2.43\ MPa$ (Governs)

$V = {v_r}\Big/\left(\frac{1}{b_O * d} + \frac{0.2884\gamma}{J} * e\right) = {2.43 * 10^{-3}}\Big/\left(\frac{1}{1220 * 160} + \frac{0.38 * 0.2884 * 1000}{3377852377} * 118.4\right) = 272.05\ kN$

### B.2.3. Shear Capacity according to ACI 318-11 **Clause 11.11**

$v_r = v_c = 0.083 * \left(2 + \frac{4}{\beta_c}\right) \lambda \sqrt{f_c'} = 0.083 * \left(2 + \frac{4}{1}\right) * 1.0 * \sqrt{41} = 3.19\ MPa$

$v_r = v_c = 0.083 * \left(2 + \alpha_s \frac{d_v}{b_o}\right) \lambda \sqrt{f_c'} = 0.083 * \left(2 + 30 * \frac{160}{1220}\right) * 1.0 * \sqrt{41} = 3.15\ MPa$

$v_r = v_c = 0.32 \lambda \sqrt{f_c'} = 0.32 * 1.0 * \sqrt{41} = 2.05\ MPa$ (Governs)

$V = {v_r}\Big/\left(\frac{1}{b_O * d} + \frac{0.2884\gamma}{J} * e\right) = {2.05 * 10^{-3}}\Big/\left(\frac{1}{1220 * 160} + \frac{0.38 * 0.2884 * 1000}{3377852377} * 118.4\right) = 229.51\ kN$

**B.2.4. Shear Capacity according to JSCE 2007** **Clause 9.2.2.3**

$$\beta_d = \sqrt[4]{\frac{1000}{d}} = \sqrt[4]{\frac{1000}{160}} = 1.58 = 1.5$$

$$\beta_p = \sqrt[3]{100\rho} = \sqrt[3]{100 * 0.0084} = 0.94$$

$$\beta_r = 1 + \frac{1}{1+0.25*\frac{3c}{d}} = 1 + \frac{1}{1+0.25*\frac{3*300}{160}} = 1.42$$

$$f_{pcd} = 0.2\sqrt{f_c'} = 0.2 * \sqrt{41} = 1.28 = 1.2\ MPa$$

$$v_r = v_c = \frac{\beta_d \beta_p \beta_r f_{pcd}}{\gamma_b} = \frac{1.5*0.94*1.42*1.2}{1} = 2.4\ MPa$$

$$V = {v_r}\Big/\left(\frac{1}{b_O*d} + \frac{0.2884\gamma}{J} * e\right) = 2.4 * 10^{-3}\Big/\left(\frac{1}{1220*160} + \frac{0.38*0.2884*1000}{3377852377} * 118.4\right) = 269.16\ kN$$

**B.3. Connection GSC-0.9-XX-0.4**

**B.3.1. Material Properties**

**B.3.1.1. Concrete**

Actual compressive strength of concrete $f_c' = 41.1\ MPa$

Material resistance factor $\phi_c = 1.0$

Concrete density factor $\lambda = 1.0$

Modulus of elasticity $E_c = 4500\sqrt{f_c'} = 4500 * \sqrt{41.1} = 28849\ MPa$

**B.3.1.2. Flexural Reinforcement**

Reinforcement ratio perpendicular to the free edge, $\rho_p$ = 0.009

Reinforcement ratio parallel to the free edge, $\rho_l$ = 0.0082

Average reinforcement ratio, $\rho = \frac{\rho_p * b_2 + 2 * \rho_l * b_1}{b_o} = \frac{0.009*460+2*0.0082*380}{1220} = 0.0085$

Modulus of elasticity perpendicular to the free edge, $E_p$ = 52460 *MPa*

Modulus of elasticity parallel to the free edge, $E_l$ = 65374 *MPa*

Average modulus of elasticity, $E = \frac{E_p * b_2 + 2 * E_l * b_1}{b_o} = \frac{52460 * 460 + 2 * 65374 * 380}{1220} = 60505\ MPa$

Modular ratio, $n = \frac{E_f}{E_c} = \frac{60505}{28849} = 2.1$

**B.3.2. Shear Capacity according to CAN/CSA S806-12** **Clause 8.7**

$v_r = v_c = \left(1 + \frac{2}{\beta_c}\right)\left[0.028\lambda\varphi_c\left(E_f\rho_f f_c'\right)^{1/3}\right] = \left(1 + \frac{2}{1}\right)\left[0.028 * 1.0 * 1.0 * (60505 * 0.0085 * 41.1)^{1/3}\right] = 2.32MPa$

$v_r = v_c = 0.147\lambda\varphi_c\left(0.19 + \alpha_s\frac{d_v}{b_o}\right)\left(E_f\rho_f f_c'\right)^{1/3} = 0.147 * 1.0 * 1.0 * \left(0.19 + 3 * \frac{160}{1220}\right) * (60505 * 0.0085 * 41.1)^{1/3} = 2.37MPa$

$v_r = v_c = 0.056\lambda\varphi_c\left(E_f\rho_f f_c'\right)^{1/3} = 0.056 * 1.0 * 1.0 * (60505 * 0.0085 * 41.1)^{1/3} = 1.55MPa$ (Governs)

$V = {v_r}\Big/\left(\frac{1}{b_O * d} + \frac{0.2884\gamma}{J} * e\right) = {1.55 * 10^{-3}}\Big/\left(\frac{1}{1220 * 160} + \frac{0.38 * 0.2884 * 1000}{3377852377} * 118.4\right) = 173.53\ kN$

**B.3.3. Shear Capacity according to ACI 440.1R-06** **Clause 9.4**

$k = \sqrt{2\rho n + (\rho n)^2} - \rho n = \sqrt{2 * 0.0085 * 2.1 + (0.0085 * 2.1)^2} - 0.0085 * 2.1 = 0.172$

$c = kd = 0.172 * 160 = 27.51\ mm$

$v_r = v_c = 0.8 * \frac{c}{d}\sqrt{f_c'} = 0.8 * \frac{27.51}{160}\sqrt{41.1} = 0.88\ MPa$

$V = {v_r}\Big/\left(\frac{1}{b_O * d} + \frac{0.2884\gamma}{J} * e\right) = {0.88 * 10^{-3}}\Big/\left(\frac{1}{1220 * 160} + \frac{0.38 * 0.2884 * 1000}{3377852377} * 118.4\right) = 98.52\ kN$

**B.3.4. Shear Capacity according to JSCE 1997** **Clause 6.3.4**

$\beta_d = \sqrt[4]{\frac{1000}{d}} = \sqrt[4]{\frac{1000}{160}} = 1.58 = 1.5$

$\beta_p = \sqrt[3]{100\rho * \frac{E_f}{200000}} = \sqrt[3]{100 * 0.0085 * \frac{60505}{200000}} = 0.64$

$$\beta_r = 1 + \frac{1}{1+0.25*\frac{3c}{d}} = 1 + \frac{1}{1+0.25*\frac{3*300}{160}} = 1.42$$

$$f_{pcd} = 0.2\sqrt{f_c'} = 0.2 * \sqrt{41.1} = 1.28 = 1.2\ MPa$$

$$v_r = v_c = \frac{\beta_d \beta_p \beta_r f_{pcd}}{\gamma_b} = \frac{1.5*0.64*1.42*1.2}{1} = 1.62\ MPa$$

$$V = {v_r}\Big/\left(\frac{1}{b_O*d} + \frac{0.2884\gamma}{J} * e\right) = 1.62 * 10^{-3}\Big/\left(\frac{1}{1220*160} + \frac{0.38*0.2884*1000}{3377852377} * 118.4\right) = 181.4\ kN$$

**B.4. Connection GSC-1.35-XX-0.4**

**B.4.1. Material Properties**

**B.4.1.1. Concrete**

Actual compressive strength of concrete $f_c' = 41\ MPa$

Material resistance factor $\phi_c = 1.0$

Concrete density factor $\lambda = 1.0$

Modulus of elasticity $E_c = 4500\sqrt{f_c'} = 4500 * \sqrt{41} = 28814\ MPa$

**B.4.1.2. Flexural Reinforcement**

Reinforcement ratio perpendicular to the free edge, $\rho_p$ = 0.0135

Reinforcement ratio parallel to the free edge, $\rho_l$ = 0.0123

Average reinforcement ratio, $\rho = \frac{\rho_p * b_2 + 2 * \rho_l * b_1}{b_o} = \frac{0.0135*460+2*0.0123*380}{1220} = 0.0128$

Modulus of elasticity perpendicular to the free edge, $E_p$ = 52460 *MPa*

Modulus of elasticity parallel to the free edge, $E_l$ = 65374 *MPa*

Average modulus of elasticity, $E = \frac{E_p * b_2 + 2 * E_l * b_1}{b_o} = \frac{52460*460+2*65374*380}{1220} = 60505\ MPa$

Modular ratio, $n = \frac{E_f}{E_c} = \frac{60505}{28814} = 2.1$

**B.4.2. Shear Capacity according to CAN/CSA S806-12** **Clause 8.7**

$$v_r = v_c = \left(1 + \frac{2}{\beta_c}\right)\left[0.028\lambda\varphi_c\left(E_f\rho_f f_c'\right)^{1/3}\right] = \left(1 + \frac{2}{1}\right)\left[0.028 * 1.0 * 1.0 * (60505 * 0.0128 * 41)^{1/3}\right] = 2.66MPa$$

$$v_r = v_c = 0.147\lambda\varphi_c\left(0.19 + \alpha_s\frac{d_v}{b_o}\right)\left(E_f\rho_f f_c'\right)^{1/3} = 0.147 * 1.0 * 1.0 * \left(0.19 + 3 * \frac{160}{1220}\right) * (60505 * 0.0128 * 41)^{1/3} = 2.72MPa$$

$$v_r = v_c = 0.056\lambda\varphi_c\left(E_f\rho_f f_c'\right)^{1/3} = 0.056 * 1.0 * 1.0 * (60505 * 0.0128 * 41)^{1/3} = 1.77MPa$$

(Governs)

$$V = {v_r}\Big/\left(\frac{1}{b_O * d} + \frac{0.2884\gamma}{J} * e\right) = {1.77 * 10^{-3}}\Big/\left(\frac{1}{1220 * 160} + \frac{0.38 * 0.2884 * 1000}{3377852377} * 118.4\right) = 198.16\ kN$$

**B.4.3. Shear Capacity according to ACI 440.1R-06** **Clause 9.4**

$$k = \sqrt{2\rho n + (\rho n)^2} - \rho n = \sqrt{2 * 0.0128 * 2.1 + (0.0128 * 2.1)^2} - 0.0128 * 2.1 = 0.207$$

$$c = kd = 0.207 * 160 = 33.05\ mm$$

$$v_r = v_c = 0.8 * \frac{c}{d}\sqrt{f_c'} = 0.8 * \frac{33.05}{160}\sqrt{41} = 1.06\ MPa$$

$$V = {v_r}\Big/\left(\frac{1}{b_O * d} + \frac{0.2884\gamma}{J} * e\right) = {1.06 * 10^{-3}}\Big/\left(\frac{1}{1220 * 160} + \frac{0.38 * 0.2884 * 1000}{3377852377} * 118.4\right) = 118.67\ kN$$

**B.4.4. Shear Capacity according to JSCE 1997** **Clause 6.3.4**

$$\beta_d = \sqrt[4]{\frac{1000}{d}} = \sqrt[4]{\frac{1000}{160}} = 1.58 = 1.5$$

$$\beta_p = \sqrt[3]{100\rho * \frac{E_f}{200000}} = \sqrt[3]{100 * 0.0128 * \frac{60505}{200000}} = 0.73$$

$$\beta_r = 1 + \frac{1}{1 + 0.25 * \frac{3c}{d}} = 1 + \frac{1}{1 + 0.25 * \frac{3 * 300}{160}} = 1.42$$

$$f_{pcd} = 0.2\sqrt{f_c'} = 0.2 * \sqrt{41} = 1.28 = 1.2\ MPa$$

$v_r = v_c = \frac{\beta_d \beta_p \beta_r f_{pcd}}{\gamma_b} = \frac{1.5*0.73*1.42*1.2}{1} = 1.87\ MPa$

$V = {v_r}\Big/\left(\frac{1}{b_O*d} + \frac{0.2884\gamma}{J} * e\right) = 1.87 * 10^{-3}\Big/\left(\frac{1}{1220*160} + \frac{0.38*0.2884*1000}{3377852377} * 118.4\right) = 207.92\ kN$

**B.5. Connection GSC-1.8-XX-0.4**

**B.5.1. Material Properties**

**B.5.1.1. Concrete**

Actual compressive strength of concrete $f_c' = 45.6\ MPa$

Material resistance factor $\phi_c = 1.0$

Concrete density factor $\lambda = 1.0$

Modulus of elasticity $E_c = 4500\sqrt{f_c'} = 4500 * \sqrt{45.6} = 30387.5\ MPa$

**B.5.1.2. Flexural Reinforcement**

Reinforcement ratio perpendicular to the free edge, $\rho_p$ = 0.018

Reinforcement ratio parallel to the free edge, $\rho_l$ = 0.0164

Average reinforcement ratio, $\rho = \frac{\rho_p * b_2 + 2 * \rho_l * b_1}{b_o} = \frac{0.009*460+2*0.0082*380}{1220} = 0.017$

Modulus of elasticity perpendicular to the free edge, $E_p$ = 52460 *MPa*

Modulus of elasticity parallel to the free edge, $E_l$ = 65374 *MPa*

Average modulus of elasticity, $E = \frac{E_p * b_2 + 2 * E_l * b_1}{b_o} = \frac{52460*460+2*65374*380}{1220} = 60505\ MPa$

Modular ratio, $n = \frac{E_f}{E_c} = \frac{60505}{30387} = 1.99$

**B.5.2. Shear Capacity according to CAN/CSA S806-12** **Clause 8.7**

$v_r = v_c = \left(1 + \frac{2}{\beta_c}\right)\left[0.028\lambda\varphi_c\left(E_f \rho_f f_c'\right)^{1/3}\right] = \left(1 + \frac{2}{1}\right)\left[0.028 * 1.0 * 1.0 * (60505 * 0.017 * 45.6)^{1/3}\right] = 3.03\ MPa$

$v_r = v_c = 0.147\lambda\varphi_c\left(0.19 + \alpha_s\frac{d_v}{b_o}\right)\left(E_f\rho_f f_c'\right)^{1/3} = 0.147 * 1.0 * 1.0 * \left(0.19 + 3 * \frac{160}{1220}\right) *$

$(60505 * 0.017 * 45.6)^{1/3} = 3.09\ MPa$

$v_r = v_c = 0.056\lambda\varphi_c\left(E_f\rho_f f_c'\right)^{1/3} = 0.056 * 1.0 * 1.0 * (60505 * 0.017 * 45.6)^{1/3} = 2.02\ MPa$

(Governs)

$V = {v_r}\Big/\left(\frac{1}{b_O * d} + \frac{0.2884\gamma}{J} * e\right) = {2.02 * 10^{-3}}\Big/\left(\frac{1}{1220 * 160} + \frac{0.38 * 0.2884 * 1000}{3377852377} * 118.4\right) = 226.15\ kN$

**B.5.3. Shear Capacity according to ACI 440.1R-06** **Clause 9.4**

$k = \sqrt{2\rho n + (\rho n)^2} - \rho n = \sqrt{2 * 0.017 * 1.99 + (0.017 * 1.99)^2} - 0.017 * 1.99 = 0.228$

$c = kd = 0.228 * 160 = 36.56\ mm$

$v_r = v_c = 0.8 * \frac{c}{d}\sqrt{f_c'} = 0.8 * \frac{36.56}{160}\sqrt{45.6} = 1.23\ MPa$

$V = {v_r}\Big/\left(\frac{1}{b_O * d} + \frac{0.2884\gamma}{J} * e\right) = {1.23 * 10^{-3}}\Big/\left(\frac{1}{1220 * 160} + \frac{0.38 * 0.2884 * 1000}{3377852377} * 118.4\right) = 137.7\ kN$

**B.5.4. Shear Capacity according to JSCE 1997** **Clause 6.3.4**

$\beta_d = \sqrt[4]{\frac{1000}{d}} = \sqrt[4]{\frac{1000}{160}} = 1.58 = 1.5$

$\beta_p = \sqrt[3]{100\rho * \frac{E_f}{200000}} = \sqrt[3]{100 * 0.017 * \frac{60505}{200000}} = 0.8$

$\beta_r = 1 + \frac{1}{1 + 0.25 * \frac{3c}{d}} = 1 + \frac{1}{1 + 0.25 * \frac{3 * 300}{160}} = 1.42$

$f_{pcd} = 0.2\sqrt{f_c'} = 0.2 * \sqrt{45.6} = 1.35 = 1.2\ MPa$

$v_r = v_c = \frac{\beta_d\beta_p\beta_r f_{pcd}}{\gamma_b} = \frac{1.5 * 0.8 * 1.42 * 1.2}{1} = 2.04\ MPa$

$V = {v_r}\Big/\left(\frac{1}{b_O * d} + \frac{0.2884\gamma}{J} * e\right) = {2.04 * 10^{-3}}\Big/\left(\frac{1}{1220 * 160} + \frac{0.38 * 0.2884 * 1000}{3377852377} * 118.4\right) = 228.55\ kN$

## B.6. Connection GSC-0.9-XX-0.2

### B.6.1. Material Properties

#### B.6.1.1. Concrete

Actual compressive strength of concrete $f_c' = 37.3\ MPa$

Material resistance factor $\phi_c = 1.0$

Concrete density factor $\lambda = 1.0$

Modulus of elasticity $E_c = 4500\sqrt{f_c'} = 4500 * \sqrt{37.3} = 27483\ MPa$

#### B.6.1.2. Flexural Reinforcement

Reinforcement ratio perpendicular to the free edge, $\rho_p = 0.009$

Reinforcement ratio parallel to the free edge, $\rho_l = 0.0082$

Average reinforcement ratio, $\rho = \frac{\rho_p * b_2 + 2 * \rho_l * b_1}{b_o} = \frac{0.009 * 460 + 2 * 0.0082 * 380}{1220} = 0.0085$

Modulus of elasticity perpendicular to the free edge, $E_p = 52460\ MPa$

Modulus of elasticity parallel to the free edge, $E_l = 65374\ MPa$

Average modulus of elasticity, $E = \frac{E_p * b_2 + 2 * E_l * b_1}{b_o} = \frac{52460 * 460 + 2 * 65374 * 380}{1220} = 60505\ MPa$

Modular ratio, $n = \frac{E_f}{E_c} = \frac{60505}{27483} = 2.2$

### B.6.2. Shear Capacity according to CAN/CSA S806-12 **Clause 8.7**

$v_r = v_c = \left(1 + \frac{2}{\beta_c}\right)\left[0.028\lambda\varphi_c\left(E_f\rho_f f_c'\right)^{1/3}\right] = \left(1 + \frac{2}{1}\right)\left[0.028 * 1.0 * 1.0 * (60505 * 0.0085 * 37.3)^{1/3}\right] = 2.25MPa$

$v_r = v_c = 0.147\lambda\varphi_c\left(0.19 + \alpha_s\frac{d_v}{b_o}\right)\left(E_f\rho_f f_c'\right)^{1/3} = 0.147 * 1.0 * 1.0 * \left(0.19 + 3 * \frac{160}{1220}\right) * (60505 * 0.0085 * 37.3)^{1/3} = 2.3MPa$

$$v_r = v_c = 0.056\lambda\varphi_c\left(E_f\rho_f f_c'\right)^{1/3} = 0.056 * 1.0 * 1.0 * (60505 * 0.0085 * 37.3)^{1/3} = 1.5MPa$$

(Governs)

$$V = {v_r}\Big/\left(\frac{1}{b_O*d} + \frac{0.2884\gamma}{J} * e\right) = 1.5 * 10^{-3}\Big/\left(\frac{1}{1220*160} + \frac{0.38*0.0884*1000}{3377852377} * 118.4\right) = 238.47\ kN$$

**B.6.3. Shear Capacity according to ACI 440.1R-06** **Clause 9.4**

$$k = \sqrt{2\rho n + (\rho n)^2} - \rho n = \sqrt{2 * 0.0085 * 2.2 + (0.0085 * 2.2)^2} - 0.0085 * 2.2 = 0.176$$

$$c = kd = 0.176 * 160 = 28.16\ mm$$

$$v_r = v_c = 0.8 * \frac{c}{d}\sqrt{f_c'} = 0.8 * \frac{28.16}{160}\sqrt{37.3} = 0.86\ MPa$$

$$V = {v_r}\Big/\left(\frac{1}{b_O*d} + \frac{0.2884\gamma}{J} * e\right) = 0.86 * 10^{-3}\Big/\left(\frac{1}{1220*160} + \frac{0.38*0.0884*1000}{3377852377} * 118.4\right) = 136.72\ kN$$

**B.6.4. Shear Capacity according to JSCE 1997** **Clause 6.3.4**

$$\beta_d = \sqrt[4]{\frac{1000}{d}} = \sqrt[4]{\frac{1000}{160}} = 1.58 = 1.5$$

$$\beta_p = \sqrt[3]{100\rho * \frac{E_f}{200000}} = \sqrt[3]{100 * 0.0085 * \frac{60505}{200000}} = 0.64$$

$$\beta_r = 1 + \frac{1}{1+0.25*\frac{3c}{d}} = 1 + \frac{1}{1+0.25*\frac{3*300}{160}} = 1.42$$

$$f_{pcd} = 0.2\sqrt{f_c'} = 0.2 * \sqrt{37.3} = 1.22 = 1.2\ MPa$$

$$v_r = v_c = \frac{\beta_d\beta_p\beta_r f_{pcd}}{\gamma_b} = \frac{1.5*0.64*1.42*1.2}{1} = 1.62\ MPa$$

$$V = {v_r}\Big/\left(\frac{1}{b_O*d} + \frac{0.2884\gamma}{J} * e\right) = 1.62 * 10^{-3}\Big/\left(\frac{1}{1220*160} + \frac{0.38*0.0884*1000}{3377852377} * 118.4\right) = 257.6\ kN$$

**B.7. Connection GSC-0.9-XX-0.6**

**B.7.1. Material Properties**

**B.7.1.1. Concrete**

Actual compressive strength of concrete $f_c' = 36.5\ MPa$

Material resistance factor $\phi_c = 1.0$

Concrete density factor $\lambda = 1.0$

Modulus of elasticity $E_c = 4500\sqrt{f_c'} = 4500 * \sqrt{36.5} = 27187\ MPa$

**B.7.1.2. Flexural Reinforcement**

Reinforcement ratio perpendicular to the free edge, $\rho_p = 0.009$

Reinforcement ratio parallel to the free edge, $\rho_l = 0.0082$

Average reinforcement ratio, $\rho = \frac{\rho_p * b_2 + 2 * \rho_l * b_1}{b_o} = \frac{0.009 * 460 + 2 * 0.0082 * 380}{1220} = 0.0085$

Modulus of elasticity perpendicular to the free edge, $E_p = 52460\ MPa$

Modulus of elasticity parallel to the free edge, $E_l = 65374\ MPa$

Average modulus of elasticity, $E = \frac{E_p * b_2 + 2 * E_l * b_1}{b_o} = \frac{52460 * 460 + 2 * 65374 * 380}{1220} = 60505\ MPa$

Modular ratio, $n = \frac{E_f}{E_c} = \frac{60505}{27187} = 2.23$

**B.7.2. Shear Capacity according to CAN/CSA S806-12** **Clause 8.7**

$v_r = v_c = \left(1 + \frac{2}{\beta_c}\right)\left[0.028\lambda\varphi_c\left(E_f\rho_f f_c'\right)^{1/3}\right] = \left(1 + \frac{2}{1}\right)\left[0.028 * 1.0 * 1.0 * (60505 * 0.0085 * 36.5)^{1/3}\right] = 2.23MPa$

$v_r = v_c = 0.147\lambda\varphi_c\left(0.19 + \alpha_s\frac{d_v}{b_o}\right)\left(E_f\rho_f f_c'\right)^{1/3} = 0.147 * 1.0 * 1.0 * \left(0.19 + 3 * \frac{160}{1220}\right) * (60505 * 0.0085 * 36.5)^{1/3} = 2.28MPa$

$v_r = v_c = 0.056\lambda\varphi_c\left(E_f\rho_f f_c'\right)^{1/3} = 0.056 * 1.0 * 1.0 * (60505 * 0.0085 * 36.5)^{1/3} = 1.49MPa$ (Governs)

$V = {v_r}\Big/\left(\frac{1}{b_O * d} + \frac{0.2884\gamma}{J} * e\right) = 1.49 * 10^{-3}\Big/\left(\frac{1}{1220 * 160} + \frac{0.38 * 0.4884 * 1000}{3377852377} * 118.4\right) = 128.73\ kN$

### B.7.3. Shear Capacity according to ACI 440.1R-06 **Clause 9.4**

$k = \sqrt{2\rho n + (\rho n)^2} - \rho n = \sqrt{2 * 0.0085 * 2.23 + (0.0085 * 2.23)^2} - 0.0085 * 2.23 = 0.177$

$c = kd = 0.177 * 160 = 28.32\ mm$

$v_r = v_c = 0.8 * \frac{c}{d}\sqrt{f_c'} = 0.8 * \frac{28.32}{160}\sqrt{36.5} = 0.86\ MPa$

$V = {v_r}\Big/\left(\frac{1}{b_O * d} + \frac{0.2884\gamma}{J} * e\right) = 0.86 * 10^{-3}\Big/\left(\frac{1}{1220*160} + \frac{0.38*0.4884*1000}{3377852377} * 118.4\right) = 74.3\ kN$

### B.7.4. Shear Capacity according to JSCE 1997 **Clause 6.3.4**

$\beta_d = \sqrt[4]{\frac{1000}{d}} = \sqrt[4]{\frac{1000}{160}} = 1.58 = 1.5$

$\beta_p = \sqrt[3]{100\rho * \frac{E_f}{200000}} = \sqrt[3]{100 * 0.0085 * \frac{60505}{200000}} = 0.64$

$\beta_r = 1 + \frac{1}{1+0.25*\frac{3c}{d}} = 1 + \frac{1}{1+0.25*\frac{3*300}{160}} = 1.42$

$f_{pcd} = 0.2\sqrt{f_c'} = 0.2 * \sqrt{36.5} = 1.21 = 1.2\ MPa$

$v_r = v_c = \frac{\beta_d \beta_p \beta_r f_{pcd}}{\gamma_b} = \frac{1.5*0.64*1.42*1.2}{1} = 1.62\ MPa$

$V = {v_r}\Big/\left(\frac{1}{b_O * d} + \frac{0.2884\gamma}{J} * e\right) = 1.62 * 10^{-3}\Big/\left(\frac{1}{1220*160} + \frac{0.38*0.4884*1000}{3377852377} * 118.4\right) = 139.99\ kN$

## B.8. Connection GRD-0.9-XX-0.4

### B.8.1. Material Properties

#### B.8.1.1. Concrete

Actual compressive strength of concrete $f_c' = 41\ MPa$

Material resistance factor $\phi_c = 1.0$

Concrete density factor $\lambda = 1.0$

Modulus of elasticity $E_c = 4500\sqrt{f_c'} = 4500 * \sqrt{41} = 28814\ MPa$

**B.8.1.2. Flexural Reinforcement**

Reinforcement ratio perpendicular to the free edge, $\rho_p = 0.0087$

Reinforcement ratio parallel to the free edge, $\rho_l = 0.0084$

Average reinforcement ratio, $\rho = \frac{\rho_p * b_2 + 2 * \rho_l * b_1}{b_o} = \frac{0.0087 * 460 + 2 * 0.0084 * 380}{1220} = 0.0085$

Modulus of elasticity perpendicular to the free edge, $E_p = 53892\ MPa$

Modulus of elasticity parallel to the free edge, $E_l = 63500\ MPa$

Average modulus of elasticity, $E = \frac{E_p * b_2 + 2 * E_l * b_1}{b_o} = \frac{53892 * 460 + 2 * 63500 * 380}{1220} = 59877\ MPa$

Modular ratio, $n = \frac{E_f}{E_c} = \frac{59877}{28814} = 2.08$

**B.8.2. Shear Capacity according to CAN/CSA S806-12** **Clause 8.7**

$v_r = v_c = \left(1 + \frac{2}{\beta_c}\right)\left[0.028\lambda\varphi_c\left(E_f\rho_f f_c'\right)^{1/3}\right] = \left(1 + \frac{2}{1}\right)\left[0.028 * 1.0 * 1.0 * (59877 * 0.0085 * 41)^{1/3}\right] = 2.31MPa$

$v_r = v_c = 0.147\lambda\varphi_c\left(0.19 + \alpha_s\frac{d_v}{b_o}\right)\left(E_f\rho_f f_c'\right)^{1/3} = 0.147 * 1.0 * 1.0 * \left(0.19 + 3 * \frac{160}{1220}\right) * (59877 * 0.0085 * 41)^{1/3} = 2.36MPa$

$v_r = v_c = 0.056\lambda\varphi_c\left(E_f\rho_f f_c'\right)^{1/3} = 0.056 * 1.0 * 1.0 * (59877 * 0.0085 * 41)^{1/3} = 1.54MPa$

(Governs)

$V = {v_r}\Big/\left(\frac{1}{b_O * d} + \frac{0.2884\gamma}{J} * e\right) = 1.54 * 10^{-3}\Big/\left(\frac{1}{1220 * 160} + \frac{0.38 * 0.2884 * 1000}{3377852377} * 118.4\right) = 172.41\ kN$

**B.8.3. Shear Capacity according to ACI 440.1R-06** **Clause 9.4**

$k = \sqrt{2\rho n + (\rho n)^2} - \rho n = \sqrt{2 * 0.0085 * 2.08 + (0.0085 * 2.08)^2} - 0.0085 * 2.08 = 0.171$

$c = kd = 0.171 * 160 = 27.36\ mm$

$$v_r = v_c = 0.8 * \frac{c}{d}\sqrt{f_c'} = 0.8 * \frac{27.39}{160}\sqrt{41} = 0.88\ MPa$$

$$V = {v_r}\Big/\left(\frac{1}{b_O * d} + \frac{0.2884\gamma}{J} * e\right) = {0.88 * 10^{-3}}\Big/\left(\frac{1}{1220*160} + \frac{0.38*0.2884*1000}{3377852377} * 118.4\right) = 98.52\ kN$$

**B.8.4. Shear Capacity according to JSCE 1997** **Clause 6.3.4.**

$$\beta_d = \sqrt[4]{\frac{1000}{d}} = \sqrt[4]{\frac{1000}{160}} = 1.58 = 1.5$$

$$\beta_p = \sqrt[3]{100\rho * \frac{E_f}{200000}} = \sqrt[3]{100 * 0.0085 * \frac{59877}{200000}} = 0.63$$

$$\beta_r = 1 + \frac{1}{1+0.25*\frac{3c}{d}} = 1 + \frac{1}{1+0.25*\frac{3*300}{160}} = 1.42$$

$$f_{pcd} = 0.2\sqrt{f_c'} = 0.2 * \sqrt{41} = 1.28 = 1.2\ MPa$$

$$v_r = v_c = \frac{\beta_d \beta_p \beta_r f_{pcd}}{\gamma_b} = \frac{1.5*0.63*1.42*1.2}{1} = 1.61\ MPa$$

$$V = {v_r}\Big/\left(\frac{1}{b_O * d} + \frac{0.2884\gamma}{J} * e\right) = {1.61 * 10^{-3}}\Big/\left(\frac{1}{1220*160} + \frac{0.38*0.2884*1000}{3377852377} * 118.4\right) = 180.77\ kN$$

# APPENDIX C

# Shear Capacity of Connections with Shear Reinforcement

## C.1. Introduction

There are no provisions in the CAN/CSA S806-12 or the ACI 440.1R-06 for designing shear reinforcement for slab-column connections; therefore, the provisions of the CAN/CSA A23.3-04 and the ACI 318-11were used with proper modifications, whenever applicable (Section 2.7). It is assumed that the critical section outside the shear reinforced zone is located at a distance 3.9*d* away from the face of the column. Also, the spacing between stud lines is taken as 0.75*d* and 0.5*d* for connections GRD-0.9-75-0.4 and GRD-0.9-50-0.4, respectively.

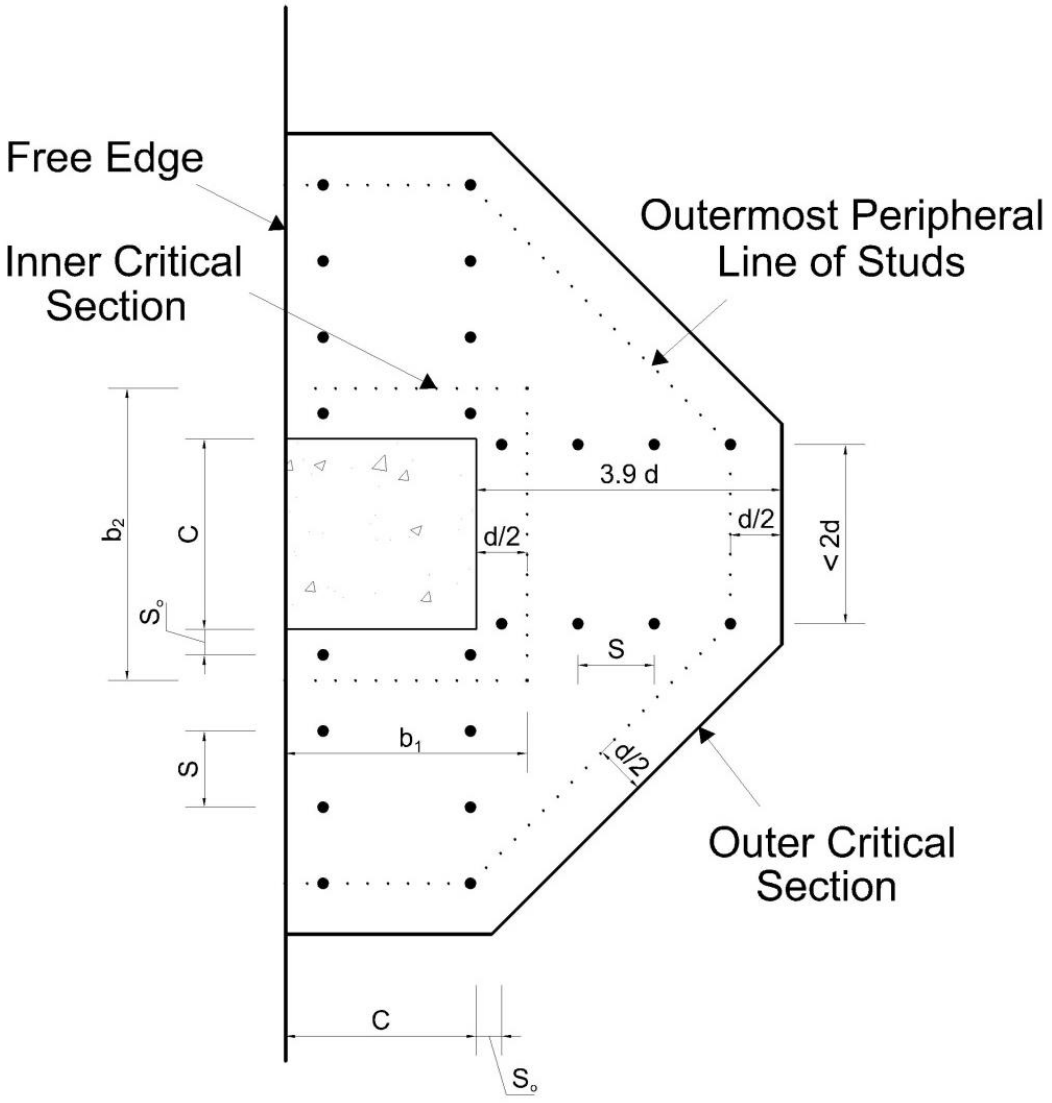


Figure C.1: Typical Arrangement of Headed Shear Reinforcement and Critical Sections

## C.2. Properties of Critical Sections

### C.2.1. Critical Section at a distance *d/2* from the column face

$d_v = 160\ mm$

$b_1 = c + \frac{d_v}{2} = 300 + \frac{160}{2} = 380\ mm$

$b_2 = c + 2 * \frac{d_v}{2} = 300 + 2 * \frac{160}{2} = 460\ mm$

$b_o = 2 * b_1 + b_2 = 2 * 380 + 460 = 1220\ mm$

$e = \frac{{b_1}^2}{2b_1 + b_2} = \frac{380^2}{2*380+460} = 118.4\ mm$

$J = 2\left(\frac{{b_1}^3 * d_v}{3} + \frac{{d_v}^3 * b_1}{12}\right) - b_o * d_v * e^2$

$= 2\left(\frac{380^3 * 160}{3} + \frac{160^3 * 380}{12}\right) - 1220 * 160 *$

$118.4^2 = 3377852377\ \text{mm}^4$

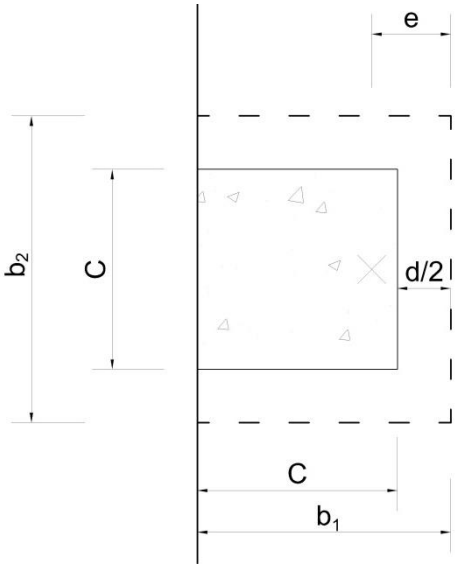


Figure C.2: Critical section at *d/2* from column face

Where *e* is the distance between the centroid and the inner side of the critical section and *J* is a property of the critical shear section analogous to the polar moment of inertia

$\beta_c = \frac{c}{c} = 1$

$\gamma_v = 1 - \frac{1}{1+\frac{2}{3}\sqrt{\frac{b_1}{b_2}}} = 1 - \frac{1}{1+\frac{2}{3}\sqrt{\frac{380}{460}}} = 0.38$

$\frac{M_o}{V} = \frac{M}{V} - \left(b_1 - e - \frac{c}{2}\right) = 0.4 - \left(0.38 - 0.1184 - \frac{0.3}{2}\right) = 0.2884\ m$ *when* $\frac{M}{V} = 0.4\ m$

**C.2.2. Critical Section at a distance 3.9d from the column face (for shear-reinforced connections)**

$l_1 = 303mm$

$l_2 = 878mm$

$l_3 = 306mm$

$l_x = 924mm$

$l_y = 1559mm$

$d_v = 160\ mm$

$b_o = 2 * (l_1 + l_2) + l_3 = 2 * (303 + 878) + 306 = \mathbf{2668\ mm}$

Taking the summation of the moments of the critical section segments about the free edge to get X:

$$\rightarrow 2 * \left(l_1 * \frac{l_1}{2} + l_2 * \frac{l_x + l_1}{2}\right) + l_3 * l_x = b_o * X$$

$$\rightarrow 2 * \left(303 * \frac{303}{2} + 878 * \frac{924+303}{2}\right) + 306 * 924 = 2668 * X$$

$$\rightarrow X = 544.2\ mm$$

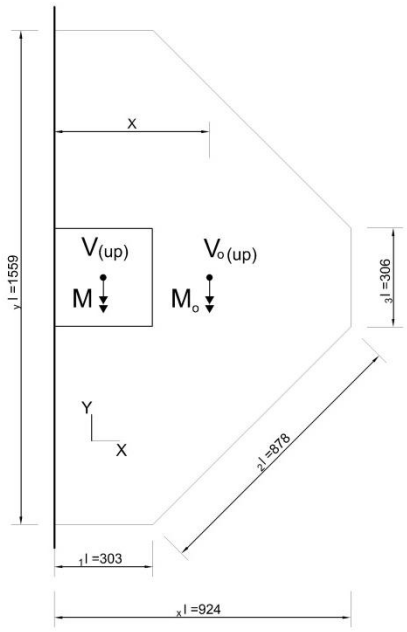


Figure C.3: Critical section outside the shear reinforced zone

Calculating *J*:

$$J = d \sum \frac{L}{3}\left(x_i^2 + x_i x_j + x_j^2\right)$$

For segment 1: $x_i = -544.2\ mm$ $x_j = -241.2\ mm$

For segment 2: $x_i = -241.2\ mm$ $x_j = 379.8\ mm$

For segment 3: $x_i = 379.8\ mm$ $x_j = 379.8\ mm$

$\rightarrow J = \frac{160}{3} * \{2 * 303 * [(-544.2)^2 + (-544.2) * (-241.2) + (-241.2)^2] + 2 * 878 *$

$[(-241.2)^2 + (-241.2) * (379.8) + (379.8)^2] + 306 * [(379.8)^2 + (379.8) * (379.8) +$

$(379.8)^2]\} = 3.314 * 10^{10}\text{mm}^4$

$\gamma_v = 1 - \frac{1}{1+\frac{2}{3}\sqrt{\frac{l_x}{l_y}}} = 1 - \frac{1}{1+\frac{2}{3}\sqrt{\frac{924}{1559}}} = 0.34$

$\frac{M_o}{V} = \frac{M}{V} - \left(X - \frac{c}{2}\right) = 0.4 - \left(0.5442 - \frac{0.3}{2}\right) = 0.0058\ m$ *when* $\frac{M}{V} = 0.4\ m$

## C.3. Reinforcement Properties

### C.3.1. Properties of Headed Shear Studs

Use No. 13bars $d_{b_{int.}} = 12\ mm$ $d_{b_{ext.}} = 13.5\ mm$ $A_b = 113\ mm^2$

Ultimate tensile strength $f_{frp_u} = 1060\ MPa$

Ultimate tensile strain $\varepsilon_{frp_u} = 1.67\ \%$

Modulus of elasticity $E_{frp} = 63500\ MPa$

### C.3.2. Flexural Reinforcement Properties

Reinforcement ratio perpendicular to the free edge, $\rho_p = 0.0087$

Reinforcement ratio parallel to the free edge, $\rho_l = 0.0084$

Average reinforcement ratio, $\rho = \frac{\rho_p * b_2 + 2 * \rho_l * b_1}{b_o} = \frac{0.0087 * 460 + 2 * 0.0084 * 380}{1220} = 0.0085$

Modulus of elasticity perpendicular to the free edge, $E_p = 53892\ MPa$

Modulus of elasticity parallel to the free edge, $E_l = 63500\ MPa$

Average modulus of elasticity, $E = \frac{E_p * b_2 + 2 * E_l * b_1}{b_o} = \frac{53892 * 460 + 2 * 63500 * 380}{1220} = 59877\ MPa$

## C.4. Connection GRD-0.9-75-0.4

### C.4.1. Concrete Properties

Actual compressive strength of concrete $f_c' = 40.7\ MPa$

Material resistance factor $\phi_c = 1.0$

Concrete density factor $\lambda = 1.0$

**C.4.2. Spacing of Studs**

$S = 0.75d = 0.75 * 160 = 120\ mm$

$S_o = 0.4d = 0.4 * 160 = 64\ mm$

**C.4.3. Capacity according to the Modified CAN/CSA A23.3-04**

**C.4.3.1. Shear Strength at the Inner Shear Perimeter (at a distance $\frac{d}{2}$ from the column face)**

**C.4.3.1.1. Concrete Contribution**

$v_c = 0.041\lambda\phi_c\left(E_f\rho_f f_c'\right)^{\frac{1}{3}}$ **Clause 13.3.8.3 (A23.3-04) Modified**

$= 0.041 * 1.0 * 1.0 * (59877 * 0.0085 * 40.7)^{\frac{1}{3}} = 1.13$ MPa

**C.4.3.1.2. Headed Bars Contribution**

$v_s = \frac{\phi_s A_v f_y}{b_o s} = \frac{\phi_s A_v f_{f_u}}{b_o s}$ **Clause 13.3.8.5 (A23.3-04) Modified**

$f_{f_u} = 0.005E_F = 0.005 * 59877 = 299.39\ MPa$ **Clause 8.4.4.9 (S806-12)**

$\rightarrow v_s = \frac{1.0*(6*113)*299.39}{1220*120} = 1.39\ MPa$

**C.4.3.1.3. Punching Shear Capacity**

$v_r = v_c + v_{sF} = 1.13 + 1.39 = 2.52\ MPa$ **Clause 13.3.7.3 (A23.3-04)**

$v_f = v_r \leq 0.11\lambda\phi_c\left(E_f\rho_f f_c'\right)^{\frac{1}{3}}$ **Clause 13.3.8.2 (A23.3-04) Modified**

$\rightarrow 0.11 * 1.0 * 1.0 * (59877 * 0.0085 * 40.7)^{\frac{1}{3}} = 3.02\ MPa > v_f = v_r = 2.52\ MPa$ OK

$V = {v_r}\Big/\left(\frac{1}{b_O*d} + \frac{0.2884\gamma}{J} * e\right) = 2.52 * 10^{-3}\Big/\left(\frac{1}{1220*160} + \frac{0.38*0.2884*1000}{3377852377} * 118.4\right) = 281.11\ kN$

**C.4.3.2. Shear Strength at the Outer Shear Perimeter (at a distance 3.9*d* from the column face)**

**C.4.3.2.1. Punching Shear Capacity**

$v_r = v_c = 0.028\lambda\phi_c\left(E_f\rho_f f_c'\right)^{\frac{1}{3}}$ **Clause 13.3.7.4 (A23.3-04) Modified**

$= 0.028 * 1.0 * 1.0 * (59877 * 0.0085 * 40.7)^{\frac{1}{3}} = 0.77$ MPa

$V = {v_r}\Big/\left(\frac{1}{b_O * d} + \frac{0.2884\gamma}{J} * e\right) = {0.77 * 10^{-3}}\Big/\left(\frac{1}{2668*160} + \frac{0.34*0.0058*1000}{3.314*10^{10}} * 379.8\right) = 325.56\ kN$

Failure is expected to be **inside** the shear reinforced zone.

**C.4.4. Capacity according to the Modified ACI 318-11**

**C.4.4.1. Shear Strength at the Inner Shear Perimeter (at a distance $\frac{d}{2}$ from the column face)**

**C.4.4.1.1. Concrete Contribution**

$E_c = 4733\sqrt{f_c'} = 4733 * \sqrt{40.7} = 30194.9\ MPa$ **Clauses 8.5 (318-11)**

$n_f = \frac{E_f}{E_c} = \frac{59877}{30195} = 1.98$

$k = \sqrt{2\rho_f n_f + \left(\rho_f n_f\right)^2} - \rho_f n_f = \sqrt{2 * 0.0085 * 1.98 + (0.0085 * 1.98)^2} - 0.0085 * 1.98 =$

0.167 **Clauses 9.4 (440.1R-06)**

$c = kd = 0.167 * 160 = 26.79\ mm$ **Clauses 9.4 (440.1R-06)**

$V_c = \frac{3}{5}\lambda\sqrt{f_c'}b_o c$ **Clauses 11.11.5.1 & 11.11.2.1 (318-11) and 9.4 (440.1R-06) Modified**

$= \frac{3}{5} * 1.0 * \sqrt{40.7} * 1220 * 26.79 = 125083.99\ N$

$\rightarrow v_c = \frac{V_c}{b_o d} = \frac{125083.99}{1220*160} = 0.64\ MPa$ **Clauses R11.11.5.1 (318-11)**

**C.4.4.1.2. Headed Bars Contribution**

$f_{f_u} = 0.004E_{f_{avg.}} = 0.004 * 63500 = 254\ MPa$ **Clause 9.2 (440.1R-06)**

$v_s = \frac{A_v f_y}{b_o s} = \frac{A_v f_{fu}}{b_o s} = \frac{(6*113)*254}{1220*117} = 1.21$ MPa **Clause 11.11.5.1 (318-11) Modified**

$v_S \geq \frac{2}{5}\sqrt{f_c'}\frac{c}{d}$ **Clauses 11.11.5.1 & 11.11.2.1 (318-11) and 9.4 (440.1R-06) Modified**

$\frac{2}{5}\sqrt{f_c'}\frac{c}{d} = \frac{2}{5}\sqrt{40.7} * \frac{26.79}{160} = 0.43\ MPa \leq v_S$ OK

**C.4.4.1.3. Punching Shear Capacity**

$v_n = v_c + v_{sF} = 0.64 + 1.21 = 1.85\ MPa$ **Clause 11.11.5.1 (318-11)**

$V = {v_r}\Big/\left(\frac{1}{b_O * d} + \frac{0.2884\gamma}{J} * e\right) = 1.85 * 10^{-3}\Big/\left(\frac{1}{1220*160} + \frac{0.38*0.2884*1000}{3377852377} * 118.4\right) = 206.37\ kN$

**C.4.4.2. Shear Strength at the Outer Shear Perimeter (at a distance 3.9*d* from the column face)**

**C.4.4.2.1. Punching Shear Capacity**

$V_n = V_c = \frac{2}{5}\lambda\sqrt{f_c'}b_o c$ **Clauses 11.11.5.4 & 11.11.2.1 (318-11) and 9.4 (440.1R-06) Modified**

$= \frac{2}{5} * 1.0 * \sqrt{40.7} * 2668 * 26.79 = 182396.18\ N$

$\rightarrow v_n = v_c = \frac{V_c}{b_o d} = \frac{182396.18}{2668*160} = 0.43\ MPa$ **Clauses R11.11.2.1 (318-11)**

$V = {v_r}\Big/\left(\frac{1}{b_O * d} + \frac{0.2884\gamma}{J} * e\right) = 0.43 * 10^{-3}\Big/\left(\frac{1}{2668*160} + \frac{0.34*0.0058*1000}{3.314*10^{10}} * 379.8\right) = 181.8\ kN$

Failure is expected to be **outside** the shear reinforced zone.

**C.5. Connection GRD-0.9-50-0.4**

**C.5.1. Concrete Properties**

Actual compressive strength of concrete $f_c' = 37.7\ MPa$

Material resistance factor $\phi_c = 1.0$

Concrete density factor $\lambda = 1.0$

**C.5.2. Spacing of Studs**

$S = 0.5d = 0.5 * 160 = 80\ mm$

$S_o = 0.4d = 0.4 * 160 = 64\ mm$

**C.5.3. Capacity according to the Modified CAN/CSA A23.3-04**

**C.5.3.1. Shear Strength at the Inner Shear Perimeter (at a distance $\frac{d}{2}$ from the column face)**

**C.5.3.1.1. Concrete Contribution**

$v_c = 0.041\lambda\phi_c\left(E_f\rho_f f_c'\right)^{\frac{1}{3}}$ **Clause 13.3.8.3 (A23.3-04) Modified**

$= 0.041 * 1.0 * 1.0 * (59877 * 0.0085 * 37.7)^{\frac{1}{3}} = 1.1$ MPa

**C.5.3.1.2. Headed Bars Contribution**

$v_s = \frac{\phi_s A_v f_y}{b_o s} = \frac{\phi_s A_v f_{fu}}{b_o s}$ **Clause 13.3.8.5 (A23.3-04) Modified**

$f_{f_u} = 0.005E_F = 0.005 * 59877 = 299.39\ MPa$ **Clause 8.4.4.9 (S806-12)**

$\rightarrow v_s = \frac{1.0*(6*113)*299.39}{1220*80} = 2.08\ MPa$

**C.5.3.1.3. Punching Shear Capacity**

$v_r = v_c + v_{sF} = 1.1 + 2.08 = 3.18\ MPa$ **Clause 13.3.7.3 (A23.3-04)**

$V = {v_r}\Big/\left(\frac{1}{b_O*d} + \frac{0.2884\gamma}{J} * e\right) = 3.18 * 10^{-3}\Big/\left(\frac{1}{1220*160} + \frac{0.38*0.2884*1000}{3377852377} * 118.4\right) = 354.7\ kN$

**C.5.3.2. Shear Strength at the Outer Shear Perimeter (at a distance 3.9*d* from the column face)**

**C.5.3.2.1. Punching Shear Capacity**

$v_r = v_c = 0.028\lambda\phi_c\left(E_f\rho_f f_c'\right)^{\frac{1}{3}}$ **Clause 13.3.7.4 (A23.3-04) Modified**

$= 0.028 * 1.0 * 1.0 * (59877 * 0.0085 * 37.7)^{\frac{1}{3}} = 0.75$ MPa

$$V = {v_r}\Big/\left(\frac{1}{b_O * d} + \frac{0.2884\gamma}{J} * e\right) = 0.75 * 10^{-3}\Big/\left(\frac{1}{2668*160} + \frac{0.34*0.0058*1000}{3.314*10^{10}} * 379.8\right) = 316.9\ kN$$

Failure is expected to be **outside** the shear reinforced zone

### C.5.4. Capacity according to the Modified ACI 318-11

#### C.5.4.1. Shear Strength at the Inner Shear Perimeter (at a distance $\frac{d}{2}$ from the column face)

##### C.5.4.1.1. Concrete Contribution

$E_c = 4733\sqrt{f_c'} = 4733 * \sqrt{37.7} = 29060.8\ MPa$ **Clauses 8.5 (318-11)**

$n_f = \frac{E_f}{E_c} = \frac{59877}{29060.8} = 2.06$

$k = \sqrt{2\rho_f n_f + \left(\rho_f n_f\right)^2} - \rho_f n_f = \sqrt{2 * 0.0085 * 2.06 + (0.0085 * 2.06)^2} - 0.0085 * 2.06 =$

0.17 **Clauses 9.4 (440.1R-06)**

$c = kd = 0.17 * 160 = 27.27\ mm$ **Clauses 9.4 (440.1R-06)**

$V_c = \frac{3}{5}\lambda\sqrt{f_c'} b_o c$ **Clauses 11.11.5.1 & 11.11.2.1 (318-11) and 9.4 (440.1R-06) Modified**

$= \frac{3}{5} * 1.0 * \sqrt{37.7} * 1220 * 27.27 = 122569.6\ N$

$\rightarrow v_c = \frac{V_c}{b_o d} = \frac{122569.6}{1220*160} = 0.63\ MPa$ **Clauses R11.11.5.1 (318-11)**

##### C.5.4.1.2. Headed Bars Contribution

$f_{f_u} = 0.004E_{f_{avg.}} = 0.004 * 63500 = 254\ MPa$ **Clause 9.2 (440.1R-06)**

$v_s = \frac{A_v f_y}{b_o s} = \frac{A_v f_{f_u}}{b_o s} = \frac{(6*113)*254}{1220*80} = 1.76$ MPa **Clause 11.11.5.1 (318-11) Modified**

$v_S \geq \frac{2}{5}\sqrt{f_c'}\frac{c}{d}$ **Clauses 11.11.5.1 & 11.11.2.1 (318-11) and 9.4 (440.1R-06) Modified**

$\frac{2}{5}\sqrt{f_c'}\frac{c}{d} = \frac{2}{5}\sqrt{37.7} * \frac{27.27}{160} = 0.42\ MPa \leq v_S$ OK

**C.5.4.1.3. Punching Shear Capacity**

$v_n = v_c + v_{sF} = 0.63 + 1.76 = 2.39\ MPa$ **Clause 11.11.5.1 (318-11)**

$$V = {v_r}\Big/\left(\frac{1}{b_O * d} + \frac{0.2884\gamma}{J} * e\right) = {2.39 * 10^{-3}}\Big/\left(\frac{1}{1220*160} + \frac{0.38*0.2884*1000}{3377852377} * 118.4\right) = 267.73\ kN$$

**C.5.4.2. Shear Strength at the Outer Shear Perimeter (at a distance 3.9*d* from the column face)**

**C.4.4.2.1. Punching Shear Capacity**

$V_n = V_c = \frac{2}{5}\lambda\sqrt{f_c'}b_o c$ **Clauses 11.11.5.4 & 11.11.2.1 (318-11) and 9.4 (440.1R-06) Modified**

$$= \frac{2}{5} * 1.0 * \sqrt{37.7} * 2668 * 27.27 = 178690.6\ N$$

$\rightarrow v_n = v_c = \frac{V_c}{b_o d} = \frac{178690.6}{2668*160} = 0.42\ MPa$ **Clauses R11.11.2.1 (318-11)**

$$V = {v_r}\Big/\left(\frac{1}{b_O * d} + \frac{0.2884\gamma}{J} * e\right) = {0.42 * 10^{-3}}\Big/\left(\frac{1}{2668*160} + \frac{0.34*0.0058*1000}{3.314*10^{10}} * 379.8\right) = 181.8\ kN$$

Failure is expected to be **outside** the shear reinforced zone.

# APPENDIX D

# Yield Line Analysis

## D.1. Yield Line Pattern

The yield line pattern shown in Figure D.1 was proposed by Mortin (1989). It consists of six plane segments and two fan-shape segments. The pattern is defined by three parameters, *a, b and c*, since the angle of the fan shape, $\varphi$, is a function of *a* only. The principal of virtual work is being used to analyze the pattern.

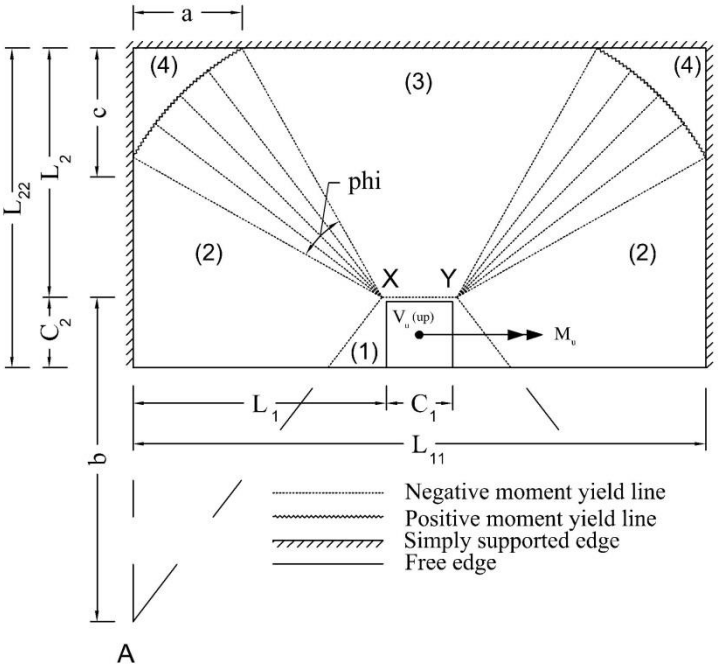


Figure D.1: Yield Line Pattern (reproduced from Mortin 1989)

The line of maximum deflection, XY, is given a unit displacement, $\delta$, in the direction of the shearing force, *V*. Plates number 4 do not move while plates number 1, 2, and 3 and the two fan-shape segments move up a distance ranging from zero at their ends to $\delta$ where they intersect with line XY. The end of plate number 1, where the displacement is zero, is the imaginary line AA if the plate was continued.

The affinity theorem is used to account for the orthotropic arrangement of the reinforcement. The orthotropic slab with moments of resistance $m_x$ and $m_y$ in the x and y directions, respectively, may be analyzed as an isotropic slab with moment of resistance $m_x$ in both directions if:

| | Orthotropic Slab | Transformation | Isotropic Slab |
|---|---|---|---|
| Dimensions: | $l_x$ | remains | $l_x$ |
| | $l_y$ | becomes | $\frac{l_y}{\sqrt{\mu}}$ |
| Applied Loads: | $V_u$ | becomes | $\frac{V_u}{\sqrt{\mu}}$ |
| | $M_u$ | becomes | $\frac{M_u}{\mu}$ |

Where $\mu = \frac{m_y}{m_x}$ and $l_x$ and $l_y$ are the dimensions of the slab in the x and y directions, respectively.

## D.2. Equivalent Plastic Moment, MP, Calculations

### D.2.1. Connection G-0.9-XX-0.4

#### D.2.1.1. Perpendicular to the Free Edge, $M_{py}$

$I_g = \frac{b*h^3}{12} = \frac{1000*200^3}{12} = 666.67 * 10^6\ mm^4$

$A_f = 1532.2\ mm^2 \quad \rho = 0.009 \quad k = 0.162 \quad n = 1.75$

$I_{cr} = \frac{b*(kd)^3}{3} + n * A_f * (d - kd)^2$

$= \frac{1000*(0.162*170.25)^3}{3} + 1.75 * 1532.2 * (170.25 - 0.162 * 170.25)^2 = 61.57 * 10^6\ mm^4$

$M_{cr} = f_r * \frac{I_g}{y_t} = 3.5 * \frac{666.67*10^6}{100} * 10^{-6} = 23.33\ kN.m$

$$f_f = 0.5 E_f \varepsilon_{c_u} \left[ \left( 1 + \frac{4\alpha_1 \beta_1 \phi_c f_c'}{\rho_f \phi_f E_f \varepsilon_{c_u}} \right)^{1/2} - 1 \right]$$

$$= 0.5 * 52460 * 0.0035 * \left[\left(1 + \frac{4 * 0.7884 * 0.8673 * 1.0 * 41.1}{0.009 * 1.0 * 52460 * 0.0035}\right)^{1/2} - 1\right] = 670.9\ MPa$$

$c = \frac{\phi_f A_f f_f}{\alpha_1 \beta_1 \phi_c f_c' b} = \frac{1.0*1532.2*670.9}{0.7884*0.8673*41.1*1000} = 36.58\ mm$

$M_n = \phi_f A_f f_f * \left(d - \frac{\beta_1 c}{2}\right) = 1.0 * 1532.2 * 670.9 * \left(170.25 - \frac{0.8673*36.58}{2}\right) = 158.71\ kN.m$

$M_{p_y} = 0.5M_n + 0.5\left(1 - \frac{I_{cr}}{2I_g}\right)\left(\frac{M_{cr}}{M_n}\right)M_{cr} = 0.5 * 158.7 + 0.5\left(1 - \frac{61.57}{2*666.67}\right)\left(\frac{23.33}{158.71}\right)23.33 =$

$80.99\ kN.m$

**D.2.1.2. Parallel to the Free Edge, $M_{px}$**

$A_f = 1228.3\ mm^2 \quad \rho = 0.0082 \quad k = 0.172 \quad n = 2.19$

$I_{cr} = \frac{b*(kd)^3}{3} + n * A_f * (d - kd)^2 = \frac{1000*(0.172*149)^3}{3} + 2.19 * 1228.3 * (149 - 0.172 *$

$149)^2 = 46.55 * 10^6\ mm^4$

$M_{cr} = f_r * \frac{I_g}{y_t} = 3.5 * \frac{666.67*10^6}{100} * 10^{-6} = 23.33\ kN.m$

$$f_f = 0.5E_f\varepsilon_{c_u}\left[\left(1 + \frac{4\alpha_1\beta_1\phi_c f_c'}{\rho_f\phi_f E_f\varepsilon_{c_u}}\right)^{1/2} - 1\right]$$

$$= 0.5 * 65374 * 0.0035 * \left[\left(1 + \frac{4 * 0.7884 * 0.8673 * 1.0 * 41.1}{0.0082 * 1.0 * 65374 * 0.0035}\right)^{1/2} - 1\right] = 778.5\ MPa$$

$c = \frac{\phi_f A_f f_f}{\alpha_1 \beta_1 \phi_c f_c' b} = \frac{1.0*1228.3*778.5}{0.7884*0.8673*41.1*1000} = 34.03\ mm$

$M_n = \phi_f A_f f_f * \left(d - \frac{\beta_1 c}{2}\right) = 1.0 * 1228.3 * 778.5 * \left(149 - \frac{0.8673*34.03}{2}\right) = 128.37\ kN.m$

$M_{p_x} = 0.5M_n + 0.5\left(1 - \frac{I_{cr}}{2I_g}\right)\left(\frac{M_{cr}}{M_n}\right)M_{cr} = 0.5 * 128.37 + 0.5\left(1 - \frac{46.55}{2*666.67}\right)\left(\frac{23.33}{128.37}\right)23.33 =$

$66.23\ kN.m$

$\mu = \frac{M_{p_y}}{M_{p_x}} = \frac{80.99}{66.23} = 1.22$

## D.3. Virtual Work Calculations

### D.3.1. Internal Work, *I*

The internal work done by the plane segments is calculated from Equation D.1 as listed in Table D.1.

$$I = m\theta l \qquad \text{Eq. [D.1]}$$

Where $I$ is the internal work done along the yield line, $m$ is the moment of resistance per unit width of the slab, $\theta$ is the relative rotation of the two segments about the yield line, and $l$ is the length of the yield line.

Table D.1: Work done by the plane segments

| Segment | $m_x$ | $\theta_x$ | $L_y$ | $m_y$ | $\theta_y$ | $L_x$ |
|---|---|---|---|---|---|---|
| 1 | *0* | *0* | *0* | $m_x$ | $\frac{\delta}{b} * \sqrt{\mu}$ | $\frac{2c_2L_1/\sqrt{\mu} + c_1b/\sqrt{\mu}}{b/\sqrt{\mu}}$ |
| 2 | $m_x$ | $\frac{\delta}{L_1}$ | $\frac{L22 - c}{\sqrt{\mu}}$ | *0* | *0* | *0* |
| 3 | *0* | *0* | *0* | $m_x$ | $\frac{\delta}{L_2} * \sqrt{\mu}$ | $L_{11}$-2*a* |
| 4 | *0* | *0* | *0* | *0* | *0* | *0* |

The work done by the two fan shape segments is calculated as follows:

$$I_{fan} = m\delta\varphi = 2 * m_x * \delta * \left[\frac{\pi}{2} - tan^{-1}\left(\frac{L_2 - C}{L_1 * \sqrt{\mu}}\right) - tan^{-1}\left(\frac{L_1 - a}{L_2} * \sqrt{\mu}\right)\right]$$

Accordingly, the total internal work done is:

$$I = m_x * \frac{\delta}{b} * \frac{2c_2L_1 + c_1b}{b} * \sqrt{\mu} + 2 * \frac{m_x}{\sqrt{\mu}} * \frac{\delta}{L_1} * (L_{22} - c) + m_x * \frac{\delta}{L_2} * (L_{11} - 2a) * \sqrt{\mu} + 2 * m_x * \delta * \left[\frac{\pi}{2} - tan^{-1}\left(\frac{L_2 - C}{L_1 * \sqrt{\mu}}\right) - tan^{-1}\left(\frac{L_1 - a}{L_2} * \sqrt{\mu}\right)\right]$$

### D.3.2. Internal Work, *E*

$$E = V * \delta + M * \theta$$

$$= \frac{V_u}{\sqrt{\mu}} * \frac{\delta * (2b - C_2) * \sqrt{\mu}}{2b * \sqrt{\mu}} + \frac{M_u}{\mu} * \frac{\delta}{b} * \sqrt{\mu}$$

$$= \frac{V_u}{\sqrt{\mu}} * \frac{\delta * (2b - C_2)}{2b} + 400 * \frac{V_u}{\sqrt{\mu}} * \frac{\delta}{b} = \frac{V_u * \delta}{\sqrt{\mu}} * \frac{800 + 2b - C_2}{2b}$$

Internal work done = External work done

$$\frac{V_u * \delta}{\sqrt{\mu}} * \frac{800 + 2b - C_2}{2b} = m_x * \frac{\delta}{b} * \frac{2c_2 L_1 + c_1 b}{b} * \sqrt{\mu} + 2 * \frac{m_x}{\sqrt{\mu}} * \frac{\delta}{L_1} * (L_{22} - c) + m_x * \frac{\delta}{L_2} * (L_{11} - 2a) * \sqrt{\mu} + 2 * m_x * \delta * \left[\frac{\pi}{2} - tan^{-1}\left(\frac{L_2 - C}{L_1 * \sqrt{\mu}}\right) - tan^{-1}\left(\frac{L_1 - a}{L_2} * \sqrt{\mu}\right)\right]$$

$$\rightarrow V_u = \frac{2bm_x}{800 + 2b - C_2}\left\{\frac{2c_2 L_1 + c_1 b}{b^2} * \mu + \frac{2(L_{22} - c)}{L_1} + \frac{(L_{11} - 2a)\mu}{L_2} + * \left[\pi - 2tan^{-1}\left(\frac{L_2 - C}{L_1 * \sqrt{\mu}}\right) - 2tan^{-1}\left(\frac{L_1 - a}{L_2} * \sqrt{\mu}\right)\right]\sqrt{\mu}\right\}$$

This equation gives the vertical load applied to the connection as a function of *a*, b and c. In order to obtain the minimum value of $V_u$, the following optimization problem was formulated:

$$V_{flex} = \min_{\{a,b,c\}} \; V_u(a, b, c)$$

$$\text{subject to} \qquad a, b, c > 0$$

Then, MATLAB® was used to solve this problem using its built-in function "fmincon" and the following results were obtained:

| Connection | Flexural Capacity, $V_{flex}$ (kN) |
|---|---|
| S-0.9-XX-0.4 | 332.6 |
| GSC-0.9-XX-0.4 | 275.9 |
| GSC-1.35-XX-0.4 | 321.6 |
| GSC-1.8-XX-0.4 | 373 |
| GSC-0.9-XX-0.2 | 331.6 |
| GSC-0.9-XX-0.6 | 232.5 |
| GRD-0.9-XX-0.4 | 353.4 |
| GRD-0.9-75-0.4 | 353.4 |
| GRD-0.9-50-0.4 | 337.9 |